Organic Material in Micrometeorites: Processes Affecting Its Delivery to Planetary Environments

Thesis

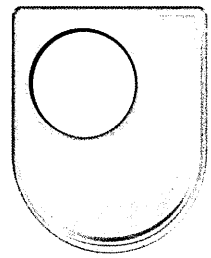

The Open University

Organic Material in Micrometeorites: Processes Affecting its Delivery to Planetary Environments

Rebecca Wilson
M.Sci. (Hons) ARSM (Imperial College London) 2004

Submitted for the degree of Doctor of Philosophy
Faculty of Science, The Open University

Supervised by:
Dr. Ian Franchi, Dr. Iain Gilmour, Dr. Victoria Pearson and Prof. Ian Wright

Submitted June 2009

DATE OF SUBMISSION : 26 JUNE 2009
DATE OF AWARD : 4 MARCH 2010

ProQuest LLC.
789 East Eisenhower Parkway
P.O. Box 1346
Ann Arbor, MI 48106 – 1346

Abstract

During their delivery to Earth, extraterrestrial dust particles (EDPs) are heated via aerodynamic braking in the upper atmosphere, liberating volatile and organic species. This study investigates the influence of atmospheric entry heating on this liberation process from Murchison (an EDP analogue), in order to assess the EDP contribution of biologically significant material to the early Earth.

Experimental simulations used a filament pulse pyrolyser to flash heat Murchison, replicating early Earth EDP atmospheric entry conditions. These simulations determined that the dehydration of phyllosilicates, the decomposition of organic and carbonate materials released H_2O, organic carbon and CO_2, respectively. Further characterisation of the released organic species (using GCxGC-TOFMS) identified a range of aliphatic, aromatic, PAH, O-bearing, S-bearing and N-bearing species; including biomolecule precursors. Relative abundances of these organic species were dependant not only on simulation peak temperature and duration, but also on their reaction with other fragments, which may have led to their production as secondary products.

In a complimentary study, comprehensive volatile organic analysis of Antarctic micrometeorites (AMMs) identified a range of aromatic, aliphatic, N-bearing, S-bearing, S-N-bearing and O-bearing species. Variations in the distribution of AMM aromatic species in comparison to the EDP analogue (as used in simulations) are consistent with i) the liberation of species during atmospheric entry heating ii) the alteration of organic material during Antarctic weathering processes and iii) a contribution from terrestrial sources. Alternatively, these deviations could reflect a different source (parent body) composition.

This investigation demonstrates that the abundance and composition of volatile and organic species liberated and retained in EDPs during entry heating (and their subsequent atmospheric reactions), may have played a role in atmospheric and climate development. EDPs additionally served as a source of prebiotic molecules and may have provided sites for chemical evolution.

Acknowledgements

I would like to thank my supervisors Ian Franchi, Iain Gilmour, Vic Pearson and Ian Wright for their continued efforts, advice and expertise over the past four years as this project has evolved. Most notably Vic, who has helped me keep the goal in sight! My thanks to Steve Sestak, for his knowledge of thermocouples; Mabs Gilmour and Jenny Gibson, for their help using the ANCA; and Diane Turner for her comprehensive training and troubleshooting in GCxGC-TOFMS – without which I would have been lost!

I would like to acknowledge Jean Duprat, Celcile Engrand and Michelle Maurrete at CSNSM CNRS-University Paris Sud for providing me with Antarctic micrometeorite and terrestrial samples from the Cap-Prudhomme site, and Elena Dobrica for her scanning electron microscope analyses of the particles.

I will be forever grateful for Bungie Studios and their development of Halo, Halo 2 and Halo 3, which provided me with a great source of stress relief throughout my Ph.D.!

Finally, I would like to thank Olly, my parents and my sister for their continued financial and emotional support throughout my university years. Without their personal sacrifices, realisation of my Ph.D. would not have been possible.


temperature
abundances
column
acids
EDP
CO2
dust
EDPs
heated
Parent
entry
identified
matter
terrestrial
experimental
contain
Murchison
gas
organic
MMs
particles
chondrites
Water
However
peak
volatile
acid
lower
Carbonate
macromolecular
increasing
presence
heating
peaks
Lunar
surface
nature
atmospheric
samples
time
Meteorites
PAHs
Flynn
species
Carbon
material
flash
micrometeorites
alkyl
release
extraterrestrial
Simulation
particle
durations
addition
IDPs
aromatic
present
similar
loss
benzene
Carbonaceous
Evolved
compounds
fragments
decomposition
AMMs
H2O
Method
suggests
average
study
Permian
cometary
temperatures
simulations
Flux
conditions
secondary
hydrocarbons
Duration
Antarctic
planetary
pyrolysis
Acta
may
also
derived
liberated
using
early
higher
percentage
within
Love
thiophenes
Toarcian
elemental
sample
thermal
molecular
amino
alteration
chemistry
interplanetary
studies
origin
Analysis
released
chemical
abundance
used
size
total
meteorite
composition
aliphatic
relative
Primary
Chondrite
Sulphur
mass
science
nitrogen
minerals
range
inorganic
Earth
mineralogy
thought
benzenes

(Wordle.net)

Contents

List of Figures

List of Tables

1. Introduction

The origin of life on Earth is a fundamental and unanswered question of science. The circumstances that gave rise to the complex chemistry that generated the first living cells are unknown, but would have required a significant reserve of organic matter, in addition to an energy source and inorganic materials. Various theories exist regarding the synthesis of pre-biotic organic materials on the early Earth (Chyba & McDonald, 1995; Lazcano & Miller, 1996; Miller & Lazcano, 1995; Orgel, 1998). Most notably Oparin (1938) proposed that the spontaneous formation of life could have occurred in the ocean, if large quantities of organic species were present. Hydrothermal vents in deep oceans have since then been suggested as a unique environment for organic synthesis (Baross & Hoffman, 1985; Corliss et al., 1981; Maher & Stevenson, 1988; Miller & Bada, 1988). Oparin (1938) also suggested that organic compounds could be synthesised in a reducing early atmosphere. Simulation of lightening discharges in a reducing atmosphere (Miller, 1953; Miller & Urey, 1959) synthesised simple organic materials such as amino acids (alanine, glycine), carboxylic acids (formic acid, acetic acid) and α-hydroxyl acids (sarcosine, lactic acid) from methane, ammonia, water and hydrogen. However, these synthesised molecules lacked diversity and complexity.

It has been proposed that a more diverse and complex range of organic materials may have been delivered to Earth by extraterrestrial impactors (Anders, 1989; Bernal, 1961; Chyba et al., 1990; Chyba, 1993; Chyba & Sagan, 1992; Oro, 1961). Throughout history, the Earth has been bombarded by extraterrestrial material, as is evident from the numerous craters present on the planet's surface. This material ranges from that of the macro-scale (impactors in excess of a few km) to that of the micro-scale (impactors < 1 mm in size). Meteorites are fragments of extraterrestrial material, >1 mm in size, that fall periodically to the Earth's surface. These fragments are produced as a result of collisions with other extraterrestrial objects. As the rocky fragments pass through the Earth's atmosphere, they are heated resulting in a fireball. Eyewitness accounts and photographs

of fireballs, allow the reconstruction of their orbits. To date 24 fireballs have been calculated as sourced from the asteroid belt (a region between Mars and Jupiter containing rocky and metallic bodies known as asteroids) (Brown et al., 2000; Docobo et al., 2008 and references there in).

Although the vast majority of meteorites originate from asteroids, there are fifty six meteorites sourced from the Moon (Korotev, 2008). Lunar origin is based on the chemistry and mineralogy of the meteorites with some matches to samples returned from the NASA Apollo missions (McSween, 1999). Forty seven meteorites originating from Mars (Classen, 2008) have also been identified based on mineralogy, chemistry and noble gas contents (McSween, 1994).

Extraterrestrial materials within our solar system < 1mm in size are known in this study as extraterrestrial dust particles (EDPs). When they pass through the Earth's atmosphere they are heated and form meteors or shooting stars. Some are completely evaporated in the atmosphere, whilst others survive and settle to the surface. Based on their composition, EDPs are thought to be of either cometary (Genge, 2005; Maurette, 2006) or asteroidal origin (Engrand & Maurette, 1998; Genge et al., 1997; Kurat et al., 1994; Noguchi, et al., 2002). EDPs are collected for study directly from the atmosphere (Brownlee, 1985), and from the Earth's surface from Greenland and Antarctic ice (Maurette, 1998; Maurette et al., 1994; Taylor et al., 1998). These μm-sized particles are the focus of this study.

1.1. Classification of Meteorites

Meteorites are classified into three broad groups based on chemical compositions - the irons, stony-irons and the stones (Bischoff, 2001)(Figure 1). The iron meteorites are composed of Fe-Ni metal alloys, while the stony irons comprise of roughly equal quantities of Fe-Ni metal alloy and silicate and oxide minerals. The stony meteorites are primarily composed of silicate and oxide minerals and are divided into the subgroups chondrites and achondrite, determined by the presence or absence of chondrules (mm-sized spheres

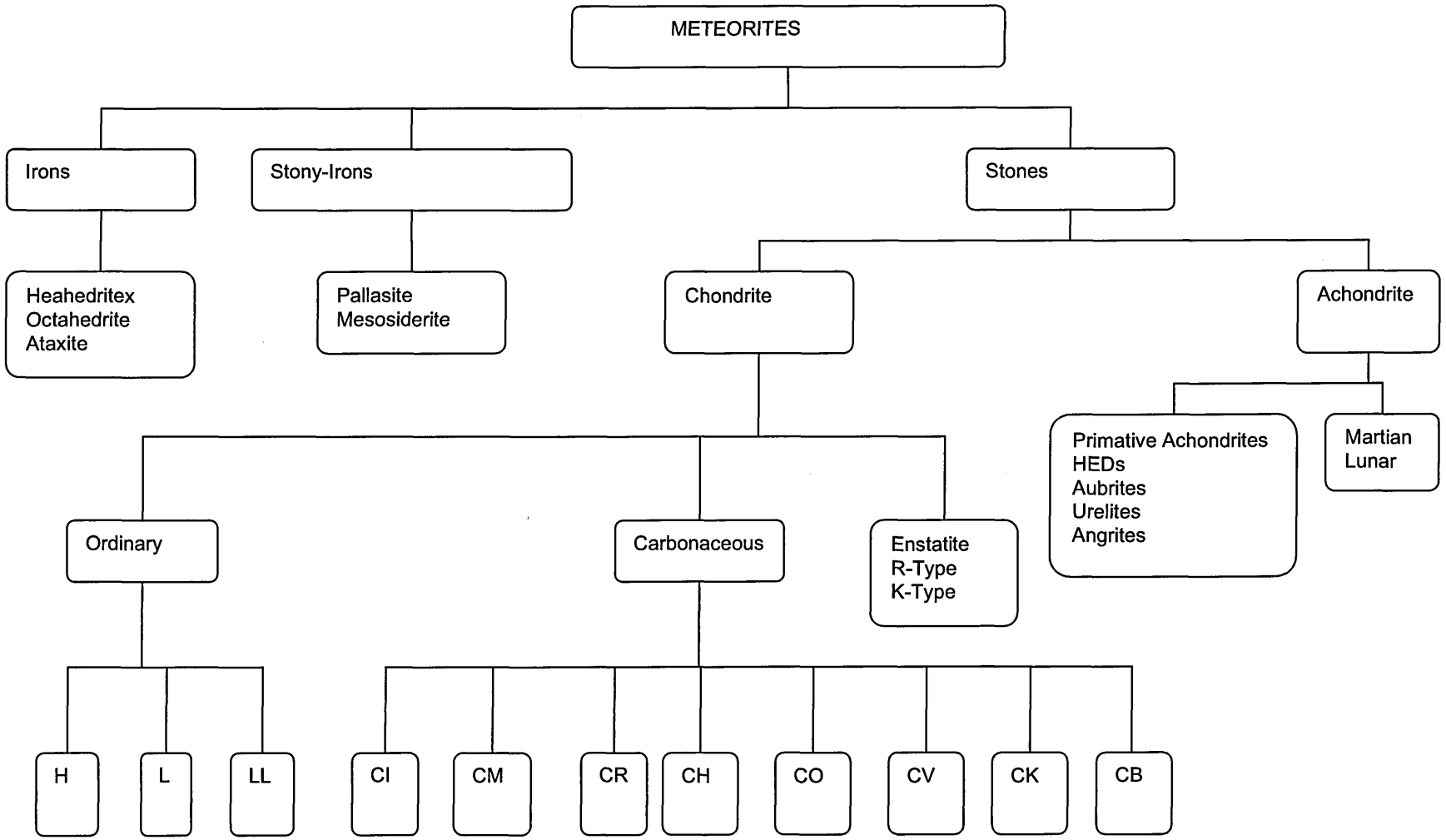

Figure 1: Classification of meteorites adapted from Bischoff (2001)

of silica melt).

The achondrites are stony meteorites that do not contain chondrules, as they have formed from recrystallisation or crystallisation and partial melting of magma. They are similar in nature to terrestrial igneous rocks. Parent bodies include asteroids, the Moon and Mars. Analysis of achondrites provides information relevant to planetary processing and differentiation of rocky bodies within the Solar System.

1.1.1. Chondrites

Chondrites are a class of stony meteorite, similar in nature to terrestrial sedimentary rocks, and represent the accretion of asteroid parent bodies from multiple components. They are the most primitive Solar System rocks, dated to 4.21-4.59 Ga (Dalrymple, 1991), with parent bodies formed from nebula materials in the same manner as the rocky planets. Chondrites have not experienced extensive alteration since their formation, unlike the achondrites that have been differentiated and processed as a result of parent body melting and recrystallisation (McSween, 1989), or terrestrial rocks that have been reworked via plate tectonics and the rock cycle (Gregor, 1992; Wilson, 1963). Chondrite analysis therefore provides a unique insight into nebular environments and processes at the time of planet formation.

Chondrites take their name from the presence of chondrules, millimetre-sized spherules of rapidly cooled silica melt formed as a result of flash heating and supercooling (Hewins & Radomsky, 1990; Hewins & Connolly, 1994; Lofgren, 1994). The Chondrite class is further subdivided into Ordinary, Carbonaceous and Enstatite and Rumaruti (R-type) based on mineralogy, non-volatile content and their oxidation state derived from the mineral compositions of olivine and pyroxene (Van Schmus & Wood, 1967). Chondrite mineralogy and texture is affected by the extent of pre-terrestrial secondary processing, enabling further sub-classification by petrologic type (Table 1).

Chemical Type	Group	PETROGRAPHIC TYPE					
		1	2	3	4	5	6
		Chondrule Texture					
		Absent	Sparse	Abundant/ distinct		Increasingly indistinct	
Ordinary Chondrites	H						
	L						
	LL						
Enstatite Chondrites	EH						
	EL						
Carbonaceous Chondrites	CI						
	CM						
	CR						
	CB[1]						
	CH[2]						
	CO						
	CV						
	CK						
R-Chondrites	R						
K-Chondrites	K						

<150 °C <200°C 400 °C 600 °C 700 °C 750 °C 950°C

Increasing aqueous alteration

Increasing thermal metamorphism

Table 1: Classification of chondrites by petrographic type adapted from Van Schmus and Wood, (1967). 1- Weisberg et al., (2001), 2- Bischoff et al., (1993)

Type 1 chondrites have experience aqueous alteration, whilst type 6 have experienced extensive thermal metamorphism (Van Schmus & Wood, 1967). Type 1 meteorites demonstrate solar bulk chemical compositions (Anders & Grevesse, 1989). Although the type 3 meteorites are petrographically the least altered, ^{13}C and ^{15}N analysis of organic matter in type 2 chondrites, suggest they may be the most primitive (Alexander et al., 1998; Sephton et al., 2003)

Evidence for aqueous processing in type 1 and type 2 carbonaceous chondrites includes the presence of indigenous water (Jarosewich, 1990) bound within hydrous phases (Barber, 1985; Barber, 1981). These components may have been derived from the aqueous alteration on the parent body (Barber, 1981; McSween, 1987; Tomeoka & Buseck, 1985; Trigo-Rodriguez et al., 2006) or by the incorporation of nebula derived materials into the parent body (Bischoff, 1998; Ciesla et al., 2003; Ciesla & Lauretta, 2005).

Although chondritic parent bodies never became hot enough to melt or differentiate, many of them reached high enough temperatures (400-950 °C) that they experienced significant thermal metamorphism in their interiors resulting in a metamorphic scale within chondrite groups (Table 1) (Keil, 2000). The source of the heat was most likely energy coming from the decay of short-lived radioisotopes such as ^{26}Al and ^{60}Fe (Grimm & McSween, 1989; Keil, 2000), present in the early solar system, which were incorporated into chondrite parent bodies during the Solar System's accretionary phase.

Collisions between asteroids and other extraterrestrial materials produce shock metamorphism as well as thermal metamorphism (Keil et al., 1997). This manifests as brecciated textures or the presence of clasts within meteorites. The extent of shock metamorphism is defined on a graded scale between S1 (low) to S6 (high) (Stöffler et al., 1991).

1.1.2. Carbonaceous Chondrites

Carbonaceous chondrites are a rare type of chondritic meteorite that are the most primitive and unaltered of all meteorites. They are composed primarily of chondrules, cm-sized clasts of refractory minerals (calcium aluminium-rich inclusions - CAIs), matrix and organic material. Primary mineralogy includes anhydrous silicates, oxides, and sulphides. In addition they contain organic materials and water and minerals that have been altered in the presence of water (Brearley & Jones, 1998).

The carbonaceous chondrites are subdivided into 8 subgroups (CM, CK, CO, CV, CR, CH, CB and CI - see Figure 1) based on refractory and volatile element concentrations (Kallemeyn & Wasson, 1981; Kallemeyn & Wasson, 1982; Kallemeyn et al., 1991). The "C" represents carbonaceous and the second letter represents the "type specimen" for the subgroup. For example CI – Ivuna, CM – Mighei, CV – Vigarano, CO – Ornans, CK – Karoonda, CR – Renazzo, CB – Bencubbin and CH – high metal. The CB chondrites are the most metal-rich of all chondrites, containing in excess of 60 vol% metal

(Weisberg et al. 2001). The CH group are similar in nature to the CBs, with a high iron content and 20-90 μm chondrules comprising 70 vol% (Hezel et al., 2003).

The bulk composition of the CIs bears resemblance to the solar photosphere (Sears & Dodd, 1988), hence their elemental abundance is seen as a record of average solar system abundances. As such, the CIs are often used as a reference composition for Solar System materials.

1.2. Carbon in Carbonaceous chondrites

Chondritic carbon is present in multiple forms, each thought to have a different origin. Elemental carbon is present in the form of nanodiamonds, graphite and silicon carbide grains (Anders & Zinner, 1993; Henning & Salama, 1998; Huss & Lewis, 1995). Nanodiamonds constitute around 400 ppm of carbon within carbonaceous chondrites, with graphite comprising 2 ppm and silicon carbide 6 ppm (Amari et al., 1990).

Carbonates comprise ~0.2 % whole rock in carbonaceous chondrites (Smith & Kaplan, 1970). Indigenous carbonates identified within the matrix include calcite, aragonite, dolomite, magnesite and breunnerite (Brearley & Jones, 1998 and references therein).

One of the most well studied chondrites is the CM2 carbonaceous chondrite Murchison, which fell in 1969. The carbon content of Murchison ranges between 1.6 - 2.70 wt.% (Naraoka et al., 2004; Pearson et al., 2006). Up to 25 % of the organic material within Murchison is solvent soluble and known as the extractable organic fraction (Hayes, 1967). The remaining ~75 % corresponds to the macromolecular material of a high molecular weight organic network, akin to terrestrial Type III kerogen (Hayatsu et al., 1977) and is insoluble in solvent extraction.

1.2.1. The Extractable Organic Fraction in Carbonaceous Chondrites

Murchison, due to its relatively pristine nature and availability, has become the standard for comparing organic material compositions within meteoritic samples. Bulk

analysis and extraction techniques have enabled the identification of indigenous amino acids, carboxylic acids, aliphatic and aromatic hydrocarbons (Table 2).

Compounds	Abundance μg g^{-1} (ppm)	Reference
Carbon dioxide	106	1
Carbon monoxide	0.06	1
Methane	0.14	1
Aliphatic hydrocarbons	12-35	2
Aromatic hydrocarbons	15-28	3
Monocarboxylic acids	332	1, 4
Dicarboxylic acids	25.7	5
α-hydroxycarboxylic acids	14.6	6
Amino acids	60	7
Alcohols	11	8
Aldehydes	11	8
Ketones	16	8
Sugar related compounds	~60	9
Ammonia	19	10
Amines	8	11
Urea	25	12
Basic N-heterocycles (pyridines, quinolines)	0.05-0.5	13
Pyridinecarboxylic acids	>7	14
Dicarboximides	>50	14
Pyrimidines (uracil and thymine)	0.06	15
Purines	1.2	16
Benzothiophenes	0.3	17
Sulfonic acids	67	18
Phosphonic acids	1.5	19

Table 2: Abundances of constituents from the free organic fraction of Murchison. 1- Yuen et al., (1984), 2- Kvenvolden et al., (1970), 3- Pering and Ponnamperuma (1971), 4- Lawless and Yuen (1979), 5- Lawless et al., (1974), 6- Peltzer et al., (1984), 7- Cronin et al., (1988), 8- Jungclaus et al., (1976 a), 9- Cooper et al., (2001), 10- Pizzarello et al., (1994), 11- Jungclaus et al., (1976 b), 12- Hayatsu et al., (1975), 13- Stoks and Schwartz (1982), 14- Pizzarello et al., (2001), 15- Stoks and Schwartz (1979), 16- Stoks and Schwartz (1981), 17- Shimoyama and Katsumata (2001), 18- Cooper et al., (1997), 19- Cooper et al., (1992)

i) Aliphatic Hydrocarbons

Over 140 aliphatic hydrocarbon species have been detected within carbonaceous chondrites (Cronin et al., 1988). These include C_1-C_{24} hydrocarbons comprising *n*-alkanes and branched alkanes, isoprenoid alkanes and alkenes (Belsky & Kaplan, 1970; Cronin & Pizzarello, 1990; Hayes, 1967; Nooner & Oro 1967; Oro & Nooner, 1967; Studieret al., 1968) in addition to C_{15}-C_{30} cycloalkanes (Cronin & Pizzarello, 1990; Kvenvolden et al., 1970).

The source of meteoritic aliphatic components is controversial. Studier et al., (1968), suggested that the range of meteoritic organic species is reflective of their formation and partial equilibration by Fischer-Tropsch synthesis (whereby catalytic reactions between CO and H_2 can yield hydrocarbons). However, the identification of the

isoprenoid alkanes, such as the common terrestrial biological compounds pristane and phytane in carbonaceous chondrites (Meinschein, 1963b; Oro & Nooner, 1967), suggests that some alkane species may be terrestrial in origin. This is supported by the distribution of aliphatic species throughout meteoritic samples, which decrease in abundance towards the sample interior (Cronin & Pizzarello, 1990; Sephton et al., 2001). Additionally, compound specific isotope analysis has demonstrated that *n*-alkanes in Murchison are relatively depleted in ^{13}C compared with other organic species and show considerable variability between specimens stored in different curatorial facilities (Sephton et al., 2001). Sephton et al., (2001) also found that the $\delta^{13}C$ values for the meteoritic *n*-alkanes were similar to petroleum *n*-alkanes, highlighting that meteoritic *n*-alkanes appear to be terrestrial contaminants possibly originating from petroleum products.

ii) Aromatic Hydrocarbons

Solvent extracts of Orgueil (CI1), Murray (CM2), Cold Bokkeveld (CM2) and Allende (CV3) have been analysed using a variety of techniques including mass spectroscopy (MS) (Meinschein, 1963a; Meinschein, 1963b), infrared and ultraviolet spectroscopy (Commins & Harington, 1966; Meinschein, 1963b) and gas chromatography (GC) (Meinschein, 1963a; Nooner & Oro, 1967) in order to identify free aromatic species. These analyses have identified aromatics from naphthalene to coronene including their alkyl derivatives (Belsky & Kaplan, 1970; Studier et al., 1968). Murchison extracts yield 1-4 carbon ringed PAHs including C_1-C_4 alkylnaphthalenes and C_1-phenanthrene (Gilmour & Pillinger, 1994; Pering & Ponnamperuma, 1971; Studier et al., 1972). Although some aromatics identified are thought to result from terrestrial contaminants (Han et al., 1969), the isotopic compositions of aromatic fractions display enrichments in deuterium and ^{13}C attributed to an interstellar contribution (Krishnamurthy et al., 1992). Additionally, the $^{12}C/^{13}C$ ratios of PAHs in the free organic fraction of Murchison increase with increasing carbon number, suggesting these species may be synthesised from lower molecular weight components (Gilmour & Pillinger, 1994).

iii) Carboxylic Acids

Carboxylic acids are the most abundant soluble compound in the carbonaceous chondrites (Table 2). Yuen and Kvenvolden (1973) were the first to characterise C_2-C_8 straight and branched chain monocarboxylic acids in Murray and Murchison using gas chromatography-mass spectrometry (GC-MS). The presence of up to C_9 branched and straight chain dicarboxylic acids were later determined (Lawless et al., 1974). More recently, studies have confirmed the presence of carboxylic acids and up to C_9-dicarboxylic acids in carbonaceous chondrites (Martins et al., 2006; Pizzarello et al., 2001) including detecting concentrations of > 300 ppm and > 30 ppm, respectively in Murchison (Pizzarello et al., 2001).

Carbon isotope measurements of monocarboxylic acids in Murchison (Huang et al., 2005; Yuen et al., 1984) demonstrated that they were isotopically heavier than their terrestrial counterparts, suggesting an extraterrestrial origin. This was confirmed by compound specific deuterium isotope measurements of Murchison carboxylic acids (Epstein et al., 1987; Huang et al., 2005), showing deuterium enrichment (with up to δD = +2024 ‰ (Huang et al. 2005)), representative of their interstellar origin or formation from interstellar materials (Krishnamurthy et al., 1992) (Section 1.2.3). Shock and Shulte (1990) have proposed that aqueous alteration on the parent body could derive carboxylic acids and amino acids from PAHs.

iv) Amino Acids

Indigenous amino acids were first identified in Murchison using the technique of ion exchange chromatography, GC and GC-MS. Initially two non-protein amino acids and five protein amino acids were identified, of which four were racemic (alanine, glutamic acid, valine and proline) suggesting an abiotic and extraterrestrial origin for the compounds (Kvenvolden et al., 1970). Over eighty amino acids have been identified in Murchison since the 1970's (Botta et al., 2002; Cronin & Chang, 1993; Cronin & Moore, 1971; Cronin & Pizzarello, 1983; Glavin et al., 2006; Lawless, 1973) and include almost

complete structural diversity of C_2-C_8 cylcic and acyclic alkanoic and alkandioic acids, many of which are not present in the terrestrial environment. α-amioisobutyric (AIB) acid and isovaline are two of the most abundant amino acids in Murchison (Kvenvolden et al., 1971) yet have a restricted presence on Earth.

v) N-Heterocycles

The presence of biologically significant N-heterocycles, such as purine and pyrimidine bases, was first established in water extracts of carbonaceous chondrites (Briggs, 1961). The nucleobases adenine and guanine, in addition to triazines, were later identified in acid hydrolysed extracts of Orgueil (Hayatsu, 1964) and Murchison (Hayatsu et al., 1975). As these compounds required prolonged acid hydrolysis for their release, they were thought to be bound within the macromolecular material (Hayatsu et al., 1975). Acid hydrolysis extracts of the Murchison meteorite confirmed the presence of 4-hydroxypyrimidines (Folsome et al., 1971; Folsome et al., 1973), later denoted contaminants of the extraction procedure (van der Velden & Schwartz, 1977).

Formic acid extracts of Murchison, Murray and Orgueil determined the additional presence of the purines hypoxanthine and xanthine (Stoks & Schwartz, 1981; van der Velden & Schwartz, 1977) with a concentration of 114-655 ppb in samples (Stoks & Schwartz, 1981). Stoks and Schwartz (1981) also identified the presence of the pyrimidine uracil in these meteorites and an absence of *s*-traizines, leading them to suggest they triazines may be artefacts synthesised during the experimental procedure of previous studies. Recent carbon isotope analysis of Murchison (Martins et al., 2008) demonstrates that uracil and xanthine have $\delta^{13}C$ of +44.5 ‰ and +37.7 ‰ respectively, reflective of an extraterrestrial origin.

GC-MS analysis of dichloromethane (DCM) and ethyl acetate extracts of the Murchison meteorite, have additionally identified alkyl pyridines, quinoline, isoquinoline and alkyl quinolines (Pizzarello et al., 1994; Stoks & Schwartz, 1982). More recently,

Pizzarello et al., (2001) identified carboxylated pyridines in water extracts of the Murchison meteorite.

1.2.2. Insoluble Organic Matter in Carbonaceous Chondrites

Initial analyses of macromolecular material focused on Murchison, Allende and Orgueil (Hayatsu et al., 1977; Levy et al., 1973). As this fraction is insoluble in common organic solvents (Hayes, 1967), its investigation has been conducted using non-destructive techniques such as infra-red spectroscopy (Hayatsu et al., 1977), nuclear magnetic resonance (NMR) spectroscopy (Cronin et al., 1987; Cody et al., 2002) and electron paramagnetic resonance (EPR) spectroscopy (Binet et al., 2002; Duchesne et al., 1964; Schulz & Elofson, 1965).

Alternatively, destructive techniques such as pyrolysis gas chromatography mass spectrometry (Py-GC-MS) has been employed since the 1960's (Gilmour, 2003; Hayatsu et al., 1977; Hayes & Biemann, 1968; Komiya & Shimoyama, 1996; Levy et al., 1973; Pearson et al., 2006; Pearson et al., 2007; Sephton et al., 2004), a process that fragments the macromolecular material into more amenable analytes. In recent years, both hydrous pyrolysis conducted with the sample in contact with water (Sephton et al., 1998; Sephton et al., 2000) and hydro-pyrolysis conducted in the presence of hydrogen (Sephton et al., 2004) have been developed to fragment macromolecular material.

Based on pyrolysis studies, the elemental composition of insoluble organic material within Murchison is thought to be $C_{100}H_{71}N_3O_{12}S_2$ (Nagy, 1975). Elemental analysis has suggested compositions of $C_{100}H_{48}N_{1.8}O_{12}S_2$ (Zinner, 1988) or $C_{100}H_{57.2}N_{2.9}$ for C, N and H compositions (Cody et al., 2002).

NMR studies suggest that the majority of carbon in the Murchison insoluble organic fraction exists as aromatic carbon (Cody et al., 1999; Cody et al., 2002; Cody & Alexander, 2005)(Table 3). Pyrolysis studies have shown that this is primarily in the form of 1- 4 ringed condensed aromatic cores such as benzene, toluene, biphenyl, naphthalene, and higher polycyclic aromatic hydrocarbons (up to chrysene, pyrene and

fluoranthene) in addition to their alkyl derivatives (Clemett et al., 1998; Sephton, 2002). The structure is thought to be a network of condensed aromatic cores, connected by aliphatic and ether linkages with a variety of functional groups attached (Cronin et al., 1987; Hayatsu et al., 1977; Hayatsu et al., 1980; Remusat et al., 2005 a; Sephton et al., 1998).

Functional Groups	NMR Response (% of total intensity)
Apparent aromaticity	62-63
C=O carbon (e.g. ketone and carboxyl)	27-36
Oxygen substituted carbon (e.g. alcohols and ethers)	17-24
Aliphatic carbon (e.g. methyl, methylene and methine)	15-22

Table 3: Estimation of functional group abundance using NMR taken from Cody and Alexander (2005)

Remusat et al., (2005 a) characterised aliphatic linkages in macromolecular material from Orgueil and Murchison. Using ruthenium tetroxide to break down macromolecular material, they generated aliphatic diacids originating from aliphatic bridging units and aliphatic side chains. The authors identified that aliphatic bridges between aromatic units were composed of C_2-C_7 aliphatics substituted by methyl, ethyl, ester or ether functional groups. In contrast, thery found that aliphatic side chains attached to aromatic units at only one end were typically less than three carbon chain length.

Several pyrolysis studies have identified the release of oxygen bearing species including phenols, benzenecarboxylic acids, aldehydes, ketones, furans, benzofurans, dibenzofurans and their associated alkylated species from meteoritic macromolecular material (Hayatsu et al., 1977; Levy et al., 1973; Komiya & Shimoyama, 1996; Pearson et al., 2006; Remusat et al., 2005 b; Sephton et al., 1998; Sephton et al., 2000; Sephton et al., 2004). Sulphur bearing compounds include thiophenes, benzothiophenes, dibenzothiophenes and their alkyl derivatives (Hayatsu et al., 1977; Levy et al., 1973; Pearson et al., 2006; Remusat et al., 2005 b; Sephton et al., 1998). In addition, a range of nitrogen containing compounds including common pyrolysis products of acetonitrile and

benzonitrile (Levy et al., 1973) and alkyl pyrimidines (Hayatsu et al., 1977) have also been identified.

1.2.3. The Origin of Meteoritic Organic Material

There are several source regions and mechanisms of formation of meteoritic organic material. Based on deuterium enrichments of macromolecular material, it is thought they may have formed, in part, from interstellar species (Botta & Bada, 2002; Cronin et al., 1995; Krishnamurthy et al., 1992; Kolodny et al., 1980; Pizzarello et al., 2001; Robert & Epstein, 1982). Simple gaseous molecules (CH_4, CH_2O, H_2O, N_2 and NH_3) residing in interstellar clouds can be ionised and fragmented by cosmic radiation (Herbst & Klemperer, 1973; Herbst, 2001; Solomon & Werner, 1971). Generated ions may then combine with neutral species, in ion-molecule reactions, producing increasingly deuterium enriched and more complex organic products. Subsequently, these enriched molecules are thought to condense onto dust grains (Kerridge, 1983; Kolodny et al., 1980; Robert & Epstein, 1982) or the surface of silicate interstellar dust grains (Greenberg, 1984; Robert & Epstein, 1982) as an icy-mantle (Sandford & Allamandola, 1993a; Sandford & Allamandola, 1993b; Sandford et al., 1993). Prolonged exposure to UV radiation or increased temperatures can drive polymerisation reactions within these icy mantles, leading to more complex and deuterium enriched products (Sandford, 1996). Incorporation of this isotopically-enriched, complex organic material would have subsequently become incorporated into chondrite parent bodies after the collapse of the interstellar cloud.

An alternative origin is the generation of organic material via Fischer-Tropsch type (FTT) reactions within the Solar Nebula. FTT reactions could have generated aliphatic hydrocarbons from CO and H_2 on the surface of mineral catalysts (Anders et al., 1973; Hayatsu et al., 1977; Kvenvolden et al., 1970; Studier et al., 1968; Studier et al., 1972). Later, thermally-induced polymerisation and aromatisation of these aliphatic species could have produced macromolecular material (Hayatsu et al., 1977). Chondritic organic

species are isomerically diverse, in contrast to that of FTT synthesised material which cannot account for the wide range of C, N and H isotopic fractionations observed in meteorites (Becker & Epstein, 1982; Yang & Epstein, 1983). Organic material in meteorites is associated with clay minerals (Pearson et al., 2002) and the surface of mineral nuclei (Alpern & Benkheiri, 1973). However, the mineral catalysts required for organic synthesis within the solar nebula could have been generated later via aqueous alteration on parent bodies (Bunch & Chang, 1980; Kerridge et al., 1979). Whilst Hayatsu et al., (1977) suggested that *n*-alkanes would be preferentially derived from FTT reactions, analysis of these chondritic species suggest that they are terrestrial contaminants (Meinschein, 1963b; Nooner & Oro, 1967; Sephton et al., 2001). Morgan et al., (1991) later proposed that chondritic macromolecular material was formed by gas-phase pyrolysis of simple aliphatics (acetylene and methane) that were present in the Solar Nebula, originating from the collapse of the interstellar cloud.

Once incorporated into chondrite parent bodies, organic material would have been affected by subsequent thermal and aqueous processing. Secondary processing or polymerisation would have been possible if volatiles (H_2O, NH_3, HCN) came in contact with interstellar precursors and mineral catalysts. For example, amino acids (Chang & Bunch, 1986; Shock & Schulte, 1990) and carboxylic acids (Shock & Schulte, 1990) could have formed on chondrite parent bodies during the aqueous alteration of macromolecular material. It has also been noted that alkyl-PAHs are associated with carbonaceous chondrites that have experienced substantial aqueous alteration (Elsila et al., 2005). Thermal metamorphism (thermal alteration) can be driven on parent bodies by a number of mechanisms such as internal heating from the decay of short-lived radionuclides (Lee et al., 1976) or residual heating following the accretion of parent bodies (Larimer & Anders, 1967). Thermal alteration of residing organic material can decrease bulk C and N abundances (Pearson et al., 2006), graphitise organic material (Abreu, 2007; Bonal et al., 2007), reduce PAH abundance (Elsila et al., 2005) and condense the aromatic network by increasing cross linkages (Sephton et al., 1998).

1.3. Extraterrestrial Dust Particles

Extraterrestrial dust particles (EDPs) are primarily rocky particles < 1mm. They comprise particles collected both from the surface of the Earth and the atmosphere. EDPs collected from the Earth's surface are known as micrometeorites (MMs) and are typically 30-1000 μm. They are typically recovered by filtering melted Antarctic ice and snow, resulting in the collection of Antarctic micrometeorites (Iwata & Imae, 2001; Maurette et al., 1991; Taylor et al., 1998). Alternatively they can be collected by sieving the sediment from cryoconite holes (Maurette et al., 1987). In contrast, interplanetary dust particles (IDPs) are collected from the Earth's stratosphere (Brownlee, 1985), but these are smaller in size (typically <30 μm).

The classification of EDPs is primarily defined by their morphology related to the degree of heating they experience upon atmospheric entry with further sub-classification based on factors such as chemical composition and grain size. Based on high abundances of presolar silicates (900 ppm - Yada et al., 2006), their high porosity and anhydrous mineralogy (Genge, 2005; Joswiak et al., 2007; Maurette, 2006) some EDPs are thought to be of cometary origin. However, similarities between EDP hydrous minerals and elemental abundances (Engrand & Maurette, 1998; Genge et al., 1997; Kurat et al., 1994; Noguchi et al., 2002) compared to that of CI, CM and CR chondrites as discussed in Section 1.4 suggest they may be of asteroidal origin.

1.3.1. The Classification of Micrometeorites

A formal classification scheme has been recently proposed by Genge et al., (2008) as summarised in Table 4 and Figure 2 and outlined in detail below. This classification is based on textural features of MMs, related to the degree of thermal processing they have undergone during their passage to the Earth's surface (Section 1.6). Further sub-categories are defined by mineralogy and chemical compositions outlined in Table 4, which can also be altered by the extent of heating during atmospheric entry (Greshake et al., 1996; Greshake et al., 1998; Toppani et al., 2001).

Group	Class	Type	Subtype	Description
Melted MMs	Cosmic Spherules (CSs)	S	CAT	Spherules with Mg/Si > 1.7 that are enriched in Ca, Ti and Al. They have barred olivine textures.
		S	Glass	Spherules consisting almost entirely of glass.
		S	Cryptocrystalline	Spherules dominated by submicron crystallites and magnetite. Some include multiple domains.
		S	Barred Olivine (BO)	Spherules dominated by parallel growth olivine within glass.
		S	Porphyritic Olivine (Po)	Spherules dominated by equant and skeletal olivine within glass. Relict-bearing varieties contain unmelted minerals.
		S	Coarse-grained	These spherules contain >50% volume relict minerals.
		G		Spherules are dominated by magnetite dendrites within silicate glass.
		I		Spherules dominated by magnetite, wustite.
Partially Melted MMs	Scoriaceous MMs (ScMMs)	-	-	Vesicular particles dominated by a mesostasis of fayalitic olivine microphenocrysts within glass. ScMMs often contain relict minerals and relict matrix areas.
Unmelted MMs	Fine-grained MMs (FgMMs)	C1		Compact, chemically homogeneous FgMMs. Often contain framboidal magnetite.
		C2		Compact, chemically heterogeneous fine-grained MMs. Often contain isolated silicates and/or tochilinite.
		C3		Highly porous FgMMs. Often contain isolated silicates and framboidal magnetite.
	Coarse-grained MMs (CgMMs)	Chondritic CgMMs	Porphyritic Olivine and/or Pyroxene	Igneous MMs dominated by pyroxene and/or pyroxene phenocrysts within glass.
			Granular Olivine and/or Pyroxene	Igneous MMs dominated by pyroxene and/or olivine without significant glass.
			Barred Olivine	Igneous MMs dominated by parallel growth olivine within glass.
			Radiate Pyroxene	Igneous MMs dominated by radiating pyroxene dendrites within glass.
			Type I/Type II	Type I CgMMs are reduced particles containing Fs and/or Fa < 10 mole%. Type II CgMMs are oxidised particles with Fs and/or Fa > 10 mole%.
		Achondritic CgMMs	-	Differentiated igneous CgMMs.
	Refractory MMs	Porous	-	Porous particles dominated by refractory minerals.
		Compact	-	Compact particles dominated by refractory minerals.
		Hydrated	-	Particles dominated by refractory minerals surrounded by Fe-rich phyllosilicates or their dehydroxylates.
	Ultracarbonaceous MMs		-	Particles dominated by carbonaceous materials with embedded

Table 4: A summary of the micrometeorite classification scheme taken from Genge et al., (2008)

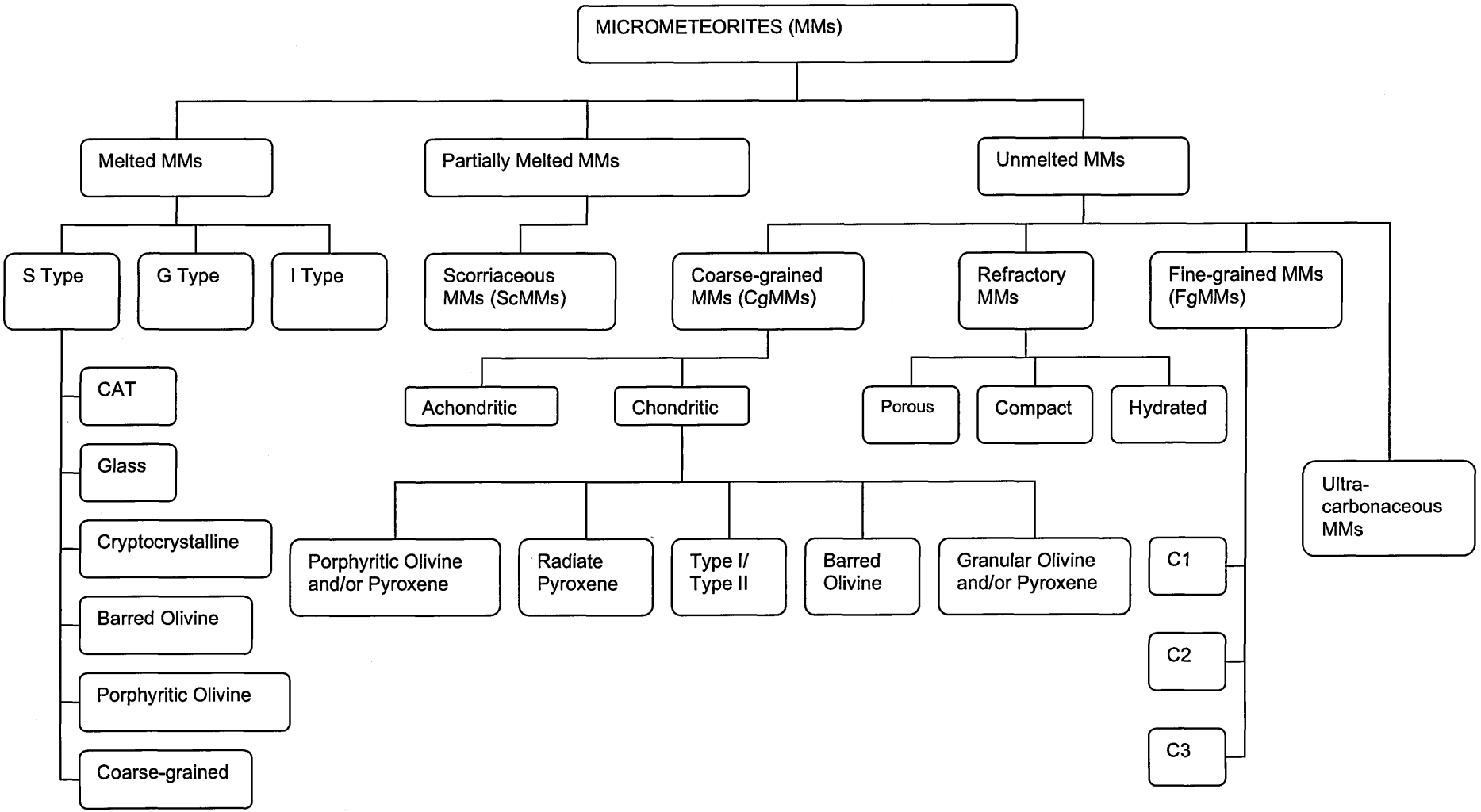

Figure 2: Micrometeorite classification scheme

Grain size is another criteria used to define subcategories of MM classification i) fine-grained MMs (fgMMs) – with a porous fine-grained groundmass of micron-sized grains and ii) coarse-grained MMs – with grain sizes of several microns, typically dominated by anhydrous silicates (Genge et al., 2008).

A) Melted Micrometeorites

Melted MMs have been exposed to high temperatures during atmospheric entry, consequently forming molten droplets which later cooled as spherical to pseudo-spherical particles and loosing their volatile and organic components (Genge & Grady, 1998; Presper et al., 1993; Toppani et al. 2001). They are dominated by a glassy mesostasis embedded with a number of features including microphenocrysts (crystallised from a melt), relict gains that have survived atmospheric entry heating and vesicles (Taylor et al., 2000).

B) Partially Melted Micrometeorites

Partially melted MMs (scoriaceous MMs, ScMMs) are highly vesicular, comprising both melted and unmelted material, and are fine or coarse grained (Genge, 2008; Kurat et al., 1994; Toppani et al., 2001). These MMs are dominated by an olivine rich mesostasis and are commonly surrounded by magnetite rims (Toppani et al., 2001). In addition, a relict fine grained matrix of Mg-rich pyroxene, olivine or enstatite is usually present. ScMMs have experienced less intense heating, relative to the melted MMs such as cosmic spherules, allowing volatile phases to escape producing a vesicular texture in addition to the survival of relict material.

Experimental simulations of MM atmospheric entry heating suggest that relict matrices survive in ScMMs as a result of thermal changes produced by the decomposition of volatile-bearing materials (phyllosilicates and organic species) during the heating process (Flynn, 1995; Genge, 2006; Jessberger et al., 2001; Toppani et al., 2001). Volatile components (Greshake et al., 1996; Greshake et al., 1998; Toppani et al., 2001)

and organic materials (Matrajt et al., 2001) survive in these MMs following atmospheric entry heating, therefore making them relevant to this study.

C) Unmelted Micrometeorites

Unmelted micrometeorites have experienced lower temperatures relative to melted MMs and ScMMs, hence have not been melted. The compositions of phyllosilicates in unmelted MMs, determined by Kurat et al. (1994), show the presence of serpentine-like minerals and cronstedtite, constituents typical of CM-type carbonaceous chondrites (Barber, 1981; Browning et al., 1996). These unmelted particles are the most likely class of MM to contain volatile and organic materials that have survived the atmospheric entry heating process, and are therefore the focus for simulations and analysis within this study. There are three types of unmelted MMs: fine-grained, coarse grained and composite.

i) Unmelted Fine-Grained Micrometeorites (fgMMs)

These particles are primarily composed of micron-sized mineral grains, and are similar in nature to the fine-grained matrix of chondritic meteorites. They comprise phyllosilicates (or their thermally decomposed products) with the accessory minerals olivine, pyroxene, magnetite, chromite and tochilinite (Genge et al., 1997). There are rare occurrences in which some unmelted fgMMs contain small quantities of refractory minerals such as spinel, perovskite, melilite, fassaite and hibonite (Genge et al., 2008).

ii) Unmelted Coarse-Grained Micrometeorites (cgMMs)

cgMMs contain mineral grains >1 μm of predominantly anhydrous silicates (pyroxene and olivine), with kamacite, plagioclase feldspar, chromite and troilite grain accessory minerals and a glassy mesostasis (Genge & Grady, 1998). Additionally some cgMMs exhibit igneous textures (e.g. barred and porphyritic) similar to those observed in chondrules.

iii) Unmelted Composite Micrometeorites (cMMs)

These MMs contain characteristics of both unmelted fgMMs and cgMMs. They typically comprise a coarse grained, igneous textured interior of predominantly anhydrous silicates and include a glassy mesostasis (similar to the cgMMs) (Genge, 2008). They are surrounded by a rim of a fine-grained matrix (Genge, 2006).

iv) Unmelted Refractory Micrometeorites

A number of micrometeorites identified by Gounelle (2001) and Kurat et al., (1994) were primarily composed of refractory minerals, similar in nature to calcium aluminium-rich inclusions present in chondritic meteorites. Some particles also contain the alteration products of refractory minerals, similar in composition to aqueously altered CAIs. Their bulk mineralogy and grain size differ slightly from those of the CM carbonaceous chondrites.

v) Unmelted Ultra-carbonaceous Micrometeorites

A total of three Antarctic micrometeorites (>200 μm in size) have been identified to contain substantially higher abundances of carbon relative to the CI carbonaceous chondrites (Nakamura et al., 2005). Dominant phases include amorphous carbon, olivine, low-Ca pyroxene, pyrrhotite and kamacite. One particle contained a high abundance of presolar silicates, suggesting it had undergone a lower degree of heating during atmospheric entry, allowing their survival.

1.3.2. The Classification of Interplanetary Dust Particles

Multiple classifications schemes exist for interplanetary dust particles (IDPs) (Bradley et al., 1988; MacKinnon & Rietmeijer, 1987; Sandford & Walker, 1985). The preferred classification scheme is primarily defined by chemical composition (Table 5), with further sub-classification based on factors such as morphology (MacKinnon et al.,

1982), related to the degree of heating a particle has experienced during atmospheric entry.

Type	Sub-type	Mineralogy/elemental signature
Chondritic	Anhydrous	Anhydrous silicates, no hydrous silicates
	Hydrous	Hydrous silicates present
Non-Chondritic	Sulphide	Fe-Ni sulphides
	Olivine	Olivine
	Pyroxene	Pyroxene
	Metal	Fe, Ni
	CAI	refractory elements Ca, Al, Ti
	Carbonate	Calcite
	Phosphate	

Table 5: A simplified classification scheme for IDPs, summarising dominant mineralogy and elemental abundances adapted from Rietmeijer, (1998)

A) Chondritic IDPs

Chondritic IDPs are the most abundant of IDP classes, so called as their bulk compositions resemble the CI chondrites (Brownlee, 1978). They typically comprise fine-grained minerals. Chondritic IDPs can be split into the subclasses hydrous and anhydrous, dependent on the presence and abundance of hydrous or anhydrous silicates within them.

i) Chondritic Anhydrous IDPs

Chondritic anhydrous IDPs tend to be highly porous particles, exhibiting a "fluffy" texture. They are composed of fine grained (<1μm) mineral grains, amorphous spherical material <2μm in diameter, carbonaceous material and glass (Bradley et al., 1988). Primary mineral phases include olivine, pyroxene and FeNi sulphides (Bradley et al., 1989; Christoffersen & Buseck, 1986; Sandford & Walker, 1985). The particles range from olivine dominant to pyroxene dominant, including mixtures of the two.

Minor phases include an alumino-silicate glass (Bradley, 1994b), FeNi metal, FeNi carbides (Bradley et al., 1984; Christoffersen & Buseck, 1986), glass with embedded metal and sulphides (Bradley, 1994a) and a fine grained matrix material with grain size typically <100nm (Bradley, 1994b).

The additional presence of Fe-sulphides with magnetite rims within chondritic olivine-rich IDPs (Flynn et al., 1993) suggests they these particles will have been heated more severely during atmospheric entry. Experimental simulations have illustrated that phyllosilicate-rich components can be altered to olivine or pyroxene-rich materials during heating (Greshake et al., 1998). Bulk elemental abundances of anhydrous chondritic IDPs closely match that of the CI chondrites (Schramm et al., 1989).

ii) *Chondritic Hydrous IDPs*

Chondritic hydrous IDPs tend to have a smooth texture compared to the "fluffy" nature of anhydrous particles. They typically consist of the same mineralogy as anhydrous IDPs (mentioned previously). In addition, they contain hydrous silicate phases (Zolensky & Lindstrom, 1992), usually smectite or serpentine.

Significant differences in mineralogy between hydrous IDPs and carbonaceous chondrite matrix have also been highlighted, for example, the presence of glass in hydrous IDPs and its absence in CI chondrite matrix material (Thomas et al., 1990). A few rare IDP particles contain hydrous minerals such as tochilinite (Bradley & Brownlee, 1991) or cronstedtite (Rietmeijer, 1992), both of which are found in the CM chondrites. Another hydrous IDP contains intergrowth of the phyllosilicates serpentine and saponite typically observed in the CI chondrites (Keller et al., 1992).

B) Non-Chondritic IDPs

Non-chondritic IDPs are those of coarse grain-size. The most common of which are dominated by sulphides, either in the form of pyrrhotite grains, polycrystalline mixtures of large sulphide grains or large sulphide grains with minor fine grained chondritic material (Zolensky & Thomas, 1995). Olivine and pyroxene dominated particles are less common (Zolensky & Barrett, 1994) whilst those dominated by refractory phases, metal grains, carbonates and phosphates are rare.

1.3.3. Summary of IDP Classification

The classification of IDPs including their mineralogical and elemental signatures is summarised in Table 5. The chondritic IDPs, in particular the hydrous sub-type are the most relevant to this study. These particles have experienced lower temperatures on atmospheric entry heating as is evident by the presence of hydrous silicates. These particles are, therefore, good candidates for retaining organic components post atmospheric entry.

1.4. Extraterrestrial Dust Particle Chemistry

1.4.1. Elemental Abundances of MMs

It has been noted that unmelted MMs contain refractory lithophile elements in abundances similar to or enriched to that of CI chondrites (Genge et al., 1997) but tend to have considerable depletions in Ca, Ni, S, Se. MMs exhibit minor depletions in lithophile and sidereophile elements (Br, Mn, Na, Mg, Cr, K, Cl, Os, Ir, Ru, Th and Fe) relative to CI chondrites (Flynn, 1991; Greshake et al., 1998; Kurat et al., 1992; Maurette et al., 1991; Presper et al., 1993). Lithophile elements more volatile than Cr and siderophile elements more volatile than Fe have highly variable abundances and can be enriched or depleted relative to the CIs in MMs (Kurat et al., 1992).

With respect to MMs collected from Antarctica, depletions of Na, Mg, Ca, Mn, and Ni are thought to be attributed to the terrestrial leaching of sulphides, sulphates and carbonates in the Antarctic environment (Kurat et al., 1994). S and Se depletions in MMs are thought to be the result of atmospheric entry heating effects as well as terrestrial leaching processes, whilst depletions in Cu, Ge, Zn, Na and Au are possibly the result of atmospheric entry heating effects (Greshake et al., 1995; Toppani et al., 2001). In contrast, the trace elemental abundances in partially melted MMs are similar to those of phyllosilicate rich MMs (Jessberger et al., 2001), except for depletions in the volatile

elements Na, K, Br, As and Se. This suggests that partially melted MMs are the altered products of phyllosilicate rich MMs, that are dehydrated during atmospheric entry heating.

The majority of MMs >100 μm, will have been heated significantly during atmospheric entry as a result of aerodynamic breaking (section 1.6) yet the presence of moderately volatile elements with abundances at or above CI abundances such as Cu , Ga (Flynn, 1991) and even Fe, Cr and in some cases Mn and Mg (Koeberl et al., 1992), suggest that MMs may not have been substantially altered during atmospheric entry heating.

1.4.2. Elemental Abundances of Interplanetary Dust Particles

The chondritic IDPs contain similar major elemental abundances (Mg, Al, Si, S, Ca, Cr, Mn, Fe and Ni) as the CI chondrites (Arndt et al., 1996). They are usually enriched in trace element abundances (Ti, Zn, Cu, V, Ge, Se, Ga, Sr, Sc, Zr, Br, Rb, As and Y) by a factor of ~ 2 relative to CI chondrites. The exception is Br, which is enriched in IDPs by a factor of up to 20,000 relative to the CI chondrites (Arndt et al., 1996), and is thought to derive from contamination of particles during their time in the atmosphere.

Bulk elemental abundances of hydrous chondritic IDPs largely correlate with CI and CM abundances, with major elemental compositions Mg, Al, Si, S, Ca, Cr, Mn, Fe, and Ni present within a factor of two of CI chondritic abundance (Brownlee, 1978). A number of particles are depleted in Ca and S relative to CIs, attributed to the abundance of iron sulphide and carbonates present in these carbonaceous chondrites. There are, however, rare particles rich in Ca or S-rich minerals, that contain enrichments of these elements relative to CIs (Brownlee, 1978).

1.4.3. Carbon in Extraterrestrial Dust Particles

The investigation of carbon content in EDPs has been inhibited by their small size and the limitations of current analytical methods. A wide range of carbon contents have been measured for EDPs present both as organic matter (section 1.4.4) and inorganic

phases, for example, carbonates (Kearsley et al., 2007; Noguchi et al., 2002; Rietmeijer, 1990; Tomeoka & Buseck, 1986) or amorphous carbon (Wopenka, 1987). Measured MM carbon abundances (Table 6) have a narrow range between 0 and ~7 wt.% (Engrand & Maurette, 1998; Matrajt et al., 2003; Maurette et al., 2001; Wright et al., 1997).

MM Type	Analytical Method	C (wt. %)	Reference
Unmelted MMs	Stepped Combustion	< 0.2	a
Unmelted MMs	Electron energy loss spectroscopy	~7	b
Unmelted MMs	Secondary ion mass spectrometry	~2.5	c
Unmelted MMs	Nuclear microprobe	0.2-2.8	d
Unmelted MMs	Nuclear microprobe	0.14 & 1.15	d
ScMMs	Nuclear microprobe	0.72-2.13	d

Table 6: The range of C contents of MMs established through a variety of techniques a- Wright et al., (1997), b- Engrand and Maurette, (1998), c- Maurette et al., (2001) and d- Matrajt et al., (2003)

In contrast, IDPs have a wider range of carbon contents of between 0 and ~50 wt. % (Figure 3). Anhydrous chondritic IDPs, thought to originate from cometary sources, tend to contain > 3 times that of CI abundances. Some hydrous IDPs also contain carbon abundances substantially higher than chondritic abundances (up to ~ 6 times that of CI abundance), suggesting they are from cometary and not asteroidal sources (Thomas et al., 1992). Thomas et al., (1993) found the average carbon abundance of 19 IDPs is 12.5 ± 5.7 wt % whilst that of Orgueil is 3.6 ± 2.1 wt. %.

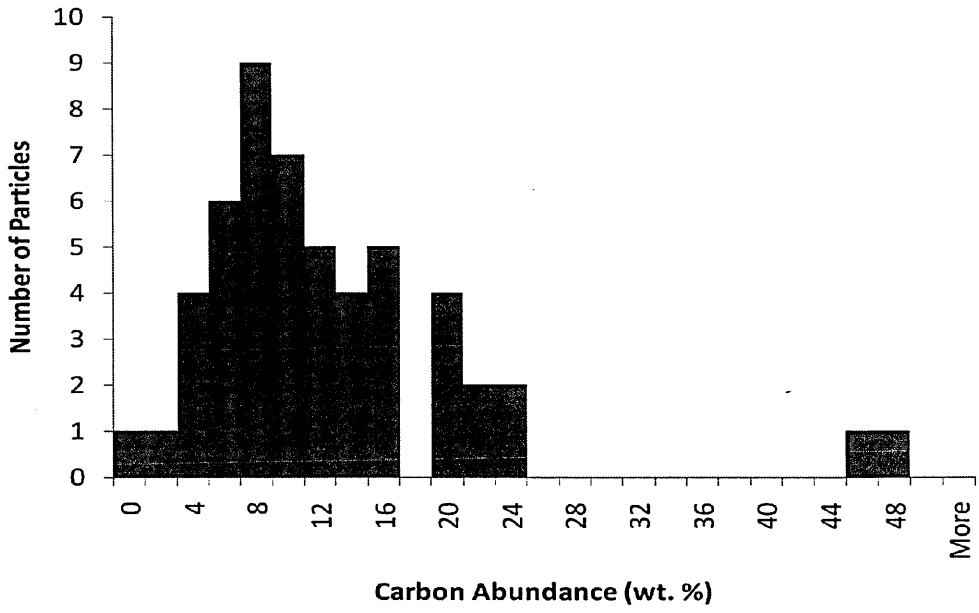

Figure 3: Distribution of bulk carbon contents (wt.%) of in individual IDPs adapted from Keller et al., (1994)

1.4.4. Organic composition of EDPs

The range and abundance of organic matter within EDPs is poorly known due to the limited availability of sample for comprehensive organic analysis using traditional techniques such as GC-MS. As such, non-destructive methods of analysis such as Fourier transform infra-red spectroscopy (FTIR) (Matrajt et al., 2001; Matrajt et al., 2005 a; Suzuki et al., 2005) and scanning transmission X-ray microscopy (STXM) (Matrajt et al., 2001) have been employed to identify functional groups present within EDPs, while very few studies have proved successful in identifying individual organic compounds as outlined below.

A) Organic Composition of Micrometeorites

Unmelted MMs are known to contain carbonaceous matrices (Maurette et al., 1995) but a very limited number of studies have been employed to identify their organic components. The spatial distribution of carbon within MMs has been investigated using a combination of energy dispersive spectrometry (EDS) and electron energy loss spectroscopy (EELS) (Maurette et al., 2000; Maurette et al., 1995), finding that carbon is uniformly distributed throughout MMs, with no apparent correlation between carbon and other elements. FTIR has identified aliphatic (methyl), aromatic and hydroxyl groups in MMs (Matrajt et al., 2001; Suzuki et al., 2005), whilst STXM has identified the carbonyl group (Matrajt et al., 2001).

Few studies have focused on the characterisation of individual micrometeoritic organic species. Microscopic double-laser mass spectrometry (μL^2MS) has been used to characterise polycyclic aromatic hydrocarbons (PAHs) (Clemett et al., 1998) and high-performance liquid chromatography (HPLC) (Brinton et al., 1998) and ion-exchange chromatography with fluorimetric detection (Matrajt et al., 2004) have both been successful in identifying a number of protein amino acids within MMs.

Clemett et al., (1998) found PAH abundances in Antarctic MMs were ten times that of Allende, with the average yield similar to that of Murchison. The MMs contained up to 5

carbon-ringed PAHs, with lower abundances of naphthalene and benzo[a]pyrene relative to Orgueil, Murchison and Allende. PAH alkylation was correlated to the abundance of vesicles present in individual particles. Clemett et al., (1998) found a greater degree of alkylated PAHs present in more vesicular particles, reflecting the thermal alteration they undergo during atmospheric entry heating. Additionally, vinyl PAHs (PAHs containing CH_2-CH- group) in the mass range 250-290 amu which are as yet undetected in meteorites, were observed in Antarctic MMs (Clemett et al., 1998).

A number of amino acids have been identified in micrometeorites with α-aminoisobutyric acid (AIB, a non-protein amino acid) and alanine (a protein amino acid) typically of high abundance (Table 7). AIB is uncommon on Earth, the only biogenic source being rare fungal peptides (Bruckner et al., 1989) whilst non-biogenic occurrences are associated with pollutants of the chemical industry (Mita & Shimoyama, 1996) or the hydrolysis products of coal gasification (Olson, 1992). The only reported geological occurrence of AIB is the K/T boundary sediments, though the delivery of this organic species is thought to be associated with the K/T bollide or was produced during the impact event (Olson, 1992; Zhao & Bada, 1989). As such AIB is strongly associated with extraterrestrial materials, and its presence within meteorites or EDPs is unlikely to be a terrestrial contaminant.

Sample	Sample Mass (μg)	AIB (ppm)
A91 - MM aliquot grain size ~100 μm	50	280
I91 - MM aliquot grain size ~ 200 μm	175	78
III91- MM aliquot grain size ~ 200 μm	310	22
IV94- MM aliquot grain size ~ 200 μm	166	<0.1
V94- MM aliquot grain size ~ 200 μm	259	20
Murchison	5000	5 – 10

Table 7: A summary of amino acid concentrations (ppm) for aliquots of MMs and Murchison (Brinton *et al.*, 1998)

The AIB content of micrometeorites was found to be between zero and over ten times that of Murchison (Table 7). Contrary to the results of Brinton et al. (1998), Matrajt et al., (2004) reported average MM AIB concentrations 6 times lower than those of Murchison. In their study, alanine and glycine were the most abundant amino acids present in all three clusters of MMs analysed. Additionally, Glavin et al. (2004) reported

detectable levels of a range of L-protein amino acids and only minor quantities (<1ppm) of non-protein amino acid, with glycine and isovaline the most abundant amino acids present. Glavin et al. (2004) also found that the distribution of amino acids in all the MMs analysed, was similar to that of Antarctic ice and glacial sands. Their study suggests that amino acids within MMs may actually be of terrestrial origin.

Despite their limited characterisation, similarities exist in terms of the organic groups identified within MMs and carbonaceous chondrites such as Tagish Lake (Suzuki et al., 2005) and Murchison (Matrajt et al., 2001). However distinct differences in PAH distributions between MMs and Murchison (Clemett et al., 1998) as well as their carbon enrichment relative to the carbonaceous chondrites (Maurette et al., 1995) suggest that MMs may represent a new population of Solar System objects worthy of more focussed and detailed analytical study.

B) Organic Composition of IDPs

Both hydrous and anhydrous IDPs contain relatively high abundances of carbon (Keller et al., 1994; Thomas et al., 1993), in the form of disordered carbonaceous material distributed throughout the fine grained matrix and present within mineral inclusions. Several groups of organic molecules have been successfully identified in IDPs using a variety of techniques. For example, using μL^2MS, Clemett *et al.,* (1993) identified a variety of PAHs in individual IDPs including naphthalene, phenanthrene, pyrene, chrysene, benzopyrene and pentacene. They observed an increased range of alkylated PAHs in IDPs relative to Allende, of up to (C-20)-alkyl-phenanthrene. This trend is similar to that observed in MMs (Clemett et al., 1998). Relatively low abundances of lower mass PAHs (up to 2 carbon-ringed PAHs) are present in IDPs (Clemett et al., 1993), thought to be the result of loss during atmospheric entry heating.

FTIR spectroscopy has been used to identify a number of organic functional groups present in IDPs, including features consistent with aliphatic CH_2 and CH_3 stretching vibrations (Flynn et al., 1998; Flynn et al., 2002; Matrajt et al., 2005 a). Matrajt

et al., (2005 a) also noted the presence of aromatic hydrocarbons and carboxylic acids. Identification of the carbonyl absorption feature in IDPs (bonded within a ketone) has also been reported (Flynn et al., 2002; Matrajt et al., 2005 a), confirming the presence of carbonyl in IDPs also identified by X-ray Absorption Near Edge Structure (XANES) spectroscopy at both C and O K-edges (Flynn et al., 2003). Additionally Flynn et al., (2003) also identified the C=C bond, most likely to be attributed to the presence of PAHs.

1.4.5. Summary of Organics in EDPs

Despite EDP heating during atmospheric entry to estimated temperatures of 400 – 1700 °C (Love & Brownlee, 1991; Love & Brownlee, 1994), they still contain up to 50 wt. % carbon (Thomas et al., 1992). In fact a range of organic species have been indentified in EDPs following their delivery to Earth including aliphatic, aromatic, hydroxyl and carbonyl bearing species (Flynn et al., 1998; Flynn et al., 2002; Matrajt et al., 2001; Matrajt et al., 2005 a; Suzuki et al., 2005), between 2-5 carbon-ringed PAHs and their alkyl derivatives (Clemett et al., 1993; Clemett et al., 1998) and a number of amino acids (AIB, alanine, glycine) (Brinton et al., 1998; Matrajt et al., 2004).

1.5. The Flux of Extraterrestrial Material to Earth and the Delivery of Organic Carbon

Estimates of the flux of extraterrestrial material to Earth have been calculated using a number of techniques. Iridium and osmium are two trace elements used to identify extraterrestrial material within snow and ice (Gounelle et al., 1999; Hammer & Maurette, 1996) and marine sediments (Barker & Edward Anders, 1968; Peucker-Ehrenbrink & Schmitz, 2001). Peucker-Ehrenbrink & Schmit (2001) analysed Os isotope compositions of sediments from the Atlantic and Pacific oceans. They deduced a total annual extraterrestrial material flux of $3.0 \pm 1.5 \times 10^7$ kg over the past 80 Ma, excluding the Chixulub K/T impact event. Another method for flux estimation has used the analysis of

meteorite weathering rates at dessert accumulation sites. Bland et al., (1996), estimate that meteorites of the mass range 10 g to 1 kg have an annual flux of 2.9-7.3 x 10^3 kg over the past 50,000 years. Up to 4500 falls a year are measured to be >1 kg in mass (Halliday et al., 1996).

In contrast, the present annual flux of EDPs is significantly greater. Direct crater counting of the space facing metallic plates on the Long Duration Exposure Facility satellite, has measured an annual global EDP flux of 4 ± 2 x 10^7 kg (Love & Brownlee, 1993). The amount of EDPs surviving to the Earth's surface has been calculated using a variety of methods. Maurette *et al.* (1990) measured the total mass of MMs >50 μm accumulated at the base of cryoconite holes on the West Greenland ice sheet. Using an ice flow model that estimated the duration of exposure of the ice to the MM flux as ~250 years, the annual flux of MMs landing on Earth was calculated at ~2 x 10^7 kg (Maurette et al., 1990)

Ir content of extraterrestrial dust extracted from a Greenland ice core (from the 1904-1915 time period) has been measured by Rasmussen et al., (1995). They found an average annual Ir input to the ice of 1.17 ± 0.47 x 10^{-15} g cm^{-2} yr^{-1} equating to an annual EDP flux to the Earth's surface of 1 ± 2 x 10^7 kg. This value is in agreement with the EDP flux measured by Love and Brownlee (1993). A size and flux distribution plot, Figure 4, illustrates that the greatest abundance of recent extraterrestrial material is delivered to Earth in the form of 10^{-8} kg EDPs and large 10^9 kg impactors (Anders, 1989; Flynn et al., 2004).

Based on the lunar cratering record, it is estimated that 3.8 – 4.5 Ga ago there was between 10^2 to 10^7 times more extraterrestrial material impacting with the earth (Hartmann et al. 2000). It is clear from the literature (Bland et al., 1996; Love & Brownlee, 1993; Maurette et al., 1990; Rasmussen et al., 1995), that EDPs presently deliver >2000 times more mass of material to Earth than meteorites. EDPs are also thought to have been the dominant contributor of extraterrestrial materials to the early Earth (Pasek & Lauretta, 2008).

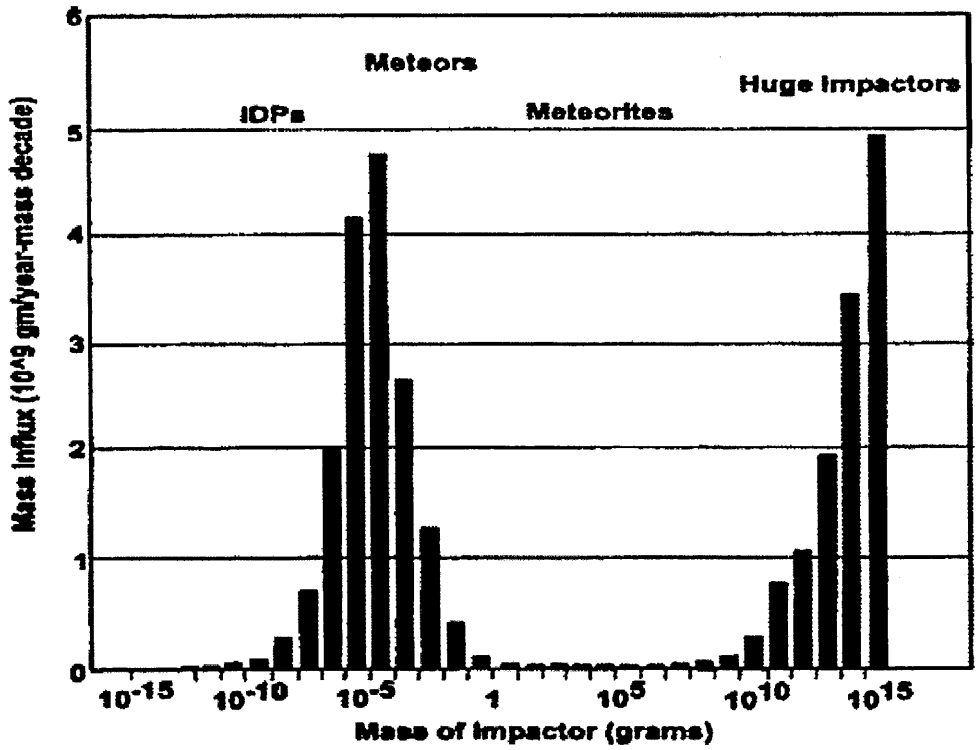

Figure 4: Size and flux distribution of extraterrestrial materials delivered to Earth (Flynn et al. 2004)

Organic C was previously thought to have accreted through large cometary and asteroidal impacts (Chyba et al., 1990; Delsemme, 1984; Oro, 1961; Svetsov, 2002). However, these high velocity impacts are so dynamic, that the resulting fireball on impact (in excess of 10^4 K) would have destroyed almost all molecular species from the impactor (Anders 1989). Later synthesis of these molecules upon cooling, would have been inefficient in the CO_2 rich atmosphere of the early Earth (Anders, 1989; McKay & Borucki, 1997). Large impacts are infrequent (Pasek & Lauretta, 2008) and would have had a damaging effect on the immediate environment upon impact, potentially destroying prebiotic materials (Chyba, 1993; Maher & Stevenson, 1988). The delivery of organic species to the early Earth by dust particles is more favourable because of their gentler deceleration in the atmosphere exposing them to lower entry heating temperatures (section 1.6). The small size of EDPs, their organic content and their high flux makes them favourable candidates for delivery of organics and volatiles to the early Earth, without the destructive nature of larger impactors.

1.6. The Effect of Atmospheric Entry Heating on Extraterrestrial Dust Particles

With the suggestion that EDPs may have delivered substantial material to the Earth during its early history (Anders, 1989; Anders et al., 1973; Maurette, 1998) it is important to investigate the conditions that EDPs experience during passage through our atmosphere. These conditions determine the composition and quantity of material evaporated from them and deposited in the atmosphere, as well as the quantity of material that will survive atmospheric entry and land on Earth.

There have previously been two approaches to understanding the effects of atmospheric entry heating on EDPs. The first is through theoretical/computational modelling of the scenario (Flynn, 1989a; Fraundorf, 1980; Love & Brownlee, 1991; Whipple, 1950; Whipple, 1951) and the second through experimental simulation of the parameters on EDP analogues (Fraundorf et al., 1982; Greshake et al., 1995; Greshake et al., 1995; Greshake et al., 1998; Klöck et al., 1994;Toppani et al., 2000; Toppani et al., 2001; Toppani et al., 2003). The results of both approaches can be compared to textural, chemical and isotopic alterations observed in EDPs that are thought to be the result of atmospheric entry heating (Greshake et al., 1996; Greshake et al., 1998; Toppani et al., 2001).

1.6.1. Theoretical Modelling

Theoretical calculations of the atmospheric entry heating affects on meteors and EDPs, was pioneered by Whipple in the 1950s. Whipple (1950; 1951) presented a theory for the passage of an EDP through the Earth's atmosphere without it suffering substantial melting or vaporisation. This theory was later adapted and applied to meteors to explain the formation of regmaglypts (cm sized depressions on the surface of some meteorites) formed by ablation of surface material during atmospheric entry (Thomas & Whipple, 1951).

With the study of EDP morphology over past decades (e.g. Genge et al., 1997; Genge et al., 2008; MacKinnon et al., 1982; MacKinnon & Rietmeijer, 1987), it is clear that a number of particles have not been melted upon atmospheric entry heating (illustrated by the classification of unmelted MMs and chondritic IDPs), true to the predictions of Whipple (1950). Thermal alteration of EDPs during deceleration upon atmospheric entry could account for differences in chemistry, morphology and mineralogy between individual EDPs. Flynn (1989a) constructed a computer simulation of the atmospheric entry deceleration and heating of EDPs and compared the predicted peak temperatures the EDPs experienced in his simulation, with those of the earlier closed-form mathematical solutions of Whipple (1950) and Fraundorf (1980). The theoretical calculations and the simulation both accurately assessed the scenario. Flynn (1989a) found that a 20 μm diameter particle (of density 1 g cm^{-3}) with a velocity of 10 km s^{-1} at infinity and entering the atmosphere at normal incidence, reached a peak temperature of 1159 K. The duration of the heating was 8 s, but the particle remained within 100 K of the peak temperature for only 1 s. As the angle of incidence decreased, it was found that the peak temperature reached on entry also decreased but the duration of the temperature pulse increased.

Further to theoretical calculations (Fraundorf, 1980; Whipple, 1950) and the computer modelling and observations of Flynn (1989a; 1989b), Love and Brownlee (1991) constructed a computer simulation to assess the relationships between EDP particle diameter (10-1000 μm), entry velocity (11.2-72 km s^{-1}) and entry angle (0-90°) during atmospheric entry heating. These are now considered the main factors affecting the peak temperature that particles are exposed to during atmospheric entry (Love & Brownlee, 1991), controlling the survival or loss of organic and volatile materials. Key findings of Love and Brownlee (1991) illustrate that total atmospheric heating durations ranged from 6-100 s with peak temperatures ranging from 700-1700 °C. As the entry angle steepened, EDPs of constant entry velocity and size were heated to a higher peak temperature with a shorter duration of heating. With increasing EDP diameter (but constant entry velocity, entry angle and heating duration) the peak temperature increased. As the entry velocity

increased, EDPs of a constant entry angle and diameter experienced similar peak temperatures yet shorter heating durations.

EDPs that experienced peak heating at <85 km altitude were completely vaporised, whilst those experiencing peak heating at an altitude of 85-100 km (within the mesosphere) survived (Love & Brownlee, 1991). The peak temperature that a 100 - 200 μm particle with an entry velocity of 20 km s^{-1} and entry angle < 45° can endure, whilst still surviving atmospheric entry, is 1700 °C (Love & Brownlee, 1991). Similar to the earlier findings of Flynn (1989a), Love and Brownlee (1991) found that EDPs remained within 100 °C of the peak temperature for only 1-2 s.

From their model, Love and Brownlee (1991) found that melted EDP particles were 1.5-2 times smaller in diameter compared to their pre-atmospheric entry size as a result of ablation of material during atmospheric entry. Furthermore, they found that EDPs <50 μm in diameter with entry velocities of 12 km s^{-1}, and those >20 μm with entry velocities of 20 km s^{-1}, survive unmelted. These particles are therefore the most likely to retain indigenous organic materials, delivering them to the Earth's surface.

1.6.2. Experimental Simulations

There have been few short duration heating experiments conducted to simulate the atmospheric entry heating on EDPs. Experiments have focused on the effects of flash heating on volatile and moderately volatile elements in carbonaceous chondrites in comparison to observations in EDPs (Greshake et al., 1995; Greshake et al., 1995; Greshake et al., 1995; Greshake et al., 1998; Toppani et al., 2000; Toppani et al., 2001; Toppani et al., 2003). Fraundordf et al., (1982) investigated pulse heating of Murchison and Orgueil fragments of uncharacterised size using a resistively heated tantalum ribbon oven capable of heating between 400-1100 °C for ~30 s. Substantial loss of sulphur was found upon heating of Murchison fragments to 800-1100 °C.

Klöck et al., (1994) heated 100 μm sized fragments of Orgueil and Alais (CI) to 600-1200°C in quartz capillary tubes for durations of 20-60 s. All phyllosilicates were

altered to anhydrous silicates at temperatures ≥1000 °C. There was also substantial loss of moderately volatile elements Zn and Ga at these temperatures, consistent with MM elemental abundances relative to CI chondrites (Section 1.4.1).

Greshake et al., (1995; 1995; 1998) conducted short duration heating experiments on 50-100 μm sized CI fragments of Orgueil and Alais. Fragments were heated to 700-1250 °C, using a high temperature furnace, for durations of 10, 20 and 60 s. Results show the loss of volatile elements S, Zn, Ga, Ge and Se as a result of short duration heating. The authors conclude that depletions of these elements (relative to CI abundances) observed in EDPs are therefore due to atmospheric entry heating (Greshake et al., 1998). The authors found that phyllosilicate phases were completely altered by dehydration to olivine and pyroxene when fragments are heated to ≥800 °C, suggesting that EDPs still containing hydrous phases are unlikely to have been heated beyond this temperature. Peak temperatures for atmospheric entry heating of EDPs were estimated to be in the order of 1100-1200 °C (Greshake et al., 1998).

Depletions of elemental sulphur upon simulation of atmospheric entry heating waere confirmed in similar investigations by Toppani et al., (2000; 2001; 2003). 200-400 μm sized fragments of Murchison and Orgueil were heated to 500-1500 °C in a closed vertical furnace for durations of 2-120 s. Large depletions in sulphur were noted, confirming that depletions of sulphur observed in MMs (Genge et al., 1997) are attributed to atmospheric entry heating. Sulphur depletions in meteorite fragments are related to the temperature experienced by the sample and its duration at the peak temperature.

Textural and mineralogical analysis of heated fragments of Orgueil, allowed the estimation of peak temperatures and durations required to produce MM textures such as fine grained particles, dehydration cracks, vesicular particles and completely melted spherules (Toppani et al., 2001) (Figure 5). Dehydration of phyllosilicates and their further alteration to anhydrous silicates, recrystallisation of minerals and the presence of spinel rims was monitored in relation to pulse heating conditions.

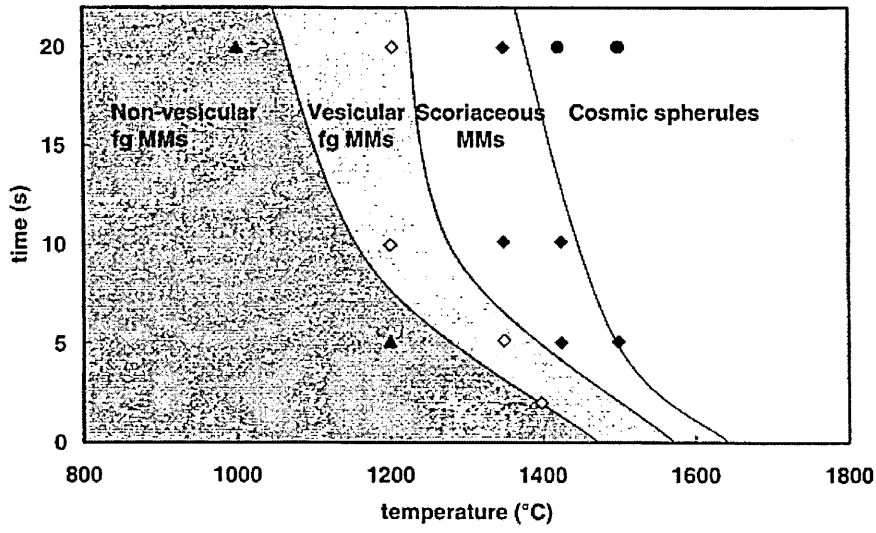

Figure 5: The conditions required upon atmospheric entry to produce various textures in 200-400µm sized MMs. △ samples showing only minor dehydration without spinel or vesiculation. ◇ samples showing a slight vesiculation and a thin spinel rim. ◆ samples showing evidence for partial melting progressing inward, well-developed vesiculation and a thick spinel rim. ● completely melted samples without vesiculation or spinel rim (Toppani et al., 2001)

Additional experiments were conducted to investigate noble gas loss during atmospheric entry (Toppani et al., 2003). Fragments of Orgueil 0.1 – 1 mg in mass, were heated in a vertical furnace to 1350 °C for durations of 2 s to 120 s. In accordance with Figure 5 fragments were heated to 1350 °C for 2 s (representing non-vesicular fine-grained MMs), 5 s (representing vesicular fine-grained MMs), 10 s (representing partially melted MMs) and 120 s (representing cosmic spherules).

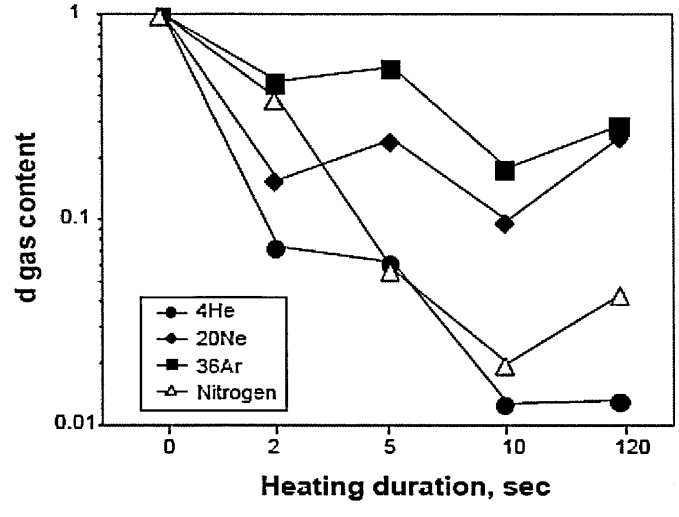

Figure 6: MM gas content as a function of heating duration, normalised to Orgueil (Toppani et al., 2003)

Figure 6 shows that substantial noble gas and nitrogen loss occurs during very short heating pulses (2-5 s). This degassing could occur in EDPs during their passage through the stratosphere, resulting in the formation of melted spherules and the vesicular texture observed in ScMMs.

1.6.3. Survival of Organic Material in Simulation Studies

Recently, investigations into the survival of organic matter upon atmospheric entry of IDPs has been conducted (Brownlee et al., 2001; Brownlee et al., 2002; Glavin & Bada, 2001; Glavin et al., 2004; Kress & Brownlee, 2002; Kress et al., 2002). Analysis of morphology, C content and mineralogy of ~100 μm sized AMMs (Brownlee et al., 2001; Brownlee et al., 2002), show that they have been severely heated and are C poor. Pulse heating experiments of coal in air (at the ram pressure EDPs experience at 90 km altitude) show substantial survival of a C ash residue after heating to temperatures of 1200 °C (Brownlee et al., 2001). Analysis of this residue, showed the retention of high concentrations of He and Ne (Palma et al., 2001), suggesting that C within EDPs can survive atmospheric entry heating, with the possibility of also preserving He and Ne.

Further investigation by intense heating experiments on a mixture of powdered coal and Allende, show that Fe and Ni facilitate the preservation of C as a char on or embedded within Fe-Ni metal beads (Kress et al., 2002) rather than being ablated during atmospheric entry. Results from the simulations are comparable to observations of a rare type of IDP - silicate spheres surrounded by FeNi metal beads and amorphous carbon (Brownlee et al., 2001). It is predicted that the atmospheric entry heating of C rich MMs could release products similar to that of coal pyrolysis such as small PAHs, tars, aliphatic hydrocarbons (e.g. CH_4, C_2H_6 and HCN) as well as CO, CO_2 and H_2O (Kress et al., 2002) which would be deposited into the atmosphere. Brownlee et al., (2002) has suggested that the remaining C ash or char may have separated from the particle upon atmospheric entry.

Glavin and Bada (1999; 2001) attempted to investigate the survival of amino acids (by means of sublimation) during simulated atmospheric heating events. Using 100 mg fragments of Murchison as a MM compositional analogue, grains were heated in a sublimation apparatus under reduced pressure. As the fragments of meteorite were heated to ~150 °C, a substantial amount of the amino acid glycine vaporised and recondensed in the sublimation apparatus and survived as the meteorite grains were heated to 550°C. The amino acids AIB and isovaline did not sublime, they were unable to survive the heating experiments.

More recent pulse heating studies to 700 - 900 °C found that a PAH (coronene), a ketone (2-pentadecanone) and an amino acid (L-lysine) embedded in a porous aluminium oxide matrix could survive such extreme conditions (Matrajt et al. 2006). Matrajt et al., (2006) suggest that the porosity of EDPs combined with the capability of inherent organic material and water to sublime, would produce ablative cooling enabling the survival of these materials under such extreme conditions.

1.6.4. Decomposition of EDP and Meteorite Components

The morphology of EDPs shows that some have been heated to such high temperatures that they have melted (Genge et al., 1997; Kurat et al., 1994). The matrix of Murchison, a compositional analogue of unmelted EDPs, melts at 1350 °C (Genge et al., 1997). It is also known that EDPs contain a variety of organic molecules, described previously. Organic species, such as amino acids, PAHs and aliphatic hydrocarbons (within the chondritic free organic fraction) decompose between 150 °C to 500 °C (Rodante, 1992; Wright et al., 1997). Thermal decomoposition of the chondritic macromolecular fraction will occur between 350-600 °C (Kristensen, 1990) as aromatic species are more thermally stable than aliphatic species (David 1975). The presence of these molecules within some EDPs suggests that they have not been heated to temperatures >600 °C, or that there is a mechanism by which organic molecules within particles are able to survive the high temperatures they are exposed to upon atmospheric

entry. Table 8 summarises the temperatures at which various meteoritic components evaporate or decompose.

Component Evaporated/Decomposed	Temperature (°C)	Reference
Amino acids	150-600	1
Macromolecular organic molecules	350-600	2
Phyllosilicate dehydration	300	3
Mg-carbonates	~350	3
Sulphides	300-600	3
Phyllosilicates	<650	3
Sulphates	600-900	3
$CaCO_3$ (calcite)	~650	3
$CaCO_3$ (aragonite)	825	4
Matrix of Murchison melts	1350	3
Significant evaporation Fe	1450	3
Mg and Si	>1500	3
Ca and Al	>1800]	3

Table 8: The decomposition/evaporation temperatures of meteoritic components. [1] Rodante (1992) [2] Kristensen (1990) [3] Genge et al., (1997) [4] Fisher (2005)

1.6.5. A Summary of Previous Studies

Computational modelling by Love and Brownlee (1991) provided detailed limits for the conditions experienced by EDPs upon atmospheric entry. Peak temperatures experienced by particles during atmospheric entry heating, were predicted to be no more than 1700 °C (Love & Brownlee, 1991). Subsequently, many experimental simulations of atmospheric entry heating of EDPs take these parameters into account (Brownlee et al., 2001; Brownlee et al., 2002; Glavin & Bada, 1999; Glavin & Bada, 2001; Greshake et al., 1995; Greshake et al., 1995; Greshake et al., 1998; Klöck et al., 1994; Kress & Brownlee, 2002; Kress et al., 2002; Matrajt et al., 2005 b; Toppani & Libourel, 2001; Toppani et al., 2000; Toppani et al., 2001; Toppani et al., 2003).

Pulse heating methods in experimental simulations have been varied. Vertical furnaces and CO_2 lasers have been used to heat fragments of carbonaceous chondrites to temperatures of 1500 °C for between 2 s and 120 s. Peak temperatures of 1100 °C to1200°C were estimated, based on comparison of experimental results with observations of MM textures (Greshake et al., 1998).

Changes in volatile element abundances such as substantial loss of S, were noted (Fraundorf et al., 1982; Greshake et al., 1998; Toppani et al., 2001). Atmospheric entry

heating can therefore explain depletions of S previously observed (Genge et al., 1997; Kurat et al., 1994) in MMs. There is very little information regarding the loss of noble gases upon atmospheric entry heating and further investigation is necessary outside the scope of this study. The possibility that EDPs may have contributed to the noble gas inventory of the early Earth, remains open. With the experimental simulations showing amino acid (Glavin & Bada, 2001) and solid carbon (Brownlee et al., 2001; Brownlee et al., 2002) survival upon atmospheric entry, there is great potential that EDPs may have had an important role in pre-biotic chemistry on Earth.

To date, investigation of the survival of EDP carbon on atmospheric entry has focussed on bulk carbon (Brownlee et al., 2001) or isolated organic groups (Glavin & Bada, 1999; Glavin & Bada, 2001; Matrajt et al., 2006). No attempt has yet been made to simulate the alteration of complete EDP organic material with respect to entry heating conditions and their subsequent interaction with the surrounding atmosphere. Comprehensive analysis of EDPs characterising individual organic species, could additionally provide clues to the parent bodies of EDPs or source of organic materials.

1.7. Aims and Objectives

Predictions of peak temperatures experienced by EDPs upon atmospheric entry heating range from 1700 °C (computational simulations of Love and Brownlee, 1991) to 1100 °C (experimental simulations Greshake et al., 1998). At such temperatures, volatile elements and low molecular weight organic species are likely to be released during atmospheric heating. Consequently, analyses of EDPs show that they are depleted in volatile elements relative to CI abundances (Greshake et al., 1995; Greshake et al., 1995; Koeberl et al., 1992; Kurat et al., 1994). Experimental simulations suggest that these volatile elements (for example S and noble gases) are lost upon atmospheric entry heating.

Despite exposure to extreme heating conditions, there is also evidence of the survival of EDP noble gases (Osawa & Nagao, 2002; Palma et al., 2001), C char

(Brownlee et al., 2001; Brownlee et al., 2002), amino acids (Brinton et al., 1998; Glavin & Bada, 1999; Glavin et al., 2004; Matrajt et al., 2004), PAHs and other aromatic species (Clemett et al., 1993; Clemett et al., 1998; Matrajt et al., 2001; Matrajt et al., 2005 a; Flynn et al., 2002). With the mass flux of EDPs to the early Earth up to $x10^2$ to $x10^7$ that of present day (Hartmann et al., 2000), and the survival of organic EDP components during atmospheric entry, EDPs may have been the dominant contributor of volatiles and organic species to the early Earth. This delivery of EDP organic material to Earth, would therefore have served as a source of organic molecules critical to the development of life here on Earth.

The aim of this study is to investigate the effects of atmospheric entry heating on the release and survival of volatile and organic species from EDP analogues. It will assess the biological significance of liberated species in order to determine whether EDPs were a feasible contributor of organic species to the early Earth. Additionally, the comprehensive organic analysis of MMs will provide clues as to the nature and possible origin of these materials.

Chapter 2 will evaluate the efficiency of experimental methods used to conduct flash heating simulations of EDPs during atmospheric entry. Additionally, the development of analytical procedures for the characterisation of the organic composition of small samples of EDPs is also outlined.

Chapter 3 will characterise the bulk volatile abundance from EDP analogues subjected to atmospheric entry heating simulations, with particular emphasis on H_2O, organic carbon and inorganic carbon. Compositional analyses of the organic species liberated during entry heating simulations are also conducted, with emphasis on alterations in volatile organic species and PAHs with changing simulation conditions.

Chapter 4 will characterise the composition and assess the indigeneity of organic matter in Antarctic micrometeorites (AMMs). A comparison of AMM organic composition, with those derived from entry heating simulations, will highlight the extent to which AMMs have been effected by atmospheric entry heating.

Chapter 5 evaluates the astrobiological significance of EDPs as a source of volatiles and organic matter to the early Earth, and the impact they may have had on the development of the early Earth environment.

2. Organic Analysis of EDPs: Samples and Method Development

Investigating the nature and characterising the volatile and organic components of micrometeoritic materials is challenging. With EDPs typically < 1 mm in size and with individual particles weighing just a few micrograms, traditional techniques (e.g. elemental analysis, Py-GCMS) utilised in meteoritic organic analysis cannot readily be applied to individual particles or clusters of particles due to limited sample size and mass. As such alternative analytical methods must be sought. Atmospheric entry heating itself is governed by a range of parameters including entry velocity, entry angle, particle size and particle density (Section 1.6), and so simulating atmospheric heating and analysing the liberated/retained volatile components requires a more sophisticated technique than has been previously applied elsewhere. Therefore in this study, exploratory heating techniques were applied to determine the most effective and efficient simulation method and a combination of analytical techniques were employed to determine the liberated and retained components. This provided an integrated study which has, to date, been lacking from the study of EDPs.

2.1. Samples

Technique development was undertaken with a series of preliminary experiments conducted using terrestrial analogues because of the limited availability and value of extraterrestrial materials. These analogues, of similar particle size, organic content and organic composition as meteorites, were used to develop and evaluate suitable methodologies and protocols for the investigation of mass, carbon and volatile loss from samples under a flash heating simulation of atmospheric entry conditions. Murchison (CM2) was used as an extraterrestrial analogue for EDPs due to its availability, good characterisation and similarities to some EDPs.

2.1.1. Terrestrial Analogue: Permian Marl (V17-2)

V17-2 is an organic rich marl, originating from the Permian Bellerophon Formation outcropping at Vigo Meano near Trento (northern Italy). It contains the debris of land plants and is composed of up to C_{30} *n*-alkanes, up to 4 ringed PAHs and their alkyl derivatives, cyclic diaryl ethers, xanthones and dibenzofurans (Sephton et al., 1999; Watson et al., 2005). The total organic carbon present is 1.8 %, the total carbonate content is 7.3 % (Watson et al., 2005). A dichloromethane extracted residue of V17-2 was used (Watson et al., 2005), which has had solvent soluble organic species removed and retains macromolecular material. It has a similar carbon content and organic composition as unmelted EDPs and Murchison (Table 9). Although it is more aliphatic-rich, it has a similar range of aromatic species to EDPs and Murchison, making it a more suitable analogue for these experiments.

Sample	Organic Carbon (wt.%)	Carbon content (wt. %)
V17-2	0.26 [a]	2.31 ± 0.08*
MMs		0 – 3 [b-d]
IDPs		0 – 50 [e]

Table 9: A table summarising the carbon content of V17-2 relative to that of MM and IDP. (a)Watson et al., (2005), (b) Wright et al., (1997), (c) Maurette et al., (2001), (d) Matrajt et al., (2003), (e) Keller et al., (1994), * this study.

Using a dual beam FEI Quanta 3D microscope, secondary electron images were taken of the sample mounted on a stub. Planimetric analysis of around 1000 particle diameters from these images was used to determine the particle size distribution (Figure 8). V17-2 particle size range is 2.5 – 426 μm with the average particle size of 31.2 μm. The majority of V17-2 particles were <30 μm in diameter, in keeping with the modelling conducted by Love and Brownlee (1991; 1994) that calculated that EDPs of equivalent diameter may experience peak temperatures < 1300 °C upon atmospheric entry.

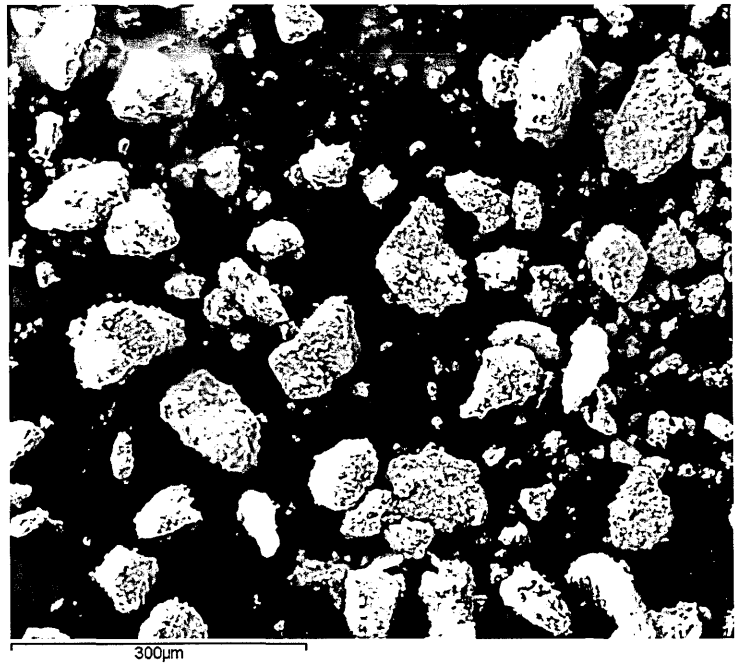

Figure 7: A secondary electron image of powdered V17-2 sample illustrating grain size distribution (20 kV electron volatage, 1.2 nA beam current)

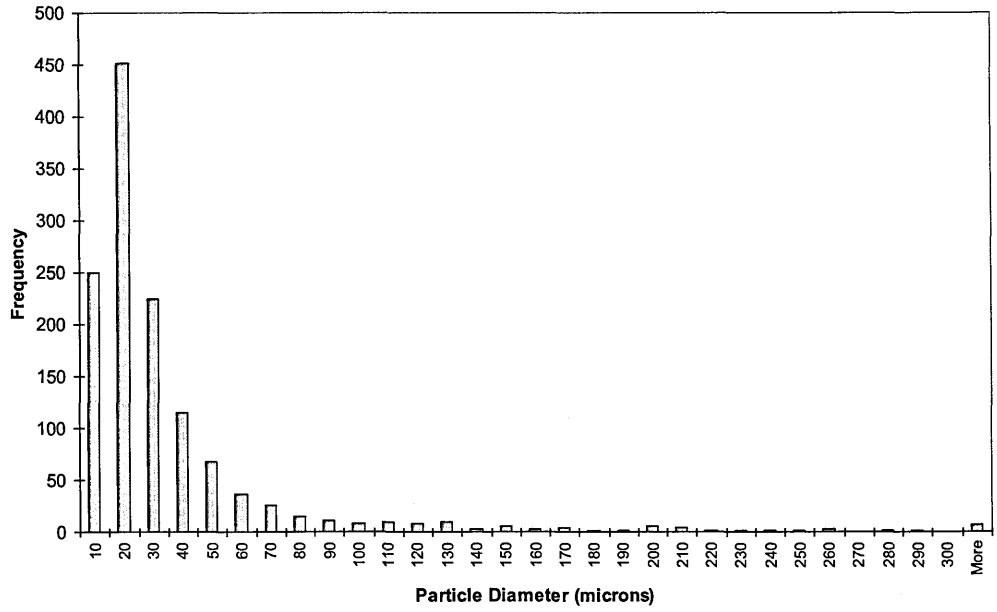

Figure 8: Particle size distribution in V17-2 as measured from BSE images of the sample

2.1.2. Terrestrial: Toarcian Shale (Tfa 00-33)

Tfa 00-33 is characterised as an organic rich grey shale, originating from the Toarcian Whitby Mudstone Formation outcropping at Port Mulgrave, North Yorkshire, UK (Harding, 2003). Bulk whole rocks samples contain carbon contents similar to EDPs (Table 10).

Sample	Organic Carbon (wt.%)	Carbon content (wt. %)
Tfa 00-33	3.66 [a]	4.08 [a]
MMs	-	0 – 3 [b-d]
IDPs	-	0 – 50 [e]

Table 10: A table summarizing the carbon content of Tfa 00-33 relative to that of MMs and IDPs.. (a) Harding (2003), (b) Wright et al., (1997), (c) Maurette et al., (2001), (d) Matrajt et al., (2003) (e) Keller et al., (1994).

Grain size distribution, determined by planimetric analysis of particle diameters in secondary electron images (e.g. Figure 9), shows a size range of 0.67 µm - 88 µm with 95 % particles are ≤ 40 µm (Figure 10) EDPs within a similar particle size as that in Tfa 00-33 are expected to experience peak temperatures of <1300 °C during atmospheric entry (Love & Brownlee, 1991; Love & Brownlee, 1994).

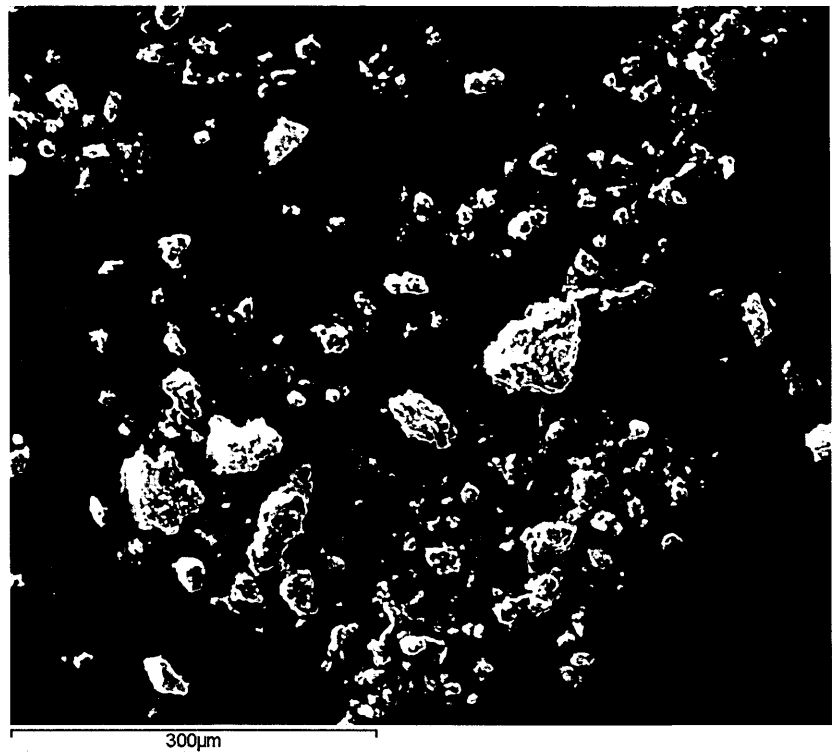

Figure 9: A secondary electron image of powdered TfA 00-33 sample illustrating grain size distribution (20 kV electron volatage, 1.2 nA beam current)

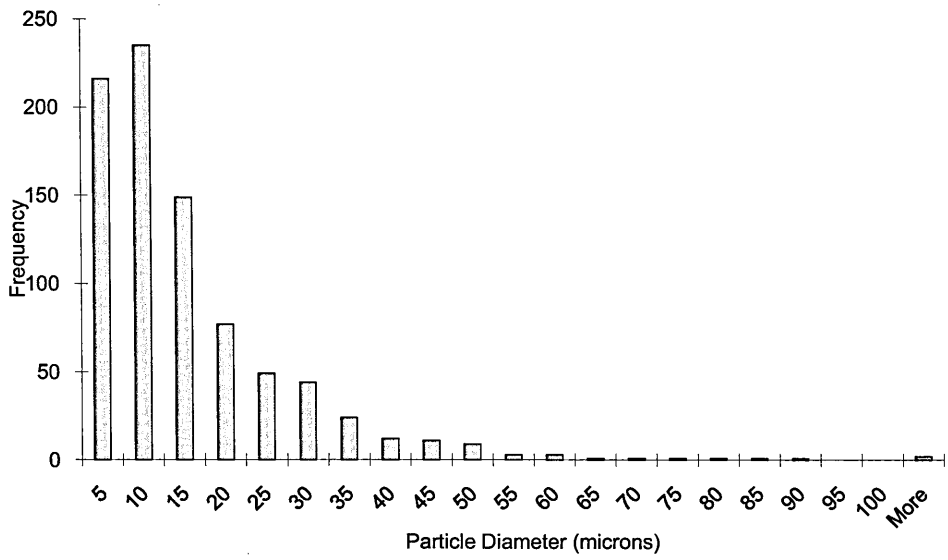

Figure 10: Grain size distribution of powdered whole rock Port Mulgrave Tfa 00-33 measured from SEM images of sample

To determine organic composition of the previously uncharacterised bulk whole rock sample, 5 g of Tfa 00-33 was pyrolysed using a CDS 1000 pyroprobe and analysed by Agilent Technologies 6890 gas chromatograph as described in Pearson et al., (2006). The total ion chromatogram (Figure 11) and corresponding table of analytes (Table 10) shows that the sample also contains up to C_{30} *n*-alkanes, C_0-C_4 benzenes, C_0-C_2 biphenyls up to C_3 PAHs and their alkyl derivatives (see Figure 11). The Mulgrave shale member is also rich in S-bearing (Scrutton, 1994) and O-bearing species (Watts et al., 1999).

Letter	Compound
a	Benzene and toluene
b	Xylene
c	Ethylmethylbenzene
d	Trimethylbenzene
e	Tetramethylbenzene
f	Naphthalene
g	Methylnaphthalene
h	Ethylnaphthalene
i	Dimethylnaphthalene
j	Trimethylnaphthalene
k	Trimethylazulene
l	Fluorene
m	Methylbiphenyl
n	Ethylbiphenyl
o	Dimethylbiphenyl
p	Methylfluorene
q	Dimethylfluorene
r	Anthracene
s	Alkylphenanthrene

Table 11: Compounds identified in the total ion chromatogram (Figure 11) of Tfa 00-33

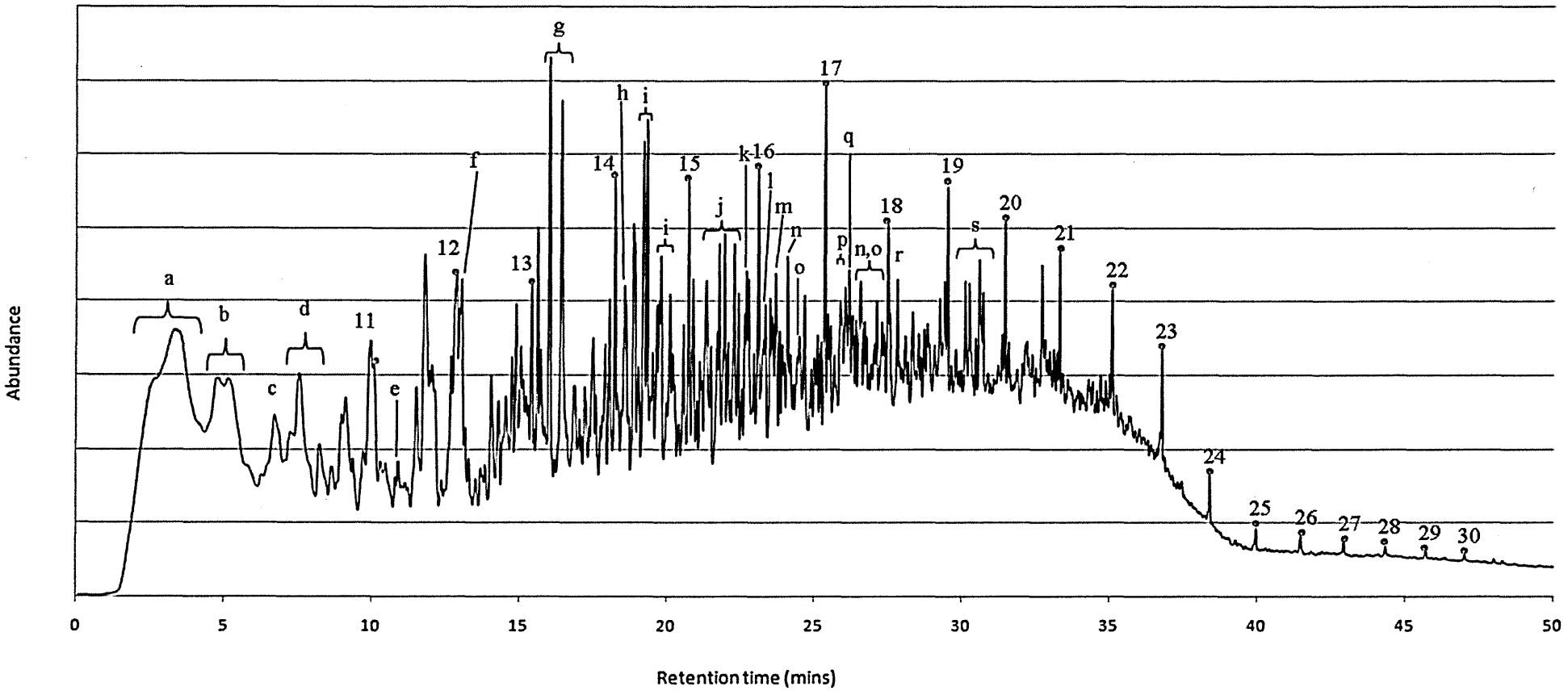

Figure 11: A total ion chromatogram of Tfa 00-33 whole rock. Numbers refer to *n*-alkane homologous series e.g. 13 = C_{13} *n*-alkane. Letters correspond to the compounds given in Table 11

2.1.3. Extraterrestrial: Murchison

The similarity between the chemistry of EDPs and CM carbonaceous chondrites has been discussed previously (Section 1.4). The carbonaceous chondrite Murchison serves as an extraterrestrial analogue for unmelted EDPs in terms of its broad mineralogy, organic composition and organic content (e.g. Table 12).

Sample	Carbon content (wt. %)
Murchison	1.6 - 2.70 [a, b]
MMs	0 – 3 [c-d]
IDPs	0 – 50 [f]

Table 12: A table summarizing the carbon content of Murchison relative to that of MMs and IDPs. (a) Naraoka et al., (2004) and references therein, (b) Pearson et al., (2006) (c) Wright et al., (1997), (d) Maurette et al., (2001), (e) Matrajt et al., (2003), (f) Keller et al., (1994)

The sample comprised a supercritical fluid extracted (SFE) residue of Murchison, whereby CO_2 was used to extract free organic matter from the sample (Sephton et al., 2001a). Pure CO_2 extraction removes the non-polar extractable organic matter (i.e. aliphatic material), thereby reducing the level of terrestrial contamination present in the sample, but leaving the predominant polar and aromatic extractable fractions largely intact. The SFE Murchison residue was homogenised using an agate mortar and pestle in a class 100 clean room. The grain size distribution was calculated using particle diameter measurements from secondary electron images (e.g. Figure 12). The grain size range (Figure 13) was 1.28 μm-106.89 μm with the majority of grains ≤60 μm, consistent with EDP size range and modelling conducted by Love and Brownlee (1994).

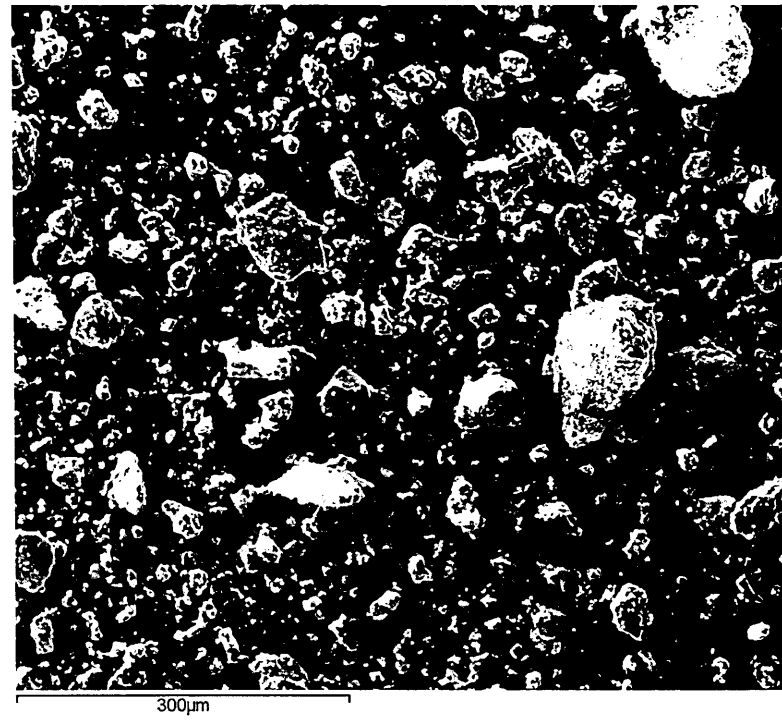

Figure 12: Secondary electron image of powdered bulk Murchison from which grain size distribution was ascertained (20 kV electron volatage, 1.2 nA beam current)

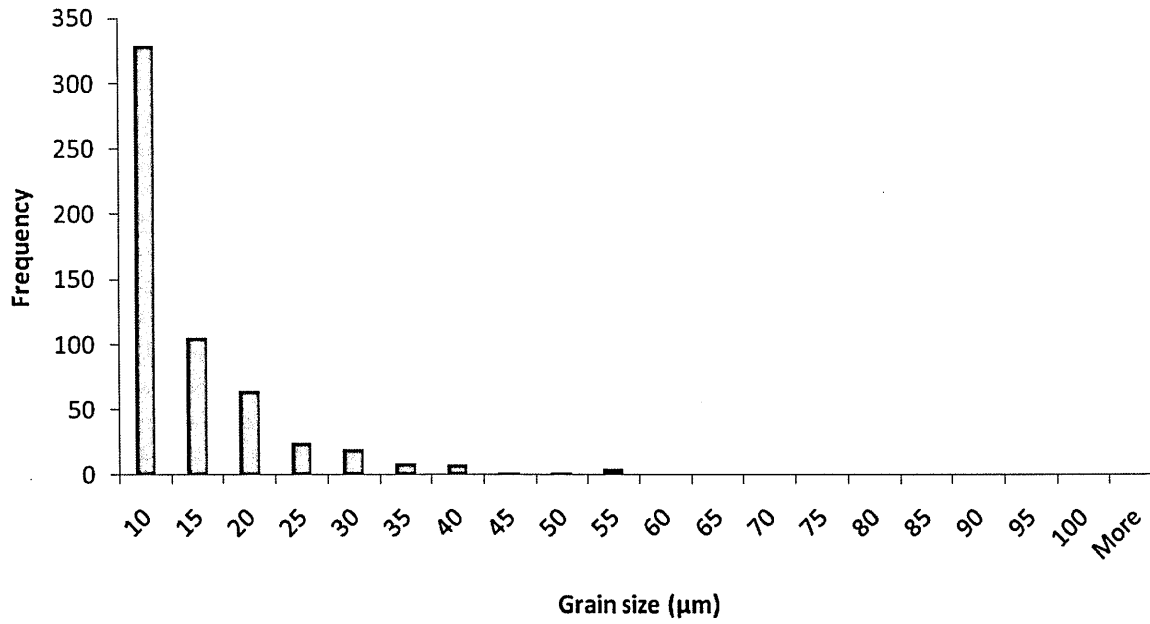

Figure 13: Grain size distribution in powdered Murchison measured directly from SEM images of the sample

2.2. Simulation of Atmospheric Entry Heating

The primary process that EDPs experience during atmospheric entry is flash heating, typically to temperatures of up to 1700 °C for 2 s – 100 s dependant on entry

velocity, entry angle, particle size and particle density (Love & Brownlee, 1991). Previous experimental simulations (Fraundorf et al., 1982; Greshake et al., 1995; Greshake et al., 1995; Greshake et al., 1998; Klöck et al., 1994; Toppani et al., 2000; Toppani et al., 2001; Toppani et al., 2003; Wright et al., 2000) have used a number of methods to simulate time intervals as short as 2 s heating duration (Love & Brownlee, 1991). Toppani et al., (2001) and Greshake et al., (1998) heated carbonaceous chondrite fragments within platinum crucibles in furnaces for 2 s to 2 mins to temperatures 500-1500 °C, in keeping with the theoretical modelling of atmospheric entry heating by Love and Brownlee (1991). However, they were unable to accurately monitor the sample temperature or heating durations. Klöck et al., (1994) and Wright et al., (2000) placed fragments of carbonaceous chondrites in Pt envelopes and inserted them into quartz tubes held in furnaces. The furnaces contained vertically mounted Pt-Rh thermocouples to monitor internal temperatures. Samples were heated for 5 mins to temperatures of 800 – 1500 °C (equivalent to the peak temperatures experience by EDPs; Love and Brownlee, 1991), but the method was not adaptable for the shorter heating durations experienced by EDPs during atmospheric entry heating. An alternative methodology is therefore required, that can provide both short heating durations of a few seconds and accurate temperature measurements.

Pyrolysis is the thermal degradation of compounds in the presence of an inert atmosphere. It is traditionally combined with gas chromatography, for separation of complex organic species (Gohlke & McLafferty, 1993 and references therein), and mass spectrometry for identification of pyrolysis products, and has been a common method for the analysis of complex organic materials since the 1960's (Barlow et al., 1961). It generally employs a flash heating approach, and as such is applicable to the study of EDP atmospheric entry heating.

Two flash heating (pyrolysis) methods were evaluated in this study, the first using a Pt coiled filament and the second using a Pt ribbon. Given the extremely small grain size of EDPs and the analytical limitations of pyrolysis-GCMS (Section 2.2.2), the bulk of

experiments on atmospheric entry simulations were undertaken using a cluster of Murchison or terrestrial analogue particles, analogous to a cluster of EDPs. However, an analytical evaluation of the feasibility of studying individual EDPs was undertaken (Section 4).

2.2.1. Flash Heating Method 1- Pt Coil

Flash heating through a coiled filament is the most common approach that has been used for both pyrolysis studies of organic materials in meteorites (e.g. Hayatsu et al., 1977; Levy et al., 1973; Pearson et al., 2006; Remusat et al., 2005 b) and more recently to simulate parent body conditions (Cody et al., 2008). An advantage of using this method, is its ability to heat relatively large sample sizes (up to 20 mg) ensuring enough residue can be collected from one simulation for post-heating analysis. In this context, it could therefore be used to heat clusters of particles and generate residues for off-line organic and volatile characterisation.

Quartz tubes 25 mm in length and of 2.5 mm external and 1.9 mm internal diameter were cleaned by soaking in nitric acid overnight and rinsing with distilled water. The tubes were then baked in a furnace overnight at 450 °C. Powdered samples (7-14 mg, see Table 13) were weighed and loaded into the tubes for heating, held in place by roasted quartz wool plugs either side (Figure 14).

Sample	Run sample mass (mg)	Heating duration (s) and replicates	Set temperature of Pt coil (°C)	Thermocouple type
Permian Marl V17-2	20	2s x 3	400, 600, 800,1000, 1200	Type K
Permian Marl V17-2	14	40s x 2 20s x 3	400, 600, 800,1000, 1200	Type K
Permian Marl V17-2	9	40s x 2 20s x 8	400, 600, 800,1000, 1200	Type K
Toarcian shale Tfa 00-33	7	40s x 3 20s x 3 10s x 3 5s x 3	400, 600, 800,1000, 1200	Grounded tip fast response type K
Murchison	9	20s x 3 10s x 3 5s x 4	400, 600, 800, (900), 1000, 1200	Grounded tip fast response type K

Table 13: Experimental conditions for preliminary flash heating experiments using Pt coil (CDS Pyroprobe 1000)

Flash heating was conducted using a coiled platinum filament connected to a CDS Analytical Inc. Pyroprobe 1000. The platinum coil has the capability of heating up to 1400 °C for a duration of up to 90 s, via resistance heating. The quartz tube containing the sample fitted snugly inside the platinum coil, hence was heated as the coil heated. Initially, a type K thermocouple was embedded in the sample to record the peak temperature that samples experienced on flash heating. Type K thermocouples are suitable for temperatures between -200 and +1200 °C, within the experimental simulation parameters. However, the continual exposure of the thermocouple to carbon during sample heating repeatedly corroded and broke the thermocouple rendering it inefficient for use in repeated simulations.

The type K thermocouple was later replaced by a fast response fine type K grounded tip insulated probe thermocouple. This meant that the thermocouple was protected from the exposure to carbon and subsequent corrosion, yet was still suitable for use at temperatures up to 1200 °C. Being finer, it also offered a faster response time and reduced thermal inertia suited for the short duration heating of simulations.

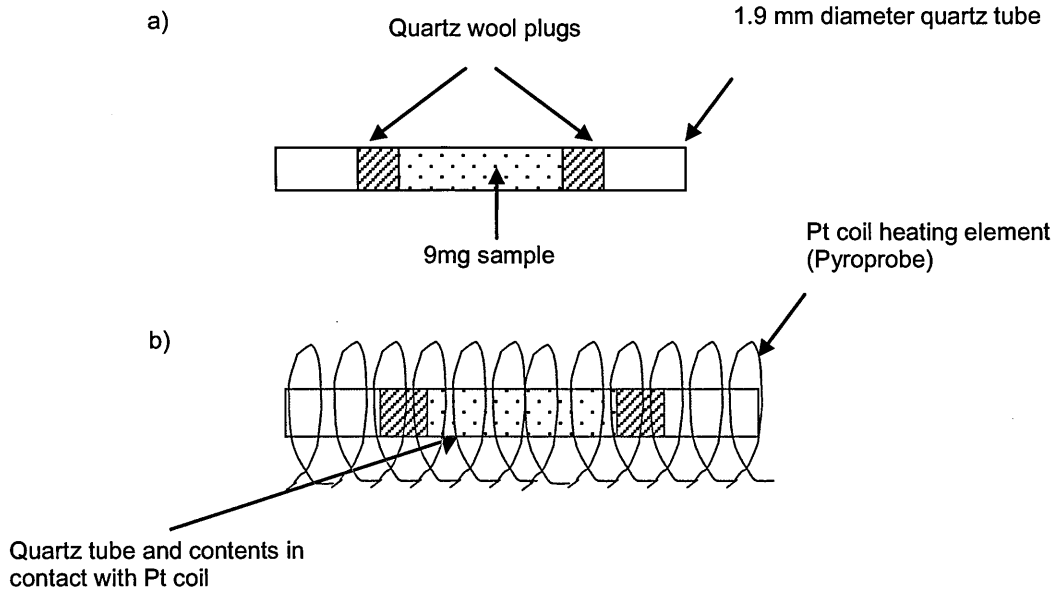

Figure 14: Sample set up a) in quartz tube and b) within Pt coil (pyroprobe)

Samples were heated in air to a range of temperatures and durations outlined in Table 13, comparable to those experienced by 30 μm sized EDPs during atmospheric entry (Love & Brownlee, 1994). Heating simulations were conducted until 10 mg of flash heated residue for each heating temperature and duration were collected for further analyses.

2.2.2. Limitations of Flash Heating Method 1

It was possible to heat all samples for durations of 5 to 20 s, however results were not reproducible. For example, Figure 15 shows the maximum temperature (T_{max}) that 9 mg V17-2 analogue was flash heated to for 2 s, using the Pt coil set to a variety of temperatures; each run was replicated eight times. For samples set to 1200, T_{max} varies by ~500 °C. These temperature anomalies can be attributed to variations in the spread of the platinum coil around the quartz tube, which can alter over time (i.e. with knocks from quartz tubes or their movement), and may not provide constant heating across the entire sample.

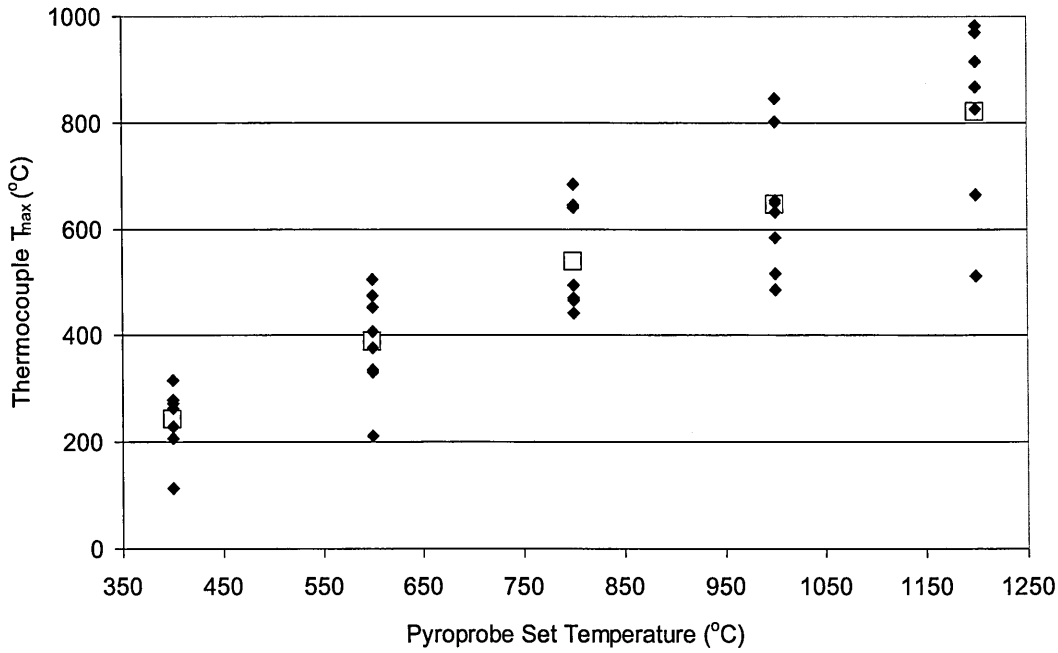

Figure 15: Pyroprobe set temperatures compared to the maximum temperature (T_{max}) logged by the thermocouple for 8 replicates (blue diamonds) of 9 mg V17-2 analogue flash heated with a Pt coil for 20 s duration. The average thermocouple temperature for each simulation temperature is given by the squares

Thermal conductivity of the quartz tube and the thermal inertia of sample grains can also account for inconsistent sample heating. This method was not suitable for simulating samples < 1 mg as the recovery of heated residues was hindered due to the sample being retained in the quartz wool. Additionally, there was a contribution by user error in placing the samples at exactly the optimum position within the quartz tube and the quartz tube at the optimum position within the Pt coil, which also affected the peak temperature of the sample.

Figure 16 shows average T_{max} for V17-2, Tfa 00-33 and Murchison samples compared to the temperature set on the Pt coil during flash heating for a variety of durations. None of the samples were subject to the temperatures set on the pyroprobe regardless of sample type, mass and heating duration. Despite extending the heating duration (extending the time period for thermal conduction) and using a lower sample mass (providing less mass for heat to conduct through), samples rarely exceeded ~ 900 °C.

Sample heating using a platinum coil is primarily inhibited by the thermal inertia of the quartz tubes in which samples are retained. Computational simulations suggest that EDPs <50 μm experience peak entry heating temperatures of 400-1200 °C for durations in excess of 2 s (Love & Brownlee, 1994). The Pt coil flash heating method is incapable of consistently reaching simulation temperatures of ~1000 °C (Figure 16) with conditions that are reproducible (Figure 15), therefore an alternative more reliable heating method was required for entry heating simulations.

These findings have a bearing on the use of the CDS 1000 pyroprobe in both organic analysis and heating simulation studies. For example, Cody et al., (2008) used the CDS 1000 pyroprobe to conduct heating experiments on 1-2 mg Murchison. They report flash heating samples to 600 °C, 800 °C, 1000 °C and 1400 °C for 10 s in order to derive thermo-kinetic expressions to establish the degree of thermal metamorphism on chondrite parent bodies. With measurements of pyroprobe sample temperatures up to ~ 300 °C below user set temperatures as highlighted in Figures 15, 16 and Appendix I,

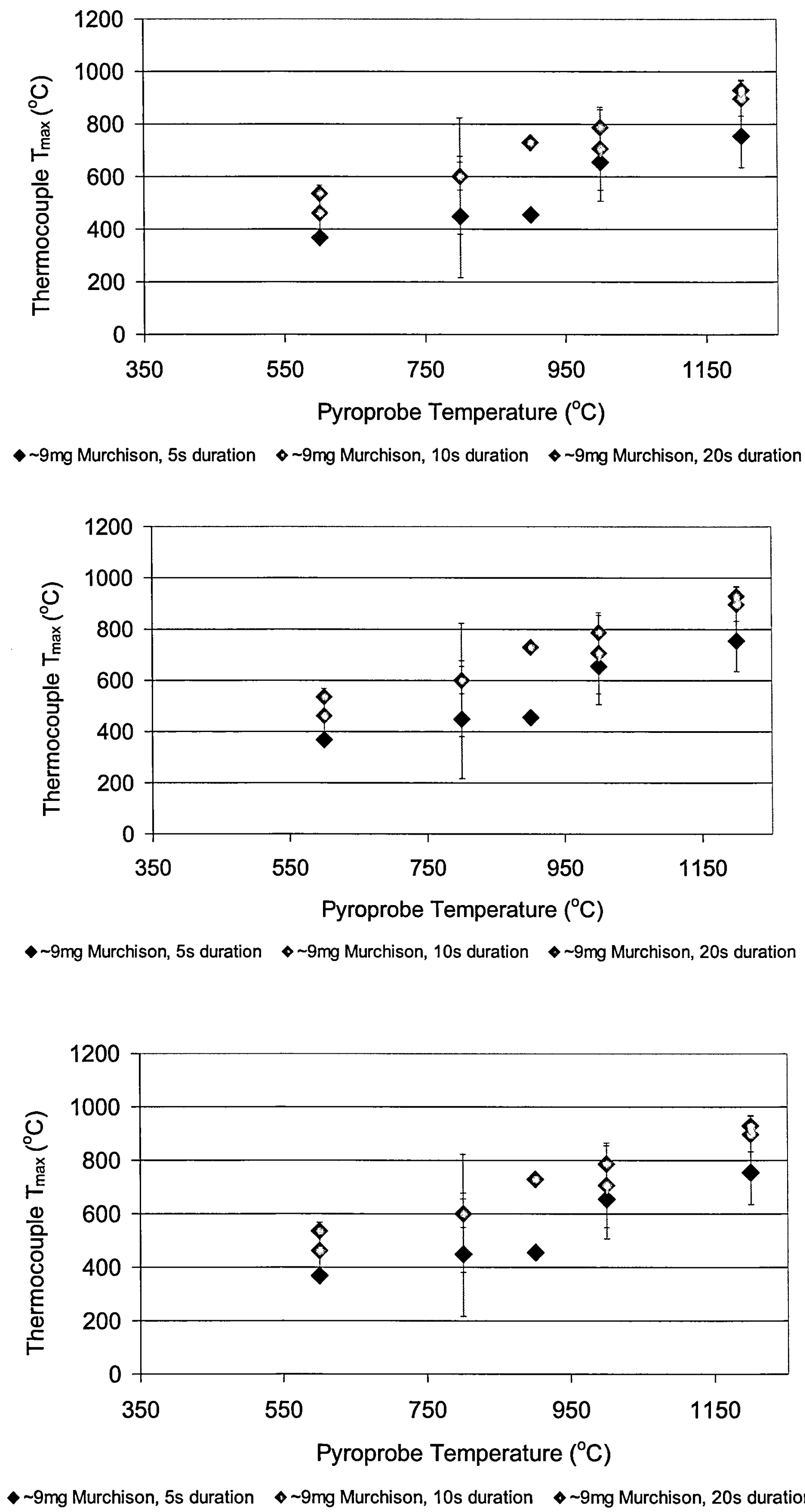

Figure 16: An example of pyroprobe set temperatures and the average T_{max} logged by the thermocouple (including errors of 2 standard deviation) for a) V17-2, b) Tfa-0033 and c) Murchison samples heated for varying durations. Raw data is available in Appendix I

it ultimately affects the validity of thermo-kinetic calculations derived from pyroprobe heating temperatures. The subsequent estimated peak thermal alteration temperatures of chondrite parent bodies predicted using such calculations (Cody et al., 2008) is also questionable.

2.2.3. Flash Heating Method 2- Pt Ribbon

In order to derive meaningful results from flash heating experiments, it is essential that the sample is heated quickly and maintained at constant temperature until it is completely pyrolysed or rapidly cooled. A Pyrola 2000 Filament Pulse Pyrolyser (Pyrolab, Sweden) is an alternative pyrolysis technique suitable for simulating the flash heating that EDPs experience upon atmospheric entry. This heats a platinum ribbon to 1400 °C in 8 ms via resistance heating.

The Pyrola 2000 consists of a control unit connected to a pyrolysis chamber and a pyrolysis probe, to which a platinum ribbon is attached. The platinum ribbon contains a well in which solid samples can be securely placed and remain within direct contact of the heating filament. The ribbon was heated in the pyrolysis chamber in a He flow held at constant temperature (Tc), by the introduction of two current pulses defined by their amplitudes (I1 and I2) and their time intervals (t1 and t2) during prior calibration. Table 14 defines the ranges of Pyrola pyrolysis parameters.

Parameter	Range
t1	0-100.0 ms
I1	0-50.0 A
t2	0-1000 ms or 1.0-600.0 s
I2	0.15.0 A
T_c	50-225 °C

Table 14: The range of Pyrola pyrolysis parameters which control the peak temperature and duration of heating. t1 and t2 are Pt ribbon heating durations, I1 and I2 control the current through the Pt ribbon and Tc represents the pyrolysis chamber temperature

The Pyrola 2000 was used for offline EDP atmospheric entry simulations, whereby materials were exposed to atmospheric entry heating conditions and the residues were

collected for further analysis. Figure 17 illustrates the experimental set up of offline simulations where the pyrolysis chamber was clamped and connected to a continuous flow of He (20 ml/ min) and was maintained at 175 °C. Online simulations were conducted with the Pyrola 2000 coupled to a Pegasus 4D (Leco Corporation) highly sensitive GCMS system in order to characterise species liberated during heating simulations (Section 2.4).

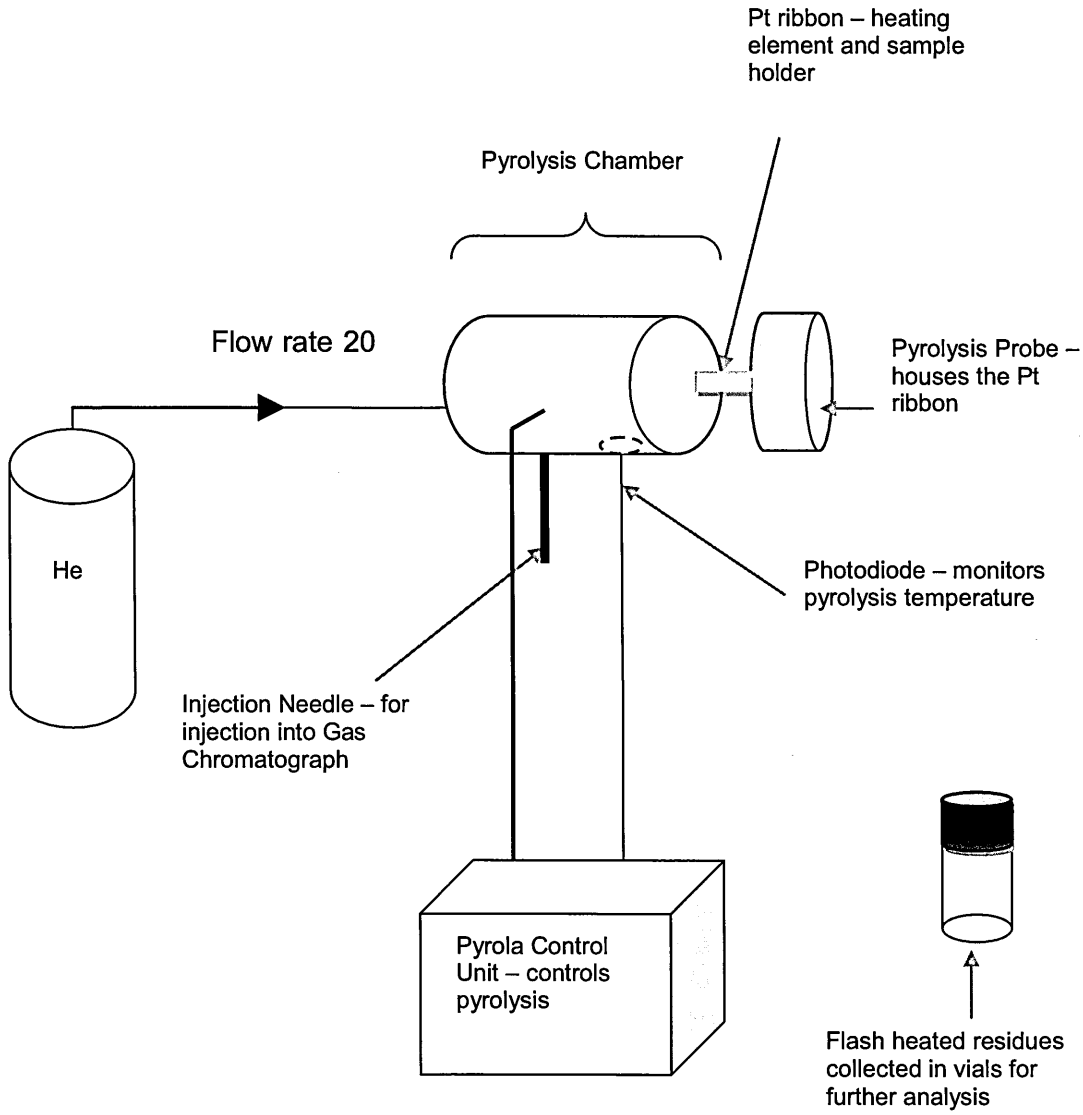

Figure 17: A diagram showing the experimental set up of offline heating simulations using the Pyrola 2000 unit

During pyrolysis, the photodiode and resistance measurements of the Pt filament temperature were displayed in the form of a time-temperature profile (e.g. Figure 18), allowing accurate temperature measurements to be recorded. An ideal time-temperature

profile is displayed in Figure 18, with the solid line representing the temperature logged by the photodiode. The dashed line represents the peak temperature maintained by the heated ribbon (T_{max}) as logged by the photodiode (circled). An example time-temperature profile (Figure 18) illustrates that the currents I1 and I2 passing through the Pt ribbon can produce the initial temperature of the Pt ribbon and then maintain it during the heating of the sample. It is noted that there is a drop in Pt ribbon temperature of approximately 100 °C following the initial introduction of current I1 and the I2 current that maintains the temperature. It represents the time interval between the initiation of the two currents and the endothermic action of heating the sample. This drop in peak temperature is more pronounced at higher set temperatures. Although this means that the heating of a sample will not spend the entire heating duration at the peak temperature set, the sample heating is still in line with the theoretical modelling of Flynn (1989a) and Love and Brownlee (1991) who found that EDPs remained within 100 °C of the peak temperature for only 1-2 s. It therefore remains an accurate simulation method of atmospheric entry heating conditions.

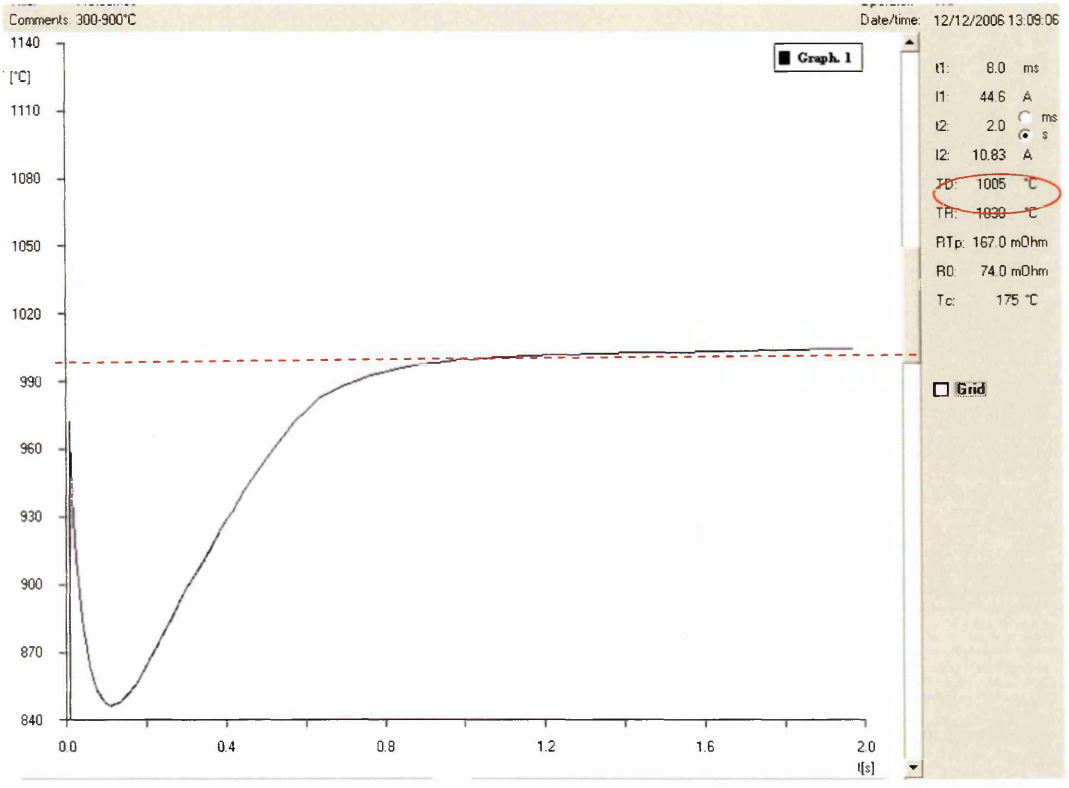

Figure 18: An example of a Pyrola time temperature profile of a sample flash heated for 2 s to 1005 °C as determined by the diode temperature (TD, circled)

A small powder pipette was calibrated to load 0.9 mg of EDP analogue into the well on the Pyrola platinum ribbon. As the filament temperature is controlled by the Pyrola 2000 unit and it is in direct contact with the sample, the sample is heated instantaneously and accurately (Table 15). Replicates were flash heated to the conditions outlined Table 15, comparable to those predicted by Love and Brownlee (1991; 1994) for the relevant grain size fraction. Differences in recorded and set filament temperature is related to heterogeneity of the sample (e.g. grain size) and the lifetime of the Pt ribbon. Samples were not heated beyond 1000 °C as components of the meteoritic matrix melts at temperatures above this (Genge et al., 1997) and would adhere to the platinum ribbon. Heating conditions were repeated until approximately 10 mg of flash heated material was collected for each temperature and duration for subsequent analyses.

Set Simulation Temperature (°C)	Heating Duration (s)	
	2 s	5 s
400	406 ± 8	409 ± 12
600	603 ± 9	599 ± 16
800	814 ± 13	790 ± 18
1000	1006 ± 59	1003 ± 30

Table 15: Recorded simulation temperatures of up to 80 replicates of flash heating method 2 for 0.9 mg samples of Murchison, taken from time-temperature profiles of photodiode measurements (temperatures > 600 °C) and the filament resistance (temperatures < 600 °C)

Advantages of the Pyrola over the Pyroprobe 1000 method include its ability to handle small sample masses (<1 mg) in direct contact with the heating element. Hence the Pyrola heats samples more accurately to the temperatures and durations set and required for precise simulation of atmospheric entry heating.

Monitoring the sample heating process by two methods (photodiode and resistance) is also beneficial and facilitates the reproducibility of experimental conditions. This experimental set-up provides the capability to flash heat samples in an inert gas lacking oxygen (a closer analogue of the early Earth atmosphere than the air of present day) and could potentially be adapted to simulate a range of planetary atmospheric compositions.

The main limitation of this flash heating method, is that it is only capable of conducting simulations on small sample sizes ~1 mg. Multiple simulations (in some cases in excess of eighty) are required to produce enough residues for some of the post-simulation analyses undertaken in this study.

2.3. Analysis of Flash Heated Residues

2.3.1. Elemental Analysis

During preliminary experiments carried out using flash heating method 1 (Section 2.2.1), bulk elemental analysis was used to monitor the change in carbon abundance in flash heated residues with respect to heating temperatures and durations, providing information on the survivability of carbon-bearing components under such conditions. Bulk carbon abundances were measured using an elemental analyser (Europa ANCA-SL [Automated Nitrogen Carbon Analysis for Solids and Liquids]) coupled to a continuous-flow mass spectrometer (Europa GEO 20-20) in combustion mode. Nitrogen abundances in simulated residues were not characterised, as they were below detection limits.

Clean 4 x 6 mm Sn buckets were filled with duplicates of approximately 2.5 mg of flash heated residues or unheated samples. Blanks were placed at the start of the sample run and consisted of empty Sn buckets to obtain the typical blank beam intensity of $x10^{-8}$ to $x10^{-9}$ C. Blanks were assessed at the beginning of each run to ensure that beam intensity was higher than $x10^{-7}$ C, to prevent decrease in precision. Typically, newly opened tubs of Sn buckets yielded the lowest blank levels and were used solely for extraterrestrial analyses. Duplicates (in some cases triplicates) of each sample were run to establish errors of ± 0.08 wt.% C.

References were placed after the blanks, after every ten samples or less and at the end of the sample run in order to monitor drift. References used for C analysis were Sn buckets filled with Chromosorb™ (a C-free absorbant) and 1 µl CANENOU (a solution of cane sugar) characterised as $\delta^{13}C$ = -11.5 ‰ or 1 µl SUCNOU (a sucrose solution) characterised as $\delta^{13}C$ = -25.8 ‰. The references contained known amounts of carbon

and nitrogen for example 1 µl of CANENOU or SOUCNOU contains 80 µg carbon. 1µl of each reference was used as the best estimated match to the amount of carbon in the terrestrial or extraterrestrial samples, ensuring a balance between beam intensities for references and samples.

Samples/blanks/references were placed into an auto-sampler and dropped into a cavity purged with He at 40 ml/min. Samples were introduced individually into a furnace maintained at 1000 °C, upon which the ignition of the Sn sample buckets raised to temperature to 1800 °C ensuring sample oxidation and complete combustion. In this first furnace carbon monoxide is oxidised by chromium oxide to carbon dioxide with copper oxide and silver wool removing sulphur. Sample gas released on combustion is directed through a second furnace, containing copper wire, maintained at 600 °C in a He flow of 60 ml/min. The second furnace reduces nitrogen oxide to nitrogen. This ensured the removal of excess oxygen. Water was removed using anhydrous magnesium perchlorate. The sample gas was then introduced into the GC oven set to 70 °C, to separate chemical species of interest and then passed to the mass spectrometer for ionisation and detection.

The VANCA automated software was used in conjunction with the ANCA-SL software to conduct daily background scans, calibrate masses of interest and perform ion source tuning prior to sample runs. Drift and blank corrections were performed automatically by the Ancapro software in addition to manual assessment of the raw values. Anomalous references were discarded and the results re-calculated for the entire sample run using the Ancapro *reprocessor* function.

2.3.2. Carbon Loss in Simulated Residues

The carbon abundances of residues from preliminary flash heating experiments (utilising heating method 1, Section 2.2.1) were monitored with respect to varying simulation temperatures. Figure 19 shows the percentage carbon lost from 14 mg samples of V17-2 flash heated for 40 s to peak simulation temperatures between 300 – 1000 °C. Carbon loss increases with increasing peak simulation temperature in an near-

linear manner, with two regions of accelerated carbon loss at ~ 700 °C (Figure 19, dark grey section) and ~ 800 °C (Figure 19, pale grey section) indicative of carbon-bound phases decomposing at specific temperatures.

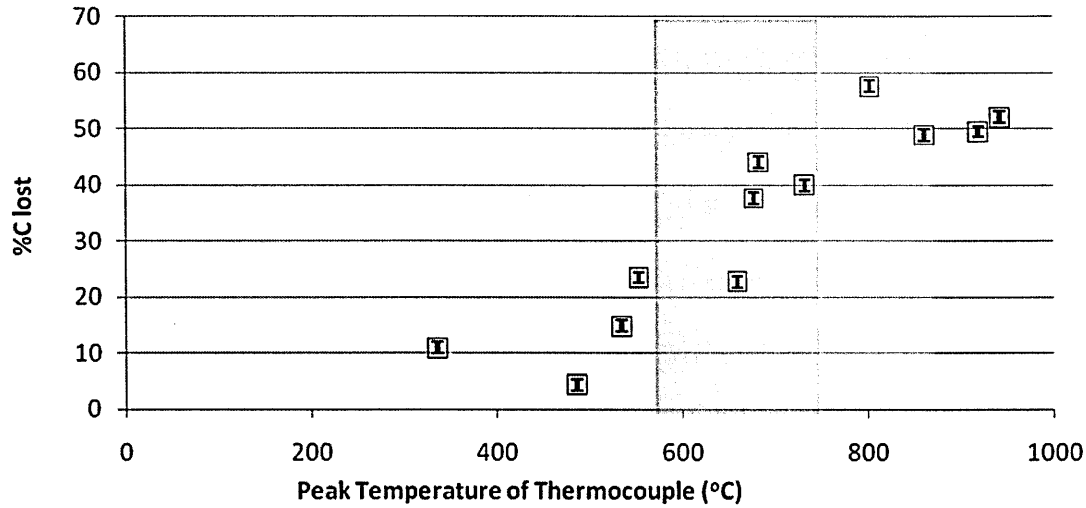

Figure 19: Percentage carbon loss (including combined errors) from V17-2 samples simulated to peak atmospheric entry heating temperatures between 300 - 1000 °C. Dark and light grey highlight regions of accelerated C loss at ~ 700 °C and ~ 800 °C respectively

2.3.3. Limitations of Elemental Analysis

Elemental analysis was able to determine changes in carbon abundance in non-simulated and simulated residues, highlighting potential simulation temperatures at which accelerated carbon loss occurs. This method, however, was not able to distinguish the survivability of individual carbon bearing components for example that of organic carbon, which is critical to this study. An alternative method could be employed to differentiate between surviving carbon in terms of organic matter, carbonate material and amorphous carbon, and provide this information using the minimal sample size generated through heating.

2.3.4. Thermogravimetric (TG) and Evolved Gas (EG) Analysis

Thermogravimetric analysis has been used to characterise material properties since the 1960's e.g. characterising the properties of polymers (Broido, 1969; Doyle,

1961; Horowitz & Metzger, 1963). The instrument records the sample weight as a function of furnace temperature during a pre-programmed pyrolysis heating regime. As a result it records cumulative volatile loss as a percentage weight, but is unable to resolve overlapping events. Evolved gas analysis, using quadrupole mass spectrometry, is a technique used to characterise the relative abundance of volatile products released from a sample as a result of heating. The two techniques combined can simultaneously record weight loss as samples are heated in a furnace and identify volatile species assigned to specific points of weight loss. The first applications of this technique to extraterrestrial samples, was determining the volatile composition and linking it to the mineralogy of the Orgueil meteorite (Gibson & Johnson, 1972) and analysing volatile composition (H_2, H_2O, N_2, CH_4, CO, CO_2 and COS) and content within Apollo lunar samples (Gibson & Hubbard, 1972). More recently it has been employed to characterise the hydrous components of carbonaceous chondrites (Morris, 2008; Morris et al., 2005) with relevance to their aqueous alteration.

In this study, TG/EGA was used to identify the volatile composition of residues before and after exposure to atmospheric entry heating conditions. The species monitored (Table 16) were selected to provide information about mineralogical and volatile compositions. Comparisons of flash heated residues with unheated samples can be used to calculate the abundance (wt.%) of each component released during simulations.

Unheated samples and those exposed to entry heating simulations were analysed for the presence of volatile and inorganic species using a Netzsch STA 449C Jupiter thermo-gravimetric analyser coupled to a Hiden Analytical HPR20 RGA evolved gas (EG) analyser.

m/z	Species	Occurrence
16	CH_4	Derived from the decomposition of organic material
18	H_2O	Present as adsorbed water and derived from the decomposition or dehydration of clay minerals
28	N_2 or CO	Derived from the decomposition of organic material
44	CO_2	Derived from the decomposition of organic material and carbonates
64	SO_2	Derived from the decomposition of sulphates

Table 16: Target species monitored during TG/EGA analysis

The Netzsch STA 449C Jupiter thermo-gravimetric analyser primarily consists of a sample carrier within a high temperature furnace attached to a sensitive µg mass balance. Between 3 – 3.5 mg of previously flash heated sample was placed in a clean Pt crucible with lid and positioned on the sample carrier within the high temperature furnace. The furnace was maintained at 20 °C under a He gas flow (10 ml/min) for 20 mins. The furnace has the capability to heat to 1500 °C at a rate between 0.1-50 °C/min using a Rhodium alloy heating element. The furnace was heated to 950 °C (so as not to melt the sample) at a rate of 10 °C/min, with the temperature monitored using a built in S-type thermocouple attached to the sample carrier. The heating regime was optimised for carbonaceous chondrite volatile analysis (*L. Baker, pers. comm.*). Throughout heating, the high precision µg balance recorded the sample mass with a sensitivity of 0.01 mg, enabling component specific calculations of mass loss (wt.%).

Analytes released on heating pass through to the Hiden Analytical HPR20 RGA EG analyser via a heated transfer line preventing their condensation prior to the mass spectrometer. The EGA comprises of an ultra high vacuum system with a heated quartz lined capillary inlet. The inlet feeds directly into a quadrupole mass spectrometer ioniser allowing fast and sensitive response to gas change. The quadrupole mass analyser filters sample ions based on their mass-to-charge ratio (m/z), hence is capable of only transmitting ions previously defined.

Raw data files were exported into Origin 6.1 (OriginLab). Peak areas of evolved gases (Table 16) are indicative of species abundance. Where necessary, peak areas were determined using the automated peak find and calculation tool in Origin 6.1, and subsequently plotted with respect to varying heating regimes.

	CO_2 evolved gas peak position (°C)		H_2O evolved gas peak position (°C)	
Sample	**carbonate 1**	**carbonate 2**	**[i]**	**[ii]**
12060802	626.3	704.5	117.1	391.5
13060801	626.4	704.7	117.6	391.7
17060801	647.9	703.8	117.0	385.5
23010602	623.5	703.6	118.5	388.1
Average	**631.0**	**704.2**	**117.6**	**389.2**
2σ	**22.7**	**1.1**	**1.4**	**5.9**

Table 17: Average peak positions of CO_2 derived from carbonates (carbonate 1 and carbonate 2 peaks) and water (H2O [i] and [ii] peaks) errors to 2σ. Determination of peak position of the evolved organic CO_2 peak was not possible as it is too broad. Further explanation of peak positions and peak identification is given in Section 3.4.1

Reproducibility of peak positions (in terms of evolved gas temperatures) has established errors (2σ) of ± 1.1 – 22.7 °C for CO_2 and between ± 1.4 - 5.9 °C for H_2O Table 17.

2.4. Analysis of Species Released on Simulation

Identification of evaporated organic species and volatiles from EDP atmospheric entry simulations is central to this study. The atmospheric entry heating simulations (flash pyrolysis) were conducted online, coupled to a highly sensitive gas chromatography and mass spectrometry system.

2.4.1. Pyrolysis (Online Heating Simulations)

The online conditions of pyrolysis are similar to the offline conditions described in (Table 15, section 2.2.3). The pyrolysis chamber was maintained at a constant temperature of 175 °C during pyrolysis and with continuous flow of He (6 ml/min), it interfaced to the gas chromatograph inlet. Powdered samples of 0.9 mg of Murchison were flash heated under the same offline conditions as described in Table 15.

A) Gas Chromatography (GC)

Gas chromatography is the method by which compounds can be separated prior to their identification by mass spectrometry. The simulation (pyrolysis) products are inserted to the Agilent Technology 6890 Gas Chromatogram by injection via a 1.2 mm (internal diameter) narrow-bore deactivated liner directly into the primary GC capillary column. The capillary column is coated with a non-volatile liquid stationary phase. The vaporised products are carried in a He flow and are separated based on volatility and affinity for the stationary phase. Gradual heating of the GC oven enables separation over a range of molecular weights.

B) 2D Gas Chromatography (GCxGC)

Two dimensional GC (GCxGC) was developed in the early 1990's (Liu & Phillips, 1991), combining two GC columns (Figure 20) separating components by different physical properties. The primary column separates by molecular weight, whilst the secondary column separates by polarity.

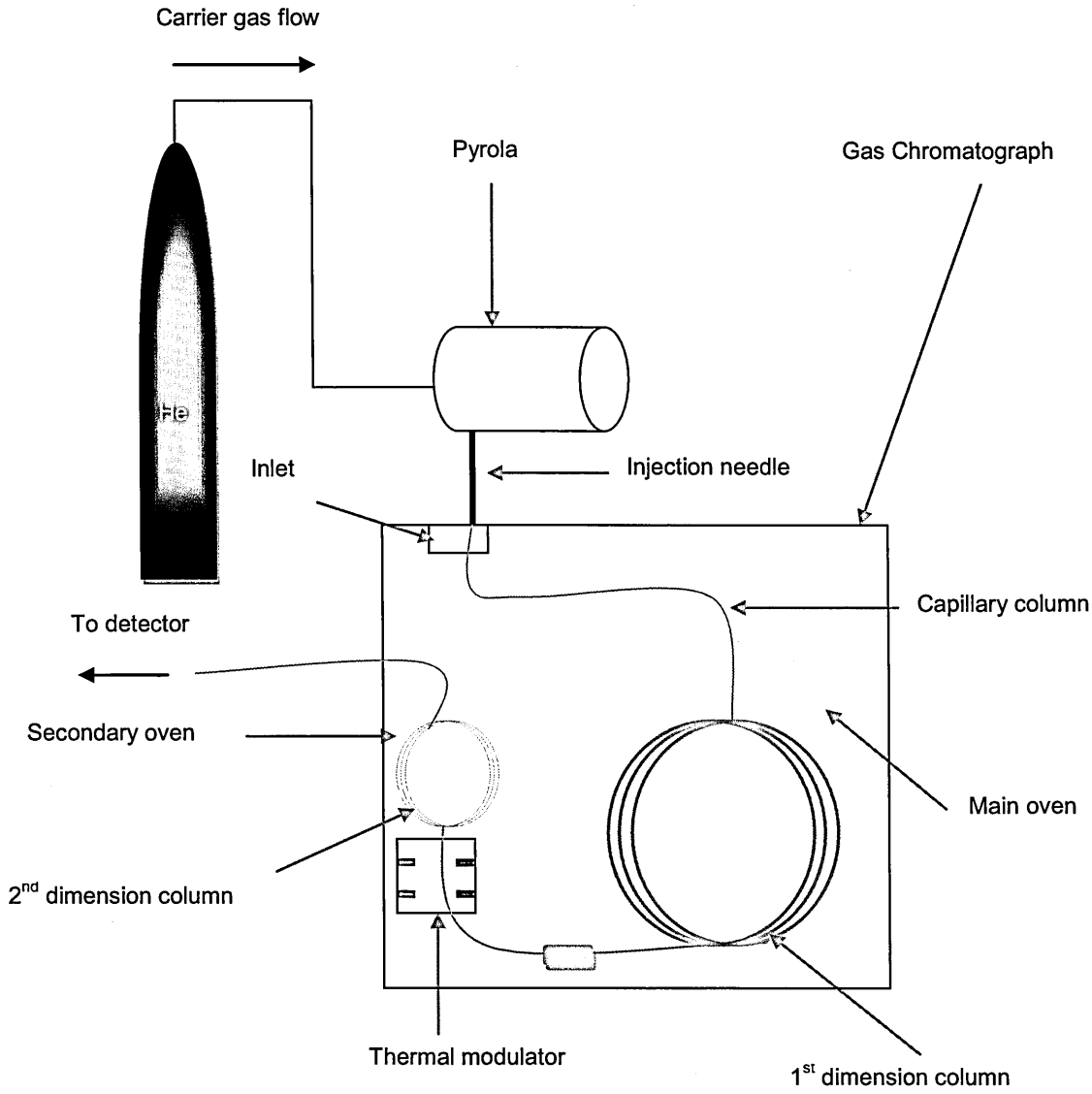

Figure 20: A schematic of the Pyrola coupled to the GCxGC system

A two-stage thermal modulator is used to trap, focus and re-inject sample from the first column to the second column, via two cryotraps (Figure 21). The sample is trapped

from the first column in the first stage using a 1.5 s cold jet (Figure 21 A); a 0.4 s hot jet then releases the concentrated sample to the cold second stage (Figure 21 B).

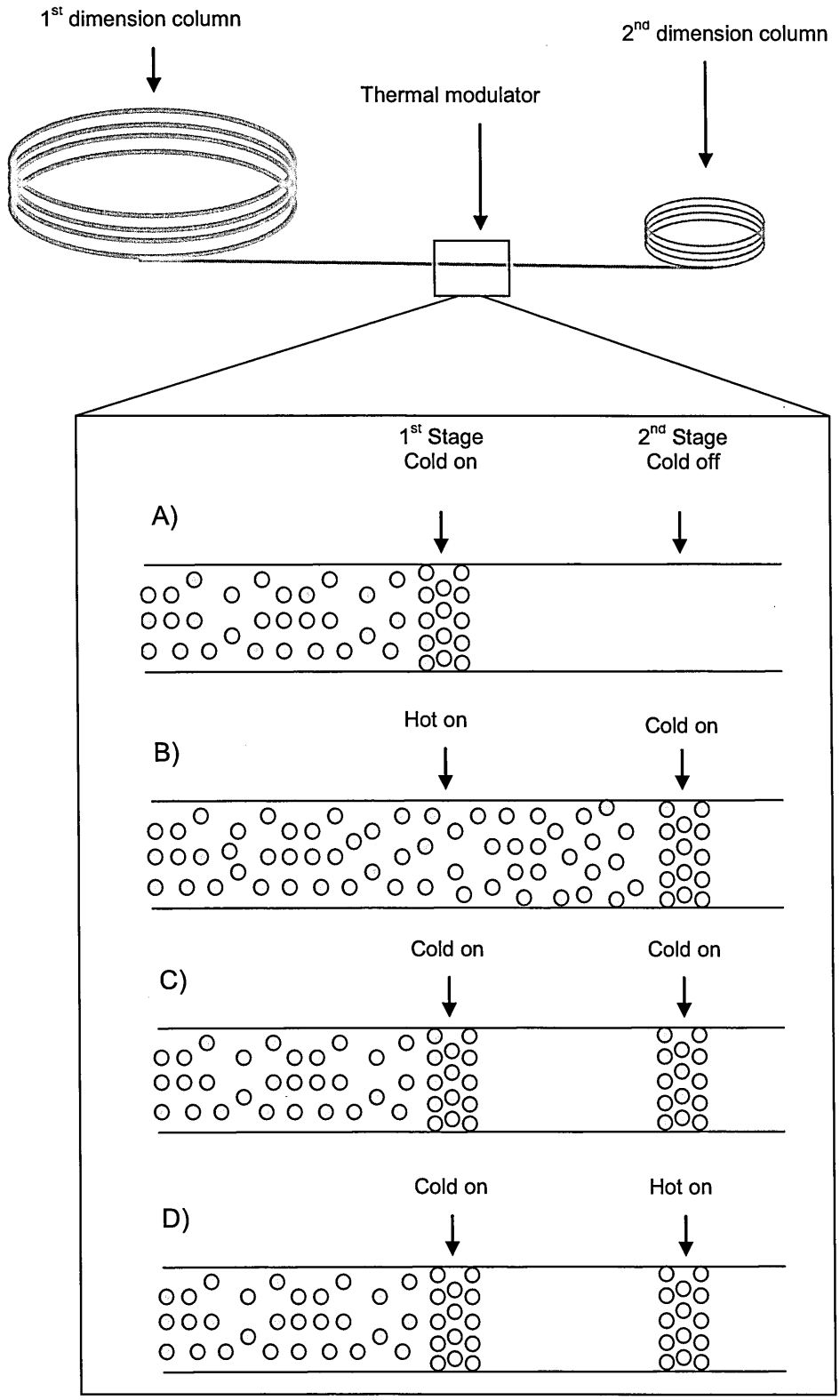

Figure 21: A diagram illustrating how the 2-stage thermal modulator traps and focuses sample from the 1st dimension column to the 2nd dimension column using a series of hot and cold jets

The second cold stage holds the sample for 1.10 s during volatile organic analysis and 1.60 s in PAH analysis as the first stage cools and traps the next sample (Figure 21 C). Once the first cold stage has trapped the next sample, the second stage heats and releases the first sample onto the secondary column (Figure 21 D). The second stage cools, then the first stage releases the next trapped sample slice continuing the sampling from column one to column two.

Separation of components on the second column occurs across a 3 s retention time. This allows continual introduction of fractions from column one, approximately every 3 s without interference, each equivalent to one peak width on column 1. Therefore each peak separating from the first column, representing a number of co-eluting peaks, is further separated on the second column. The sampling frequency can be set to preserve the resolution available on the first column (usually 3-4 samples, known as slices, per first dimension peak width). The sampling period is equal to the modulation period and the separation time on column two. Due to the high separation power, this technique has predominantly been used to characterise complex petrochemical mixtures (Bloomberg et al., 1997). Further applications include oil spill source identification (Gaines et al., 1999), crude oil biomarker analysis (Frysinger & Gaines, 2001), characterisation of unresolved complex mixtures in petroleum contaminated sediments (Frysinger et al., 2003) and the screening of PAHs in soils (Hyötylainen et al., 2002; Ong et al., 2003). A review of terrestrial applications of GCxGC is available in Marriot and Shellie (2002). More recently, GCxGC has been used to characterise the organic material within meteorites (Greenwood et al., 2007; Pearson et al., 2007 a & b; Watson et al., 2005).

i) *Primary Column Selection*

Two sets of online simulations were conducted, one focussed on the identification of highly volatile species released and the other on higher molecular weight species. The primary column selected for volatile species identification was the SGE BP624 coated with a mid-polar phase (cyanopropylphenyl polysiloxane). It has a maximum operating

temperature of 240 °C suitable for volatile organic and alcohol analysis. The primary column selected for higher molecular weight species analysis was the SGE BPX5, a low bleed column coated with a non-polar 5% phenyl polysilphenylene-siloxane stationary phase. It has a maximum operating temperature of 370 °C and is suitable for routine analysis of pesticides, hydrocarbons and drugs.

i) Secondary Column Selection

The secondary column selected for volatile species identification was the SGE BP20, a WAX column coated with a polar phase (polyethylene glycol). It has a maximum operating temperature of 270 °C suitable for alcohol, ketone, ester and aldehyde analysis. It is useful for the separation of aromatic isomers such as those of xylene. The secondary column selected for higher molecular weight species analysis was the SGE BPX50, a low bleed column coated with a mid-polar 50% phenyl polysilphenylene-siloxane stationary phase. It has a maximum operating temperature of 370 °C and is best suited for routine analysis of pesticides, hydrocarbons and pharmaceuticals.

C) Advantages of GCxGC

The primary advantage of GCxGC is its high resolving power and the capability to separate complex mixtures (Phillips & Xu, 1995). Theoretical calculations suggest that an optimised GCxGC system has a separation performance an order of magnitude greater than a 1D GC counterpart (Blumberg, 2003). GCxGC can potentially separate a larger fraction of analytes in a complex mixture, resolving peaks that co-elute in standard GC techniques (Figure 22). Overall, the increased resolution relative to traditional GC methods enables easier characterisation of lower abundance peaks. With its high peak capacity, GCxGC is a powerful tool for analyte separation and is ideally suited to unravelling the complex nature of meteoritic and micrometeoritic organics.

Figure 33 shows a comparison of a conventional Murchison GC-MS total ion chromatogram (TIC) trace (inset, Pearson et al., 2006) with that from a GCxGC-TOFMS

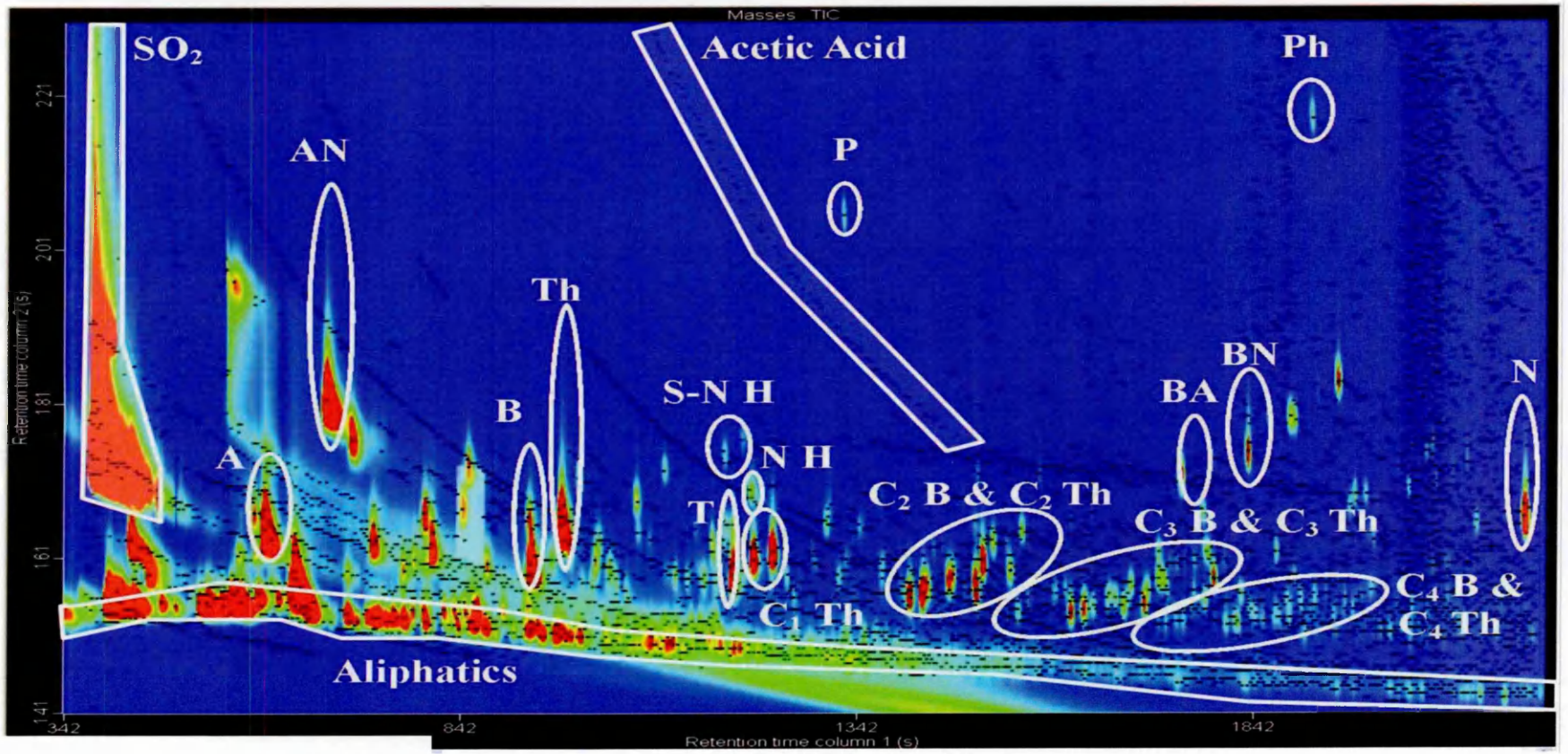

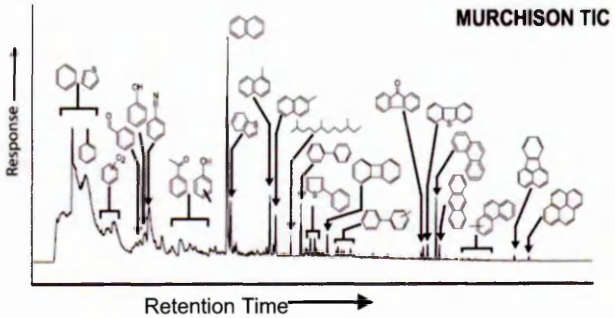

Figure 22: Above, a TIC of Murchison (pyrolysed to 632 °C for 2 s) identifying key species. A = acetone, AN = acetonitrile, B = benzene, BA = benzaldehyde, BN = benzonitrile, N= naphthalene, N H = nitrogen heterocycle, P = pyrrole, Ph = phenol, S-N H = sulphur-nitrogen heterocycle, T = toluene and Th = thiophene. Left, For comparison, an annotated Murchison TIC trace displaying dominant compounds (Pearson et al., 2006)

2D TIC. The 2D TIC is taken under standard pyrolysis conditions (610 °C for 2 s) with columns suited for volatile organic analysis up to naphthalene (128 amu). The volatile end of the GCMS TIC is dominated by one broad peak to which benzene, thiophene and methylbenzene have been assigned. The corresponding region on the 2D TIC illustrates multiple compounds identifiable in this region including sulphur dioxide, acetone, acetonitrile, benzene, thiophene and toluene. The 2D TIC also illustrates how clearly more polar compounds such as acetic acid and phenol can be identified, whilst the less polar fraction (i.e. column bleed) plots beneath the aliphatic species and does not obscure the analysis.

D) Limitations of GCxGC

Samples utilising pyrolysis GCxGC can not be set up as automated runs, and combined with the quantity of liquid nitrogen necessary, they require manual initiation of analyses. Due to separation on two columns, GCxGC has a higher peak capacity compared to conventional GCMS methods. Consequently, identifying key components within samples, more specifically identifying isomers that traditionally co-elute, takes a greater amount of time.

2.4.2. Time of Flight Mass Spectrometry (TOF-MS)

Mass spectrometry can identify and quantify individual components within a mixture in conjunction with the retention order of compounds as separated in the gas chromatography column. The limit of detection (i.e. the lowest concentration that can be established from a blank) is around 10^{-9} M depending on analytes, for conventional GC coupled to quadrupole mass spectrometer (Vandenabeele-Trambouze et al., 2001). The GCxGC thermal modulator traps, focuses and re-injects sample from the first column to the second column resulting in peak widths which are typically < 0.2 s (Marriott & Shellie, 2002), therefore requiring high spectral acquisition rates from the MS system. Scanning MS systems are not suitable for GCxGC because of mass spectral skewing (Marriott &

Shellie, 2002) and their spectral acquisition rates are too low, just a few scans per second. Time-of-flight MS (TOF-MS), capable of rapid spectral acquisition (>100 or more spectra per second) instantaneously records all masses in the chamber and is best suited for GCxGC applications.

TOF-MS, developed in the 1950's (Wiley & McLaren, 1955) involves acceleration of an ion of known electrical charge and unknown mass, by an electrical field of known strength within the mass spectrometer. Using the time of flight of the particle to reach the detector, along with known experimental parameters, the mass-to-charge ratio (m/z) of charged particles, atoms and molecules can be established.

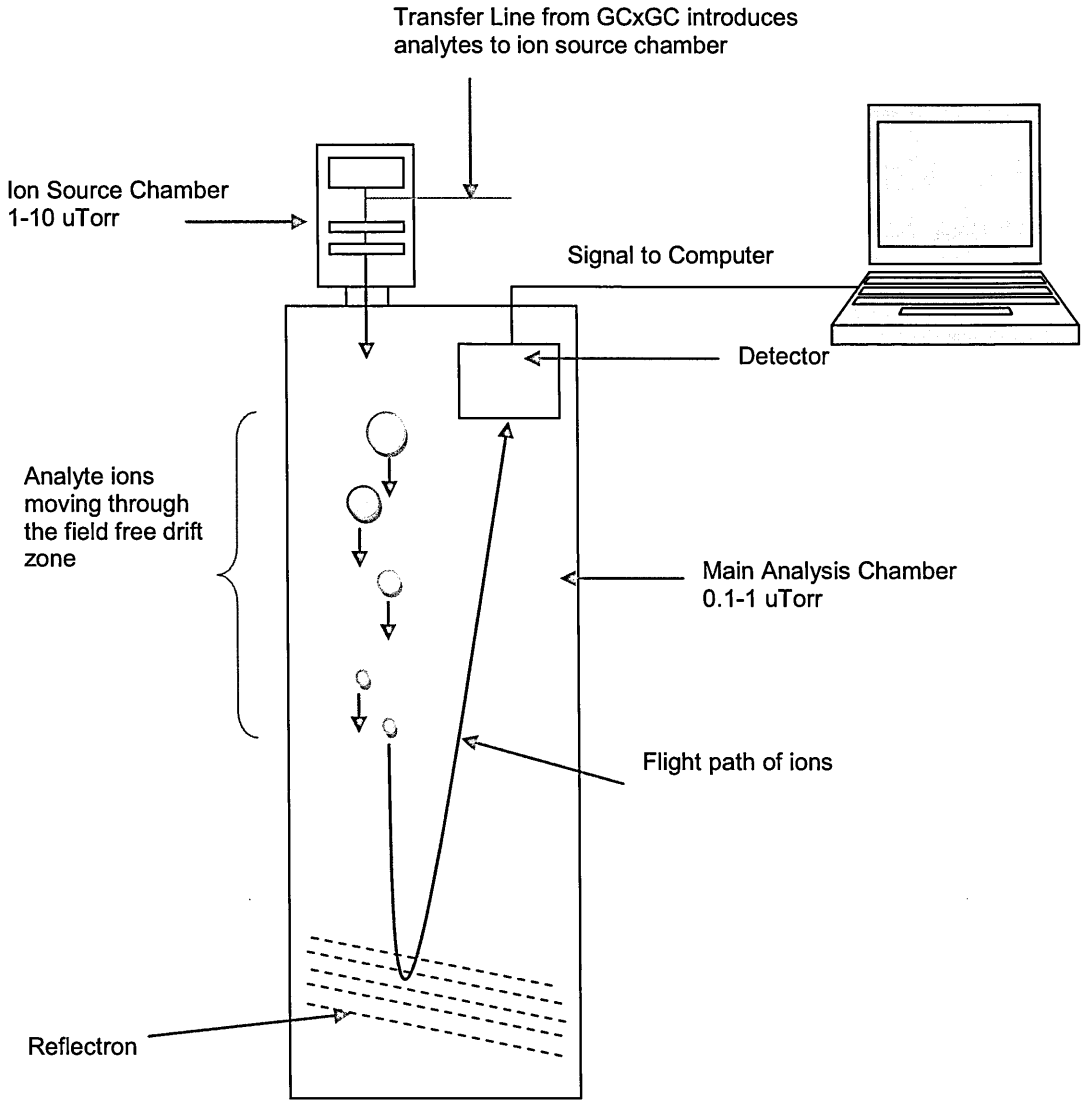

Figure 23: A schematic of the TOF-MS and the flight path of ions detected

The GC column outlet is passed through a heated transfer line, connecting the GC column oven to the MS ion source (Figure 23). Consequently, analytes separating from the GC column are fed directly into the electron impact ionisation source chamber with He carrier gas flow rate of 1 ml/min. Molecules introduced to the ion source chamber are ionised through bombardment with a beam of electrons (~ 70 eV).

As a result of increased internal energy during ionisation, these molecular ions may break up into varying amounts of fragment ions of lower masses. A mass spectrum is the fragmentation pattern unique for each molecule (relative amount vs. m/z ratio). Ions are pushed out of the ion source and those with equal kinetic energies have velocities dependant solely on their mass-to-charge ratios (m/z). The m/z of ions created is determined by measuring the time taken for ions to travel from the ion source to the detector, known as the time of flight. Ions of different m/z ratios have varying velocities, a heavier particle will have a lower velocity and a lighter particle will have a higher velocity.

Slight variations in ion kinetic energies results in differences of times-of-flight in ions of the same m/z ratio, affecting the mass resolution of the mass spectrometer. An electrostatic device known as a reflectron reflects the ion beam toward the detector allowing ions of differing energies to strike the detector simultaneously. This minimises the differences in ion time-of-flight, hence, improving mass resolution.

Ion detection is carried out using a microchannel plate type electron multiplier which amplifies the signal from one ion and facilitates ion detection and processing of the resulting signal. To ensure the survival of ions from the ion source to the detector, both the ion source chamber and the analyser chamber are under a vacuum.

A) Advantages and Limitations of TOFMS

Compared to alternative MS methods (e.g. quadrupole, ion trap and magnetic sector) TOFMS has a short mass spectrum acquisition time and allows simultaneous sampling of all ions in the ion chamber. This both greatly reduces the analysis time and

improves the quality of analytical results. It is highly sensitive, hence well suited to detecting trace levels of organics.

As TOFMS records all ions in the chamber a large amount of data can be accumulated (it is not unusual for meteorite chromatograms to contain thousands or tens of thousands of peaks). As a consequence data processing and analyte identification can be extremely time consuming and file sizes are extremely large (in the order of 1 GB per sample).

B) Data Processing

The increased resolution achieved by GCxGC results in the identification of a large number of peaks, on average approximately 12000 peaks per sample. As such, a partially automated system of deconvoluting peaks and processing data including computing the baseline, finding peaks, identifying peaks and measuring peak areas is employed using the Chromatof software. The data processing method used the parameters outlined in Table 18, along with peak measurements to correct for peak broadening on columns 1 and 2, before a library match was assigned to an unknown peak.

Data Processing Parameter	Volatile Organic Identification	High Molecular Weight Organic Identification	Notes
Baseline offset	0.5	0.5	Baseline = middle of noise
Data points for smoothing	3	7	
Max number unknown peaks	1000000	1000000	
Signal to noise ratio	25	25	
GCxGC match to combine	85%	85%	% match to combine markers as a single peak
Max molecular weight	400 amu	600 amu	
Min similarity for match	60%	60%	% match relative to library

Table 18: Data processing parameters for volatile organic and higher molecular weight organic compounds

In 2D chromatograms, the x-axis demonstrates retention times on the primary column (increasing volatility), the y-axis demonstrates retention times on the secondary column (increasing polarity). In 3D chromatograms the additional z-axis represents species abundance. Abundance is further highlighted in 2D and 3D chromatograms by

the automatically assigned contour colours - blue for species of lowest abundance through to red for species of highest abundance. Chromatograms are automatically scaled relative to the species of highest abundance. In the case of the 2D TIC in Figure 22 (pyrolysis of Murchison at 632 °C for 2 s) this is sulphur dioxide. As such, not all peaks are clearly visible in the TIC, as they have a very low abundance relative to sulphur dioxide. The Chromatof software, however, denotes a black peak marker (black dot) at the position of potential peaks. For example, in excess of 12000 peak makers were identified in the Murchison meteorite using the automated data processing software. In many cases groups of peak markers represented one individual organic species peak. Peaks are characterised using a combination of the 1D conventional chromatograms, the 2D chromatograms (like that in Figure 22) and the built in database of compounds.

2.4.3. GCxGC-TOFMS Experimental Conditions – Organic Volatile Analysis

GCxGC-TOFMS conditions were optimised, complimentary to column selection, for the analysis of volatile organic compounds up to the molecular weight of naphthalene. Pyrolysis products directly entered the injector inlet in split mode, which was sustained at 230 °C, the He (99.9999%) carrier gas was 1 ml/min during the entire run. The primary column (first dimension) situated in the primary oven, was a BP624 column (30 m x 250 µm x 1.4 µm) connected to the secondary (second dimension) BP20 column (2.0 m x 100 µm x 0.1 µm) housed in the secondary oven. Due to the nature of the column phases, the primary column had a maximum operational temperature of 230 °C.

The primary oven was held at 30 °C for 1 min, then raised to 230 °C at a rate of 5 °C/min and held for 10 mins. The secondary oven was offset by +15 °C from the primary oven. A liquid nitrogen cooled modulator was used with an offset from the primary oven of +30 °C for modulation on the secondary column, with a frequency of 3 s. The transfer line to the TOFMS was constant at 240 °C. The TOF-MS ion source was maintained at 230 °C, with an electron ionisation of -70 eV. The spectral acquisition rate was 200 spectra/s for a mass range of 33 – 401 amu.

2.4.4. GCxGC-TOFMS Experimental Conditions – Higher Molecular Weight Analysis

GCxGC-TOFMS conditions were optimised, complimentary to column selection, for the analysis of higher molecular weight compounds comprising polycyclic aromatic hydrocarbons (PAHs) up to pyrene. Pyrolysis products directly entered the injector inlet in split mode, which was sustained at 250 °C, the He (99.9999%) carrier gas was 1 ml/min during the entire run. The primary column (first dimension) situated in the primary oven, was a BPX5 column (30 m x 250 µm x 0.25 µm) connected to the secondary (second dimension) BPX50 column (1.8 m x 100 µm x 0.1 µm) housed in the secondary oven.

The primary oven was held at 35 °C for 1 min, then raised to 300 °C at a rate of 5 °C/min and held for 5 mins. The secondary oven was offset by +15 °C from the primary oven. A liquid nitrogen cooled modulator was used with an offset from the primary oven of +30 °C for modulation on the secondary column, with a frequency of 3 s. The transfer line to the TOFMS was constant at 280 °C. The TOF-MS ion source was maintained at 230 °C, with an electron ionisation of -70 eV. The spectral acquisition rate was 135 spectra/s for a mass range of 33 – 401 amu.

2.5. Summary of Experimental Development

Two flash heating techniques, the pyroprobe Pt coil and the Pyrola Pt filament, were assessed in terms of their ability to simulate short duration EDP entry heating conditions (between 400 – 1200 °C for durations of 2 – 20 s). The pyroprobe was unable to reach set temperatures for short durations of heating (2 s – 20 s) and additionally had poor reproducibility. The Pyrola, however, was able to reach set temperatures of ~1000 °C in as short as 2 s. As peak heating temperatures were recorded (by a photodiode and the resistance of the Pt filament) and were reproducible, the Pyrola was the most suitable method for simulating EDP atmospheric entry heating conditions.

Simulated residues were analysed using two techniques – elemental analysis and thermogravimetric analysis. Preliminary investigations demonstrated that carbon was lost during EDP entry heating simulations, however elemental analysis was unable to characterise the nature of surviving carbon (Section 2.3.2). Thermogravimetric and evolved gas analysis of simulated residues were capable of identifying remaining volatiles (H_2O, N_2/CO, CO_2, O_2 and SO_2), with the ability to determine their source within the sample (Chapter 3).

Online experiments, with the Pyrola coupled to a Pegasus 4D GCxGC-TOFMS, enabled the identification of organic species released from samples during simulations (Chapter 3). As the GCxGC system gives a greater separation of analytes in comparison to standard GCMS techniques, it is ideally suited to characterising the complex organic composition of released species from EDP simulations. As the Pyrola is ideal for handling small sample masses, coupled to the GCxGC-TOFMS, it was utilised to analyse the complex organic composition of clusters of micrometeorite particles and their terrestrial counterparts (Chapter 4).

3. The Release of Organic Material from EDPs During Atmospheric Entry: A Simulation Study

3.1. Introduction and Review of Previous Simulation Studies

One source for the organic components needed for the birth of life on Earth could be from extraterrestrial sources such as comets (Chyba et al., 1990; Oro, 1961), asteroids (Anders, 1989) or extraterrestrial dust particles (EDPs) (Anders, 1989; Maurette, 1998). As asteroid and cometary impacts occur at high velocities, on average ~ 20 km/s (Stuart & Binzel, 2004) and 55 km/s (Artemieva & Shuvalov, 2008) respectively, the majority of the impactor is vaporised along with the target rocks in the vicinity of the impact (Pierazzo et al., 1997; Pierazzo et al., 1998), damaging the immediate terrestrial environment and limiting the survival potential of any organic species they contain (Anders, 1989). EDPs, in contrast, predominantly travel at lower velocities <20 km/s and experience aerodynamic braking during atmospheric entry (Section 1.6), thus decreasing their velocity and enabling them to settle to the surface rather than "impact".

Some EDPs have been found to retain a range of organic molecules, broadly similar to those in carbonaceous chondrites (Section 1.4.4). Consequently, it has been suggested that unmelted EDPs, that have not experienced extreme heating, may therefore have been a significant contributor to the terrestrial organic inventory (Anders, 1989; Maurette, 1998).

EDPs make up the majority of extraterrestrial materials delivered to the present day Earth (Anders, 1989; Flynn et al., 2004), with a present day flux in the region of 2-4 x 10^7 kg yr^{-1} (Love & Brownlee, 1993; Maurette et al., 1990). However, it is estimated that the total flux of extraterrestrial material on the early Earth from 3.8 – 4.5 Ga ago was between 10^2 to 10^7 times higher than that of the present day (Hartmann et al., 2000), with

a mid-range value of 10^5 times the present flux over this time period. There is evidence from the similarity in the abundances of volatile elements in the Earth's crust and CI chondrites, to suggest that significant amounts of C, N and H and other volatile elements were acquired as a late veneer of carbonaceous material (Anders, 1968; Anders & Owen, 1977), a process that would have continued through the late stages of the Earth's accretion. Passing through the primitive Earth's atmosphere and depositing evaporated and volatilised species, EDPs may have contributed to atmospheric evolution. Additionally, the delivery of retained EDP organic molecules and volatiles to the early Earth's surface, may have served as a reservoir of suitable raw materials for pre-biotic evolution or even sustenance for emerging life (Anders, 1989; Maurette, 1998; Maurette, 2006a; Maurette et al., 1995). This concept is applicable to any young planetary surface, for example, that of Mars. However, understanding the role that EDPs may have played in contributing to the organic inventory of the early Earth and Mars requires a better comprehension of the processes affecting EDPs during their atmospheric entry.

Direct observation of the ablation products of meteors during atmospheric entry is problematic: atomic carbon does not have strong optical emissions in the visible or near-IR making remote sensing difficult. Smaller molecules are more easily detected; e.g. CN, CH and C_2. Recently, near-IR spectra of Leonid meteors demonstrate that they lack or contain very low abundances of CN (Jenniskens et al., 2004; Taylor et al., 2007) and atomic carbon emission features (Taylor et al., 2007), suggesting that organic matter from meteors does not decompose into smaller constituents upon ablation. Instead, it is thought that larger organic compounds are evolved from meteors during their descent through the atmosphere (Jenniskens et al., 2004).

Experimental simulations provide a means of assessing the changing mineralogy, morphology and elemental chemistry of EDPs during atmospheric entry heating (Greshake et al 1995; Greshake et al., 1995; Greshake et al., 1995; Greshake et al., 1998; Toppani et al., 2000; Toppani et al., 2001; Toppani et al., 2003), providing potentially much greater chemical information than can be obtained by remote sensing,

although it is important to bear in mind that simulations are invariably conducted on materials thought to be analogous with EDPs. Consequently, experimental simulations have generally flash heated carbonaceous chondrite fragments using a variety of methods for a range of durations and peak temperatures.

For the majority of studies, furnaces and ovens have been the preferred heating method for EDP atmospheric entry heating simulations (Fraundorf et al., 1982; Greshake et al., 1995; Greshake et al., 1998; Toppani et al., 2000; Toppani et al., 2001; Toppani et al., 2003). Fraundordf et al., (1982) used a resistively heated tantalum ribbon to heat Murchison and Orgueil fragments of uncharacterised size to 400-1100°C for ~30 s. Two 0.5-1 mm chromel-allumel thermocouples were positioned in contact with the heated tantalum ribbon and the sample holder, with one additional thermocouple free floating between the two. The thermocouples recorded temperatures ± 50 °C of each other. Fraundorf et al. (1982) also noted that the temperature of the sample holder lagged by approximately 15 s behind that of the heated ribbon, most noticeably at lower temperatures. Despite these inaccuracies in peak heating temperature, Fraundorf et al., (1982) recorded a decrease in S/Fe ratios in Murchison fragments heated to 800-1100°C associated with release of sulphur during the degradation of S-bearing minerals (sulphides) in Orgueil and Murchison (Gao & Thiemens, 1993) accounting for the S depletions found in micrometeorites (Greshake et al., 1995; Kurat et al., 1994).

Greshake et al., (1998) conducted short duration heating experiments on 50-100 μm fragments of Orgueil and Alais heated to 700-1250 °C, using a high temperature furnace, for durations of 10-60 s. The furnace consisted of four silicon carbide heating elements, capable of heating to 1700 °C with an error of ± 3 °C. Although these authors report that a Pt-PtRh thermocouple was placed in the furnace adjacent to the sample, they do not give the peak temperature of their furnace during simulations. In addition, the peak temperature the samples experience during heating is not measured; hence the temperature conditions during simulations are not well constrained. Results show the loss of volatile elements (S, Zn, Ga, Ge and Se) and the alteration of phyllosilicates to olivine

and pyroxenes were a consequence of the short heating duration used. However, the reliability of these findings is uncertain due to the lack of temperature constraints on the initial heating experiments.

Toppani et al., (2000; 2001; 2003) heated 200-400 μm sized fragments of Murchison and Orgueil to 500-1500 °C in a closed vertical furnace for durations between 2-120 s. A $PtRh_{10}$-Pt thermocouple recorded the temperature of the hot zone of the furnace. Samples were placed in Pt buckets surrounded by Pt wire spirals, facilitating conduction during heating. Toppani et al., (2001) confirmed large depletions of sulphur in flash heated samples in addition to textural changes, consistent with sulphur volatisation during entry heating (Greenwood & Hutchison, 1993).

Heating conditions	Sample	Observations
20 s at 1000 °C compared to 500 °C	Murchison	Increase in dehydration cracks, decrease in volume attributed to dehydration of layer silicates. No formation of polycrystalline spinel.
20s at 1200 °C	Murchison	Abundant vesicles, anhydrous silicates present, continuous polycrystalline spinel rim.
20 s at 1350 °C	Murchison	Recrystallisation texture, vesicles outlined with spinel rim, continuous polycrystalline spinel rim surround entire particle,
20 s at 1500 °C	Murchison	Completely melted particle, quench dendritic spinel, scarce anhydrous silicates.

Table 19: A summary of textural and mineralogical observations in atmospheric entry heating simulations of 200-400 μm sized Murchison fragments from Toppani et al., (2001)

Heating Duration/ Temperature	1200 °C	1350 °C
5 s	no spinel rim, no recrystallised spinel, minor dehydration cracks, magnetite and iron-rich phases destabilise leading to iron-rich domains along dehydration cracks.	ovoid vesicles, increased vesiculation towards particle edge, spinel rim, minute spinels embedded in the fragment.
10 s	same observations as 5 s at 1200 oC	partial melting of fragments, small spinel crystals and euhedral anhydrous silicates occur toward the core of the particle, significant vesiculation, spinel rim
20 s	polycrystalline spinel rim.	same observations as 10 s at 1350 °C
40 s	abundant vesiculation and increased thickness of spinel rim.	prominent recrystallisation texture (anhydrous silicates and spinel embedded in glass), less continuous spinel rim than shorter durations
120 s	not determined	large recrystallised zoned anhydrous silicates and spinels. No spinel rim.

Table 20: A summary of textural and mineralogical observations in heating simulations of 200-400 μm sized Orgueil fragments varying with simulation temperature and duration from Toppani et al., (2001)

Textural and mineralogical analyses of heated fragments of Orgueil allowed the estimation of peak temperatures and durations required to produce EDP textures such as

fine grained particles, dehydration cracks, vesicular particles and completely melted spherules (Figure 5, Section 1.6.2) and are summarised in Table 19 and Table 20.

Klöck et al., (1994) heated 100 μm sized fragments of carbonaceous chondrites to 600-1200 °C in quartz capillary tubes for durations of 20-60 s. The authors do not elaborate on the method of heating, nor the apparatus used to establish sample heating temperatures. As such, no assessment of heating accuracy and reproducibility can be determined. Klöck et al., (1994) observed Zn, Ge and Ga loss in heated samples in addition to the dehydration of phyllosilicates at higher temperatures, however with no constraints on the temperature samples experience, the validity of their results is questionable.

Theoretical modelling indicates that particles up to 100 μm in size typically experience peak temperatures of between 600–1700 °C for periods of approximately 1-5 s (Flynn, 1989a; Love & Brownlee, 1991). Analysis of EDPs show they are not fully melted suggesting that they experience lower temperatures (perhaps <600 °C) on passage through the atmosphere. A number of limitations can be identified in the previous experimental simulations discussed above: (a) most have not accurately monitored peak heating conditions and (b) they have not (with the exception of Toppani et al., (2001)) simulated peak temperatures for periods as short as 2 s duration.

To date, few studies have been conducted to assess the survival of carbonaceous species in flash heated EDP analogues (Brownlee et al., 2001; Kress & Brownlee, 2002; Wright et al., 2000). Undetermined sized fragments of Allende (CV3), Weston (H4) and Goalpara (ureilite) meteorites were flash heated within a quartz tube in a high-temperature furnace to 800 °C and 1500 °C (Wright et al., 2000). Although the furnace temperature was monitored by a Pt-Rh thermocouple, the sample temperature within the quartz tube was not recorded. Using stepped combustion, a technique able to distinguish different carbon components, Wright et al., (2000) were able to establish that only refractory carbonaceous material within the 800-1200 °C combustion steps, survived their flash heating experiments. It has been suggested that this char-like material is a by-product of

flash heating following the decomposition of existing carbon bearing components (Kress & Brownlee, 2002).

3.2. Aims and Objectives

Previous work (Greshake et al., 1998; Love & Brownlee, 1991; Toppani et al., 2001) has shown that EDPs experience a range of heating regimes during atmospheric entry dependant on EDP size, entry velocity and entry angle. As discussed in the previous section, experimental simulations have also generally focussed on changes in mineralogy or elemental composition (Greshake et al., 1998; Klöck et al., 1994; Toppani et al., 2001; Fraundorf et al., 1982). Substantial loss of S (Fraundorf et al., 1982; Greshake et al., 1998; Toppani et al., 2001), Zn (Greshake et al., 1995; Klöck et al., 1994), Ge (Greshake et al., 1995), Ga (Greshake et al., 1998; Klöck et al., 1994) have been reported, in addition to the dehydration of phyllosilicates to olivine and pyroxenes (Greshake et al., 1998; Toppani et al., 2001). Few studies of the carbonaceous components have been undertaken; those conducted have suggested that only refractory components survive atmospheric entry heating (Brownlee et al., 2001; Kress & Brownlee, 2002; Wright et al., 2000).

This study aims to characterise the volatile and organic components released or retained during "flash" heating simulations. It examines the effects of heating on the abundance and distribution of volatile components (such as H_2O, CO_2), volatile organic compounds and polycyclic aromatic hydrocarbons (PAHs) in EDPs over a range of peak temperatures (400-1000 °C) and heating durations (2-20 s). For the purposes of the simulation, chondritic meteoritic material is used as an analogue for EDPs (Section 2.1.3).

3.3. Experimental

3.3.1. Simulation Method and Samples

Between 50 and 150 replicates of 0.9 mg samples of supercritical fluid extracted (SFE) Murchison residue (see Section 2.1.3 for a full description of samples) were pyrolysed offline using a Pyrolab Pyrola 2000 (Section 2.2.3), to the temperatures and durations described in Table 21. SFE residues were used as they minimise the risk of terrestrial contamination by volatile species, which are removed by the SFE extraction (Sephton et al., 2001). Although SFE extraction, using high purity carbon dioxide, will also remove some non-polar indigenous organic matter, the majority of the indigenous polar species and the predominant macromolecular organic component of CM chondrites is left intact (Sephton et al., 2001b). Simulations were conducted in a He carrier gas (flow rate 20ml/min), creating a chemically inert environment. 3.5 mg of heated residues were collected for thermogravimetric and evolved gas analysis.

Simulation Duration (s)	Simulation Temperature (°C)	Average Peak Simulation Temperature (°C)
2	400	406 ± 8
2	600	603 ± 9
2	800	814 ± 13
2	1000	1006 ± 59
5	400	409 ± 12
5	600	599 ± 16
5	800	790 ± 18
5	1000	1003 ± 30

Table 21: Offline simulation conditions. Errors of 2 σ are given for up to 80 replicates of each sample

3.3.2. Thermogravimetric and Evolved Gas Analysis

3–3.5 mg of each sample (comprising up to 80 replicates for each offline simulation condition, and the Murchison reference sample) was analysed by thermogravimetric (TG) and evolved gas (EG) analysis as described in Section 2.3.4. TG analysis was used to determine the percentage mass of evolved gas remaining in flash heated residues, with EG analysis enabling characterisation of the remaining volatiles. Release of inorganic and organic components were monitored including H_2O, CO or N_2,

O_2, CO_2, and SO_2. Volatile components are responsible for evolved gas species released at < 600 °C, whilst evolved species at > 600 °C derive primarily from the decomposition of minerals. While the analytical method provides data on the volatile components remaining after each flash heating simulation, it is also possible to determine, by difference, both the amount and composition of volatiles released in each flash heating experiment.

3.3.3. Py-GCxGC-TOFMS – Volatile Organic Analysis

Organic species evolved as a result of flash heating were studied using an online approach, i.e. direct coupling of the pyrolyser to the analytical instrument. This enabled individual 0.9 mg samples of SFE Murchison to be studied in heating simulations using the Pyrola 2000 coupled to a GCxGC-TOFMS, optimised to characterise the volatile organic species released over a range of different peak temperatures and durations (Section 2.4). Heating temperatures and durations are outlined in Table 22. For comparison, one 0.9 mg sample of unheated SFE Murchison (referred to hereafter as the Murchison reference sample) was analysed under standard pyrolysis conditions (610 °C for 2 s).

Simulation Duration (s)	Simulation Temperature (°C)	Simulation Peak Temperature for Volatile Organic Compound Analysis (°C)	Simulation Peak Temperature for PAH Analysis (°C)
(Murchison reference sample)			
2	610	632	598
2	400	425	395
2	800	834	829
2	1000	1026	1005
5	400	404	396
5	600	599	605
5	800	802	805
5	1000	1009	999
20	400	438	420
20	600	614	634
20	800	801	810
20	1000	992	962

Table 22: Simulation conditions for volatile organic and PAH characterization used during online simulation experiments

The pyrolysis chamber was maintained at 200 °C, with pyrolysis temperatures accurately monitored using both filament resistance and a photodiode. The injector inlet, in split mode, had a split flow of 5 ml/min and a total flow of 6 ml/min. The inlet was sustained at 230 °C, the He (99.9999%) carrier gas had a flow of 1 ml/min during the entire run. The primary column (first dimension) situated in the primary oven, was a BP624 column (30 m x 250 µm x 1.4 µm) connected to the secondary (second dimension), BP20 column (2.0 m x 100 µm x 0.1 µm) housed in the secondary oven. The BP624 column was coated with a polar phase, ideally suited for volatile organic compound and alcohol analysis. The BP20 is coated with a very polar phase suited for alcohol, ester, ketone and aldehyde analysis. Due to the nature of the column phases, the primary column had a maximum operational temperature of 230 °C. As such, these columns were selected to optimise the analysis of volatile organic species from the samples but it was not possible to use them to analyse higher molecular weight material. A second set of online simulations using the same samples and similar conditions was carried out using a column set and GCxGC conditions optimised for PAH identification (Section 3.3.4).

The primary oven was held at 30 °C for 1 min, then raised to 230 °C at a rate of 5 °C/min and held for 10 mins. The secondary oven was offset by +15 °C from the primary oven. A liquid nitrogen cooled modulator was used with an offset from the primary oven of +30 °C for modulation on the secondary column, with a frequency of 3 s. The transfer line to the TOFMS was constant at 240 °C. The acquisition rate was 200 spectra/s for a mass range of 33-401 amu.

3.3.4. Py-GCxGC-TOFMS – Analysis of PAHs and high molecular weight species

Different analytical conditions were required to study the higher molecular weight species evolved. As with volatile species, individual 0.9 mg samples of SFE Murchison were heated in online simulations for similar peak temperatures and durations. Flash

heating was conducted online according to the conditions outlined on Table 22, using a Pyrola 2000 (Pyrolab, Sweden) coupled to a Pegasus 4D GCxGC-TOFMS (LECO Corporation). For comparison, one 0.9 mg sample of Murchison reference material was analysed under standard pyrolysis conditions (610 °C for 2 s).

Conditions were as described in Section 3.3.3 with the following exceptions. The pyrolysis chamber was maintained at 175 °C, and the injector inlet held at 250 °C. The primary column (first dimension) was a BPX5 column (30 m x 250 µm x 1.4 µm) connected to the secondary (second dimension), BPX50 column (2.0 m x 100 µm x 0.1 µm). With their high maximum operating temperature of 370 °C, they are ideally suited to the analysis of higher molecular weight organics.

The primary oven was held at 35 °C for 1 min, then raised to 300 °C at a rate of 5 °C/min and held for 5 mins. The secondary oven was offset by +15 °C from the primary oven. A liquid nitrogen cooled modulator was used with an offset from the primary oven of +30 °C for modulation on the secondary column, with a frequency of 4 s. The transfer line to the TOFMS was constant at 280 °C. The acquisition rate was 135 spectra/s for a mass range of 33-401 amu.

3.4. Results and Discussion

3.4.1. Thermogravimetric and Evolved Gas Analysis of Unheated Samples

Thermogravimetric analysis reveals that Murchison reference material contains a total of 14.7 wt % evolved species corresponding to total percentage mass loss (Figure 24). As indicated by the steeper gradient in the mass loss profile (red line), there is an increase in mass loss between 300 – 550 °C. Evolved gas analysis (EGA) enables these individual evolved species to be characterised, which correspond predominantly to the release of H_2O and CO_2 (Figure 24) further discussed below.

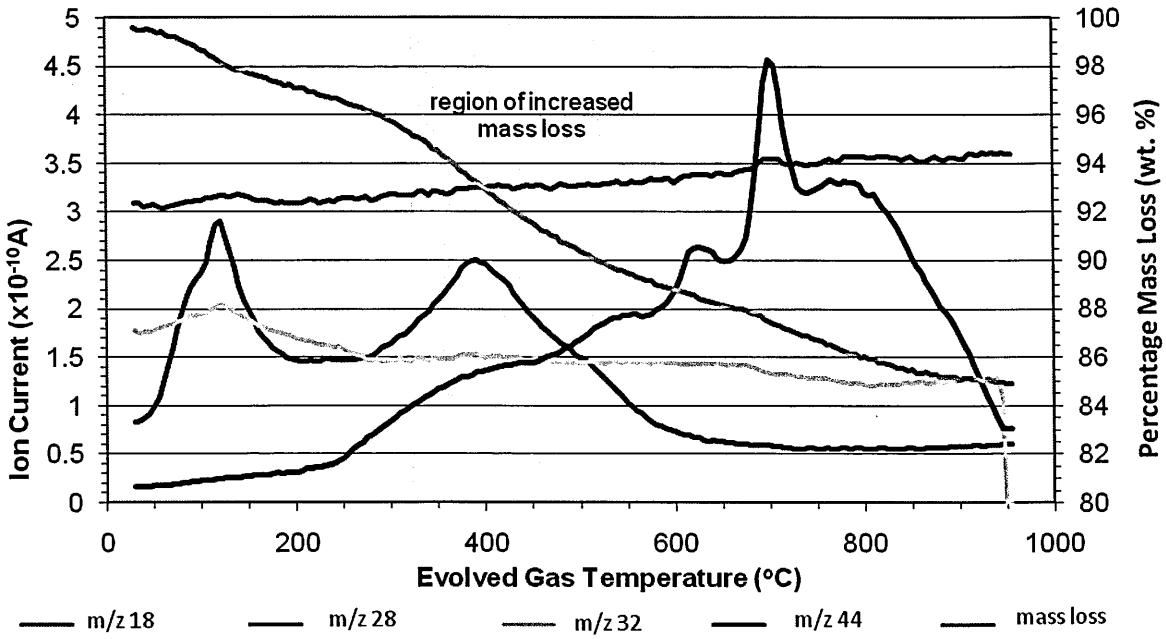

Figure 24: The correlation between percentage sample mass and evolved gas release in a SFE Murchison sample (non simulated) as determined by thermogravimetric and evolved gas analysis

A. Water (m/z 18)

The abundance of m/z 18 (water) released from Murchison reference material at evolved gas temperatures 0-950 °C is shown in Figure 25. There are two identifiable peaks – [i] a sharp peak at 117 °C and [ii] a broader peak at 386 °C. The exposure of the sample to low temperatures during EGA (< 250 °C) removes adsorbed water (Parsons et al., 1997) and the weakly bonded water from hydrated minerals such as phyllosilicates or sulphates (gypsum) (Morris, 2008), corresponding to peak [i]. Peak [ii] is consistent with the removal of structurally bound water (OH^-) released upon the dehydration of clay minerals (Morris, 2008; Wicks & Ramik, 1990) at EG temperatures in excess of 300 °C. Notably the Fe-phyllosilicate cronstedtite, which exhibits a very broad evolved CO_2 peak at 416 °C, has been matched to Murchison structural water which exhibits a peak at 386 °C (Morris, 2008). Peak [ii] is very broad; Morris (2008) has postulated that a second poorly resolved Mg-phyllosilicate, an intermediate between Fe- and Mg- end member serpentines, is a contributor of evolved H_2O at ~500 °C. Murchison matrix material analysed in this study may therefore contain cronstedtite (Buseck & Hua, 1993; Brearley &

Jones, 1998) and minor clay minerals (tochinilite/ Mg-, Fe-serpentines). The dehydration of organic species such as alcohols (Fox & Whitesell, 2004; Kristensen, 1990) may be a minor contributor to EG evolved water.

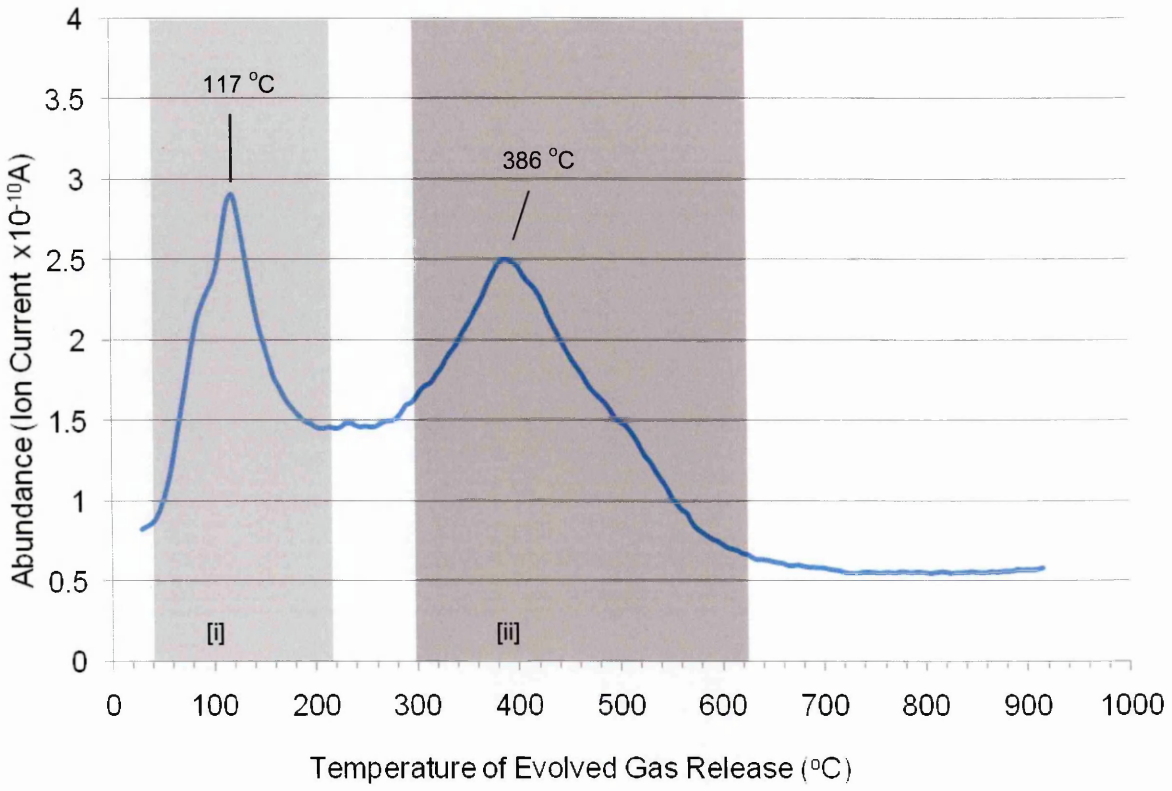

Figure 25: Evolved gas release of H_2O in an unheated reference Murchison sample. Peaks [i] and [ii] correspond to adsorbed and mineral bound water respectively

B. Carbon Dioxide (m/z 44)

Figure 26 displays multiple m/z 44 peaks present in Murchison reference material, primarily within regions [a], [b] and [c], representing CO_2 releases. CO_2 evolved at 300-600 °C (broad peak [a]) represent organic carbon (Lauer et al., 2006) and can be attributed to CO_2 generated by the degradation of organic components (Rodante, 1992; Shimoyama, 1997; Wright et al., 1997). Typically, free organics and the more thermally labile side-chain components will be released at temperatures <350 °C as a result of the decarboxylation of carboxylic (Blake & Jackson, 1969; Kristensen, 1990) and amino acids (Bada, 1991) and the cleaving of weak bonds. Evolved gas temperatures between 350-600 °C predominantly correspond to the thermal degradation macromolecular material (Kristensen, 1990), or its oxidation by matrix components e.g. metal cations (Shiota et al.,

2005) derived from oxide minerals present in the Murchison matrix. The release of CO_2 over such a large temperature range is reflective of several phases of organic matter present in the sample.

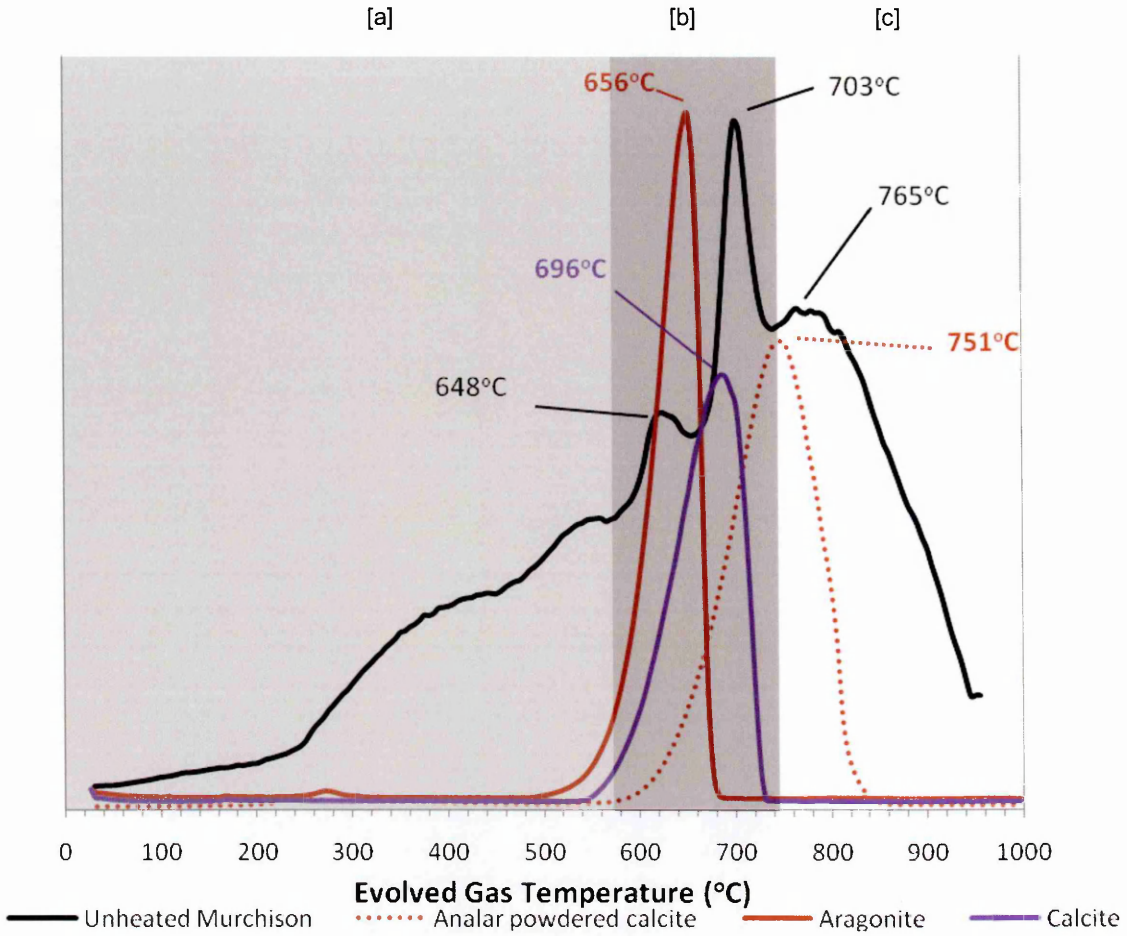

Figure 26: Evolved gas traces for CO_2 in unheated Murchison, terrestrial aragonite[1], terrestrial calcite[1] and Analar grade calcite[1]. Murchison peaks in regions [a] correspond to organic material, peaks in regions [b] and [c] correspond to carbonate material. 1 – M.Miller (*unpublished data*)

CO_2 evolved in excess of 600 °C, peaks b and c, are most probably the result of decarbonation of carbonate minerals. Carbonates in Murchison comprise ~ 0.4 vol.% (Brearley et al., 1999) and consist of calcite, aragonite with minor dolomite (Barber, 1981; Benedix et al., 2003; Brearley & Jones, 1998; Brearley et al., 1999). Table 23 summarises the decarbonation temperatures of common carbonate species, in addition to their associated CO_2 EG peak temperatures compiled from ExoMars TEGA data (Lauer et al., 2000), controlled carbonate decomposition experiments (Engler et al., 1988) and routine analysis of pristine carbonates (M.Miller *unpublished data,* Figure 26). Evolved

CO_2 at 648 °C (Figure 3) is attributed to aragonite, a minor carbonate component in the Murchison matrix (Barber, 1981; Brearley & Jones, 1998), typically released at 656 °C (Table 23).

Carbonate	Temperature of decomposition/ decarbonation[1]	Evolved CO_2 peak temperatures[2]
Aragonite	793-803 (decomposes to calcite)	656×
Calcite	1067 – 1177 830 – 940 *	751× 700◆ (finely ground)
Dolomite	-	650-750• 550-765+
Magnesite	867-897	615
Siderite	773	500-533, 600
Rhodocrocite	-	524-560, 545-610
Smithsonite	-	495, >730
Nesquehonite	-	170, 450, 537
Hydromagnesite	460-543	240, 450

Table 23: Decarbonation temperature of common carbonates and their evolved CO2 peak positions. (1- Boynton et al. 2001 and references there in, 2 - Lauer et al. 2000, * Blazek 1973, + - Engler et al. 1988, ×- M.Miller (*unpublished data*), ◆ - Norman & Palin (1982), • - Lauer et al., (2006))

Assigning the peaks at 703 °C and 765 °C is more complex. Calcite, the dominant carbonate in Murchison (Barber, 1981), typically evolves CO_2 at 751 °C (M.Miller *unpublished data,* Figure 26) and is assigned to the broad peak at 765 °C. Despite no petrographic evidence of dolomite within Murchison, the presence of this carbonate has been inferred from observations of released CO_2 in oxygen isotope extractions (Benedix et al., 2003). It is possible that dolomite may also be contributing to this peak wither the 703 °C or 765 °C evolved CO_2 peaks. Typically dolomite evolves CO_2 in two stages over 550-750 °C (Engler et al., 1988; Lauer et al., 2006), but at low concentrations it will evolve under one peak at 750-775 °C (Parsons et al., 1997) making it indistinguishable from calcite (Milodowski & Morgan, 1980; Parsons et al., 1997).

Finely ground calcite evolves CO_2 at 700 °C (Norman & Palin, 1982). Calcite does occur in Murchison as 1-80 μm sized grains (Fuchs et al., 1973), it is likely the decarbonation of this fine-grained component is contributing to the peak at 703 °C (Figure 26). In addition, the combustion of kerogen with H_2O and O_2 evolved from Murchison components (e.g. phyllosilicates, sulphates) may also be a contributor to CO_2 evolved between 650-750 °C (Lauer et al., 2006; Parsons et al., 1997). Furthermore, graphite

comprises ~2 ppm in CM2 chondrites (Anders and Zinner, 1993), it combusts between 700-900 °C (Wright & Pillinger, 1998) and may be contributing to peak [c].

C. Nitrogen (m/z 28), Carbon monoxide (m/z 28), Oxygen (m/z 32) and Sulphur Dioxide (m/z 64)

There are minor m/z 28 peaks at 150 °C and 700 °C (Figure 24). The peak at 150 °C represents the liberation of nitrogen from N-bearing organic species (e.g. N-heterocycles, nitriles, amines, amides) (Pizzarello et al., 1994; Stoks & Schwartz, 1982) and nitride grains (Hoppe et al., 1996). The peak at 700 °C is most likely attributed to a CO release associated with decarbonation of carbonates (M.Miller, *unpublished data*) or a consequence of evolved carbon dioxide reacting with residual carbon via the Boudouard reaction (Basu, 2006). A minor peak of m/z 32, representing oxygen, was identified at 120 °C, which coincides with the release of adsorbed water within the matrix material.

Murchison has a total sulphur content of 1.6-4.1 wt.% (Fuchs et al., 1973) comprising S-bearing minerals sulphides (troilite and pentlandite), the sulphate gypsum and organic sulphur (S-heterocycles, N-S heterocycles). Despite relatively high sulphur content, evolved sulphur dioxide (m/z 64) from unheated Murchison was negligible (Figure 27) compared to that of water or carbon dioxide. This suggests that sulphur containing materials within Murchison are perhaps more resistant to thermal degradation and may require intensive conditions i.e. oxidation for their release. As such, sulphur may have been retained in meteoritic and EDP materials without contributing substantial release into the early Earth atmosphere.

Although previous studies have focussed on the volatisation and subsequent loss of sulphur during flash heating (Fraundorf et al., 1982; Toppani et al., 2001), sulphur containing material in this study constitute very minor components in the Murchison reference sample relative to the dominant evolved H_2O and CO_2 peaks. Consequently, it was not possible to determine sulphur bearing components from evolved SO_2 gas species of simulated samples.

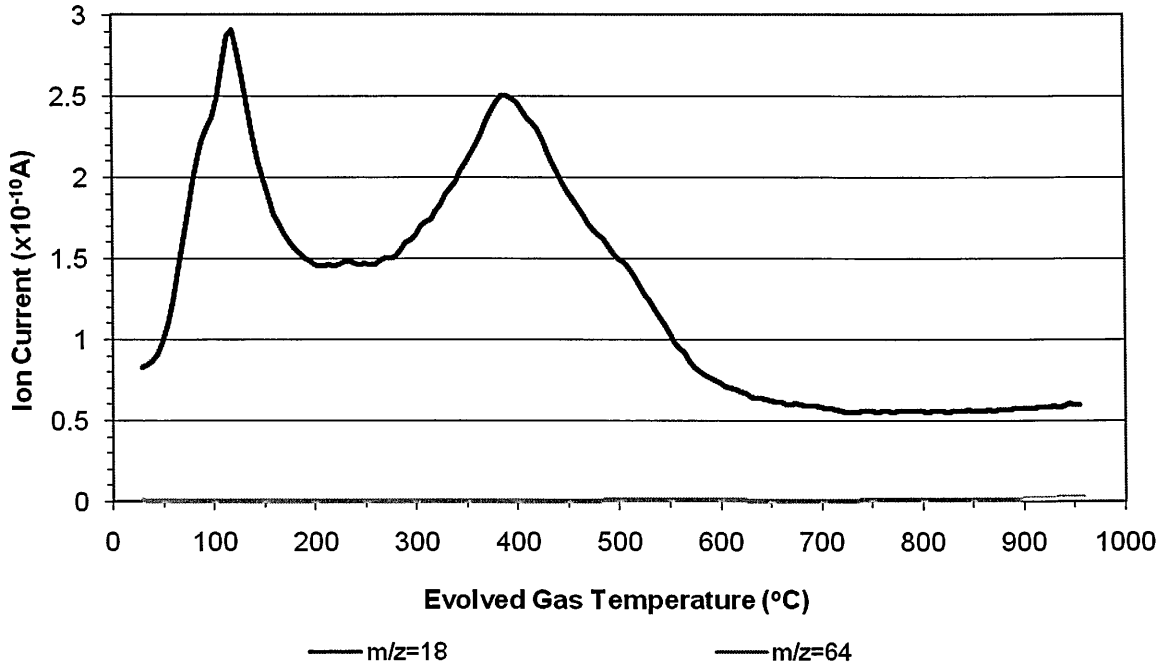

Figure 27: Evolved gas release of sulphur dioxide (m/z 64) in comparison to water (m/z 18) in a SFE Murchison reference sample (unheated) as determined by evolved gas analysis

3.4.2. Volatile Survival in Flash Heated Residues

A. Evolved Gas Content

Figure 28 shows the percentage mass loss from flash heated residues corresponding to total evolved gas. Residues collected from higher peak simulation temperatures contain less evolved species than those from lower peak simulation temperatures because of the cumulative loss of volatile species via the processes outlined in Section 3.4.1. For example, residues collected from simulations of 2 s to 814 °C contain just 3.9 wt. % evolved species, whilst residues from simulations of 2 s to 406 °C contain 12.4 wt. % evolved species. Even simulated residues collected from exposure to temperatures of 1006 °C for 2 s show the presence of 1.1 wt. % evolved gases. The same trend can be seen for the longer simulation duration of 5 s.

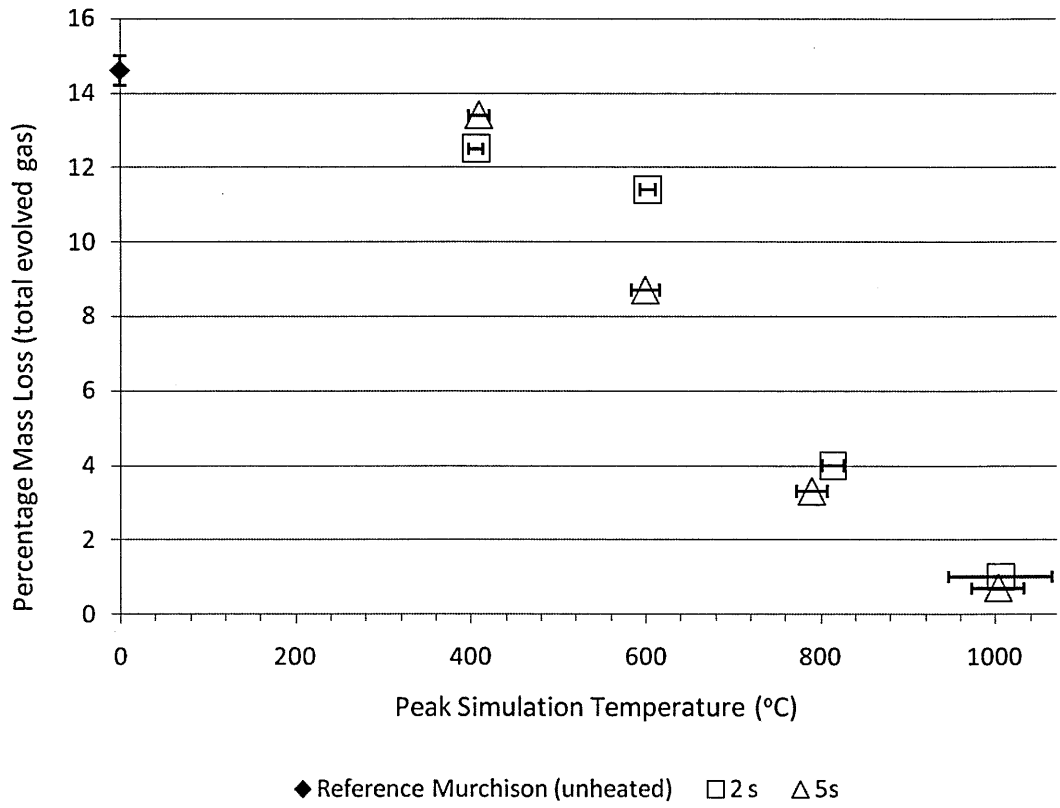

Figure 28: Total evolved gas (wt. %) in unheated reference Murchison and in flash heated samples of Murchison heated to a range of peak temperatures and durations of 2s and 5s (errors to 2σ)

B. Evolved CO_2

Although evolved gas traces of individual samples are not directly comparable in terms of peak abundances, their peak positions can demonstrate the source of evolved species within simulated residues. Figure 29 and Figure 30 shows the CO_2 evolved gas profiles for residues simulated for 2 s and 5 s respectively. The Murchison reference sample is dominated by a broad peak [a] representative of organic species and several carbonate peaks within region [b]. As simulation temperature increases, peaks [a] and [b] both progressively become absent, with peak [c] dominating in samples heated to 1006 °C and 1003 °C for 2 s and 5 s respectively. Samples heated to 600 °C have lost organic carbon but retain carbon within carbonate minerals, whilst samples heated to > 600 °C have lost organic carbon and a portion of their inorganic carbon via carbonate decomposition. The loss of organic carbon and carbon bound within carbonate minerals via decomposition, decarboxylation and decarbonation (as discussed in Section 3.4.1)

and their subsequent survival in samples is directly related to their peak simulation temperature.

In samples heated to 1003 °C for 5 s and 814 °C for 2 s, there is a minor peak at ~220 °C corresponding to organic carbon. During flash heating, macromolecular material may react with degradation products (Lauer et al., 2006) (e.g. H_2O and O_2 released from phyllosilicates or organic components) producing volatile organics such as carboxylic acids and CO_2 (Larson & Ji, 2000) which may account for the minor presence of organic material in these samples.

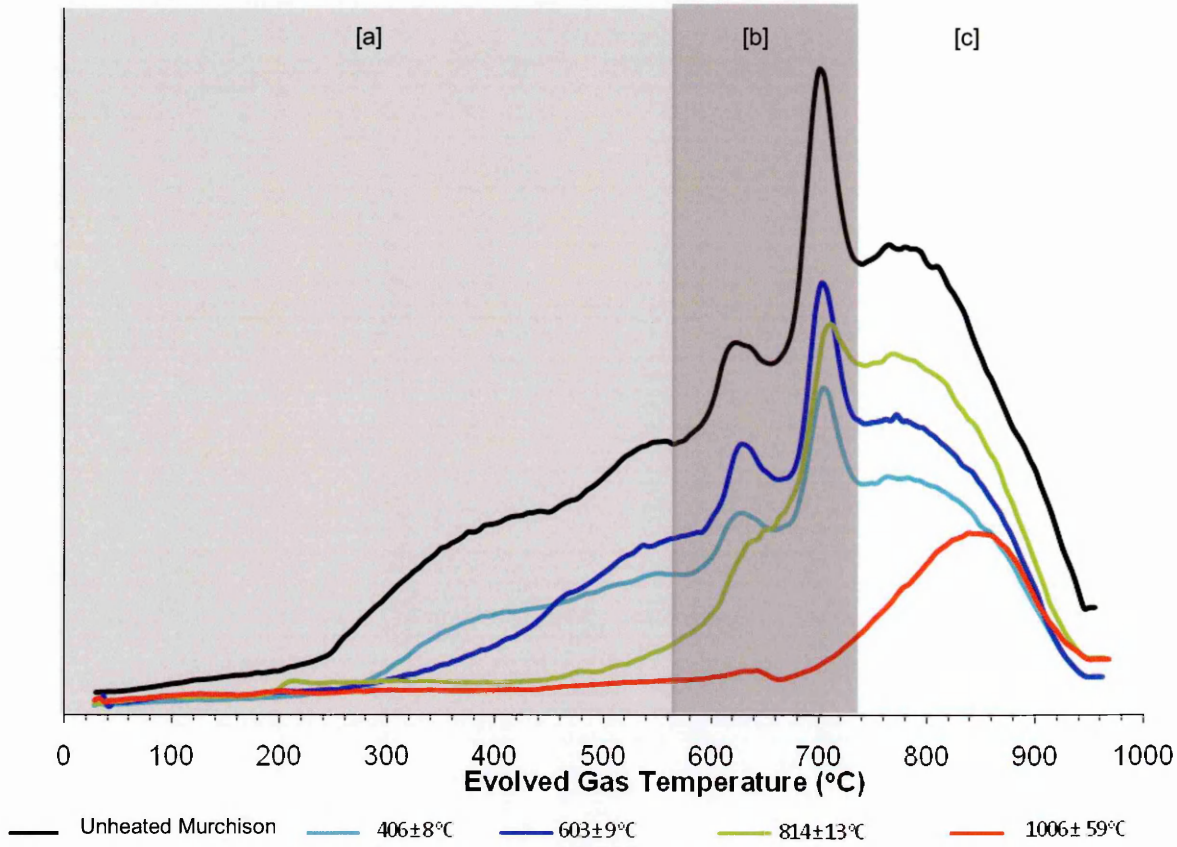

Figure 29: CO_2 evolved gas release in residues simulated for 2 s and unheated reference Murchison demonstrating the form of carbon remaining. Peaks in [a] – represent organic carbon, [b]- carbonate minerals [c] – carbonate minerals

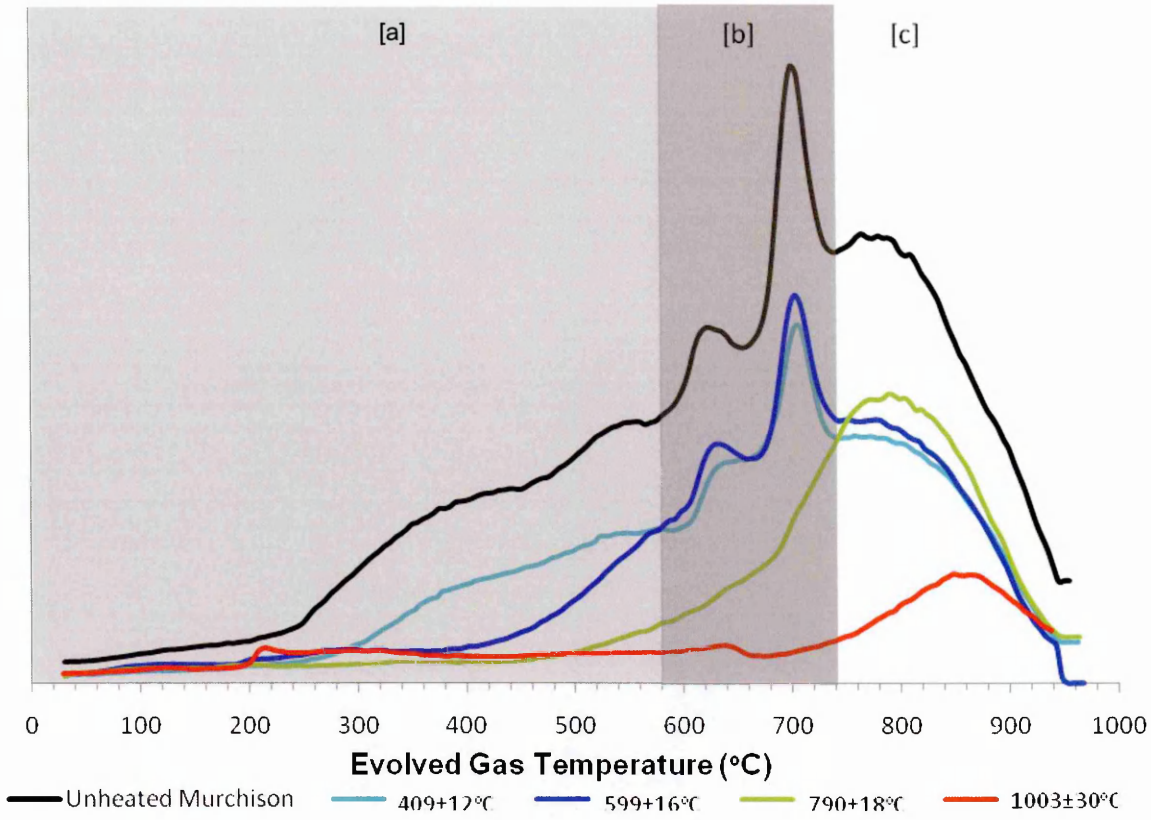

Figure 30: CO_2 evolved gas release in residues simulated for 5 s and unheated Murchison reference sample demonstrating the form of carbon remaining. Peaks in [a] – represent organic carbon, [b]- carbonate minerals [c] – carbonate minerals

C. Evolved H_2O

Figure 31 and Figure 32 illustrate H_2O evolved gas traces in samples simulated for 2 s and 5 s respectively, demonstrating the source of any retained H_2O. Adsorbed water, peak [i], is present in all flash heated residues, with a minor peaks in samples simulated for 2 s and 5 s for to >800 °C) (Figure 31 and Figure 32). Any indigenous adsorbed water will have been evaporated from mineral surfaces during all heating simulations in excess of 100 °C. However, the recondensation on to mineral surfaces of water derived from the dehydroxylation of phyllosilicates, may account for the minor peak [i] in samples heated in excess of 800 °C for 2 s and 5 s.

As simulation temperatures were increased (regardless of duration) the presence of structural water (peak [ii]) within flash heated residues diminished. Structural water was barely present in samples heated to >800 °C (Table 24), indicative of extensive dehydration of phyllosilicate material at these higher temperatures. Structurally bound

water was substantial in samples experiencing temperatures of approximately 400-600 °C suggesting less intense dehydration of phyllosilicates.

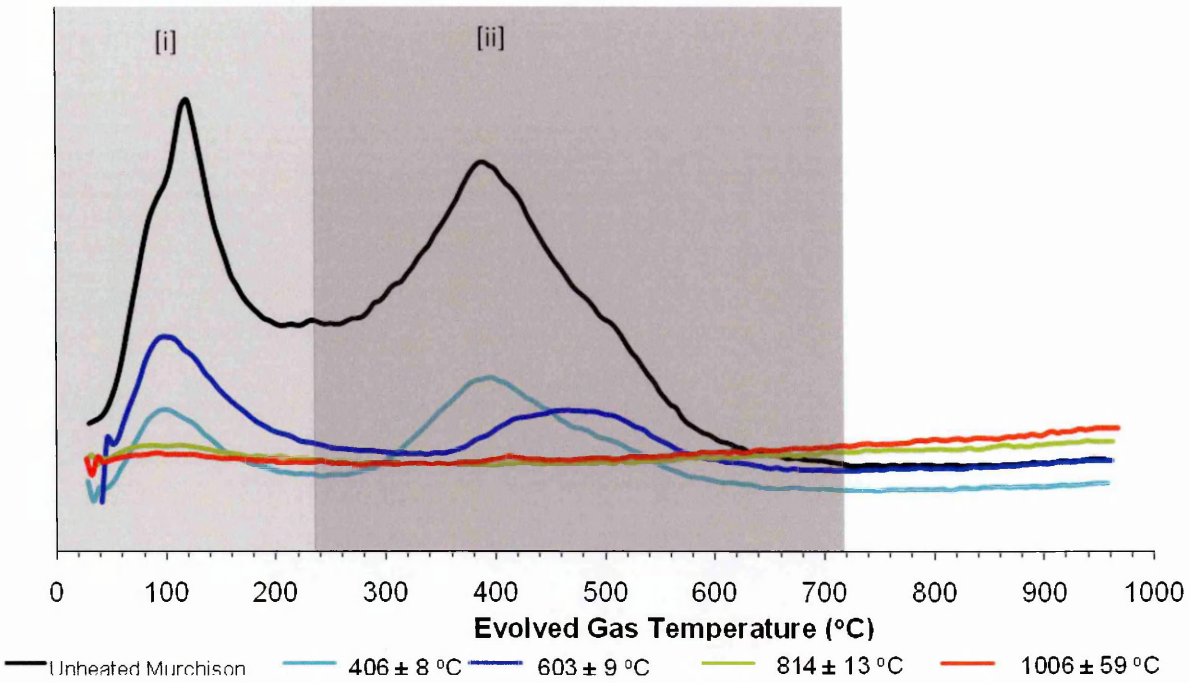

Figure 31: H_2O evolved gas release in residues simulated for 2 s and unheated reference Murchison, demonstrating the source of remaining H_2O, where peaks within [i] represent adsorbed H_2O and [ii] represent structurally bound H_2O

An interesting feature of peak [ii] in heated samples, is that in samples heated to ~600 °C the peak position of remaining phyllosilicates shifted from 386 °C to 480 °C and 540 °C for 2 s and 5 s durations respectively. At simulations to ~ 600 °C there has been extensive dehydration of the Fe-phyllosilicate cronstedtite, demonstrated by the absent evolved H_2O peak at 386 °C. At this simulation temperature, the incomplete dehydration of the Mg-phyllosilicate component that contributes to the broad peak [ii], may account for the retention of structural water that is evolved at a slightly higher temperature. At simulations to temperatures >800 °C, both the Fe- and the Mg- phyllosilicate components are extensively dehydrated, hence no structural water is identified in the evolved gas analysis of simulated samples. The presence of a minor evolved H_2O peak at 420 °C in the sample heated to 1006 °C, suggests that despite extensive heating and consequent dehydration of phyllosilicates, a very small fraction of cronstedtite still survives.

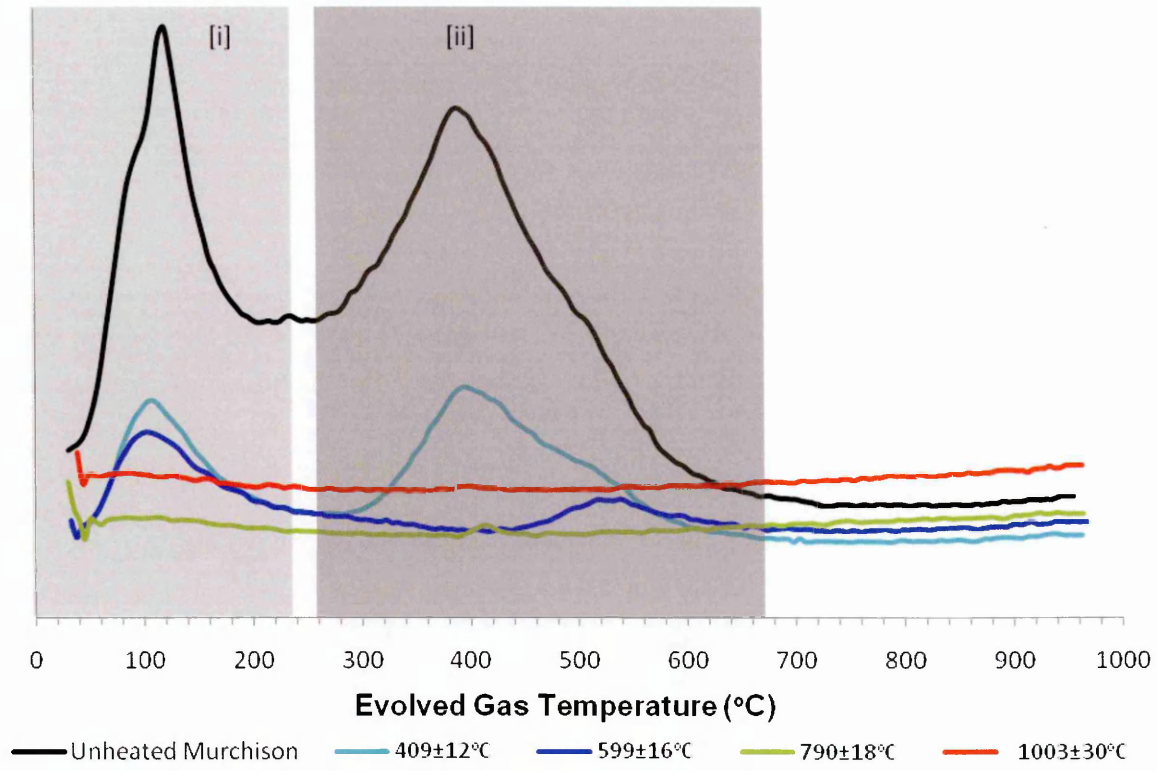

Figure 32: H_2O evolved gas release in residues simulated for 5 s and unheated reference Murchison demonstrating the source of remaining H_2O, where peaks within [i] represent adsorbed H_2O and [ii] represent structurally bound H_2O

D. A Summary of TG and EG Analysis

Table 24 summarises the total evolved gas content (wt. %) and the composition of remaining components as deduced from evolved CO_2 and H_2O peaks within flash heated samples. It demonstrates that the survival of both organic carbon and inorganic carbon (bound in carbonate minerals) is dependent on the extent of flash heating. Murchison matrix contains a range of phyllosilicate compositions from Mg- to Fe-bearing phyllosilicates). Similarly, the survival of structurally bound water is also dependent on the extent of heating conditions, with Mg-bearing phyllosilicates dehydrating at marginally higher temperatures than the Fe-bearing phyllosilicate component of Murchison. The increased dehydration of phyllosilicates, loss of organic material and decarbonation of carbonates at higher simulation temperatures is consistent with textural observations of increased desiccation cracks and vesicles in samples simulated to higher temperatures (Toppani et al., 2001) (Table 19).

Duration (s)	Peak Temperature (°C)	Evolved gas (wt. %)	Adsorbed Water [i] 0-200°C	Phyllosilicates [ii] 300-600°C	Organic Material [a]<600°C	Carbonates (plus Organic Carbon?) [b] 600-750°C	Carbonates [c] 750°C
0	0	14.6	✓	✓	✓	✓	✓
2	406 ± 8	12.5	✓	✓	✓	✓	✓
2	603 ± 9	11.4	✓	✓[1]	✓	✓	✓
2	814 ± 13	4.0	✓	×	✓	✓	✓
2	1006 ± 59	1.1	✓	minor	minor	✓	✓
5	409 ± 12	13.4	✓	✓	✓	✓	✓
5	599 ± 16	8.7	✓	✓[2]	✓	✓	✓
5	790 ± 18	3.3	minor	minor	minor	×	✓
5	1003 ± 30	0.7	minor	×	minor	minor	✓

Table 24: A summary of evolved gas contents and composition of flash heated samples and the reference Murchison . ✓= distinct peak identified ([1] peak shift to 450 °C , [2] peak shift to 520°C). Minor = minor peak and × = no peak

Based on abundances of the water (average 8.2 %) and organic material (upper limit of 2%) within Murchison (Table 25), the ratio of water:organic material is 4:1. Utilising the known volatile content determined by thermogravimetric analysis of the reference sample and flash heated samples, and the ratio of water:organic material in Murchison, quantification of the respective components is calculated (Table 26). It is assumed that all mass loss below 600 °C is the result of dehydration of phyllosilicates and a contribution by decomposition of organic material, whilst above 600 °C it is a result of liberated CO_2 from inorganic material (carbonates, graphite).

Water Abundance (%)	Organic Carbon abundance (%)
6.5[1]	2[3]
10.5[2]	>1.5[4]
7.72	
Average = 8.2	

Table 25: Abundances of water and organic carbon within the Murchison bulk meteorite 1- Tyburczy et al., (1986), 2 – Baker et al., (1998), 3- Kvenvolden et al., (1970), 4- Sephton et al., (1998)

The majority of mass loss from the flash heated samples is due to the release of water. Organic carbon is released at increasing simulation temperatures, with organic carbon corresponding to > 1 wt % of the total sample released at temperatures >800 °C for 2 s and > 600 °C for 5 s. Substantial inorganic carbon loss only occurs in simulations to ~1000 °C. Fluctuations in inorganic carbon abundance in samples heated to 409 °C and 599 °C for 5 s may be reflective of Murchison heterogeneity.

Duration (s)	Peak Temperature (°C)	Retained in Samples[1]			Released during simulations[2]		
		H_2O (wt. %)	CO_2: organic material (wt. %)	CO_2: inorganic (wt. %)	H_2O (wt. %)	CO_2: organic material (wt. %)	CO_2: inorganic (wt. %)
0[3]	0	8.6	2.2	4.0	n/a	n/a	n/a
2	406 ± 8	6.8	1.7	4.0	1.8	0.5	0.0
2	603 ± 9	5.9	1.5	4.0	2.7	0.7	0.0
2	814 ± 13	0.2	0.1	3.7	8.4	2.1	0.3
2	1006 ± 59	0.0	0.0	1.0	8.6	2.2	3.0
5	409 ± 12	7.2	1.8	4.4	1.4	0.4	-0.5
5	599 ± 16	3.5	0.9	4.3	5.1	1.3	-0.3
5	790 ± 18	0.1	0.0	3.2	8.6	2.1	0.8
5	1003 ± 30	0.0	0.0	0.7	8.6	2.2	3.3

Table 26: Calculated percentages of water, organic carbon and inorganic carbon based on thermogravimetric measurements of evolved gases from heated samples (1) and the average of duplicate Murchison reference sample (3). The percentage of water, organic carbon and inorganic carbon released during simulations (2) is determined by comparison between flash heated samples and the average composition of duplicate Murchison reference samples (3)

3.5. The Organic Composition of the Reference Murchison Sample

Characterisation of the organic species liberated during offline heating simulations (Section 3.4.2) is necessary to identify the range of species that may have been deposited in the early atmosphere, and to infer those that were subsequently retained by particles. Despite numerous studies that have characterised the soluble and insoluble organic fractions of carbonaceous chondrites (Section 1.2), limited studies of CO3 (Pearson et al., 2007), CR2 (Pearson et al., 2007) and CM (Watson et al., 2005) macromolecular material have been conducted using GCxGC-TOFMS. It has been necessary to constrain the organic composition of the reference Murchison sample (unheated) using this technique (Wilson, et al., 2007a; Wilson, et al., 2007b), in order to compare it with simulated samples.

Pyrolysis of the Murchison reference sample (which contains limited free organic material due to SFE) releases volatile organic species, due to the decomposition of macromolecular material. In this study, BP624 and BP20 columns are used to identify volatile organic species (up to the molecular weight of napthalene), shown in the total ion chromatogram (TIC) (Figure 33). Aliphatic hydrocarbons up to C_{12} *n*-alkanes, up to C_{10} branched alkanes and C_3-C_9 alkenes were released (Figure 34), consistent with previous

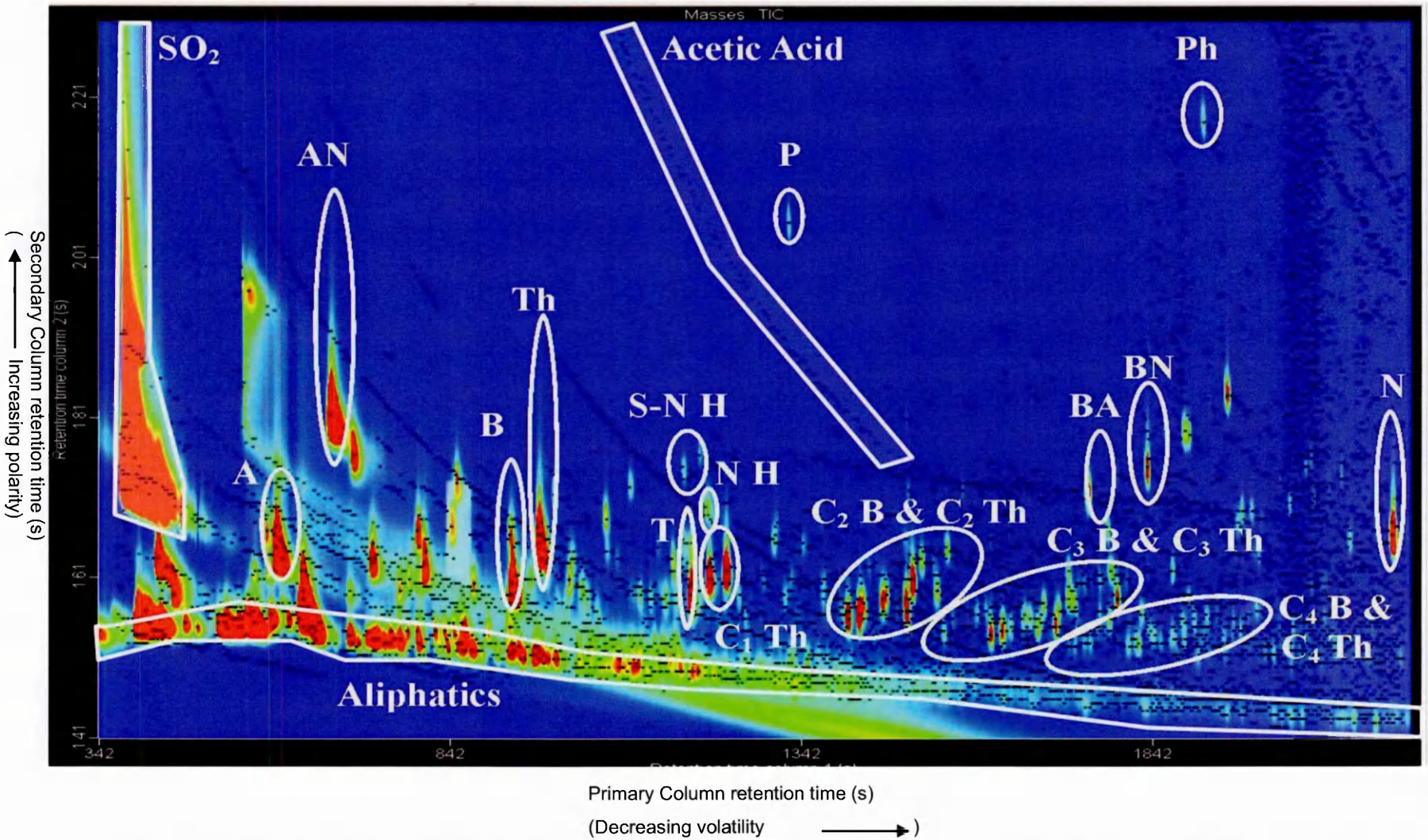

Figure 33: A TIC of unheated Murchison identifying key species using BP624 and BP20 columns. A = acetone, AN = acetonitrile, B = benzene, BA = benzaldehyde, BN = benzonitrile, N= naphthalene, N H = nitrogen heterocycle, P = pyrrole, Ph = phenol, S-N H = sulphur-nitrogen heterocycle, T = toluene and Th = thiophene

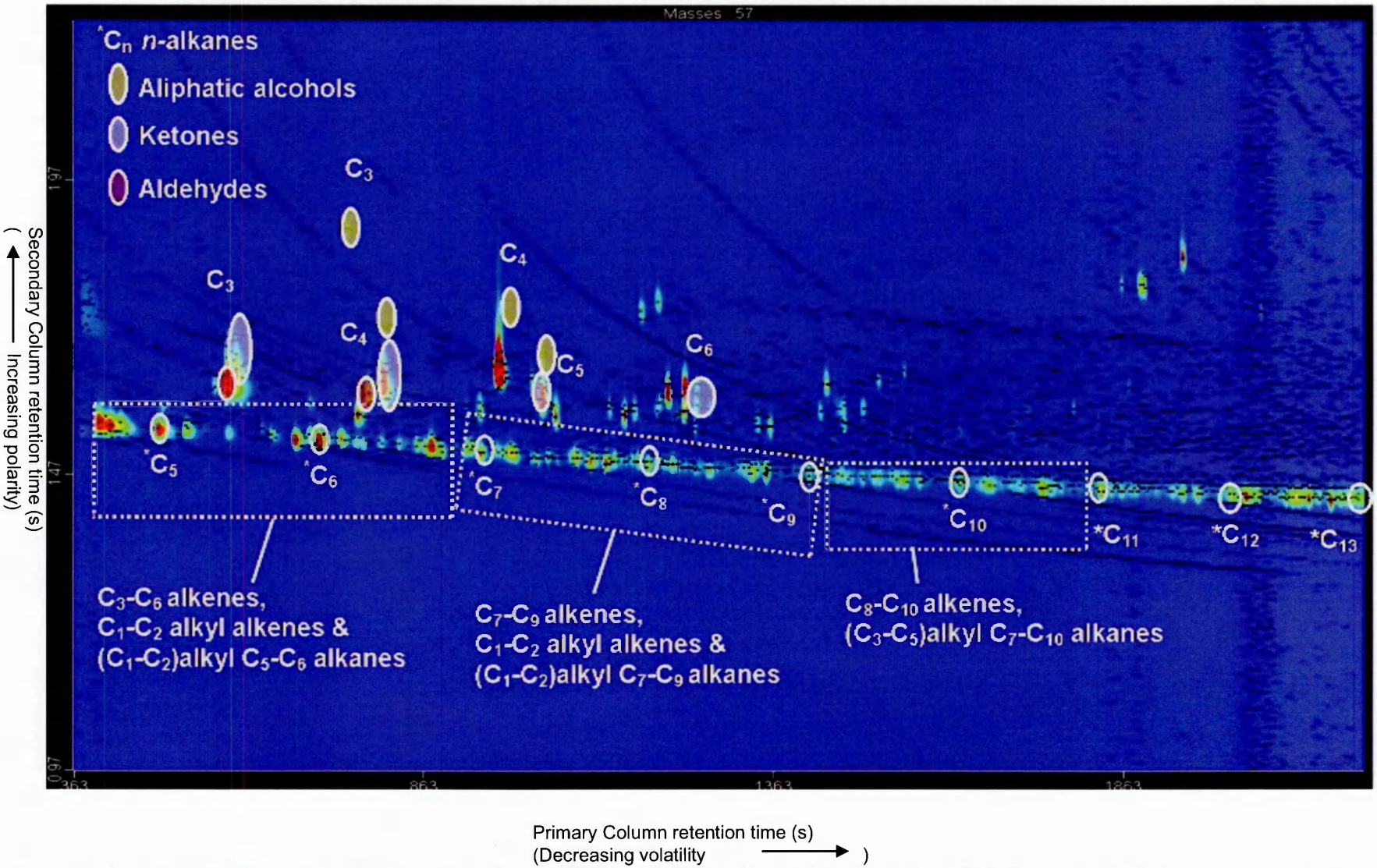

Figure 34: An RIC (mass 57) of unheated Murchison (using BP624 and BP20 columns) identifying key aliphatic species including *n*-alkanes, C_3-C_6 aliphatic ketones and C_3-C_4 aliphatic aldehydes

pyrolysis studies that have identified up to C_{13} *n*-alkanes (Hayatsu et al., 1977; Levy et al., 1973).

Free, aliphatic, non-polar material including > C_{15} *n*-alkanes (Sephton et al., 2001b) should have been removed from Murchison during SFE extraction. Therefore the identification of lower molecular weight aliphatic species in the Murchison reference sample could be the result of either trapped aliphatic material being retained following SFE, or the cleaving of aliphatic linkages identified within the macromolecular material (Remusat et al., 2005 a).

Dominant acids are acetic acid and aminomethansulfonic acid, although higher carboxylic acids have been previously characterised in Murchison from derivatised extracts (Martins et al., 2006; Pizzarello et al., 2001) and aryl carboxylic acids have previously been identified in Murchison macromolecular material using infra-red spectroscopy (Hayatsu et al., 1977). It is thought that -COOH functional groups are contained within the aromatic polymer (Bitz & Nagy, 1966). As acetic acid is a very polar compound, it would not have been removed during the extraction procedure and could originate from the free organic fraction. Instead of appearing as a peak in the chromatogram, the acetic acid peak tails from left to right along the primary (non-polar) column and appears as a continuous line. Derivitising such compounds prior to analysis, or conducting tetramethylammonium hydroxide (TMAH) assisted pyrolysis (Remusat et al., 2005 b) would aid their identification in the chromatogram.

Up to C_5 aliphatic alcohols and branched aliphatic alcohols are also present, compared to the C_4 aliphatic alcohols previously identified in Murchison solvent extracts (Jungclaus et al., 1976). The C-OH stretching vibration of alcohols/phenol has been identified in Murchison insoluble organic material using infra-red spectroscopy (Hayatsu et al., 1977), and OH functional groups are believed to reside in the macromolecular network (Bitz & Nagy, 1966). Oxygen-bearing species within the Murchison reference sample include phenol, C_3-C_6 ketones, C_3-C_4 aldehydes and benzaldehyde (Figure 33, Figure 34).

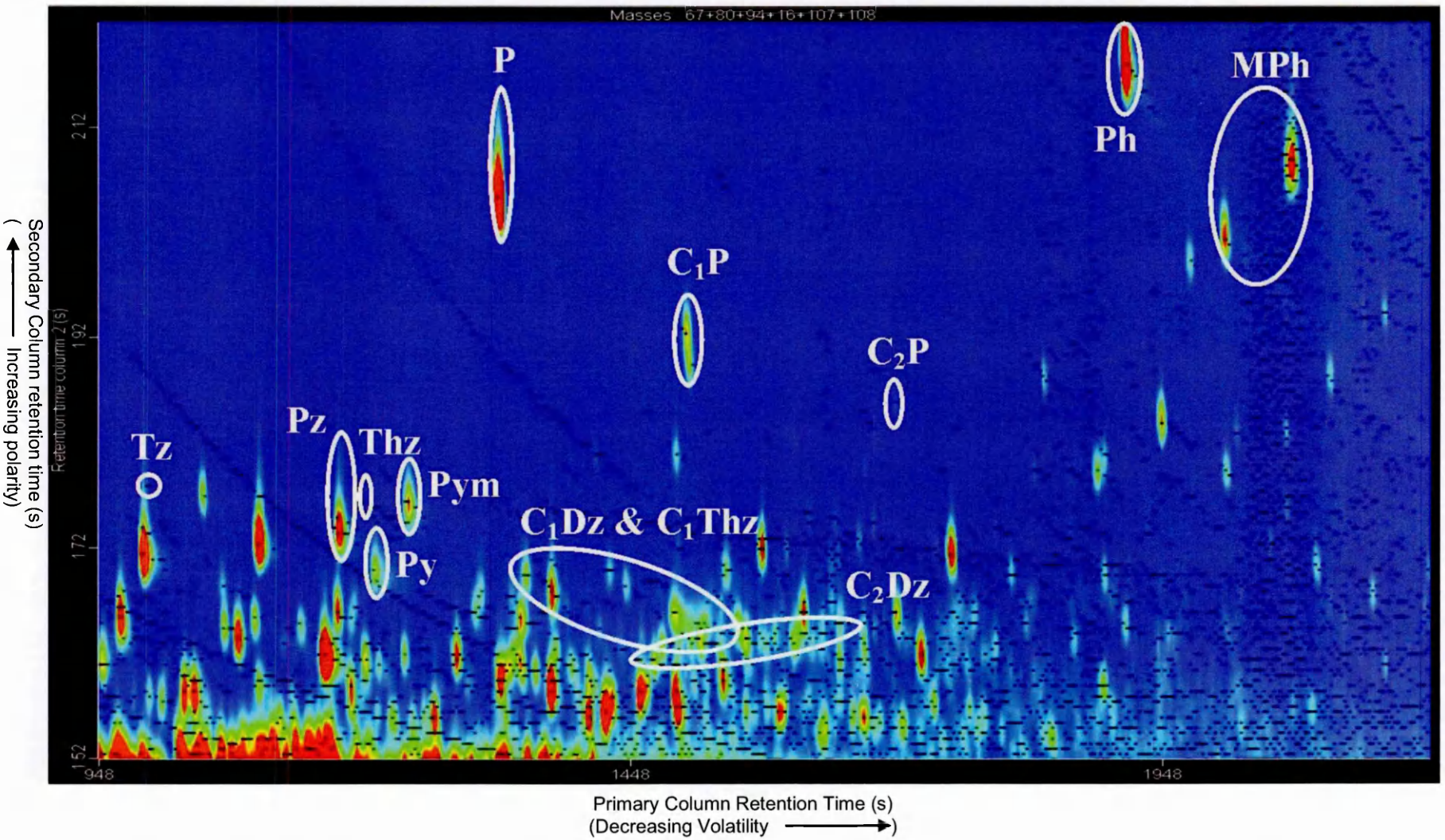

Figure 35: An RIC of masses 67+80+94+107+108 (using BP624 and BP20 columns) identifying nitrogen and sulphur-nitrogen heterocyclic compounds and phenols. Dz = diazine, MPh = methylphenol, P = pyrrole, Ph = phenol, Py = pyridine, Pym = pyrimidine, Pz = pyrazine, Thz = thiazole and Tz = triazine

Using NMR spectroscopy, Cody and Alexander (2005) have identified CO moieties within Murchison macromolecular material thought to derive from ketones, confirming earlier identification of aryl and unsaturated ketones (Hayatsu et al., 1977) by infra-red spectroscopy. The aliphatic ketones identified in this study may be the result of the cleaving of side chains from macromolecular material or incomplete SFE using CO_2. Other aromatic species identified include benzene, C_1-C_4 alkylbenzenes and C_1-C_6 *n*-alkane substituted species (Figure 33), consistent with previous analysis (Hayatsu et al., 1977; Levy et al., 1973). Naphthalene is the largest molecule identified due to the constraints of the BP624 column conditioned for volatile organic compound elution.

A range of sulphur (S-) bearing species are identifiable in the TIC of Murchison reference material (Figure 33) including inorganic components (e.g. SO_2), N-S heterocycles and S-bearing aromatics. One of the most dominant peaks in the TIC is that of SO_2 released from the decomposition of S-containing minerals within Murchison such as troilite and pentlandite (Brearley & Jones, 1998; Burgess et al., 1991) and the degradation of S-bearing organic material (Haraldson, 1962). However, TG and EG analysis of Murchison reference material demonstrated that SO_2 was a very minor component relative to total evolved CO_2 and H_2O species (Section 3.4.1). SO_2 quantities may have been below the detection limits of the TG/EGA.

The dominant S-aromatic species are thiophene and its C_1-C_3 alkyl-substituted species. The N-S heterocycle thiozole and its C_1-C_2 alkyl derivatives consistent with the previous identification of S-bearing species in Murchison (Hayatsu et al., 1977; Levy et al., 1973; Pearson et al., 2006; Remusat et al., 2005 b; Sephton et al., 1998). It is reported that 24 % organic sulphur in Murchison macromolecular material is present as thiophene units (Derenne et al., 2002; Derenne & Robert, 2008; Remusat et al., 2005), based on K-edge sulphur XANES analysis. The remaining organic sulphur comprises aliphatic sulphide linkages (Derenne et al., 2002). During pyrolysis, the cleaving of thiophenic moieties from macromolecular material and the oxidation of sulphide linkages may be responsible for the subsequent identification of thiophenes in pyrolysates. Additional S-

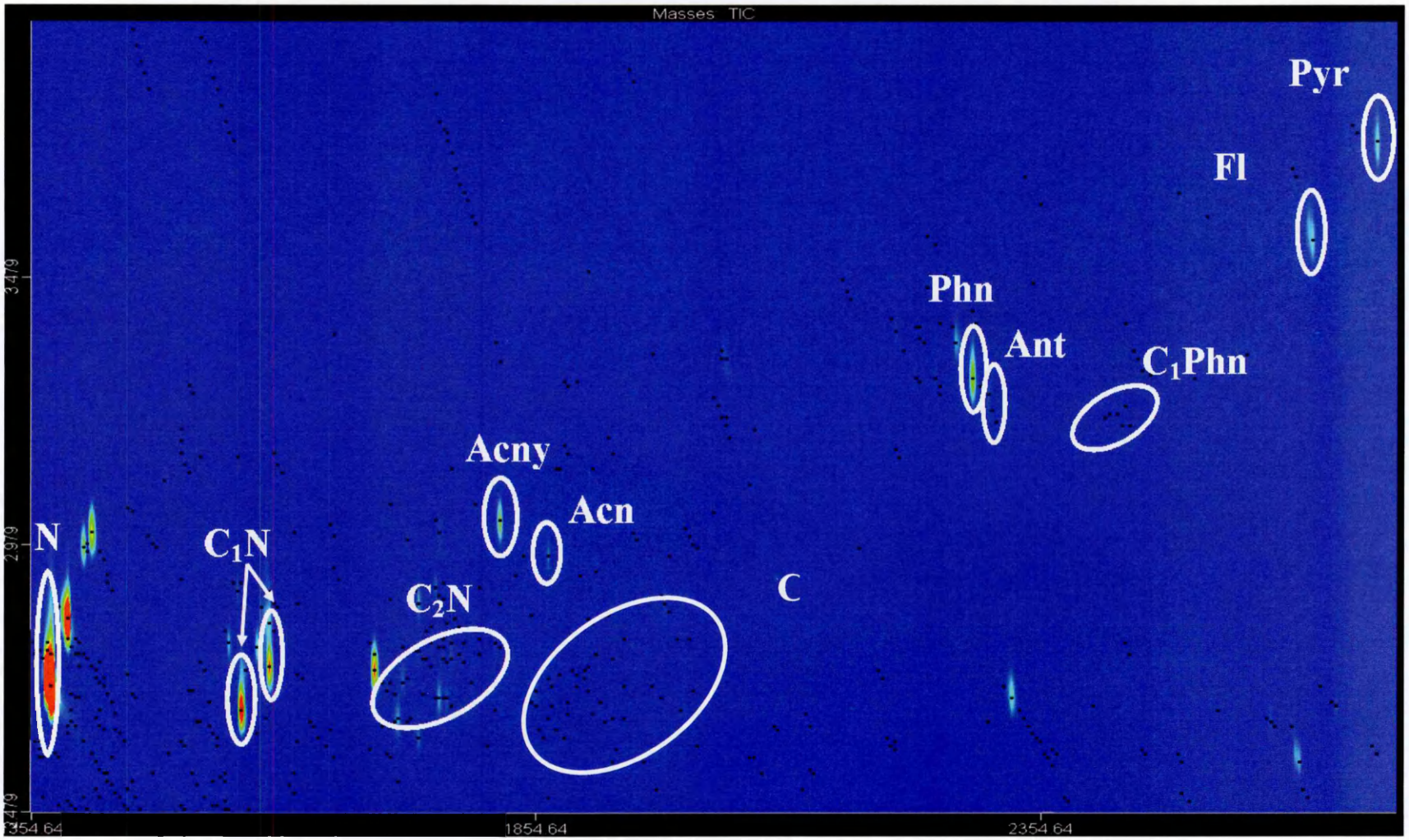

Figure 36: A TIC identifying PAHs in Murchison using BPX5 and BPX50 columns. Acen = acenaphthene, Acny = acenaphthylene, Ant = Anthracene, Fl = Fluoranthene, N= naphthalene, Phn = Phenanthrene, Pyr = Pyrene

bearing species include sulfonic acid, previously identified in Murchison solvent extracts (Cooper et al., 1992; Cooper, 1993), and carbon disulphide. Carbon disulphide may in fact be a pyrolysis product of low molecular weight alkanes reacting with elemental S (Burgess et al., 1991; Holleman & Wiberg, 2001) present in the matrix or a product of pyrolytic thiophene decomposition (Wynberg & Bantjer, 1959).

One of the most diverse groups of compounds within Murchison reference material are N-bearing species (Figure 35). These include the nitriles acetonitrile and benzonitrile, and a variety of N- heterocycles (pyridine, pyrazine, diazine, triazine, pyrimidine and pyrrole). Whilst acetonitrile and benzonitrile can be identified in the free organic fraction, N-hetrocycles are typically found in Murchison macromolecular material (Hayatsu et al., 1975; Hayatsu et al., 1977; Levy et al., 1973) but can be released from the macromolecule via acid hydrolysis. Alkyl derivatives of these heterocycles (C_1-C_3 alkyl pyrimidines, C_1-C_4 alkyl pyrazines, C_1-C_2 alkyl pyrimidines, methyl pyridazine and methylpyrrole) are also present. NMR spectroscopy has identified the presence of N-heterocylces within Murchison insoluble organic matter (Derenne & Robert, 2008). The presence of pyrrole, indole and carbazole moieties in Orgueil have also been detected by NMR spectroscopy and it is suggested that these exist too in Murchison (Remusat et al., 2005 b). It is likely that the N-heterocycles in Murchison reference material pyrolysates are therefore cleaved from macromolecular material on pyrolysis, or remain following incomplete SFE CO_2 extraction.

The only amines identifiable are benzenamine and methyl benzenamine. Although previous studies of Murchison extracts have identified a variety of aliphatic amines (Jungclaus et al., 1976; Pizzarello, 2002) through their derivitised products, these compounds have never been identified in pyrolysates. It is possible that these benzenamines are derived from secondary reactions involving carboxylic acids during pyrolysis e.g. via the Schmidt reaction (Schmidt, 1924), reduction of the corresponding nitroaromatic, amonolysis of phenol and amination of the aromatic ring (Amini & Lowenkron, 2003).

Utilising a different column set (BPX5 and BPX 50), it was possible to identify higher molecular weight species, illustrating that the Murchison reference material contains 1-4 ring aromatic hydrocarbons (Figure 36): benzene, naphthalene, acenaphthylene, acenaphthene, phenanthrene, anthracene, pyrene and fluoranthene within the constraints of the primary column. Additionally the complete suite of C_1-C_3 alkyl naphthalenes, up to C_4 n-alkyl substituted naphtalene and C_1 phenanthrenes were also identified. These species have been identified in previous Murchison pyrolysates (Hayatsu & Anders, 1981; Pearson et al., 2006; Remusat et al., 2005 b), in addition to C_1 anthracenes (Remusat et al., 2005 b) which were lacking in this study. Two step laser desorption/ionisation mass spectrometry as identified up to 4 carbon ringed PAHs including chrysene and alkylated species including C_1-C_2 phenanthrenes (Clemett et al., 1998), confirming pyrolysis results.

A summary of PAHs, aromatic species and *n*-alkanes characterised by in this study during volatile organic analysis and higher molecular weight organic analysis are given in Table 27, Table 28 and Table 29 respectively.

Species	1st Dimension Retention Time (s)	2nd Dimension Retention Time (s)	Peak on Chromatograms
Naphthalene	1374.62	2.716	N
1-methylnaphthalene	1590.41	2.753	C_1N
2-methylnaphthalene	1562.44	2.671	C_1N
1,2-dimethylnaphthalene	1814.18	2.797	C_2N
1,3-dimethylnaphthalene	1754.24	2.694	C_2N
1,4 & 2,3-dimethylnaphthalene	1790.21	2.723	C_2N
1,5-dimethylnaphthalene	1798.20	2.775	C_2N
1, 6-dimethylnaphthalene	1766.23	2.694	C_2N
1,7-dimethylnaphthelne	1758.24	2.694	C_2N
1,8-dimethylnaphthalene	1850.15	2.849	C_2N
2,6-dimethylnaphthalene	1734.26	2.642	C_2N
2,7-dimethylnaphthalene	1738.26	2.620	C_2N
1-ethylnaphthalene	1718.28	2.657	C_2N
2-ethylnaphthalene	1722.28	2.723	C_2N
C_3-naphthalene	1910.09	2.664	C_3N
C_3-naphthalene	1922.08	2.649	C_3N
C_3-naphthalene	1942.06	2.716	C_3N
C_3-naphthalene	1970.03	2.716	C_3N
C_3-naphthalene	1994.00	2.805	C_3N
C_3-naphthalene	2005.99	2.805	C_3N
Acenaphthylene	1818.18	3.027	Acny
Acenaphthene	1866.13	2.960	Acn
Phenanthrene	2285.71	3.293	Phn
C1-phenanthrene	n.d.	n.d.	C_1Phn
Anthracene	2301.70	3.263	Anth
Fluoranthene	2621.38	3.552	Fl
Pyrene	2685.31	3.737	Pyr

Table 27: A summary of PAHs identified in Murchison reference material using BPX5 and BPX50 columns (n.d. not determined)

Species	1st Dimension Retention Time (s)	2nd Dimension Retention Time (s)	Peak on Chromatograms
Inorganic			
Sulphur Dioxide	n.d.	n.d.	SO_2
Aromatics			
Benzene	930	1.605	B
Toluene	1185	1.590	T
Ethylbenzene	1410	1.560	C_2B
p & *m*-xylene	1425	1.565	C_2B
o-xylene	1491	1.570	C_2B
Isopropylbenzene	1545	1.545	C_3B
Propylbenzene	1611	1.540	C_3B
1-ethyl-3-methylbenzene	1626	1.545	C_3B
1-ethyl-4-methylbenzene	1641	1.550	C_3B
1-ethyl-2-methylbenzene	1677	1.550	C_3B
1,2,4-trimethylbenzene	1704	1.550	C_3B
1,2,3-trimethylbenzene	1782	1.560	C_3B
Tertiary butylbenzene	1695	1.530	C_4B
Isobutylbenzene	1722	1.525	C_4B
Secondary butylbenzene	1731	1.525	C_4B
1-methyl-3-isopropylbenzene	1746	1.530	C_4B
1-methyl-4-isopropylbenzene	1752	1.530	C_4B
1-methyl-2-isopropylbenzene	1791	1.530	C_4B
1-methyl-3-propylbenzene	1809	1.525	C_4B
1-methyl-4-propylbenzene	1818	1.525	C_4B
1,4-diethylbenzene	1821	1.530	C_4B
n-butylbenzene	1827	1.525	C_4B
1,2-diethylbenzene	1842	1.530	C_4B
1-methyl-2-propylbenzene	1854	1.530	C_4B
1,4-dimethyl-2-ethylbenzene & 1,3-dimethyl-2-ethylbenzene	1872	1.535	C_4B
1,2-dimethyl-4-ethylbenzene	1887	1.535	C_4B
1,3-dimethyl-2-ethylbenzene	1911	1.540	C_4B
1,2-dimethyl-3-ethylbenzene	19.41	1.540	C_4B
1,2,4,5-tetrametylbenzene	1956	1.545	C_4B
1,2,3,5-tetramethylbenzene	1965	1.545	C_4B
1,2,3,4-tetramethylbenzene	2040	1.550	C_4B
Naphthalene	2181	1.665	N
Oxygen, Hydroxyl and Carboxyl Bearing			
Acetic Acid	n.d.	n.d.	Acetic Acid
Benzaldehyde	1749	1.715	BA
Acetone	594	1.650	A
Phenol	1914	2.180	Ph
Methylphenol	2007	2.015	MPh
Methylphenol	2070	2.090	MPh
Sulphur-Bearing			
Thiophene	969	1.655	Th
2-methylthiophene	1212	1.610	C_1Th
3-methylthiophene	1236	1.620	C_1Th
2-ethylthiophene	1431	1.580	C_2Th
2,5-dimethylthiophene	1458	1.585	C_2Th
2,4-dimethylthiophene	1464	1.590	C_2Th
2,3-dimethylthiophene	1491	1.585	C_2Th
3,4-dimethylthiophene	1536	1.595	C_2Th
2-isopropylthiophene	1557	1.560	C_3Th
3-isopropylthiophene	1593	1.565	C_3Th
2-propylthiopehene	1629	1.560	C_3Th
2-ethyl-4-methylthiophene	1656	1.560	C_3Th
2-ethyl-5-methylthiophene	1668	1.560	C_3Th
C_3-Thiophene	1734	1.570	C_3Th
C_3-Thiophene	1767	1.570	C_3Th
Thiazole	1197	1.765	Thz
Isothiazole	1173	1.750	IThz
C_1-Thiazole	n.d.	n.d.	C_1Thz
Nitrogen Bearing			
Acetonitrile	672	1.815	AN
Benzonitrile	1833	1.750	BN
Pyrazine (Diazine)	1173	1.735	Pz
Pyridine	1206	1.700	Py
Pyrimidine (Diazine)	1239	1.765	Pym
Pyrrole	1323	2.055	P
C_1-Pyrrole	1500	1.925	C_1P
C_2-Pyrrole	1698	1.860	C_2P
Triazine	996	1.780	Tz

Table 28: A summary of volatile organic species in Murchison reference material using BP624 and BP20 columns

n-alkane	1st Dimension Retention Time (s)	2nd Dimension Retention Time (s)	Peak on Chromatograms
pentane	483	1.550	*C_5
hexane	711	1.530	*C_6
heptane	942	1.510	*C_7
octane	1182	1.485	*C_8
nonane	1413	1.470	*C_9
decane	1629	1.455	*C_{10}
C_{11}	1827	1.445	*C_{11}
C_{12}	2013	1.440	*C_{12}
C_{13}	2187	1.435	*C_{13}

Table 29: A summary of *n*-alkanes identified in Murchison reference material using BP624 and BP20 columns

The range of organic species identified in the pyrolysate of Murchison reference material by GCxGC-TOFMS accounts for the broad evolved CO_2 peak between 200 °C-600 °C in the reference sample derived from EG analysis (Figure 26), which undergoes a slower heating rate and longer heating regime.

The broad nature of the organic evolved CO_2 peak suggests heterogeneity of Murchison organic material, with thermally labile components released at lower evolved gas temperatures (<350 °C). Such components exist in the Murchison TIC e.g. carboxylic acids and a broad range of aliphatic species. Similarly the large range of aromatic species including PAHs and N-, S- and O- bearing aromatics are more resistant to thermal degradation than aliphatic components (David, 1975), thus accounting for CO_2 evolved between 350 °C – 600 °C.

3.5.1. Volatile Organic Species Released During Simulations

Although absolute species abundance is not directly measureable by GCxGC-TOFMS, the species peak area can be used to determine the relative abundances between species and can therefore serve as a proxy for comparing relative abundance across all samples. Chromatogram peak areas are used as a means to quantify organic species as it was not possible to get absolute concentrations during this study. Appendix II summarises the chromatogram peak areas used to compile the graphs depicting percentage and relative proportions.

A. Aliphatic Species

The distribution of *n*-alkanes released on simulations is displayed in Figure 37. At all simulation durations and temperatures, C_5 and C_6 *n*-alkanes were released in greatest relative abundance. There were additional large relative percentages of C_{11}-C_{13} *n*-alkanes released at all simulation temperatures for 2 s and 20 s durations. Considering, simulations were conducted on SFE extracted residues of Murchison (i.e. with non-polar extractable organic matter such as aliphatics removed), it seems likely that *n*-alkanes released during simulations could be derived from the thermolysis of aliphatic hydrocarbons associated within the macromolecular network as short alkyl substituents or cross linkages (Cody & Alexander, 2005; Cronin et al., 1987; Cronin et al., 1988; Hayatsu et al., 1977; Hayatsu et al., 1980; Levy et al., 1973). Ruthenium tetroxide oxidation of Murchison macromolecular material (Remusat et al., 2005 a) has revealed that up to C_3 aliphatic side chains are present within the aromatic network, with up to C_7 hydrocarbons between aromatic units as aliphatic cross linkages. Alkanes could also be produced via the decomposition of alkylsubstituted aromatics (e.g. decomposition of alkylbenzenes, alkylthiophenes and alkyl heterocyclics released from the macromolecular structure) (Mochida & Yoneda, 1967; Watson et al., 1997) or by the cracking of larger alkanes, to produce lower weight alkanes and alkenes (Raseev & Suciu, 2003). For example octane cracks to form hexane and propene under conditions similar to pyrolysis (Olah & Molnar, 2003).

Up to C_{24} straight chain and branched chain alkanes are present in Murchison solvent extracts (Cronin & Pizzarello, 1990), known terrestrial contaminants (Sephton et al., 2001 a), and up to C_{18} n-alkanes have been identified in Murchison pyrolysates (Levy et al., 1973; Pearson, 2003). These *n*-alkanes within pyrolysates are thought to originate in the free organic fraction and are likely to be terrestrial contaminants arising from incomplete solvent extraction, or introduction post-extraction. In the event of incomplete extraction with supercritical CO_2, the sample used in this study may have retained some of these larger alkanes, which would crack on pyrolysis into smaller alkanes and alkenes

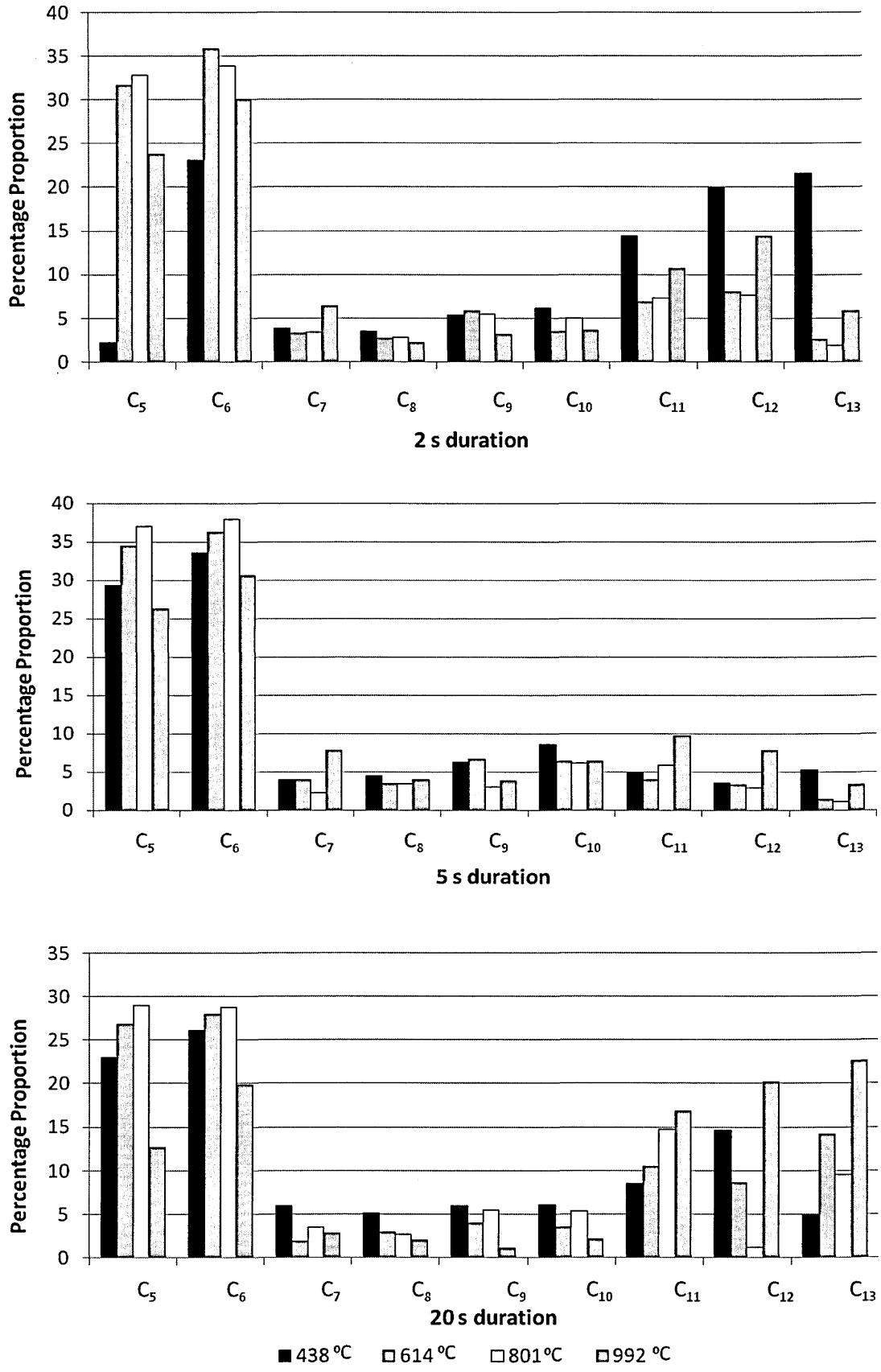

Figure 37: Distribution of n-alkanes released on EDP entry heating simulations. Cn corresponds to carbon number (derived from chromatogram peak area abundances). Percentage proportion represents the percentage of total C_5 to C_{13} alkanes

(Raseev & Suciu, 2003). Intensive heating to higher temperatures facilitates cracking, with an increased release of $>C_{11}$ *n*-alkanes at longer durations of 20 s than the short 2 s simulation durations. It is suggestive that there may be a terrestrial contribution to aliphatic species in the Murchison pyrolysate.

B. Aromatic Species

Benzene and the full suite of C_1-C_4 alkylbenzenes and C_1-C_6 *n*-alkane substituted species were released during all simulation conditions. The percentage proportions of parental and alkyl benzenes expressed as a percentage of total C_0-C_4 benzenes with changing simulation conditions is given in Figure 38. Percentage proportions of total (C_1-C_4) alkylbenzenes decrease with increasing peak simulation temperature. Alkylbenzenes are the thermal fragmentation products of Murchison macromolecular material (Komiya et al., 1993; Levy et al., 1973). They are formed from predominantly the β-cleavage of monoaromatic macromolecular bound moieties i.e. cleavage of the C-C bond between α and β carbon atoms of the macromolecular linked aromatic moiety side chain (Hartgers et al., 1994), with a minor contribution from γ- and δ- bond cleavages. A range of pyrolysis products can be derived from β- and γ- cleavages depending on macromolecular- bound monoaromatic precursors (Hartgers et al., 1994). Alkylbenzene substitution patterns are therefore pyrolysis products reflective of the monoaromatic precursor bound to the macromolecular structure.

The decreased release at higher temperatures may be, in part, the result of cleaved radicals combining to form larger components, which condense at higher temperatures producing higher aromatic structures (Juntgen, 1987a; Juntgen, 1987b). There are some CM chondrites thought to have experienced unusually high parent body thermal metamorphism at a similar temperatures to simulations in this study, 250 °C – 900 °C (Kitajima et al. 2002 and references therein). These meteorites have undergone a similar process of carbonisation and graphitisation (Kitajima et al. 2002; Komiya et al., 1993). Flash heating simulations conducted on Murchison samples to between 600 °C-

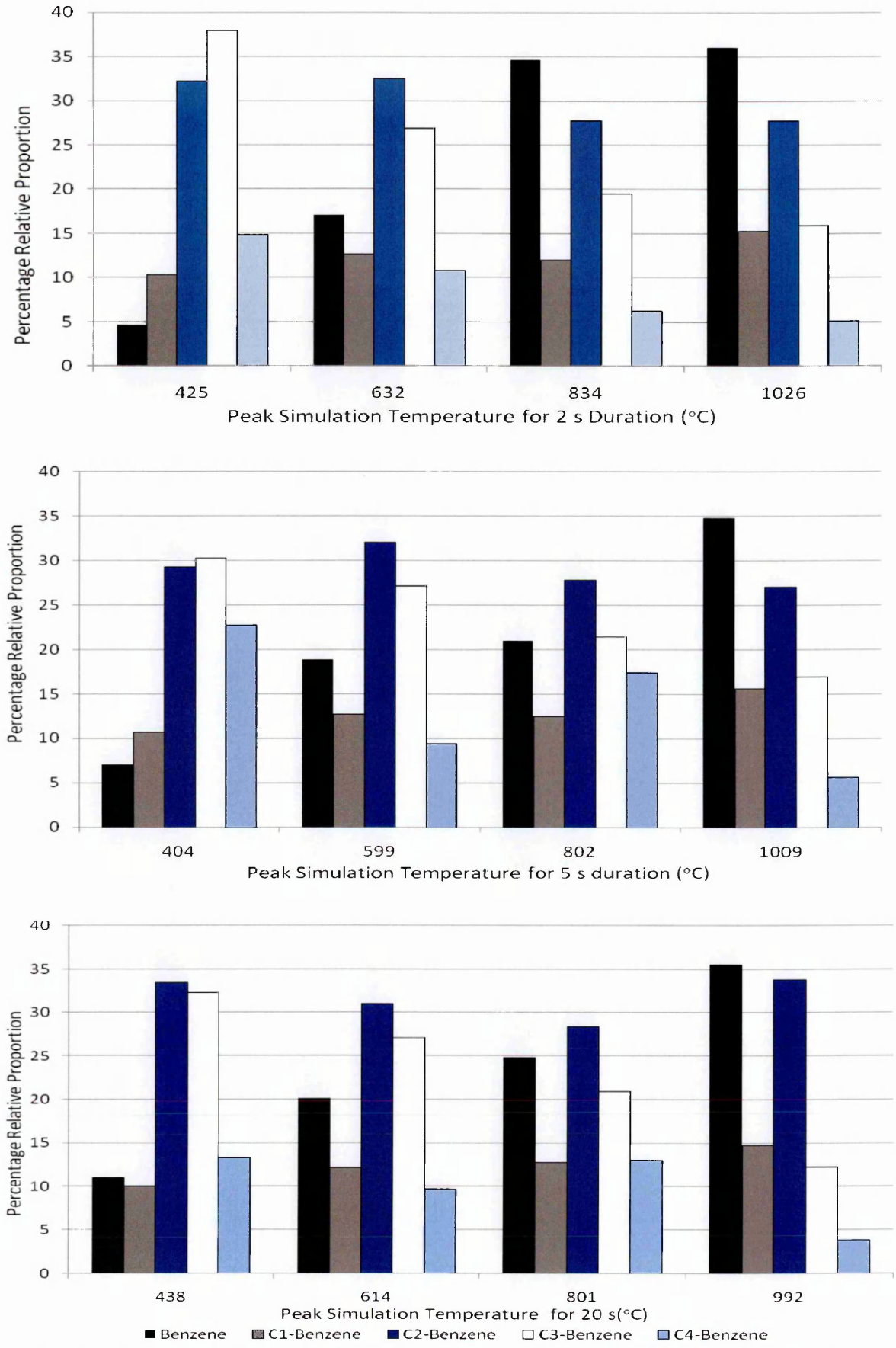

Figure 38: The relative proportions of benzene and C1-C4 alkyl substituted benzenes released on simulations for 2 s (top), 5 s (middle) and 20 s (bottom), expressed as a percentage of the total C_0-C_4 benzenes in each sample (derived from chromatogram peak area abundances)

1400 °C for undetermined durations (Cody et al., 2008), reveal that graphite is more prevalent in residues that have been heated to higher temperatures. During parent body thermal alteration, the thermally labile organic fraction is lost from macromolecular material and their extractable organic compounds (Shimoyama, 1997), consequently yielding an overall lower abundance and variety of pyrolysates, compared to unmetamorphosed CMs (Kitajima et al., 2002). This trend is visible across the carbonaceous chondrite groups, whereby the more thermally metamorphosed groups (CO, CV) exhibit a lack of pentagonal ring PAHs (indene, acenaphthene, acenaphthylene, fluorene and fluoranthene) and altered insoluble organic material (Yabuta et al., 2007).

The percentage proportional release of C_1-benzene remains almost constant, whilst that of benzene increases with increasing simulation temperature (Figure 38). Subsequent cracking of C_2-C_4 alkylbenzenes results in their dealkylation to benzene (Mochida & Yoneda, 1967), with the cracking of larger alkyl side chains generating benzenes with shorter alkyl side-chains such as C_1-benzene (Watson et al., 1997).

64 % of total benzenes released during simulations for 2 s to 1006 °C are alkylbenzenes, compared to 95 % at 425 °C. Both the condensing of aromatic structures and cracking of larger alkylbenzenes contribute to the decrease in percentage proportions of alkylbenzenes with increasing simulation temperatures. Similar trends are visible for the longer simulation durations of 5 s and 20 s.

C. Sulphur Bearing Species

The full range of S-bearing species identified in the Murchison reference sample were released during all simulations. These include SO_2, carbon disulphide, dimethylsulphide, thiophene, C_1–C_3 alkylthiophenes and C_1-C_5 *n*-alkane substituted thiophenes. Thiophenes and their alkyl derivatives are typical pyrolysis products of previous carbonaceous chondrite analyses (Levy et al., 1973; Studier et al., 1972; Sephton et al., 1998). The relative proportions of C_0-C_3 thiophenes (Figure 39) in species released during simulations for 2 s remain almost constant over peak temperatures

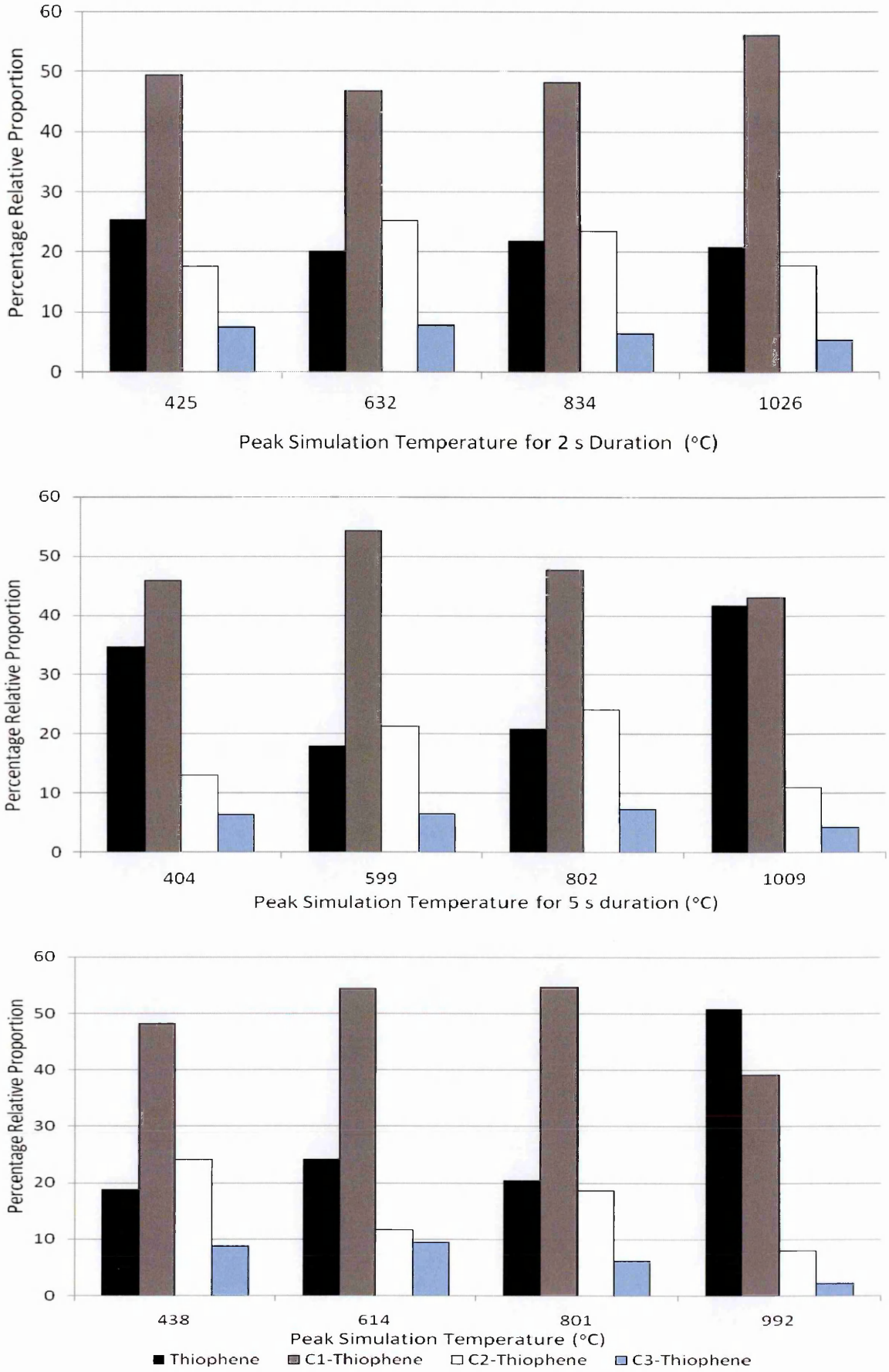

Figure 39: The relative proportions of thiophene and C_1-C_3 alkyl substituted thiophenes released on simulations for 2 s (top), 5 s (middle) and 20 s (bottom), expressed as a percentage of the total thiophenes in each sample (derived from chromatogram peak area abundances)

ranging from 425 °C to 1026 °C. During simulations for 5 s, the ratio of alkyl to parental thiophenes was highest (4.6) in simulations to 599 °C and lowest (just 1.4) in simulations to 1009 °C.

Elemental sulphur in samples can generate H_2S on heating via the dehydrogenation of organic components, which can subsequently lead to the formation of secondary thiophenes and other S-bearing species (Simmonds et al., 1969). However, the effect of this process is thought to be minimal (Hayes & Biemann, 1968) as it is limited by the small sample size pyrolysed and the short heating durations.

Alkylthiophenes are thought to be released from macromolecular material via a similar mechanism to that of the alkylbenzenes, predominantly the β- cleavage, γ-hydrogen rearrangement and γ-cleavage of macromolecular-bound thiophenic moieties (Hartgers et al., 1994). Similar to the distribution of alkylbenzenes, that of the alkylthiophenes is dependent on the thiophenic precursors bound to the macromolecular structure. Oxidation of Murchison macromolecular material using sodium dichromate (Hayatsu et al., 1980) and XANES (Derenne et al., 2002) reveal the presence of such sulphur bearing moieties (substituted benzothiophenes and dibenzothiophenes).

Pyrolysis experiments on terrestrial kerogens, coals and asphaltenes at 350 °C found trace amounts of alkylthiophenes, whilst at 610 °C a broad variety of alkylthiophenes are released (Sinninghe Damsté et al., 1989). A similar increased release of alkylthiophenes in Murchison samples heated to ~ 600 °C relative to ~ 400 °C is only noticeable in short duration simulations (2 s and 5 s). Sinninghe Damsté et al., (1989) suggest that higher pyrolysis temperatures (610 °C) enables the cleaving of C-C bonds (which has a high bonding energy *ca.* 350 kJ/mol) in addition to S-S and C-S bonds (bond energies *ca.* 250 kJ/mol and 275 kJ/mol respectively). Under lower temperature pyrolysis conditions, the authors suggest that only S-S and C-S bonds are cleaved. However, for 2 s simulations at temperatures >600 °C, the percentage proportions of thiophene and total alkyl thiophenes remains constant suggesting simulation heating conditions do not effect thiophenes in a similar manner as benzenes.

The thermal decomposition of thiophene occurs under pyrolysis at 800–850 °C (Wynberg & Bantjer, 1959) to yield CS_2, C, H_2S, volatile and non-volatile hydrocarbons. At temperatures of 1023-1127 °C benzene is also produced (Cullis & Harris, 1972). More recently, Winkler et al., (2002) observed that at >800 °C, secondary reactions occur between thiophene starting species (thiophene, benzothiophenes and dibenzothiophene) and their fragments from decomposition, leading to the formation of 1-4 carbon ringed PAHs and S-bearing polycyclic hetarenes. In addition, their breakdown is potentially contributing to the generation of S-bearing species (CS_2), PAHs and benzene at higher simulation temperatures.

D. Nitrogen Bearing Species

(i) Nitriles

Benzonitrile and acetonitrile, common in Murchison pyrolysates (Levy et al., 1973; Yabuta et al., 2007) are liberated from all simulated samples. Their ratios to benzene liberated at each simulation condition are given in Figure 40. There is a reduction in acetonitrile release with increasing simulation temperature and heating duration. The same trend is observed in benzonitrile for 2 s and 5 s hating durations. Recent NMR studies (Derenne & Robert, 2008) demonstrate that nitrogen within chondrite macromolecular material is present within N-heterocycles and to lesser extent nitriles.

This simulation study suggests that their release from the breakdown of macromolecular material is either inhibited at higher temperatures, perhaps as a consequence of condensing aromatic units (as is outlined for other aromatic species in Section 3.5.1B). Alternatively, released acetonitrile may be thermally decomposing to methane and hydrogen cyanide at higher simulation temperatures (Lifshitz & Tamburu, 1998). During simulations for 20 s, optimal release of benzonitrile occurs at heating to ~ 600 °C, at increasingly higher temperatures the abundance released decreases. At temperatures of 500-600 °C under pyrolysis conditions in the presence of nitrogen (derived from the decomposition of N-bearing organic species), benzonitrile fragments to

products including hydrogen cyanide and benzene (Etemad-Rad & Metcalfe, 1993) which may be contributing to its reduced release at higher simulation temperatures.

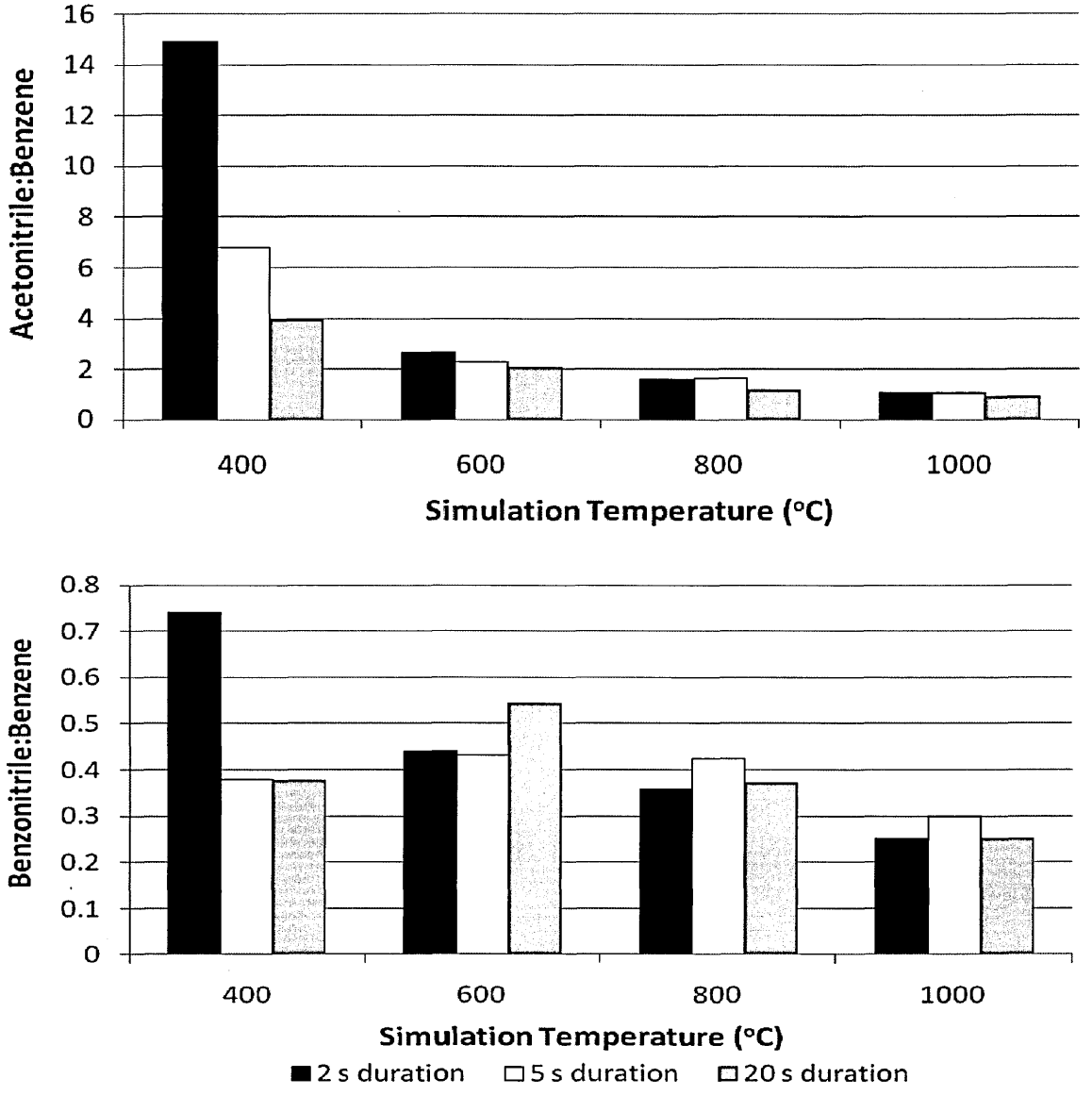

Figure 40: Chromatogram peak area abundance ratios of acetonitrile:benzene (top) benzonitrile:benzene (bottom) for varying simulation conditions

(ii) Nitrogen Heterocycles

A range of nitrogen heterocycles are identified in simulation products. These include six-member rings – pyridine, pyrimidine, pyrazine, pyridazine and triazine and the five-member ring pyrrole. Additionally alkylated nitrogen heterocycles C_1–C_3 alkylpyridines, C_1-C_4 alkylpyrazines and C_1–C_2 alkylpyrimidines, methylpyridazine and

methyl-1H-pyrrole are also identified. The Murchison macromolecular material is known to comprise N-containing moieties in the form of N-heterocycles (Derenne & Robert, 2008; Hayatsu et al., 1977), analogous to coal nitrogen which comprises pyrrolic and pyridinic N-heterocycles (Solomon & Colke, 1978). Similar to coal pyrolysis (Hambly, 1998), Murchison macromolecular pyrolysis will preferentially break bonds of low bond energy first (i.e. C-H bonds of low bond energy 338.4 kJ/mol, Handbook of Chemistry and Physics (2008)), releasing N-heterocycles and alkyl substituted species from macromolecular material in a similar manner to benzenes and thiophenes detailed previously.

The abundances of these nitrogen heterocycles varies significantly with simulation conditions. Changing abundances of pyrrole, pyridine, pyrazine and pyrimidine relative to those of Murchison reference sample are plotted for varying peak simulation temperatures for 2 s, 5 s and 20 s simulation durations (Figure 41). No pyridine or pyrimidine was detected in the gas released from simulations conducted at 425 °C for 2 s, indicating that a minimum temperature is required for the release of these compounds. The absence of these N-heterocylces in pyrolysates at low temperatures suggests that these species orginate in the insoluble orgnic fraction within macromolecular material. The greatest abundance of each species released during simulations for 2 s and 5 s was at 834 °C and 802 °C respectively.

The amount of pyrrole released during a 2 s duration simulation to 834 °C was almost x 2.4 that in Murchison reference material. In the case of pyridine, pyrazine and pyrimidine released during simulations for 5 s durations, abundances from simulations to 802 °C were x 1.1, x 1.4 x and x 1.4 that of Murchison reference material, respectively. It suggests that there is optimal release of these nitrogen heterocycles at approximately 800 °C, with lower temperatures not providing the energy required to release these species. At higher simulation temperatures (~1000 °C), C-N bond breaking (high bond energy 750.0 k/mol, Handbook of Chemistry and Physics (2008)) may be occurring causing the decomposition of N-heterocycles to HCN, NH_3 and N_2 as it does in pyrrolic and pyridinic

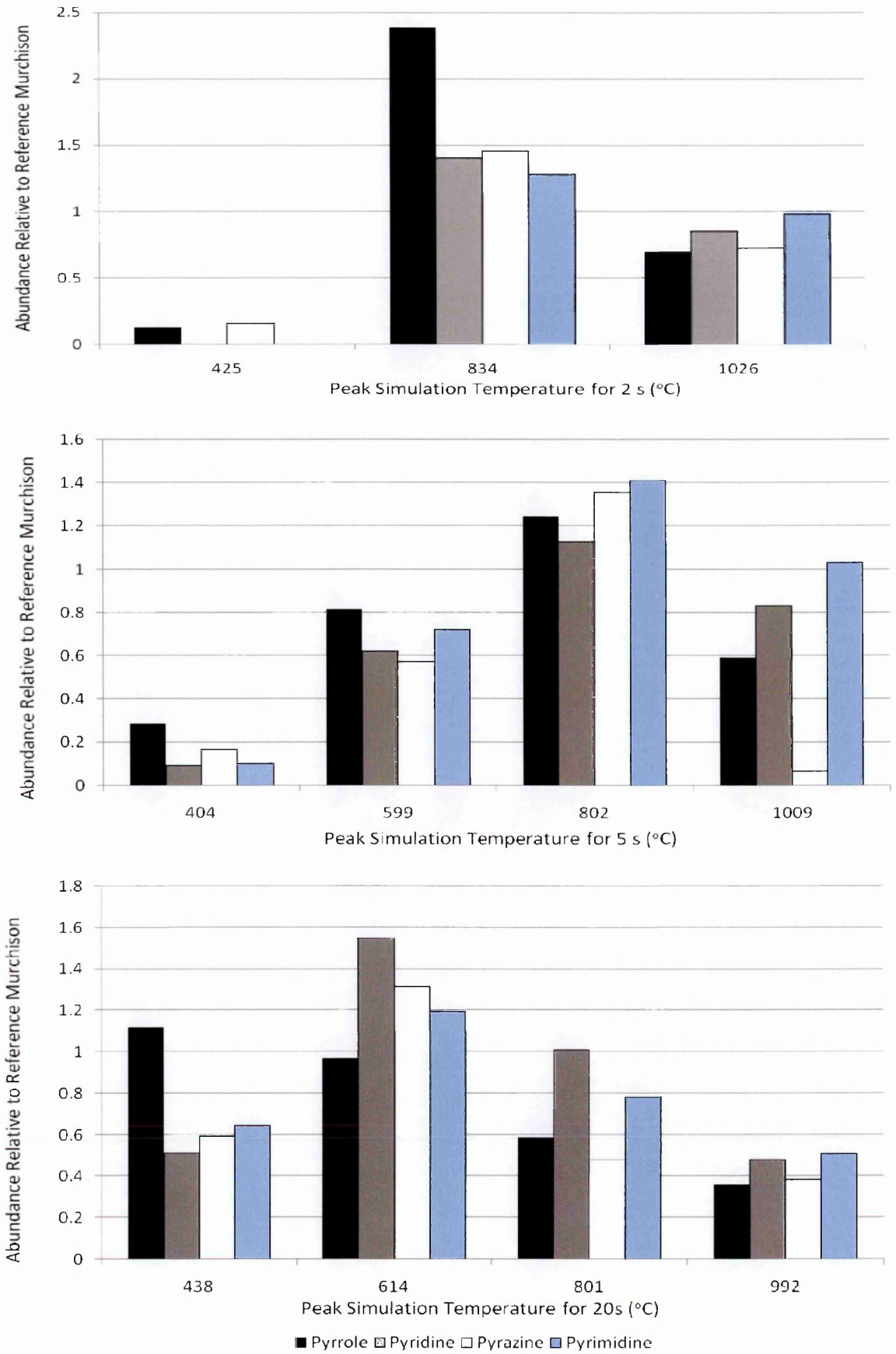

Figure 41: Chromatogram peak area abundances of N-heterocycles (relative to that in the unheated Murchison reference sample) released during simulations for 2 s, 5 s and 20 s to various peak temperatures

coals (Solomon & Colket, 1978). Alternatively condensation of the aromatic structure may be occurring during more extensive heating (longer durations and at higher temperatures), thus limiting the release of further N-heterocyles from macromolecular material.

This may explain the low abundance of N-heterocycles liberated during simulations for a 20 s duration to temperatures >600 °C (Figure 41). Similar trends in the abundance of the thiazole released during simulations (Figure 42), suggesting a similar fate for N-S heterocylic species.

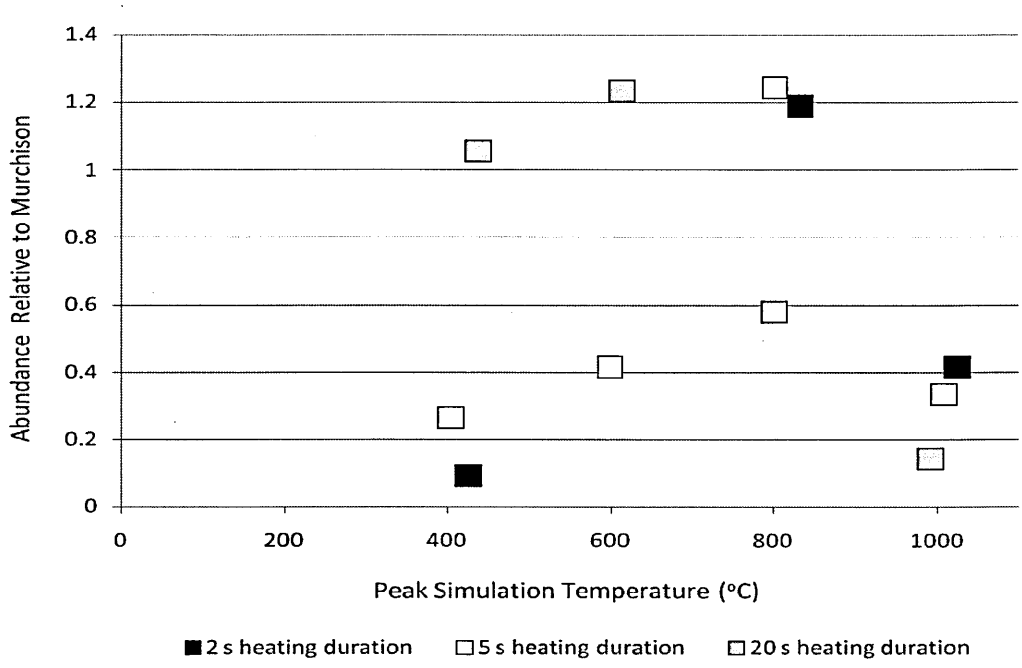

Figure 42: Chromatogram peak area abundances of thiazole released in simulations of varying conditions relative to reference Murchison

D. Oxygen, Hydroxyl and Carboxyl Bearing Species

Up to C_5 aliphatic alcohols, benzaldehyde, phenol, C_1-phenol and the carboxylic acid acetic acid are identified in liberated species of all simulation conditions. Polar compounds (alcohols and acids) have very broad peak areas, some of which tail across the primary column. Without well defined peaks, it is not possible to use some peak areas as indicators of abundance for oxygen-bearing species. During short duration simulations of 2 s and 5 s, the relative abundances of phenol and methyl phenol (Figure 43) tend to increase with increasing simulation temperature. This suggests substantial cleaving of

macromolecular ether cross linkages present in Murchison (Cody & Alexander, 2005; Hayatsu et al., 1980; Sephton et al., 1998) at increasing temperatures, analogous to that

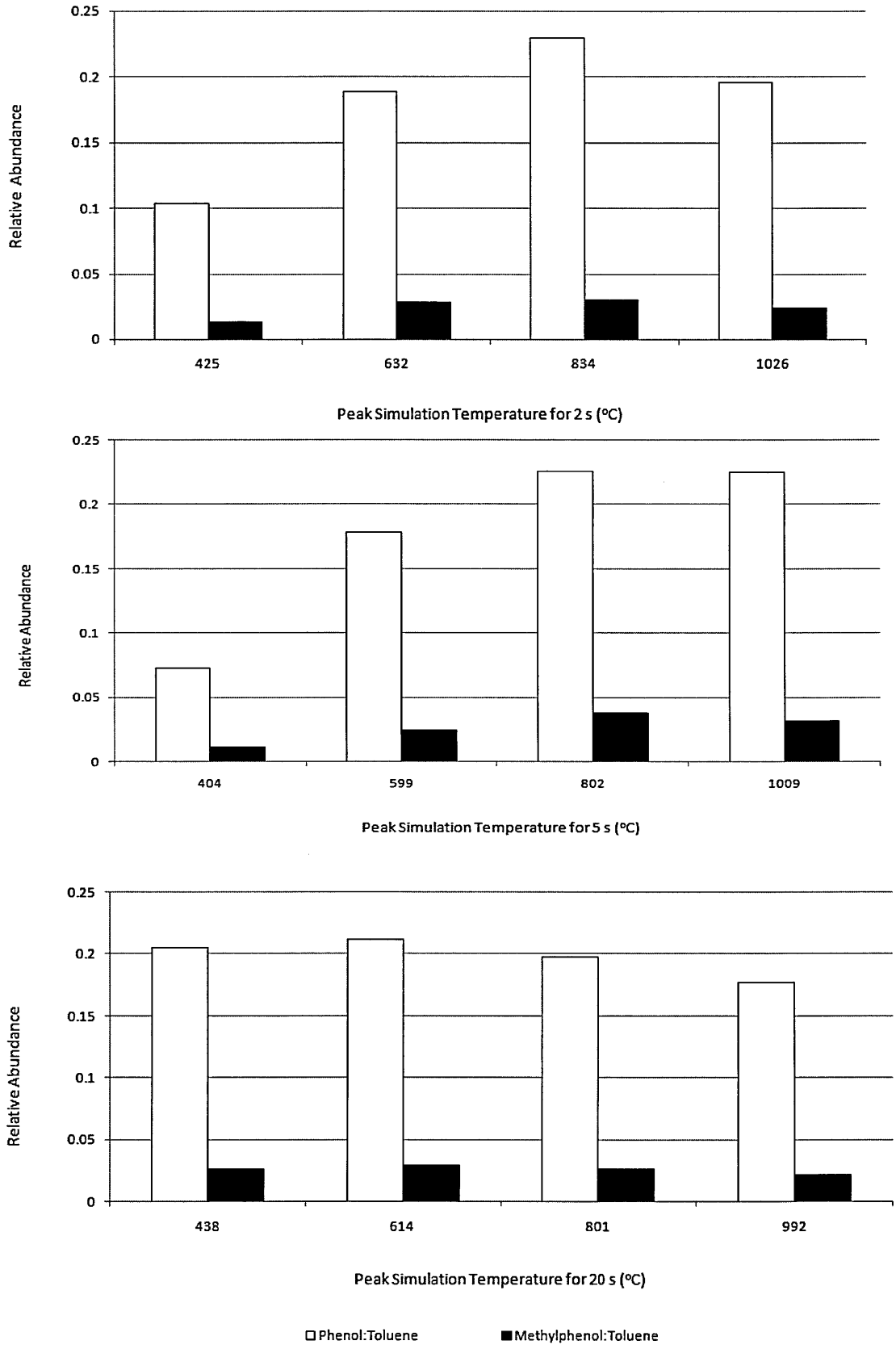

Figure 43: Chromatogram peak area abundances of phenols (relative to that of toluene in each sample) released during simulations for 2 s, 5 s and 20 s to various peak temperatures

occurring during coal pyrolysis (Schlosberg et al., 1981; Siskin & Aczel, 1983). It is possible that intermolecular rearrangements (Schlosberg et al., 1983) or the oxidation of liberated benzene by Fe-bearing cations (Shiota et al., 2005) derived from iron oxides in the Murchison matrix (Fuchs et al., 1973) may also contribute to the enhanced abundance of phenol released at higher temperatures.

In simulations for longer durations (20 s), the relative abundances of phenols released decreased with increasing simulation temperature. This may be the result of the thermal decomposition of phenol (Brezinsky et al., 1998) under extreme heating conditions to benzene, or a consequence of the aromatic network condensing at higher temperatures (Juntgen, 1987a; Juntgen, 1987b).

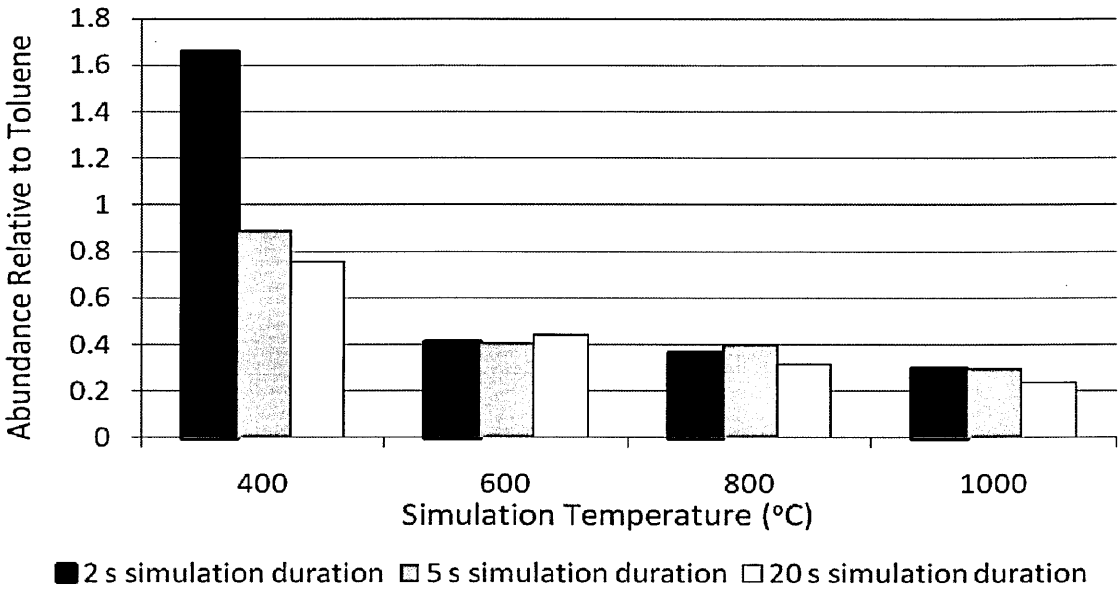

Figure 44: Chromatogram peak area abundances of benzaldehyde (relative to toluene) for all simulation conditions

Benzaldehyde decreased with increasing simulation temperature and heating duration (Figure 44), suggesting that at higher simulation temperatures, benzaldehyde is decomposing (Smith & Hinshelwood, 1940). Benzene is the primary decomposition product, thus contributing to the increasing release of benzene observed at increasing simulation temperatures (Figure 38).

3.5.2. PAH Release During Simulations from High Molecular Weight Simulations

Figure 45 shows the distribution of 1-4 ringed aromatic cores expressed as a percentage of total aromatic cores detected in pyrolysates. Whilst 1-ringed aromatic cores (benzene) show a maximum release of 84 % at simulations to 829 °C for a 2 s duration, the release of 2- ringed core aromatics (naphthalene) is at a minimum (just 15 % of total aromatic cores). In simulations for longer durations (5 s and 20 s) the abundance of 1-ringed aromatic cores increases with increasing simulation temperature, while 2-ringed, 3-ringed and 4-ringed aromatic cores decrease in abundance. Analysis of the volatile organic compounds released during simulations (Section 3.5.1) suggests that while aromatic macromolecular structure will condense at higher simulation temperatures (Juntgen, 1987a; Juntgen,1987b) accounting for the decreased release of 2-4 ringed PAHs, benzene can also be produced by the cracking of C_2-C_4 alkylbenzenes (Mochida & Yoneda, 1967), contributing to increasing benzene abundances at higher simulation temperatures. Additionally thiophene decomposition at temperatures in simulations at >800 °C contributes to 1-4 ringed PAH abundances (Winkler et al., 2002).

Substantial loss of naphthalene (2-ringed PAH) occurs at all simulation durations, but decreases with increasing simulation temperature. In an analogous scenario, reduced abundances of naphthalene are observed in the free organic fraction of CK meteorites and the Coolidge C4 chondrite (Elsila et al., 2005), that have experienced thermal alteration on their parent bodies between 550 – 1000 °C (Geiger & Bischoff, 1991; Kallemeyn et al., 1991; Kallemeyn & Rubin, 1995). More extensive thermal metamorphism of carbonaceous chondrite parent bodies results in significant volatilisation and subsequent loss of parental and alkyl PAHs (Elsila et al., 2005), producing more condensed, graphitised aromatic units within chondritic macromolecular material (Kitajima et al. 2002; Komiya et al., 1993).

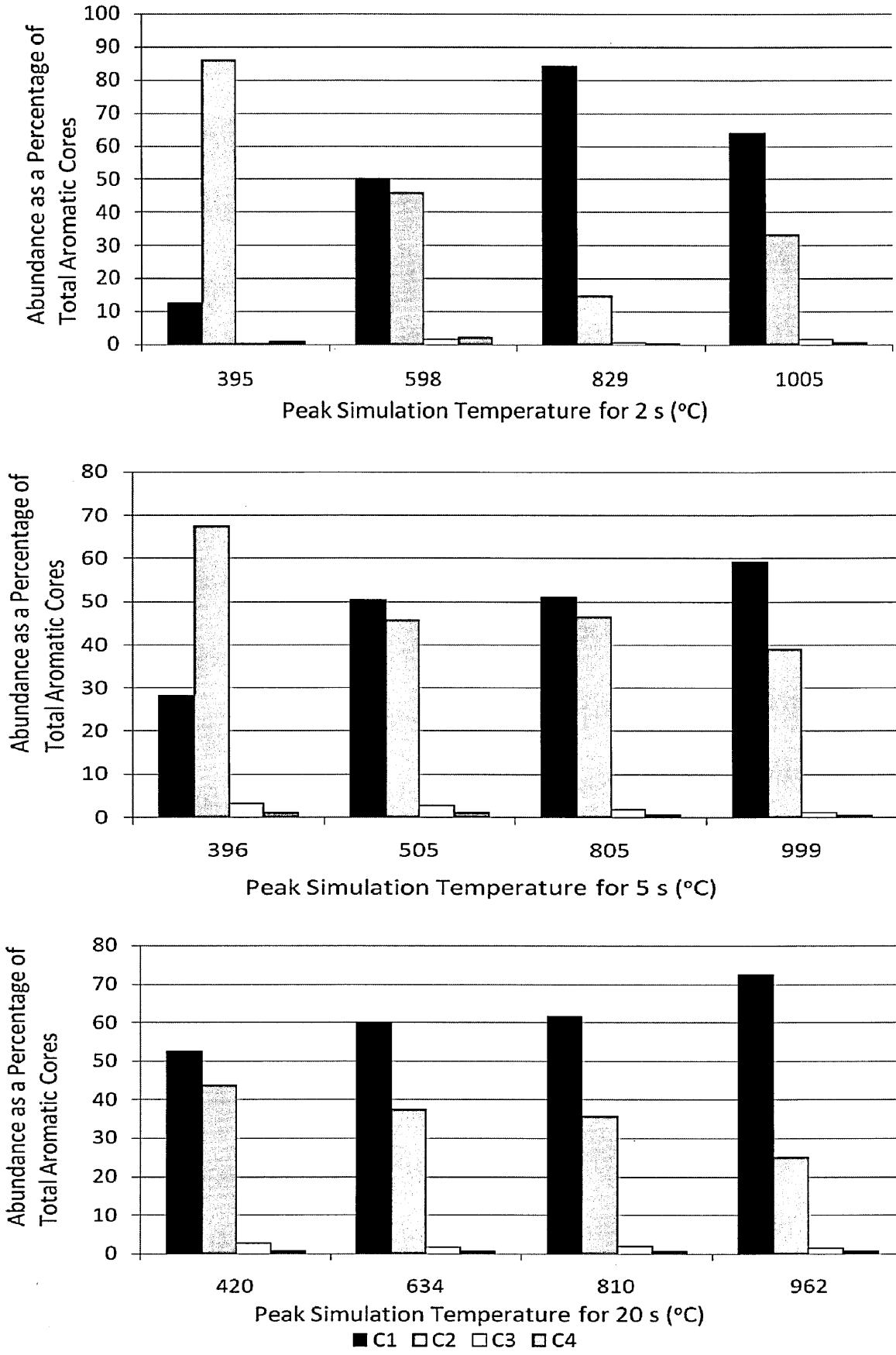

Figure 45: Chromatogram peak area abundances of 1-4 ringed aromatics (C1-C4) expressed as a percentage of total aromatic cores

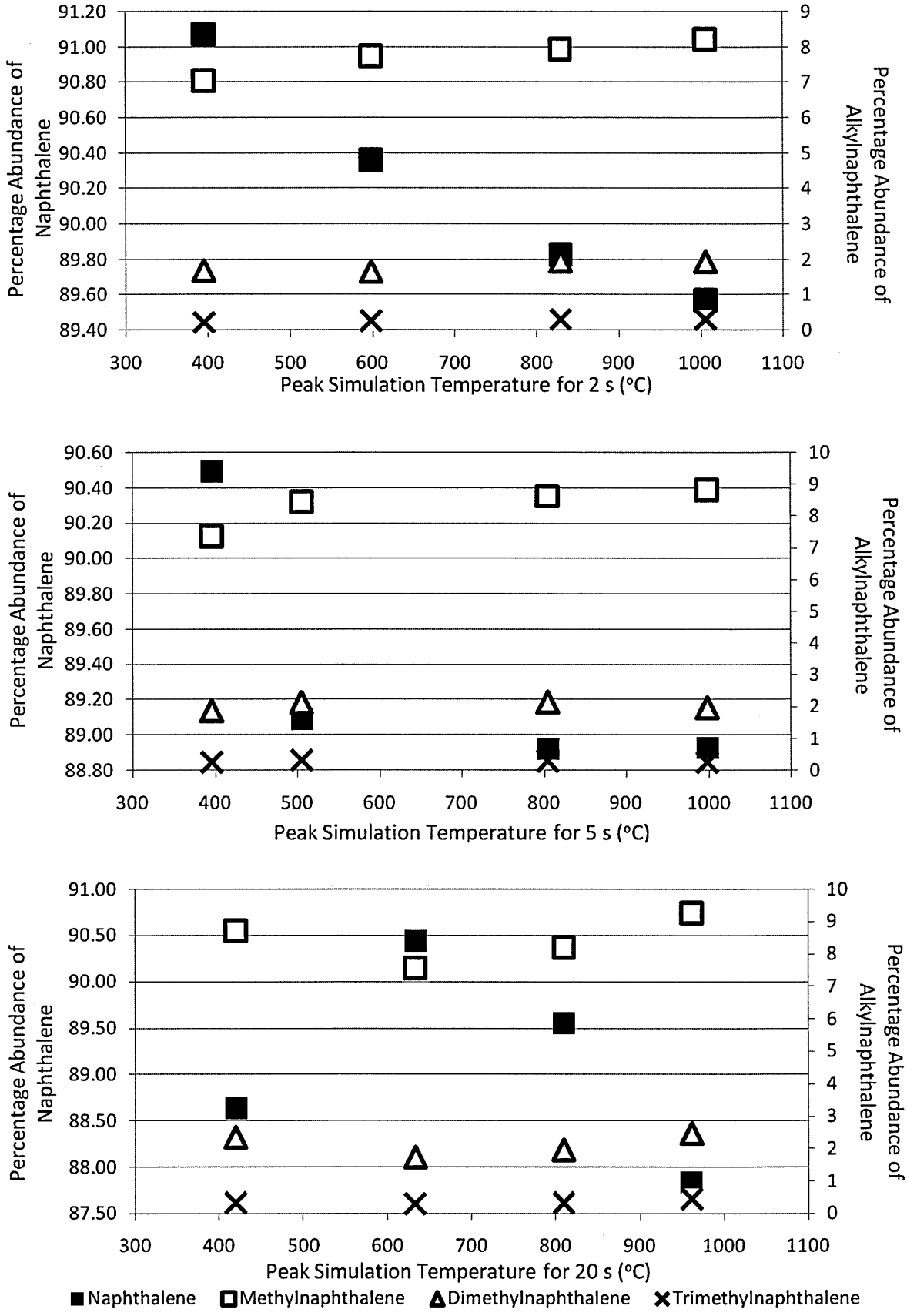

Figure 46: Chromatogram peak area abundances of naphthalenes expressed as a percentage of total naphthalene, methyl- dimethyl- and trimethyl-naphthalenes

The abundance of naphthalenes for all simulation conditions is given in Figure 46 as a percentage of total naphthalene and alkylnaphthalene (methyl-, dimethyl- and trimethylnaphthalene). In simulations for 2 s and 5 s, naphthalene abundances decrease with increasing simulation temperature, whilst those of the alkylnaphthalenes increase. Despite an enhanced release of naphthalene at 634 °C during 20 s simulation durations, there is an increase in the release of alkylnaphthalenes with increasing simulation temperature. These trends in parental and alkyl naphthalene release are analogous to compositional changes of kerogen-containing sediments within close proximity to dykes and sills (George, 1992; Murchison & Raymond, 1989). Depending on distance from an intrusion, the organic material would be subject to temperatures of 250–1200 °C for long durations of days or months. Analysis of bitumen extracts from a siltstone within 0.18m of a quartz-dolerite dyke contained higher ratios of parent to alkyl PAHs (George, 1992) compared to samples further from the dyke. Samples close to the intrusion, experiencing higher temperatures, would result in thermally destroying or volatising a greater proportion of alkyl PAHs. A similar trend is observed in the atmospheric entry heating simulations, as increasing abundances of alkylnaphthalenes (methyl-, dimethyl- and trimethyl-naphthalenes) are released from macromolecular material at higher simulation temperatures for 2 s and 5 s Figure 46.

A. Methylnaphthalene Ratios and Thermal Maturity

The relationship between 1-methylnaphthalene (1-MN) and 2-methylnaphthalene (2-MN) (Equation 1) has traditionally been used as an indicator of thermal maturity of free organic fractions of terrestrial kerogens (George, 1992; Radke et al., 1982; Raymond & Murchison, 1992). Pyrolysis (Pearson et al., 2006; Remusat et al., 2005 b; Shimoyama, 1997) and hydrous pyrolysis (Sephton et al., 2000) studies of carbonaceous chondrites have identified MNRs as an indicator of thermal processing.

$$\text{Methylnaphthalene ratio (MNR)} = \text{2-MN}/\text{1-MN} \qquad \textbf{(Equation 1)}$$

Typically, 1-MN dominates at lower temperatures, whilst 2-MN is more dominant at higher temperatures as it is thermodynamically favourable. Therefore, the methylnaphthalene ratio (MNR) increases with increasing temperature as the methyl group shifts from α to β configuration (dominance shifts from 1-MN to 2-MN).

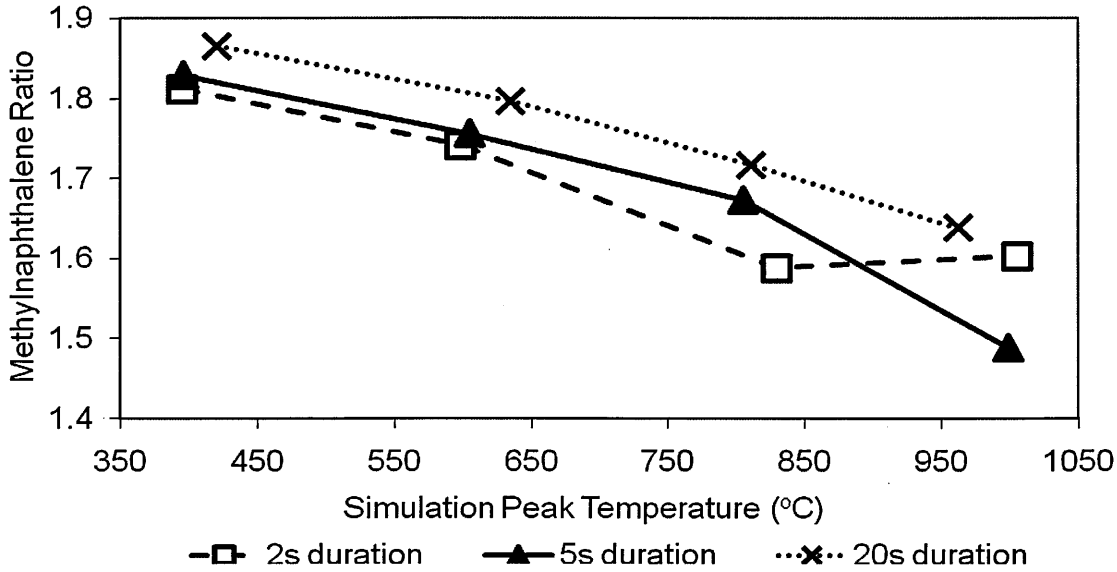

Figure 47: Variations in methylnaphthalene ratios of released simulation species with respect to simulation durations and peak temperatures

Regardless of simulation duration, the MNR of liberated species decreases with increasing simulation temperature (Figure 47). At increasing simulation temperatures, whilst almost a constant low percentage abundance of the more thermally stable 2-methylnaphthalene is released (typically 0.05-0.06 % of total naphthalene, methyl-dimethyl- and trimethyl- naphthalenes), an increasing percentage abundance of 1-methylnaphthalene is released from samples (Figure 48).

The flash heating of samples in this simulation, volatilises the less stable 1-methylnaphthalene. Subsequently, thermally altered residues would be depleted in 1-methylnaphtalene and therefore would exhibit a "high" MNR. For example, under standard pyrolysis conditions, Orgueil has a lower MNR than Murchison (Remusat et al., 2005 b) reflecting its lower degree of thermal alteration than Murchison.

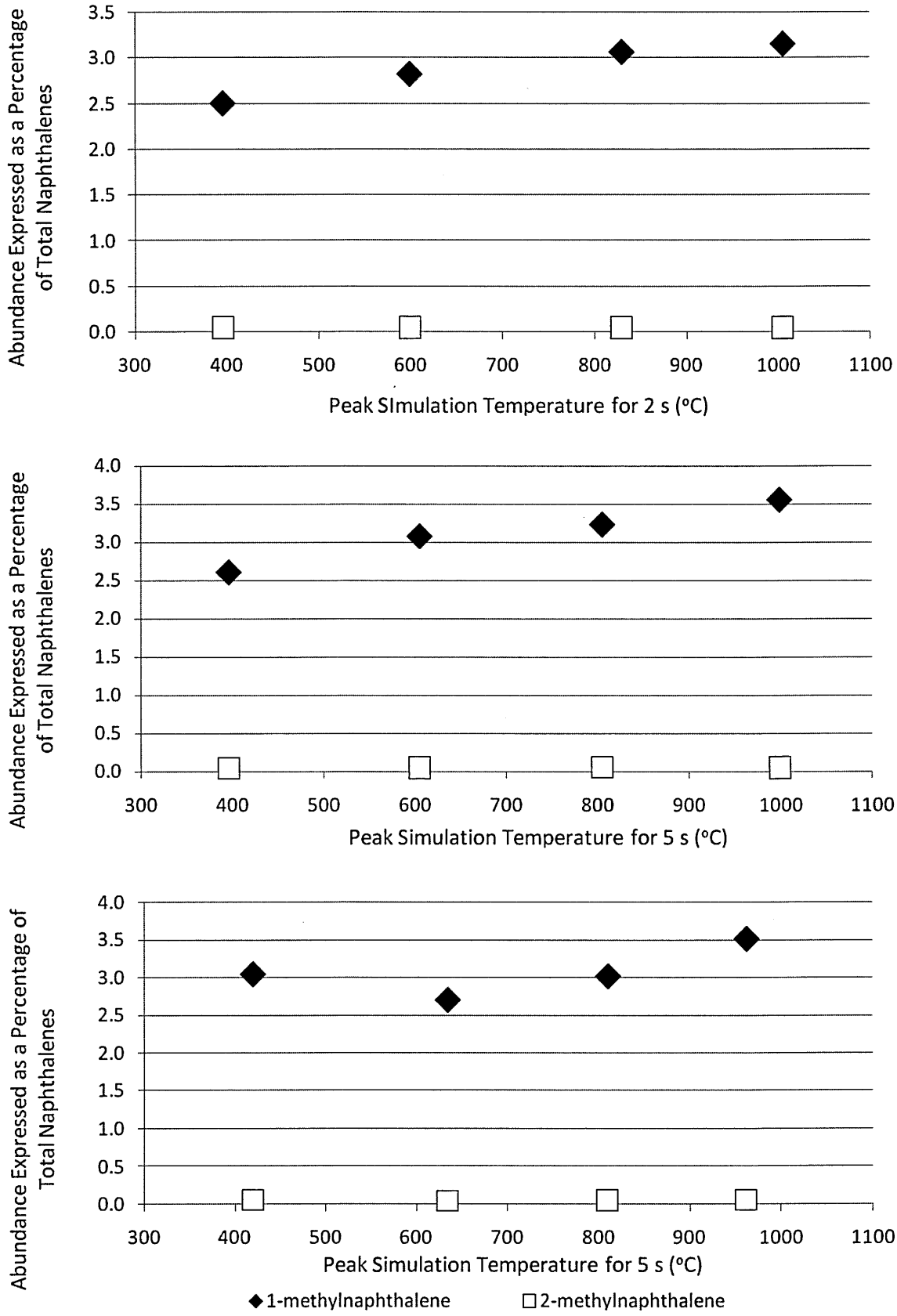

Figure 48: Abundances (derived from chromatogram peak areas) of 1-methylnaphthalene and 2-methylnaphthalene expressed as a percentage of total naphthalenes (naphthalene, methyl- dimethyl- and trimethyl- naphthalenes)

3.5.3. A Summary of the Organic Species Liberated in Simulations

A vast range of organic species are released upon simulations of EDP atmospheric entry heating, the abundances of which are directly affected by simulation conditions (peak temperature and heating duration). Many of these compounds and functional groups have been identified in MMs that have survived entry heating (Section 1.4.4) and their composition is thought to be analogous to CM2 chondrites (Section 1.4). Assuming MMs are composed of a similar macromolecular structure as carbonaceous chondrites, they will undergo similar mechanisms to liberate organic species. Benzenes, thiophenes and N- N-S heterocycles and their alkyl derivatives released in simulations, are thought to originate from predominantly the β-cleavage of monoaromatic macromolecular bound moieties within Murchison macromolecular material with similarities to a process in coal, kerogen and asphaltene pyrolysis (Hartgers et al., 1994).

Total C_1-C_4 alkyl benzenes decrease with increasing simulation temperature, a consequence of heating to higher temperatures resulting in cleaved radicals combining to form larger components which condense producing higher aromatic structures (Juntgen, 1987a; Juntgen, 1987b). Additionally cracking of C_2-C_4 alkylbenzenes results in their dealkylation to benzene (Mochida & Yoneda, 1967), yielding increased benzene and short alkyl chains at higher simulation temperatures. There are additional contributions of released benzenes at higher simulation temperatures from the decomposition of thiophenes (Winkler et al., 2002) and benzonitrile (Etemad-Rad & Metcalfe, 1993).

The abundances of parental and total alkyl thiophenes remain relatively constant throughout varying simulation conditions, contrary to that of the benzenes. At heating temperatures >800 °C, thiophenes decompose and secondary reactions can produce benzenes and 1-4 ringed PAHs (Winkler et al., 2002). Similar to thiophenes, N-heterocycles decompose when C-N and C-S bonds are broken at simulation temperatures ~1000 °C, thus contributing to their lack of release at higher simulation temperatures. Released nitriles also decrease in abundance with increasing simulation temperature. Acetonitrile and benzonitrile decomposition to methane and HCN (Lifshitz & Tamburu,

1998) and HCN and benzene (Etemad-Rad & Metcalfe, 1993) respectively at higher simulation temperatures may be a contributing factor.

Phenol and methylphenol relative abundances in liberated species, increased with increasing simulation temperature for short durations of 2 s and 5 s. This may reflect the increased cleaving of phenolic precursors at higher temperatures from the aromatic network. In contrast the reduction in benzaldehyde released during simulations at increasing temperatures, suggests it may be susceptible to thermal decomposition (Smith & Hinshelwood, 1940).

With the exception of benzene, PAH cores are released in decreasing abundances with increasing temperatures. This is reflective of condensation of aromatic units within Murchison macromolecular structure with increasing simulation temperature, in a process analogous to the consequence of thermal metamorphism on chondrite parent bodies. Chondrites that have experienced extensive thermal metamorphism of parent bodies and consequential volatisation and loss of parental and alkyl PAHs (Elsila et al., 2005), produce more condensed, graphitised aromatic units within chondritic macromolecular material (Kitajima et al., 2002; Komiya et al., 1993).

Additionally, phenol, thiozole and N-heterocycles (pyrrole, pyridine, pyrazine, pyrimidine) all exhibit a temperature of maximum liberation during simulations. For example in short duration simulations (2 s and 5 s) a maximum relative abundance of these species is released at around 800 °C, suggesting it is an optimal release temperature for these compounds.

3.6. Limitations of the Simulations

Carbonaceous material is not homogenously distributed within the Murchison meteorite (Binet et al., 2002; Brearley, 2002). This heterogeneity is a contributing factor in minor compositional variation of samples used in both offline and online simulations.

As the analysis of simulations on this scale are labour intensive, no replicates of online simulations have been carried out. Although simulations were conducted on

relatively small samples, < 1mg, these were still carried out on multiple grains representing a cluster of EDPs and may not necessarily be representative of single grain behaviour. Heating of multiple grains could still result in grain shielding or insulation, just not to the extent as was observed during preliminary investigations using a Pt coil heating method (Section 2.2.1). Such shielding effects may account for recondensation of some volatiles and organics released at high temperatures back onto grains as is demonstrated by the retention of adsorbed water in samples simulated to >800 °C for 2 s and 5 s (Section 3.4.2). Such effects would be negligible in smaller sample masses, ideally of individual grains.

3.7. Conclusions

The release of volatile and organic material from EDP simulation studies is dependent on peak heating temperatures and durations as is indicated by the progressive dehydration of phyllosilicates, loss of organic material and the decarbonation of carbonates in offline simulations. Up to 8.6 wt. % water and 2.2 wt. % organic carbon was released during simulations for 2 s and 5 s to 1000 °C. Textural observations of EDPs and comparison to previous heating simulations (Toppani et al., 2001) show they exhibit desiccation cracks and vesicles, which are consistent with the substantial loss of volatile and organic material during simulation conditions of this study.

Online simulations (coupled to GCxGC-TOFMS) have been successful in identifying a range of organic species volatised from samples during heating experiments including benzenes, thiophenes, N- and S-N heterocycles, nitriles, PAHs and aliphatic species. Abundances of these species released during simulations is dependant not only on peak temperature and heating durations in order to release them from macromolecular material, but also on their reaction with other fragments, leading to their production as secondary products. Furthermore, there is evidence that some components (N-heterocycles and N-S heterocycles in particular) have an optimal release temperature in the region of 800 °C during simulations for 2 s and 5 s. In particular, biomolecule

precursors pyridine and pyrimidine are not released during gentle heating simulations (425 °C for 2 s).

4. Analysis of Antarctic Micrometeorites by Comprehensive 2-dimensional (GCxGC) Chromatography

4.1. Introduction

Micrometeorites (MMs) have been proposed as significant contributors of prebiotic material to the early Earth (Anders, 1989; Maurette et al., 1995) and have consequently been investigated using a variety of techniques in attempts to characterise their organic carbon contents. The spatial distribution of carbon within MMs has been studied using a combination of energy dispersive spectrometry (EDS) and electron energy loss spectroscopy (EELS) (Maurette et al., 1995). These observations have found that carbon is uniformly distributed throughout MMs, with no clear correlations between carbon and other elements (Maurette et al., 2000; Maurette et al., 1995). More specific information on the nature of organic matter has come from Fourier transform infrared spectroscopy (FTIR) (Matrajt et al., 2001; Suzuki et al., 2005) which has identified aliphatic (methyl), aromatic and hydroxyl groups in MMs, whilst scanning transmission X-ray microscopy (STXM) (Matrajt et al., 2001) has identified the carbonyl group. However, to date, attempts to more fully characterise the organic constituents of micrometeorites have been limited by the extremely small size of individual MMs and the subsequent need to work with larger clusters of a sample set that is and hard to obtain.

The carbonaceous chondrites are known to contain a diverse range of organic material (Anders et al., 1973; Botta & Bada, 2002; Briggs, 1961; Cronin et al., 1988; Sephton, 2002), and so a fundamental question arises as to nature of any relationship between organic matter in chondritic meteorites and chondritic micrometeorites. Of the limited studies that have been undertaken, microscopic L^2MS indentified polycyclic aromatic hydrocarbons (PAHs) in individual MMs, up to 5-ring PAHs and their alkyl derivatives (Clemett et al., 1998). HPLC (Brinton et al., 1998) and ion-exchange

chromatography with fluorimetric detection (Matrajt et al., 2004) have also been successful in identifying a number of protein amino acids in the free organic fraction including glycine and alanine, although assessing the indigeneity of these species was inconclusive.

From the studies so far undertaken, it is evident that some similarities exist between the organic species identified within MMs and those within carbonaceous chondrites such as Tagish Lake (Suzuki et al., 2005) and Murchison (Matrajt et al., 2001). However, a closer examination reveals that distinct differences in PAH distributions are also apparent (Section 1.4.4 A), for example between MMs and Murchison (Clemett et al., 1998), as well as the marked enrichment in carbon abundance of MMs relative to carbonaceous chondrites (Maurette et al., 1995 a; Maurette et al., 1995 b).

4.2. Aims and Objectives

The development of methodologies for the analysis of µg-sized quantities of extraterrestrial materials was reported in Chapter 2 and applied to the analysis of volatile and high molecular weight organic species released from MM atmospheric entry heating simulations in Chapter 3. In this chapter, the same technique is utilised to characterise the organic composition of Antarctic micrometeorites (AMMs) and is contrasted with complementary Antarctic terrestrial particles collected alongside AMMs during their recovery. Whilst previous work has attempted to characterise PAHs in AMMs (Clemett et al., 1998), this study focuses on the wider range of volatile organic species. Comparison of AMM volatile organic composition with that of Antarctic terrestrial particles will serve a potential indicator of the level of terrestrial contamination, the indigeneity of organic species and Antarctic processing. Comparative analysis of AMMs with that of carbonaceous chondrites such as Murchison will provide constraints on the possible origins of organic species in micrometeorites and their parent bodies.

4.3. Experimental

4.3.1. Samples and Sample Handling

This study analyses previously uncharacterised particles recovered as sample #141 in 1994, by melting blue ice from the Antarctic Cap-Prudhomme site and filtering the melt water through stainless steel sieves with openings of 25 μm, 50 μm, 100μm and 400 μm size (Maurette et al., 1991; Maurette et al., 1994). Batch #141 comprises particles in the 100 - 400 μm grain size sieved fraction and includes a mixture of AMMs, terrestrial particles and glacial sand.

Samples were manipulated under a binocular microscope using a nylon brush (previously cleaned in distilled water) and a drop of distilled water. The pale brown glacial sand particles were readily identified and separated from the sample, leaving the remaining fraction of black coloured particles consisting of AMMs and Antarctic terrestrial particles. Of the remaining fraction, twenty-four dark coloured particles were separated and fragmented using a scalpel cleaned with distilled water. This enabled a portion of each particle to be analysed using scanning electron microscopy (E.Dobrica) to confirm terrestrial or extraterrestrial origin (Appendix III), and illustrate that seven of the eight MM fragments exhibited a "fluffy" texture possibly representing unmelted or partially melted MMs (Maurette, 2006a; Genge et al., 2008).

The remainder of each particle was available for organic analysis. A batch of eighteen particles of "play" sand served as a procedural blank. These were baked at 450 ^{o}C overnight to remove any organic material. Particles were divided into the following sample batches for organic analysis (Table 30) and were imaged under a light microscope in a class 100 clean room, to determine grain/fragment diameters and calculate estimated sample masses.

Samples were manipulated under a binocular microscope onto the Pyrola filament for pyrolysis, using a nylon brush (previously sonicated in methanol) and a drop of

pesticide grade methanol (< 2 ppm residue). The methanol was evaporated from the sample under the light of the binocular microscope prior to pyrolysis.

In addition, 0.9 mg Murchison was also analysed under standard pyrolysis conditions (2s, 600 °C) to serve as a reference.

Batch Name	Description	Sample mass
S	Roasted sand - 18 particles	1.49 mg
T2	Antarctic terrestrial particles - 15 fragments from 8 particles	1.19 mg
ET	AMMs - 21 fragments from 8 particles	0.27 mg
Murchison	Powdered Murchison referenfce material – grain size ≤ 60 µm	0.9mg

Table 30: A table summarising sample batches for organic analysis (see Appendix IV for raw data)

4.3.2. Py-GCxGC-TOFMS

Samples were pyrolysed for 2 s to the temperatures described in Table 31, in a He flow of 1ml/min, using a Pyrola 2000 (Pyrolab, Sweden) coupled to a Pegasus 4D GCxGC-TOFMS (LECO Corporation). The pyrolysis chamber was maintained at 200°C, with pyrolysis temperatures accurately monitored using both filament resistance and a photodiode. The injector inlet was operated in split mode and was maintained at 200 °C, the He (99.9999%) carrier gas had a flow of 1 ml/min during the entire run. The primary column (first dimension) situated in the primary oven, was a SGE BP624 column (30 mx250 µmx1.4 µm) connected to the secondary (second dimension), SGE BP20 column (1.8 m x 100 µm x 0.1 µm) housed in the secondary oven. The BP624 is a cyanopropylphenly polysiloxane coated column, a polar phase designed primarily for volatile organic compound analysis. The SGE BP20 is polyethylene glycol coated column, a very polar phase designed for alcohol, ester, ketone and aldehyde analysis. Due to the nature of the column phases, the primary column had a maximum operational temperature of 230 °C. These columns were selected to optimise the analysis of volatile organic species from the samples but are not suited to the study of higher molecular weight material.

The primary oven was held at 30 °C for 1 min, then raised to 230 °C at a rate of 5 °C/min and held for 10 mins. The secondary oven was offset by +15 °C from the primary oven. A liquid nitrogen cooled modulator was used with an offset from the primary oven of +30 °C for modulation on the secondary column, with a frequency of 3 s. The transfer line to the TOFMS was constant at 240 °C. The acquisition rate was 200 spectra/s for a mass range of 33-401 amu.

Batch Name	Pyrolysis Temperature Photodiode (°C)	Pyrolysis Temperature Resistor (°C)
S	614	614
T2	623	614
ET	625	600
Murchison	632	620

Table 31: Sample peak pyrolysis temperatures, pyrolysis conditions set to 610 °C for 2 s

Figure 49 shows the total ion chromatogram (TIC) for the procedural blank (roasted sand). The chromatogram is dominated by siloxane derivatives typical of column bleed, with typical ion counts of 40,000–200,000. Remaining peaks are extremely poorly defined, and because of their extremely low ion counts relative to the chromatogram baseline they are predominantly unidentifiable.

Data processing was conducted using the LECO ChromaTOF software with peak identification methods set according to peak broadening on both columns throughout the run and a signal to noise ratio of 25. Peaks of the same species were combined both automatically (if they had a minimum of an 85 % spectral match) and manually. Peak identification was conducted using the ChromaTOF built-in library, with a minimum similarity match of 60 % between the sample and library spectra. Peak identification was possible up to mass 128 (naphthalene).

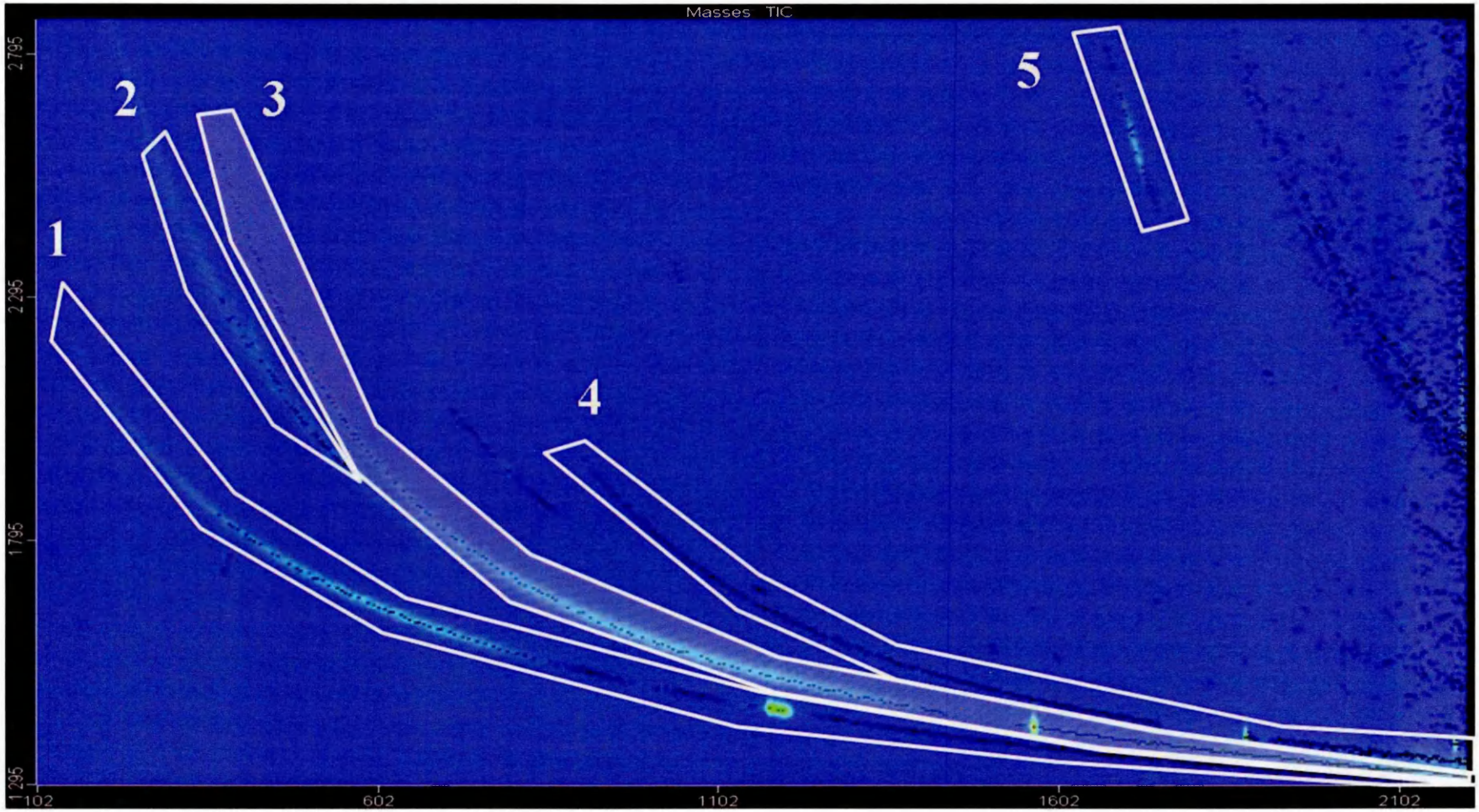

Figure 49: A TIC of the procedural blank (roasted sand) consisting primarily of column bled. 1 - hexamethyl-cyclotrisiloxane, 2 – inconclusive CO_2 or N_2O peak, 3 – octamethyl-cyclotetrasiloxane, 4 – decamethyl-cyclopentasiloxane and 5 – siloxane derivative

4.4. Results and Discussion

4.4.1. The Organic Inventory of Murchison

The volatile organic inventory of a supercritically fluid extracted (SFE) residue of Murchison (as examined by pyrolysis 2 dimensional GC-TOFMS) is fully described in Section 3.3.3. Briefly, it was found to consist of aliphatic hydrocarbons with species up to both C_{13} *n*-alkanes and C_{10} branched aliphatics identified. Additionally aliphatic alcohols (up to C_5) and branched aliphatic alcohols (up to C_{10}) in addition to phenol and methylphenol are present. Dominant acids are acetic acid and aminomethansulfonic acid. Other oxygen-bearing species are acetone and benzaldehyde. Benzene, C_1-C_4 alkylbenzenes and C_1-C_6 n-alkane substituted species are present; with naphthalene the largest aromatic species identified using BP SGE BP624 and SGE BP20 columns, although Murchison is known to contain much larger aromatic species (Section 1.2). The dominant S-aromatic species are thiophene and its C_1-C_3 alkyl-substituted species and the nitrogen-sulphur heterocycle thiozole and C_1-C_2 alkyl derivatives. Additional sulphur-bearing species include sulfonic acid and carbon disulphide. Murchison contains nitrogen-bearing species which include the nitriles acetonitrile and benzonitrile, and a variety of nitrogen heterocycles (pyridine, pyrazine, diazine, triazine, pyrimidine and pyrrole) (Section 3.5). Alkyl derivatives of these heterocycles (C_1-C_3 alkyl pyrimidines, C_1-C_4 alkyl pyrazines, C_1-C_2 alkyl pyrimidines, methyl pyridazine and methylpyrrole) are also present. The only amines identifiable in Murchison pyrolysates are benzoamine and methyl-benzoamine.

4.4.2. The organic inventory of Antarctic Micrometeorites

A 2D total ion chromatogram (TIC) of AMMs is given in Figure 50, identifying major species. These include a aromatic species (benzenes and thiophenes) with their alkyl counterparts, a number of N- and S-N heterocycles, acetic acid, phenol and a range of aliphatic species. Figure 51 comprises a reconstructed ion chromatogram (RIC) of mass

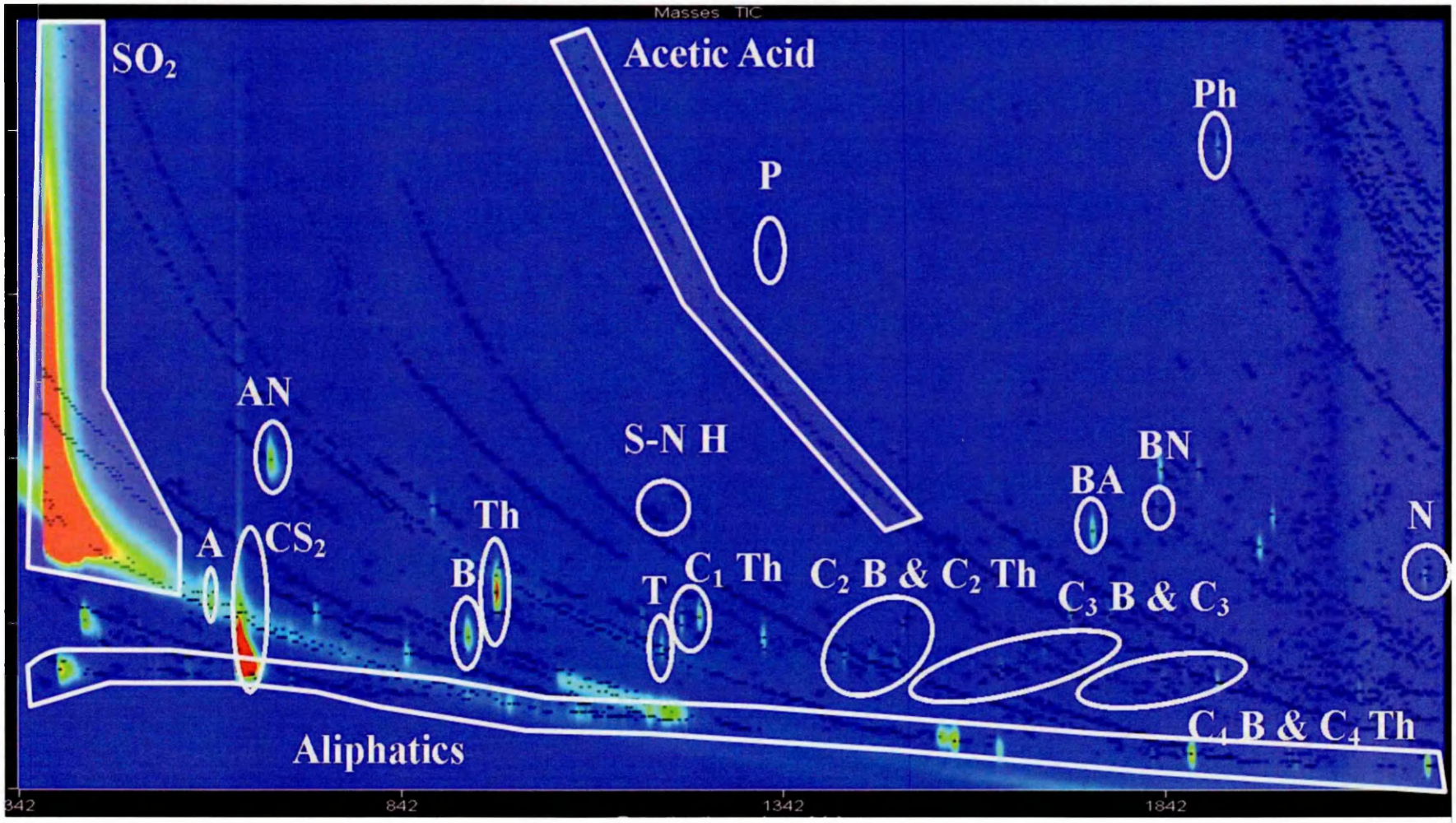

Figure 50: A TIC of AMMs identifying key species. A = acetone, AN = acetonitrile, B = benzene, BA = benzaldehyde, BN = benzonitrile, N= naphthalene, N H = nitrogen heterocycle, P = pyrrole, Ph = phenol, S-N H = sulphur-nitrogen heterocycle, T = toluene and Th = thiophene

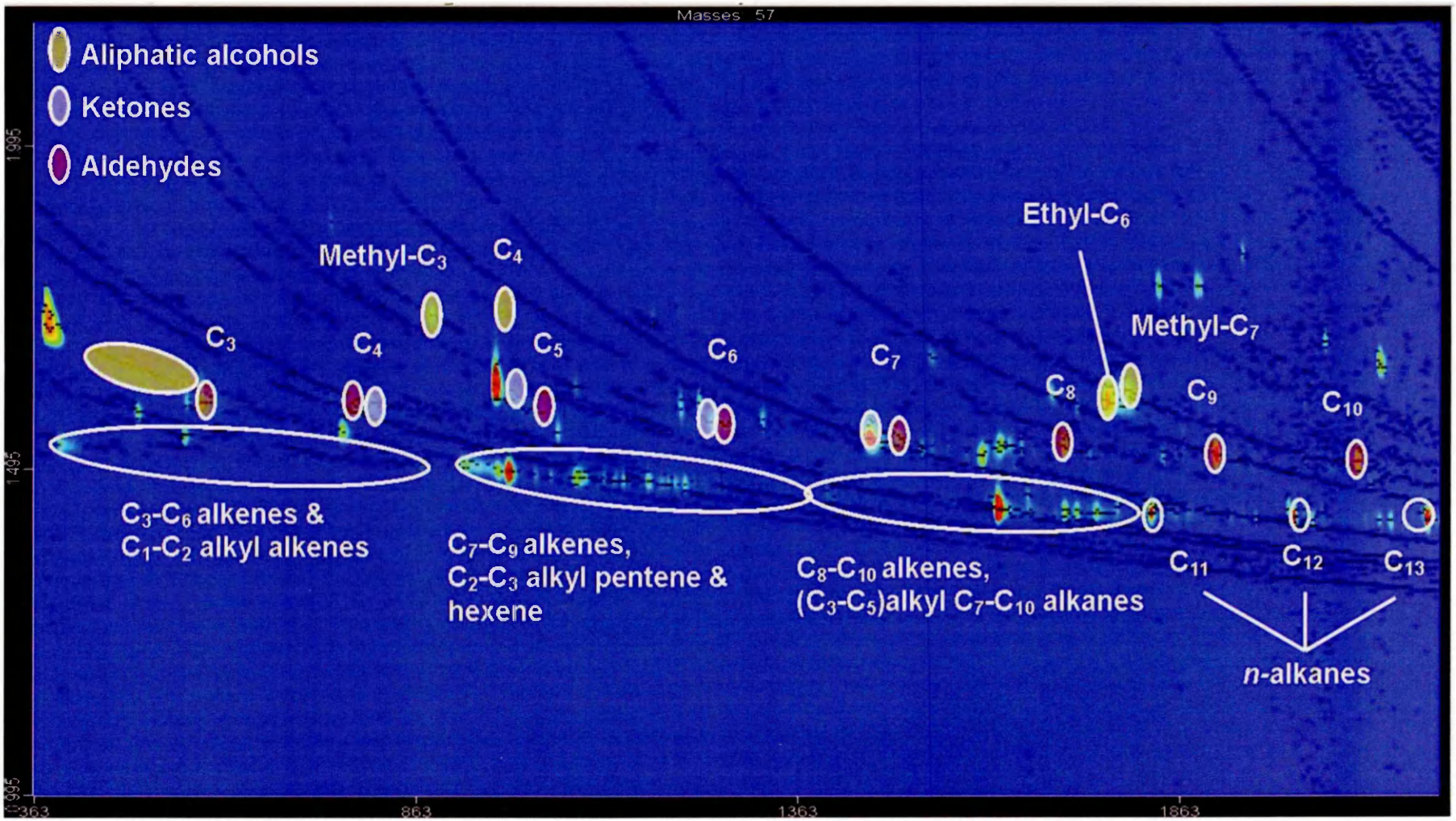

Figure 51: An RIC (mass 57) of AMMs identifying aliphatic species

57 amu, highlighting the variety of aliphatic species characterised in AMMs. C_3-C_9 unsaturated hydrocarbons (alkenes) with up C_1-C_3 alkyl derivatives exist in the sample. C_{11}-C_{13} *n*-alkanes and branched C_7-C_{10} aliphatics are also identified. Additionally up to C_7 aliphatic alcohols and branched aliphatic alcohols were also present in the AMMs studied.

FTIR analyses have identified the aliphatic CH_2 asymmetric and symmetric stretching, CH_3 stretching and C-H bend absorption features identified in both AMMs (Matrajt et al., 2001; Suzuki et al., 2005; Osawa et al., 2001) and IDPs (Flynn et al., 1998; Flynn et al., 2002; Matrajt et al., 2005 a; Sandford & Walker, 1985). Suzuki et al., (2005; 2007) have used the intensities of the CH_2 and CH_3 stretching absorptions to infer aliphatic relative chain lengths. The authors found that the majority of AMMs contain a CH_3/CH_2 ratios >0.63 (which represents C_{18} straight chain hydrocarbons), suggesting that AMM aliphatics are of shorter chain length. Pyrolysis GCxGC analysis (Figure 51) has enabled the identification of individual aliphatic componants (up to C_{13} hydrocarbons) including both polar and alkyl-substituted species.

Acetic acid is the only carboxylic acid identifiable in AMMs in this study; however the identification of larger carboxylic acids traditionally requires derivitisation. The only aromatic alcohols identified in AMMs are phenol, methylphenol and benzylalcohol, consistent with the O-H stretch absorption feature previously identified in MMs by FTIR (Suzuki et al., 2005). However, as the O-H stretch absorption feature could also be indicative of free and structurally bound water within phyllosilicates (Engrand et al., 1999; Gounelle et al., 2005), this study provides evidence of organic phenolic moieties in AMMs. Other oxygen-bearing species present include a series of C_3 to C_{10} aldehydes, a suite of C_3-C_7 ketones and benzaldehyde. The C=O bond has thus far only been detected in MMs by STXM, exhibiting C-C and C=O features typical of carbon rings (Matrajt et al., 2001).

Aromatic species in the form of benzene, C_1 – C_4 alkyl-benzenes and C_1-C_5 *n*-alkyl substituted benzenes are present in AMMs (Figure 52). With the emphasis of this study on characterising volatile organics, naphthalene was the species of highest mass identified in the AMM fragments, confirming its previous detection in AMMs using μL^2MS

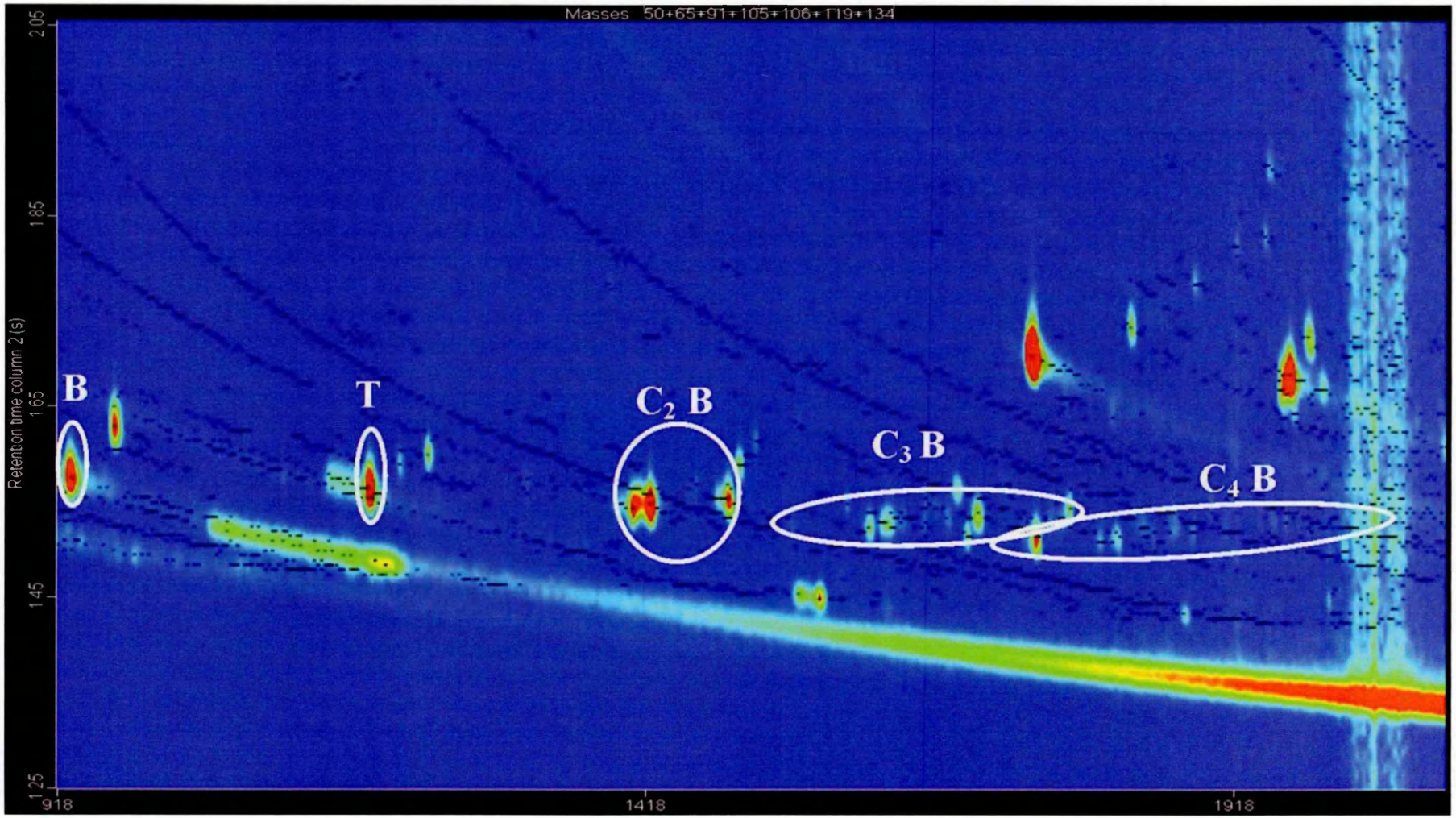

Figure 52: A RIC of masses 50+65+91+105+106+119+134 illustrating the distribution of benzene and C_1-C_4 alkylbenzenes in AMMs

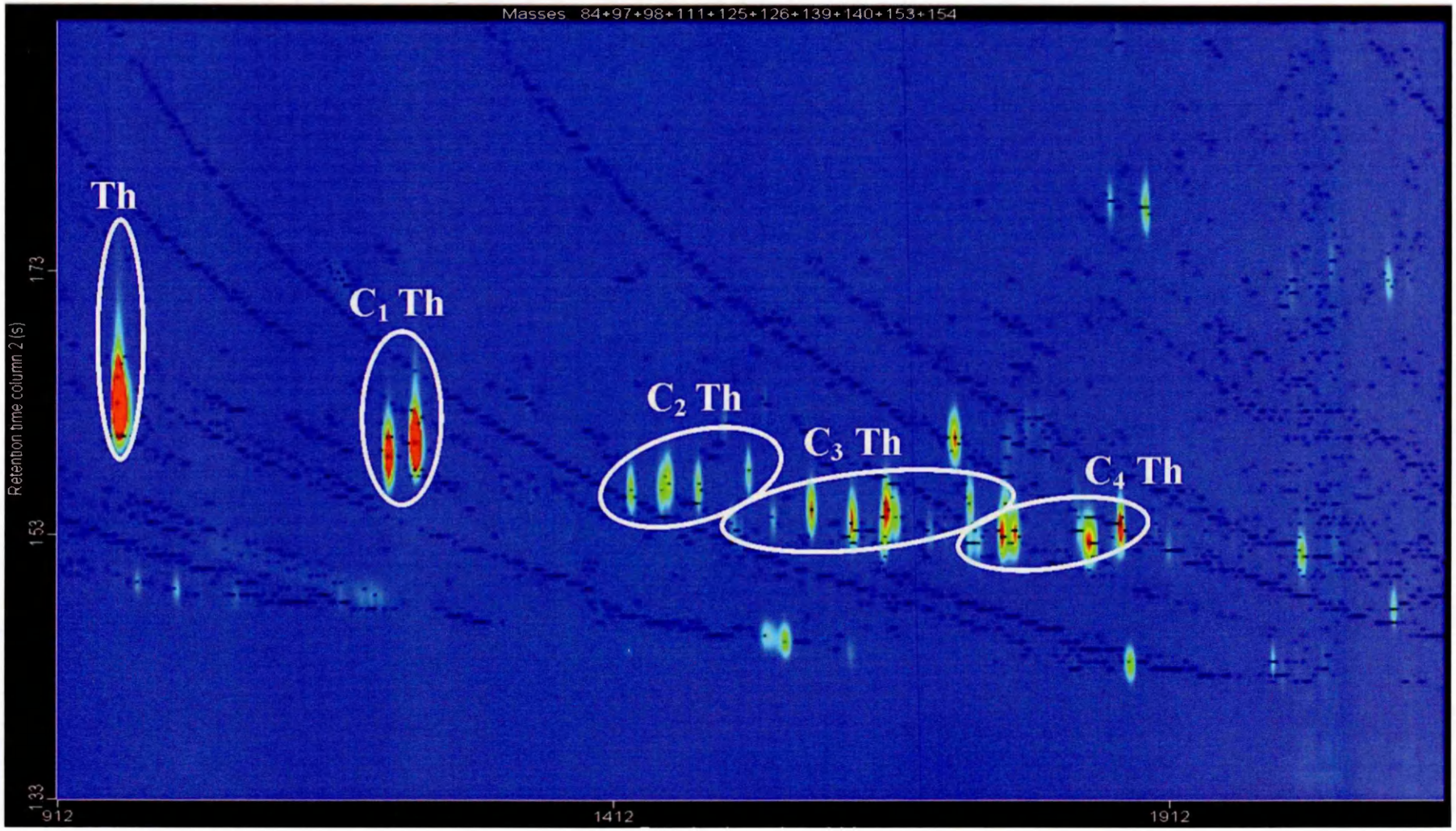

Figure 53: A RIC of masses 84+97+98+111+112+125+126+139+140+153+154 illustrating the distribution of thiophene and C1-C4 alkylthiophenes in AMMs

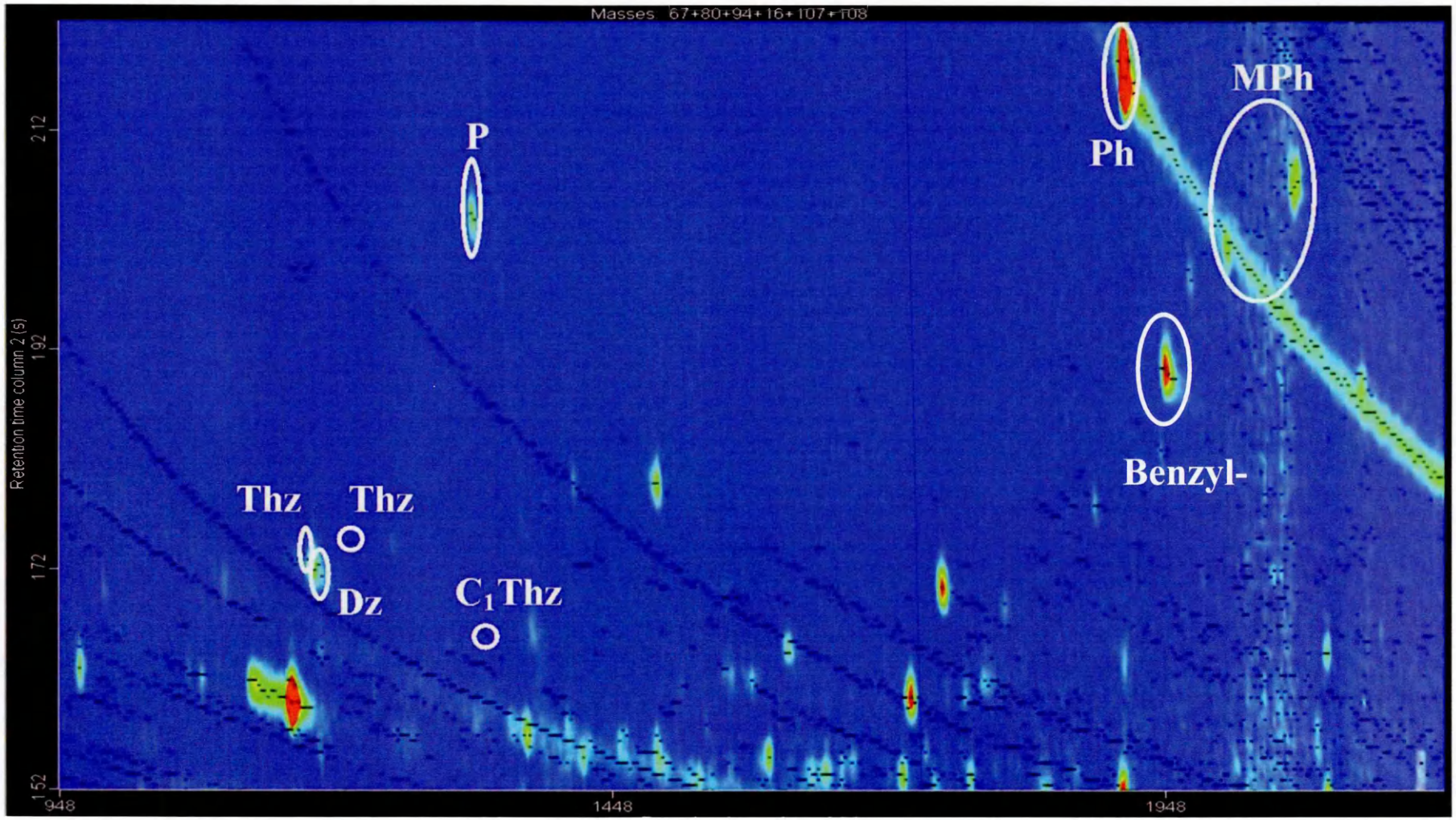

Figure 54: A RIC of masses 67+80+94+107+108 illustrating the distribution of nitrogen- and sulphur-nitrogen heterocycles in AMMs

Species	1st Dimension Retention Time (s)	2nd Dimension Retention Time (s)	Chromatogram Annotation
Inorganic			
Sulphur Dioxide	381	1.780	SO_2
Carbon disulphide	630	1.560	CS_2
Aliphatics			
C_{11} *n*-alkane	1827	1.430	C_{11}
C_{12} *n*-alkane	2013	1.425	C_{12}
C_{13} *n*-alkane	2187	1.420	C_{13}
Aromatics			
Benzene	930	1.575	B
Toluene	1182	1.565	T
Ethylbenzene	1407	1.545	C_2B
p & m-xylene	1422	1.550	C_2B
o-xylene	1488	1.555	C_2B
Isopropylbenzene	n.d.	n.d.	C_3B
Propylbenzene	1608	1.525	C_3B
1-ethyl-3-methylbenzene	1623	1.530	C_3B
1-ethyl-4-methylbenzene	n.d.	n.d.	C_3B
1-ethyl-2-methylbenzene	1674	1.535	C_3B
1,2,4-trimethylbenzene	1701	1.540	C_3B
1,2,3-trimethylbenzene	1779	1.545	C_3B
Tertiary butylbenzene	1692	1.515	C_4B
Isobutylbenzene	n.d.	n.d.	C_4B
Secondary butylbenzene	n.d.	n.d.	C_4B
1-methyl-3-isopropylbenzene	1749	1.515	C_4B
1-methyl-4-isopropylbenzene	1752	1.515	C_4B
1-methyl-2-isopropylbenzene	n.d.	n.d.	C_4B
1-methyl-3-propylbenzene	1803	1.510	C_4B
1-methyl-4-propylbenzene	1806	1.510	C_4B
1,4-diethylbenzene	1815	1.510	C_4B
n-butylbenzene	1821	1.515	C_4B
1,2-diethylbenzene	n.d.	n.d.	C_4B
1-methyl-2-propylbenzene	n.d.	n.d.	C_4B
1,4-dimethyl-2-ethylbenzene	n.d.	n.d.	C_4B
1,3-dimethyl-2-ethylbenzene	n.d.	n.d.	C_4B
1,2-dimethyl-4-ethylbenzene	1884	1.520	C_4B
1,3-dimethyl-2-ethylbenzene	n.d.	n.d.	C_4B
1,2-dimethyl-3-ethylbenzene	n.d.	n.d.	C_4B
1,2,4,5-tetrametylbenzene	n.d.	n.d.	C_4B
1,2,3,5-tetramethylbenzene	1962	1.530	C_4B
1,2,3,4-tetramethylbenzene	n.d.	n.d.	C_4B
Napthalene	2181	1.650	N
Oxygen, Hydroxyl and Carboxyl Bearing			
Acetic Acid	1035	2.385	Acetic Acid
Benzaldehyde	1746	1.705	BA
Acetone	594	1.610	A
Phenol	1911	2.170	Ph
Methylphenol	2004	2.015	MPh
Methylphenol	2067	2.075	MPh
Benzylalcohol	1950	1.900	Benzyl-OH
Sulphur-Bearing			
Thiophene	966	1.630	Th
2-methylthiophene	1209	1.590	C_1Th
3-methylthiophene	1233	1.600	C_1Th
2-ethylthiophene	1428	1.565	C_2Th
2,5-dimethylthiophene	1455	1.565	C_2Th
2,4-dimethylthiophene	1461	1.570	C_2Th
2,3-dimethylthiophene	1488	1.570	C_2Th
3,4-dimethylthiophene	1533	1.580	C_2Th
2-isopropylthiophene	1554	1.545	C_3Th
3-isopropylthiophene	1590	1.550	C_3Th
2-propylthiopehene	1626	1.540	C_3Th
2-ethyl-4-methylthiophene	1653	1.545	C_3Th
2-ethyl-5-methylthiophene	1665	1.545	C_3Th
C3-Thiophene	1731	1.555	C_3Th
Thiazole	1203	1.750	Thz
C_1-Thiazole	n.d.	n.d.	C_1 Thz
Isothiazole	1173	1.730	IThz
Nitrogen Bearing			
Acetonitrile	672	1.790	AN
Benzonitrile	1833	1.750	BN
Pyrazine (Diazine)	1179	1.720	Pz (Dz)
Pyrrole	1320	2.045	P

Table 32: A summary of species characterised in AMMs (n.d.= not determined)

(Clemett et al., 1998). In addition, the authors identified up to 5 ringed PAHs, with a greater degree of alkylation of 3 and 4 ringed PAHs than is observed in carbonaceous chondrites. This study using pyrolysis GCxGC data, however, demonstrates that mono-aromatic species dominate the volatile organic fragments of AMM material, in addition to a substantial structural diverstity of the alkylbenzenes. These may represent fragments of alkyl-linked macromolecular polyaromatic structures, similar to those present in CM2 chondrites.

A broad range of sulphur-bearing species were observed including sulphur dioxide, carbon disulphide, dimethylsulphide, thiophene, C_1 – C_3 alkylthiophenes and C_3-C_5 *n*-alkane substituted thiophenes are all present in AMMs. The distribution of thiophene and alkylthiophenes in AMMs is given in Figure 53. Thiazole and methyl thiazole are the only S-N heterocycles identified (Figure 54). As a consequence of column restrictions (i.e. columns selected for volatile organic analysis) it was not possible to analyse benzothiophenes. Nitrogen-bearing species in AMMs include acetonitrile and benzonitrile. Nitrogen containing functional groups have not been previously identified in MMs, however, isotopic and abundance studies of nitrogen within MMs (Marty et al., 2005) suggest it is associated with a carbon component thought to originate as part of the aromatic structure of MM organic matter. This is consistent with the presence of the N-heterocycles pyrrole and diazine within AMMs.

4.4.3. AMMs vs. Murchison

A significantly lower number of peaks are identifiable in AMMs compared with Murchison reference sample, this is likely to be a consequence of analysing a smaller sample mass or may reflective of a different parent body. Similar to the Murchison reference pyrolysate (Section 3.5), AMMs show the same broad groups of compound classes: aliphatics, aromatics and NSO components (Table 32). The range of aliphatic hydrocarbon species is comparable to that found in Murchison as described in Section

3.5.1. However, previous studies of Murchison have identified a much greater range up to C_{26} *n*-alkanes (Cronin & Pizzarello, 1990), although the *n*-alkanes are thought to represent terrestrial contaminants. There is a greater range of straight chain aliphatic alcohols and a restricted variety of branched aliphatic alcohols identified in AMMs compared to Murchison.

Although acetic acid is the only carboxylic acid identifiable in AMM and Murchison in this study, previous studies have identified up to C_9 mono- and di-carboxylic acids within Murchison extracts (Yuen & Kvenvolden, 1973; Martins et al., 2006). Oxygen bearing species in AMMs are similar to those of Murchison (phenol, methylphenol, benzaldehyde and acetone). Phenol:toluene and methylphenol:toluene ratios in AMMs are substantially (40 times) higher than both Antarctic terrestrial particles and Murchison Table 33. These are discussed in more detail in Section 4.4.4.

Sample	Phenol:Toluene	Methylphenol:Toluene
Unheated Murchison	0.19	0.03
AMMs	7.37	0.18
T2	0.35	0.01

Table 33: Phenol:toluene and methylphenol:toluene ratios for unheated Murchison, AMMs and Antarctic terrestrial particles, derived from chromatogram peak areas

Table 34 and Figure 55 illustrate that both Murchison and the AMM fragments contain similar distributions of benzenes and alkylbenzenes.

	Benzene Peak Areas					Benzene Ratios			
Sample	C_0	C_1	C_2	C_3	C_4	C_1/C_0	C_2/C_0	C_3/C_0	C_4/C_0
Murchison	19432064	14370337	36913639	30470148	12215803	0.74	1.90	1.57	0.63
AMMs	655384	80951	474503	211049	169134	0.12	0.72	0.32	0.26
T2	21085823	1419766	2665015	405012	643295	0.07	0.13	0.02	0.03

Table 34: Peak areas for C_0-C_4 benzenes calculated from RIC (masses 50+65+91+105+106+119+134) peak areas (representative of abundance). Ratios of alkyl-parental benzenes in Murchison, AMMs and batch T2 Antarctic terrestrial particles

They are dominated by alkyl-substituted benzenes comprising 83 % and 59 % of total benzenes respectively. The AMM fragments also contain a noticeably higher relative proportion of benzene and a lower relative proportion of C_1 and C_3 benzenes compared to Murchison. However, Murchison and AMM fragments contain similar relative proportions of C_2 and C_4 alkylbenzenes. C_2 and C_3 alkyl benzenes dominate in AMMs and Murchison,

whilst C_1 and C_2 alkyl benzenes dominate Antarctic terrestrial particles. These trends could reflect the possibility AMM organic material is not as alkylated as that of Murchison, or that these are generated during pyrolysis but the starting materials are different.

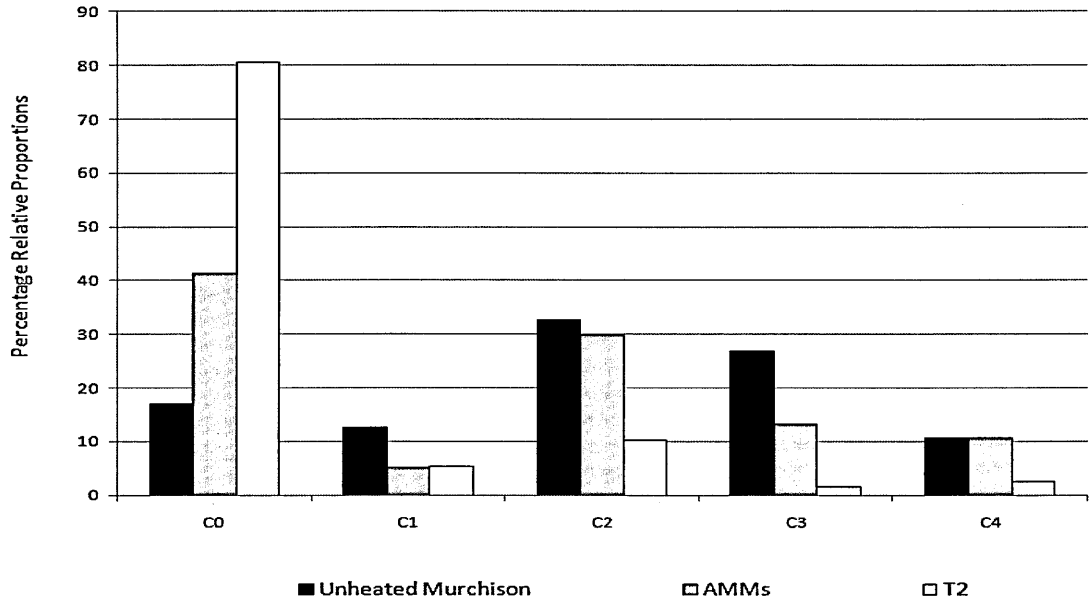

Figure 55: A graph showing the percentage of C_0-C_4 alkyl substituted benzenes in unheated Murchison, AMMs and batch T2 of Antarctic terrestrial particles expressed as a percentage of the total benzenes in each sample

The distribution of thiophenes and alkyl thiophenes present in AMMs is consistent with those found in Murchison (Table 35 and Figure 56). However alkyl:parental abundances are different. AMMs contain a significantly higher percentage of thiophene than Murchison (58 % and 20 % respectively), some of which may be of terrestrial contribution. Murchison contains a significantly greater percentage of C_1 and C_2-thiophenes than AMMs. Both Murchison and the AMM fragments contain similar percentages of C_3-thiophenes (8 % and 10 % respectively).

	Thiophene Peak Areas				Thiophene Ratios		
Sample	**C_0**	**C_1**	**C_2**	**C_3**	**C_1/C_0**	**C_2/C_0**	**C_3/C_0**
Murchison	18021008	41685190	22386108	6926768	2.31	1.24	0.38
AMMs	3811920	1686580	434841	647924	0.44	0.11	0.17
T2	420805	89758	3791	35181	0.21	0.01	0.08

Table 35: Peak areas for C_0-C_3 thiophenes and ratios of alkyl-parental thiophenes in Murchison, AMMs and batch T2 Antarctic terrestrial particles derived from RIC (masses 84+97+98+111+112+ 125+126+ 139+ 140+153+154)

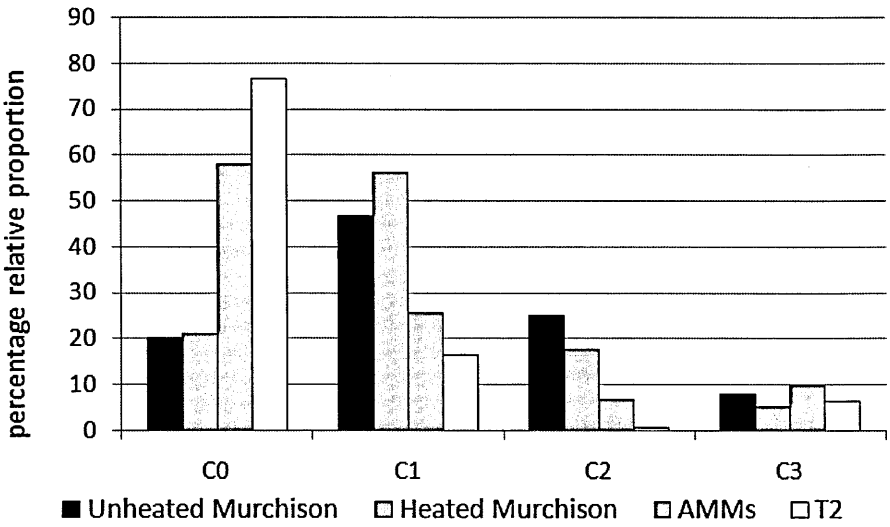

Figure 56: A graph showing the percentage of thiophene and C_1-C_3 alkyl substituted thiophenes in unheated Murchison, heated Murchison (simulation results 1026 °C, 2 s), AMMs and batch T2 Antarctic terrestrial particles expressed as a percentage of the total thiophenes in each sample

Although acetonitrile, benzonitrile, pyrrole and diazine are found in both AMMs and Murchison, AMMs lack the diversity of other nitrogen bearing species (N- heterocycles and S-N heterocycles) that are observed in Murchison. This may be indicative of a lower occurance of N-bearing moieties in the AMM macromolecular structure relative to that of Murchison. Alternatively N-heterocylces may be of such low abundance, they are not within the detection limits of this analysis.

4.4.4. Assessing the Indigeneity of Micrometeorite Organics: AMMs vs. Antarctic Terrestrial Particles

Antarctic terrestrial particles (batch T2) are dominated by aliphatic, aromatic and NSO species (Figure 57). Figure 58 shows that Antarctic terrestrial particles contain both saturated and unsaturated hydrocarbons, with a complete series of C_5-C_{13} *n*-alkanes, up to C_{10} alkenes and up to C_{10} branched aliphatics. Additionally, up to C_7 aliphatic alcohols and branched aliphatic alcohols are also present. The *n*-alkanes in meteorites are typically regarded as terrestrial contaminants (Cronin & Pizzarello, 1990; Sephton et al., 2001) possibly originating from petroleum products introduced during atmospheric entry,

during collection or by direct contact with samples within the Antarctic environment (Section 4.4.6).

However, EDP entry heating simulations (Chapter 3) demonstrate the substantial loss of the more volatile *n*-alkanes (C_5 and C_6) across all simulation temperatures and durations (2 - 20 s, 400 - 1000 °C). Extensive loss of higher *n*-alkanes (C_{10}-C_{13}) was achieved with longer heating durations (20 s). Therefore the lack of < C_{10} *n*-alkanes within AMMs, may be a consequence of the loss of these more volatile components on atmospheric entry heating. This implies that *n*-alkanes within the AMMs may be indigenous and not terrestrial contaminants.

Similar to Murchison and AMMs, the only aromatic alcohols identified are phenol and methylphenol (Figure 59), whilst the oxygen-bearing species include C_3-C_6 ketones, C_3-C_4 and C_8 aldehydes and benzaldehyde (Figure 57 and Figure 58). In contrast AMMs exhibit a complete series of C_3-C_7 ketones and C_3-C_{10} aldehydes. Unlike Murchison and AMMs, acetic acid is not present in the Antarctic terrestrial particles.

The terrestrial particles do contain benzene, C_1-C_4 alkylbenzenes and up to C_5 *n*-alkane substituted benzenes, however their parental:alkyl ratios are very different to those of AMM fragments and Murchison. Figure 55 illustrates that AMM fragments contains a significantly higher relative proportion of C_1-C_4 alkylbenzenes than Antarctic terrestrial particles (batch T2), 59 % and 20 % respectively. Additionally, 24 % of total benzenes comprise C_3 and C_4 alkylbenzenes, compared to just 4 % of total benzenes in terrestrial particles.

There is also a more restricted range of other S-bearing species in the terrestrial particles relative to both AMM fragments and Murchison. The only sulphur-bearing species in T2 are carbon disulphide, thiophene and methylthiophene, whilst sulphur dioxide is absent. The terrestrial particles contain thiophene and an incomplete series of C_1-C_3 thiophenes (Figure 61), unlike Murchison and AMMs which exhibit the full range of C_1-C_3 alkylthiophenes. Figure 56 shows that Antarctic terrestrial particles are dominated

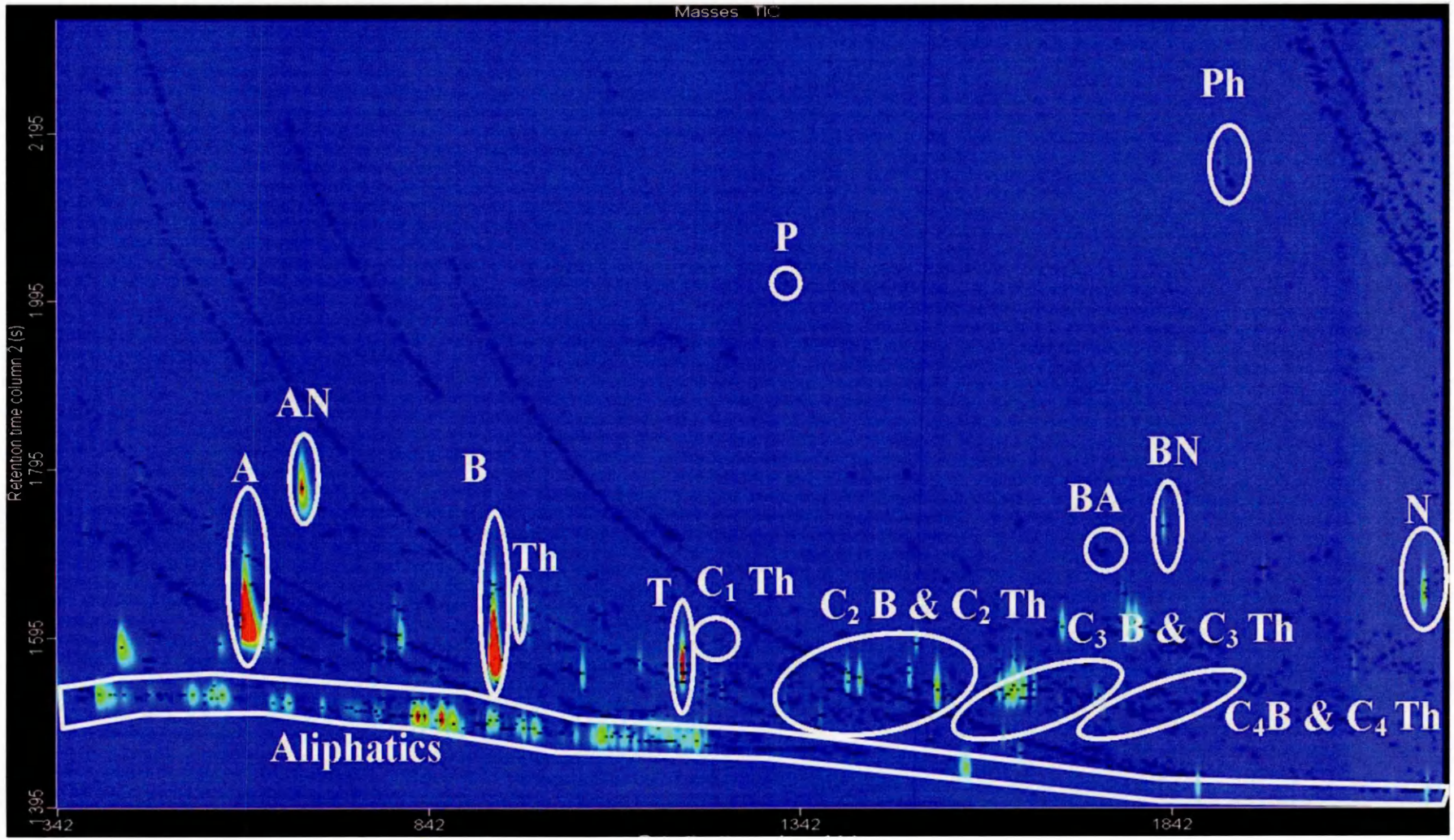

Figure 57: TIC of batch T2 Antarctic terrestrial particles identifying key species. Al=aliphatics, AN = acetonitrile, B = benzene, BA= benzaldehyde, BN= benzonitrile, N=naphthalene, T= toluene, Th = thiophene, Thz= thiazole.

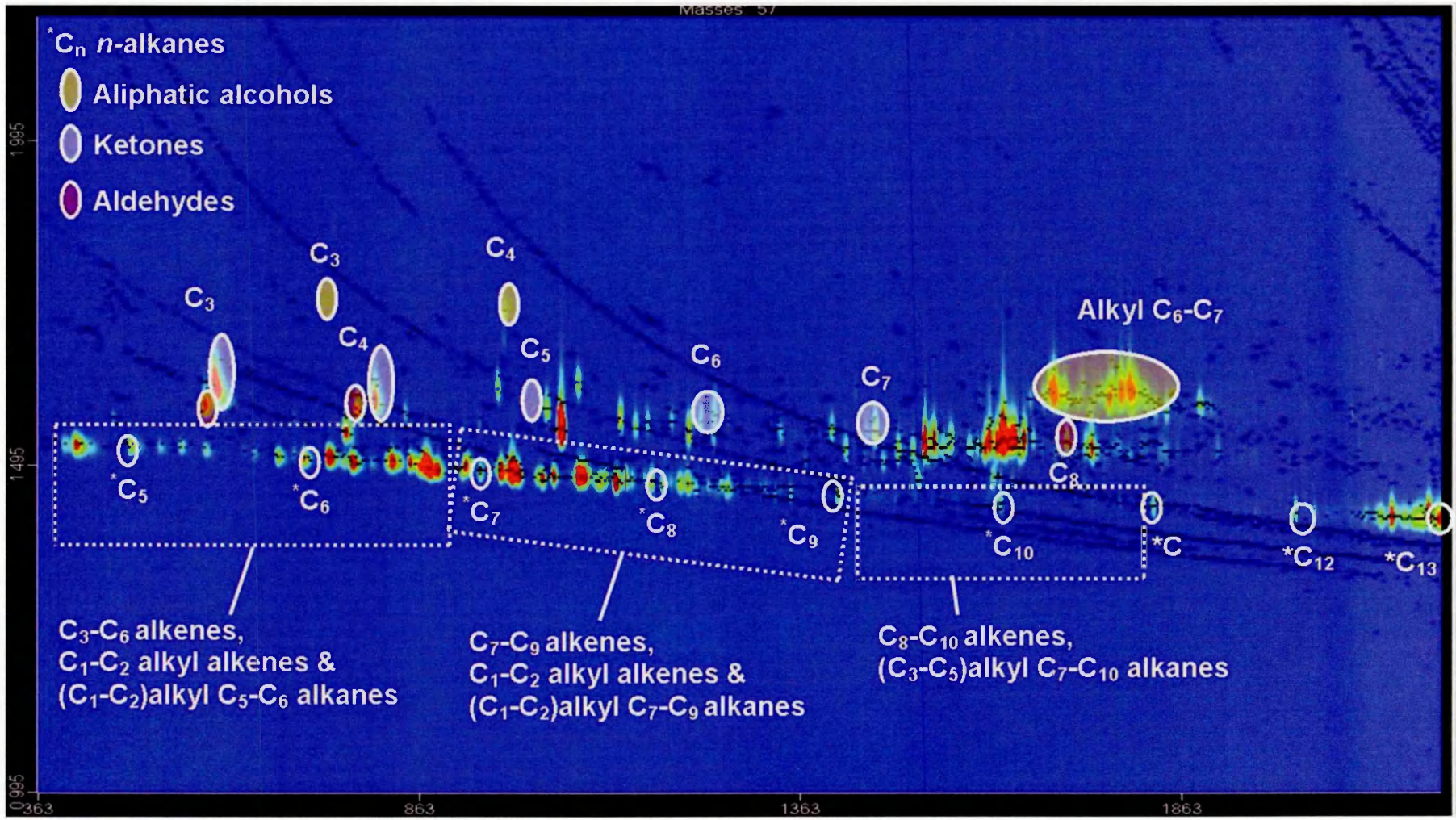

Figure 58: An RIC of mass 57 illustrating the distribution aliphatic species in Antarctic terrestrial particles (batch T2)

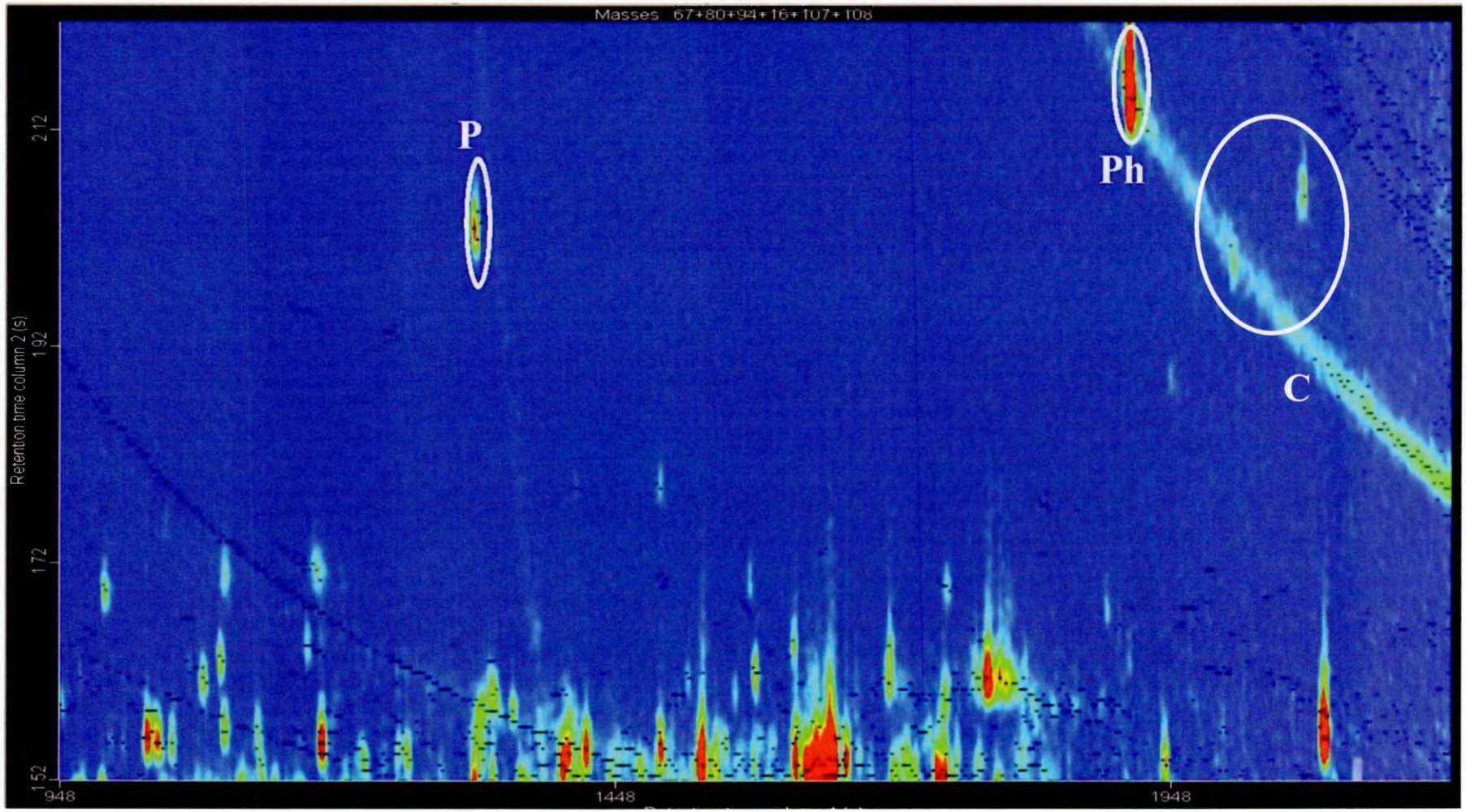

Figure 59: A RIC of masses 67+80+94+107+108 illustrating the distribution of nitrogen-heterocycles and phenol in batch T2 Antarctic terrestrial particles

by thiophene, with alkyl thiophenes comprising just 24 % of total thiophenes compared to 42 % in AMMs and 80 % in Murchison. The terrestrial particles contain an extremely low percentage of C_2 thiophenes (< 1 %), compared to Murchison (25 %) and AMMs (7 %). Identical to the AMM fragments, acetonitrile, benzonitrile and pyrrole are the only nitrogen-bearing species (Figure 57 and Figure 59). In contrast to AMMs and Murchison, no further nitrogen or sulphur-nitrogen heterocycles are present. This suggests that at least diazine, if not all AMM N-heterocycles, must derive from N-precursors in the macromolecular material.

The organic inventory of AMMs in this study is consistent with the functional groups (aliphatic, aromatic, hydroxyl and carbonyl) previously identified in MMs (Clemett et al., 1998; Matrajt et al., 2001; Suzuki et al., 2005). However, the presence of phenol, nitriles, ketones, aldehydes and pyrrole in both AMM fragments and Antarctic terrestrial particles does not rule out the possibility that they may be terrestrial contaminants introduced during their residence time on Earth, or during the collection procedure.

Organic species present only in AMMs and Murchison include diazine, thiazole and methylthiazole, suggesting these are derived from S-moieties within the macromolecular material integral to AMMs. An alternative possibility is that their precursors were present, allowing their generation on atmospheric entry heating. SO_2 also present in Murchison and AMMs, could be derived from the degradation of S-bearing organic species or that of any sulphide mineral assemblages that may be present in samples. Additionally no lower *n*-alkanes ($<C_{10}$) are identified in AMMs in contrast to the complete series of C_5-C_{13} *n*-alkanes observed in Antarctic terrestrial particles and Murchison. Although there are similarities in the range of C_0-C_4 benzenes and C_0-C_3 thiophenes, their relative proportions in AMMs is significantly different to terrestrial samples suggesting they may also be indigenous to the samples.

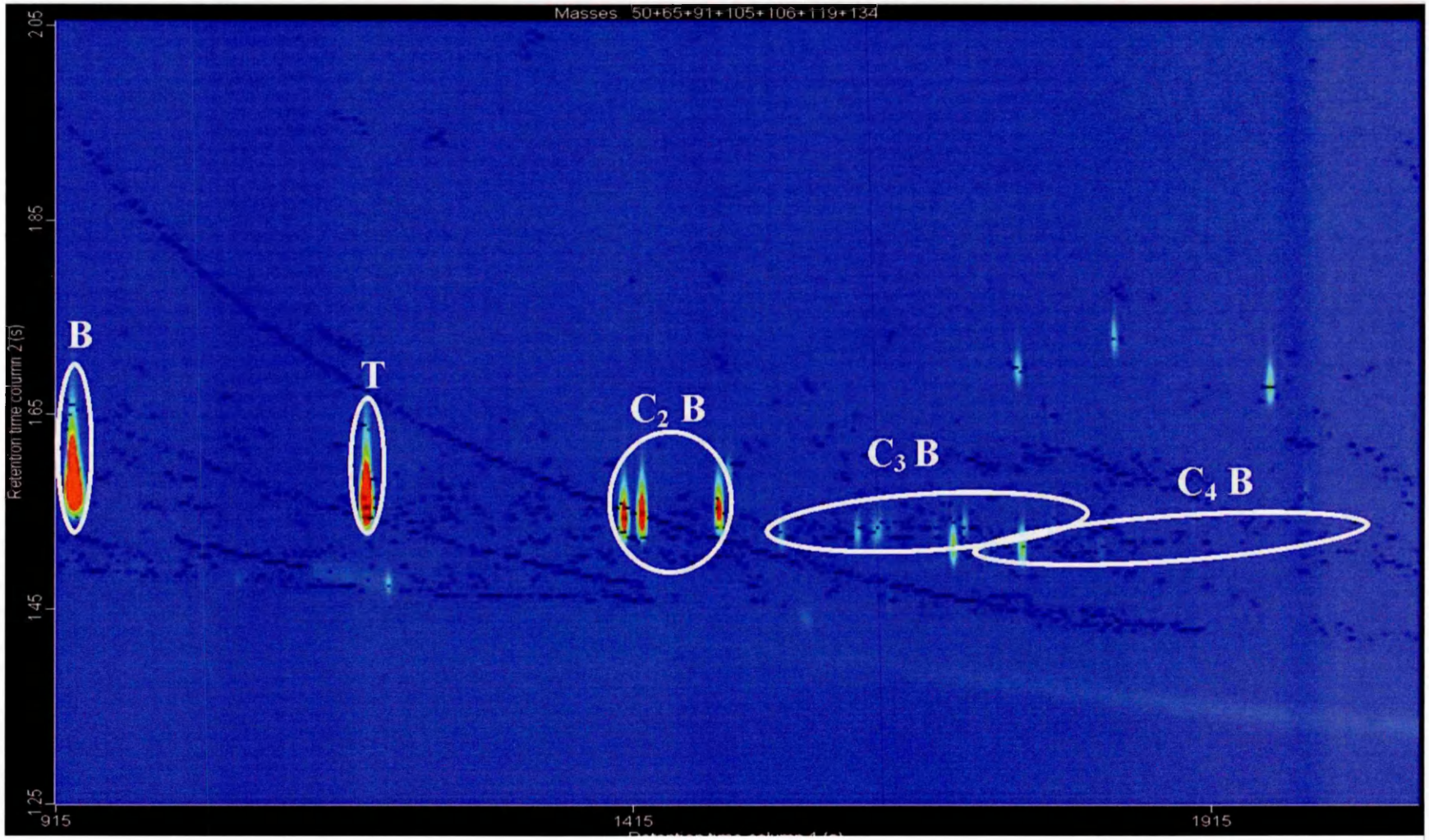

Figure 60: A RIC of masses 50+65+91+105+106+119+134 illustrating the distribution of benzene and C_1-C_4 alkylbenzenes in batch T2 Antarctic terrestrial particles

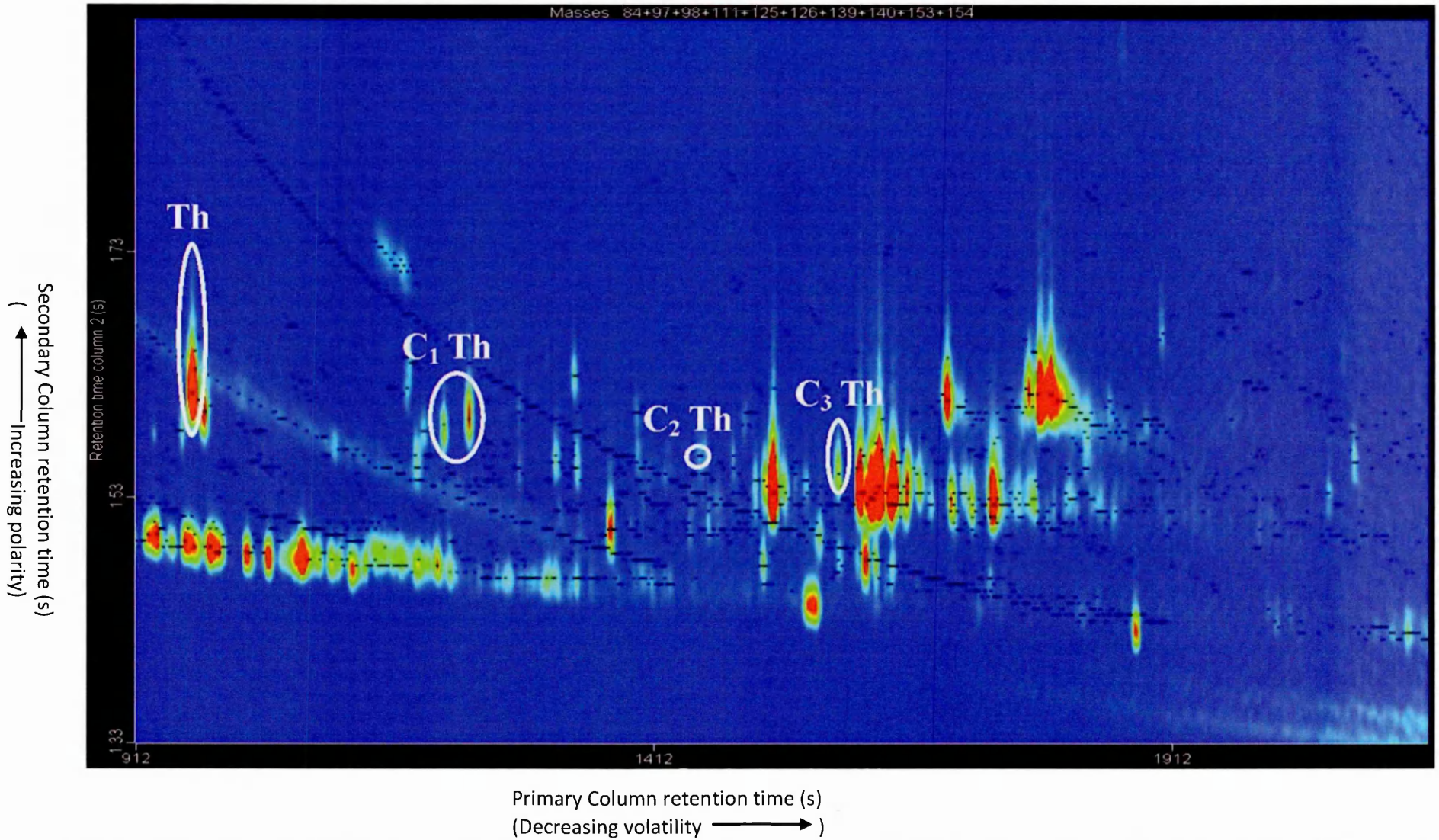

Figure 61: A RIC of masses 84+97+98+111+112+125+126+139+140+153+154 illustrating the distribution of thiophene and C1-C4 alkylthiophenes in batch T2 Antarctic terrestrial particles

4.4.5. AMMs vs. Entry Heating Simulations

Simulations presented in Chapter 3 investigated the effect of atmospheric entry heating on the organic composition of MM analogous material. Variations of specific organic functional groups under simulation conditions can account for differences in organic composition of Murchison and AMMs, which ultimately would have undergone a similar heating regime during their passage to Earth.

Phenol:toluene ratios of species liberated during simulations (Chapter 3) significantly increased at simulation temperatures at or above 600 °C for short durations of 2 s. This suggests that macromolecular ether cross linkages, in a similar manner to those in coal (Schlosberg et al., 1981; Siskin & Aczel, 1983) and in carbonaceous chondrites (Sephton et al., 1998), are extensively cleaved or undergo intermolecular rearrangements (Schlosberg et al., 1983) at higher simulation temperatures, liberating substantial phenol. The high phenol:toluene ratio observed in AMMs (Table 33), is an indicator of substantial ether linkage degradation within the macromolecule during atmospheric entry heating, resulting in the phenols in AMM pyrolysates.

The high relative proportion of benzene observed in AMMs suggests that they may have not experienced extreme heating regimes, or that the organic material significantly differs to Murchison. Simulations (Section 3.5.1) identified increasing release of benzene (and decreasing release of total alkyl benzenes) occurred during EDP entry heating simulations at higher temperatures and durations. Contributory factors to the increased loss of benzene included a) its generation by secondary reactions during heating e.g. the cracking of alkylbenzene side chains (Mochida & Yoneda, 1967; Watson et al., 1997) and the thermal decomposition of thiophenes (Cullis & Harris, 1972) or benzonitrile (Etemad-Rad & Metcalfe, 1993) and b) the recombining of cleaved macromolecular radicals at higher temperatures thereby condensing aromatic structures releasing a lower abundance of alkylbenzenes.

In contrast, EDP entry heating simulations (Chapter 3) found no correlation between peak temperature and the release of thiophenes at heating durations of 2 s, the

predicted duration of maximum heating in EDPs (Love & Brownlee, 1991). This suggests that thiophene distribution in AMMs represents indigenous precursor macromolecular material that has not been altered by atmospheric entry heating.

4.4.6. The Effect of the Antarctic Environment on AMMs

In the Cap-Prudhomme Antarctic environment, MMs reside encased in ice for the majority of their ~ 50,000 year duration on Earth (Maurette et al., 1994). While Antarctic meteorites can be shielded from the outside extreme conditions such as temperature fluctuations (Koeberl & Cassidy, 1991), AMMs are dark particles that can absorb sunlight, melting a thin layer of ice surrounding them causing them to sink to the subsurface of blue ice fields (Duprat et al., 2007). As a consequence of freeze-thaw cycles, and exposure to melted ice at a few ° C for up to ~ 8 hours during the collection procedure (Maurette, 1998), these AMMs will undergo a degree of terrestrial aqueous alteration. Evidence for terrestrial alteration of AMMs includes their depletions of Na, Mg, Ca, Mn, and Ni with respect to CI chondrites, from terrestrial leaching of sulphides, sulphates and carbonates in the Antarctic environment (Kurat et al., 1994; Presper et al., 1993).

Iron sulphide and carbonate minerals are known mineralogical indicators of the degree of terrestrial weathering in Antarctic meteoritic samples, as acidic water can both react with iron sulphides (Pratt & Nesbitt, 1997) and dissolve carbonates thereby removing them. Between 10-20 % of AMMs from Cap-Prudhomme contain iron sulphides, with no carbonates identified in these samples (Duprat et al., 2007). In comparison, Duprat et al., (2007) found 65 % of AMMs from the Concordia collection (collected from central Antarctic snow in a region of low precipitation rates) contained iron sulphides and the first known occurrence of a carbonate (dolomite) within an AMM. In contrast IDPs (collected directly from the stratosphere, having experienced no terrestrial aqueous alteration) are known to contain iron sulphides (Zolensky & Lindstrom, 1992; Zolensky & Thomas, 1995) and carbonates (Tomeoka & Buseck, 1985; Zolensky & Lindstrom, 1992). Based on the lower occurrence of iron sulphides and the absence of carbonate minerals

within Cap-Prudhomme AMMs, it indicates that they have experienced more terrestrial aqueous alteration than those in the Concordia collection (Duprat et al., 2007). Alternatively, the absence or low occurrence of these minerals may be reflective of the AMM parent body. For example, recent analyses of Stardust cometary particles indicate an absence of extraterrestrial carbonate minerals in samples (Keller et al., 2006; Wirick et al., 2007), whilst IR observations of the Deep Impact ejecta from comet Tempel 1 (Lisse et al., 2005; Lisse et al., 2007) and independent observations of Halley (Bregman et al., 1987) identify their presence. With the limited identification of the presence and absence of carbonates within cometary materials, it is impossible to rule out a cometary source of AMMs in this study.

As a consequence of terrestrial weathering, more labile organic species may have leached from AMMs or in the case of amino acids (Glavin et al., 2004), even introduced to AMMs from terrestrial sources during their residence time in Antarctic ice. Carbonate is a known scavenger of PAHs in polar ice (Becker et al., 1997). As carbonate minerals are absent in Cap-Prudhomme AMMs, nor present in any substantial abundance within Concordia AMMs (of a younger terrestrial age) (Duprat et al., 2007), it suggests that AMM PAHs in this study are indigenous and not the products of terrestrial leaching into the MM particles.

The solubility of C_4-C_8 *n*-alkanes in water at room temperature decreases exponentially with increasing carbon number (McAuliffe, 1963) and combined with the level of terrestrial aqueous processing Cap-Prudhomme AMMs have undergone, could account for the absence of $<C_{10}$ *n*-alkanes in AMMs. In contrast, the solubility of *n*-alkanes $>C_{11}$ is much lower, as consequence of forming an aggregate rather than molecular dispersion in water (Baker, 1967), which in turn can explain the presence of C_{11}-C_{13} *n*-alkanes retained in AMMs.

The extent to which Antarctic weathering affects meteorites has been investigated extensively (Gooding, 1986; Koeberl & Cassidy, 1991; Velbel et al., 1991). CR, CM and CO Antarctic meteorites are found to contain no significant differences in C, N or H

elemental abundances or isotopic compositions compared to their non-Antarctic counterparts, suggesting that the Antarctic environment does not play a significant role in the removal of these components (Pearson et al., 2006) even though macromolecular structural differences exist that are attributed to Antarctic weathering processes (Sephton & Gilmour, 1998; Sephton et al., 2004).

Sephton et al. (2004) found that Antarctic CM meteorites lack phenols and contain fewer alkylated benzenes and thiophenes compared to their non-Antarctic counterparts (Table 36). Phenol is bound to chondritic macromolecular material by ether linkages (Hayatsu et al., 1980), with more extensively altered meteoritic matter depleted in macromolecular phenol precursors (Sephton et al., 2000). Sephton et al., (2004) have suggested that the absence of phenol from pyrolysates of Antarctic meteorites is a result of Antarctic weathering removing phenolic precursors from the macromolecular material. Analogously, aqueous alteration on chondrite parent bodies is thought to be responsible for degrading ether linkages in chondritic macromolecular material (Sephton et al., 1998; Sephton et al., 2000) giving rise to phenolic species in meteorite pyrolysates (Pearson et al., 2006).

Despite AMMs being more susceptible to terrestrial aqueous alteration (because of their high surface:volume ratio, porosity and chemical reactivity under prolonged exposure to water; Engrand & Maurette, 1998) they contain C_0-C_1 phenols, with significantly higher phenol:toluene ratios than both Murchison and Antarctic terrestrial particles (Table 33). It suggests that phenols, the products of ether link cleaving (Schlosberg et al., 1981; Siskin & Aczel, 1983) or intermolecular rearrangements (Schlosberg et al., 1983) during atmospheric entry heating have not been removed in the Antarctic environment by terrestrial alteration processes. Alternatively, it could suggest that AMM indigenous organic material is different to that of carbonaceous chondrites.

The extent of alkylation in the AMM pyrolysate in comparison to Antarctic meteorites and Antarctic terrestrial particles show that they bear resemblance to non-Antarctic CM meteorites. The AMM fragments have a greater degree of alkylation (up to

C_4 alkyl benzenes and thiophenes) than Antarctic meteorites, equivalent to those of non-Antarctic meteorites such as Murchison. Antarctic carbonaceous chondrites exhibit a reduction in the alkylation of these species compared to non-Antarctic carbonaceous chondrites (Table 36). It suggests that these particular AMMs may not been subject to extensive Antarctic weathering. Alternatively, the differences in alkylation may be reflective of different indigenous organic material. In comparison, the Antarctic terrestrial particles exhibited an incomplete series of C_0-C_4 alkyl benzenes and C_0-C_3 thiophenes with minor C_0-C_1 phenol which may be representative of the degree of processing that the organic matter has experienced prior to the Antarctic environment.

Sample	Benzenes	Thiophenes	Phenols	Ref.
Non-Antarctic				
Mighei	C_0-C_4	C_0-C_5	C_0-C_1	a
Nogoya	C_0-C_4	C_0-C_4	C_0	a
Murchison	C_0-C_5	C_0-C_4	C_0-C_1	a
Antarctic				
ALH 82100	C_0-C_2	C_0-C_1	Not detected	a
EET 83250	C_0-C_3	C_0-C_2	Not detected	a
Y-791824	C_0-C_3	C_0-C_2	Not detected	a
This Study				
AMMs	C_0-C_4	C_0-C_5	C_0-C_1	
Murchison reference material	C_0-C_4	C_0-C_3	C_0-C_1	
Antarctic terrestrial particles	C_0-C_4 incomplete series	C_0-C_3 incomplete series	minor C_0-C_1	

Table 36: compounds and their extent of alkylation in pyrolysates of whole rock CM meteorites, AMMs and Antarctic terrestrial particles. [a = from Sephton et al., (2004)]

As a result of low precipitation rates and the absence of bedrock, Concordia MMs yield a higher ratio of extraterrestrial:terrestrial particles, containing less contaminants (Duprat et al., 2007). The collection also has well constrained terrestrial ages in the order of a few hundred years, and have therefore experienced lower degrees of terrestrial aqueous alteration compared to other AMM collections (Duprat et al., 2007). The analysis of MMs from more pristine Antarctic sources, such as the Concordia collection, may advance the findings of this study.

4.4.7. The effect of atmospheric entry heating on MMs

During atmospheric entry, MMs are subject to flash heating to peak temperatures of between 600 - 1700 °C (Flynn, 1989; Greshake et al., 1998; Love & Brownlee, 1991).

At such temperatures, the chemical composition and morphology of the MM particle is altered. For example, mineralogical changes can occur at relatively low temperatures, between 600-800 °C, the decomposition, dehydration or replacement of phyllosilicate minerals (Section 3.3.2) to/with anhydrous minerals, including olivine and magnetite, highlights the phase transformation from hydrous to anhydrous minerals in MMs (Nakamura et al., 2001) at these relatively low heating temperatures.

At temperatures between 1000–1600 °C (depending on heating duration), volatile loss will increase particle porosity, as is evident by the increased vesicular nature of particles (Toppani et al., 2001). Experimental simulations of atmospheric entry heating on CI analogous materials have shown the loss of S, Zn, Ga, Ge and Se from fragments 50-100 μm in size (Greshake et al., 1998; Toppani et al., 2000; 2001; 2003), suggesting this may be the case for MMs. In the most extreme circumstances, at temperatures between 1350 °C (the melting temperature of Murchison matrix) and 1800 °C, particle melting will occur decreasing particle porosity (Genge et al., 1997; Kurat et al., 1994).

With MM flash heating conditions affecting both the chemical composition and morphology of particles, some studies have investigated the related effects on organic species. Organic species such as amino acids, PAHs, aliphatic and aromatic hydrocarbons typically decompose between 150-500°C (Rodante, 1992; Wright et al., 1997). The presence of aliphatic and aromatic hydrocarbons within AMMs in this study and previous studies (Clemett et al.,1998; Matrajt et al., 2001; Suzuki et al., 2005) suggests that either they have not been heated to temperatures >150-500°C, or that there is a mechanism by which organic molecules within particles are able to survive the high temperatures they are exposed to upon atmospheric entry. Glavin and Bada (2001) investigated the survival of amino acids from MM analogous material during MM atmospheric entry simulations. The subsequent recovery of glycine from Murchison fragments heated for 30 s at temperatures up to 550 °C, suggest that sublimation ensures these species are not decomposed under such heating conditions. Furthermore, Matrajt et al. (2006) have demonstrated that it is possible for the PAH coronene and the ketone 2-

pentadecanone to survive flash heating to 900 °C provided it is embedded in a porous substrate. It is suggested that pore spaces shelter organic species against direct contact with extreme conditions during flash heating.

Pyrolysis studies have shown that it is possible for minerals present within a sample to catalyze reactions between indigenous organic species, in a similar way to sulphur-bearing species being generated as an artifact during long duration pyrolysis (Simmonds et al., 1969). However analysis of S-bearing species in whole rock and benzene extracts of terrestrial material suggest that there is no generation of thiophenes, benzothiophenes or dibenzothiophenes upon introduction of S during pyrolysis (Hayes & Biemann, 1968). The pyrolysis time in this study is extremely short (2 s), eliminating the possibility of thiophene generation in AMM samples during analysis. A broader range of alkylthiophenes and S-containing compounds are identified in AMMs relative to Antarctic terrestrial particles, suggesting they are extraterrestrial in origin. Although the generation of sulphur-bearing species during atmospheric entry heating may be possible, atmospheric entry simulation experiments (Section 3.5.1) find no correlation between simulation temperatures (400-1000 °C) or heating durations (2- 20 s) and the percentage relative abundances of thiophenes released on simulation. The exception is at the high simulation temperature of ~ 1000 °C, where increasing abundances of thiophene and decreasing abundances of C_1-C_3 alkylthiophenes are released with increasing heating durations.

In addition, changes in alkylation of benzenes during simulated atmospheric entry heating conditions (Section 3.5.1) suggest that prolonged heating durations and higher peak temperatures lead to their dealkylation and an increase in the relative abundance of benzene. This is a similar effect rendered by exposure of samples to Antarctic weathering (Sephton et al., 2004). The dealkylation of AMM benzenes during atmospheric entry heating would account for the lower abundance of alkyl benzenes within AMMs in comparison to reference Murchison (Section 3.5). Similarly, higher abundances of phenolic species were liberated from EDP simulations for short durations (2 s and 5 s) to

> 800 °C, relative to unheated samples (Section 3.5.1). This suggests that flash heating degrades macromolecular O-moieties accounting for the increased presence of phenols observed in AMMs despite exposure to terrestrial weathering processes.

4.4.8. Astrobiological Significance

There are a number of species identified in this study that are unique to AMMs (and Murchison) such as the N-heterocycle diazine (of which pyrazine, pyrimidine and pyradazine are isomers). Many N-heterocycles are the precursors of essential biomolecules, for example DNA and RNA nucleobases are derivatives of pyrimidine. Folic acid and folate (its anion form) are pyrazine derivatives, essential for the production and maintenance of new cells and DNA synthesis, function and replication (Kamen, 1997).

The carboxylic acid, acetic acid, was also identified in AMMs. Carboxylic acids in free organic material in carbonaceous chondrites are thought to originate as a result of aqueous alteration on their parent bodies (Cronin & Chang, 1993) via the hydrolysis of nitrile, carboxamide and lactam precursors (Cooper & Cronin, 1995), the cleavage and oxidation of macromolecular hydrocarbons or the oxidation of alkenes. The presence of indigenous acetic acid in AMMs suggests the pre-terrestrial aqueous processing of the AMM parent body. Carboxylic acids can be converted to amines and amides via the Schmidt reaction (Laue & Plagens, 2005; Schmidt, 1924) which could then be utilised in amino acid formation.

The delivery of aromatic hydrocarbons (benzenes, thiophenes and naphthalene) may not have been of direct biological importance. However their involvement in secondary reactions (hydrolysis, substitution, oxidation and reduction) on the planet's surface would have contributed to prebiotic chemistry. With the flux of extraterrestrial dust particles to the early Earth 4.0-4.5 Ga up to a billion times that of the present day (Hartmann et al., 2000), the delivery of biologically important species (such as those identified during this study) would have served as a source of organics during prebiotic chemical reactions.

4.4.9. Micrometeorites – Cometary or Asteroidal?

The origin of MMs is controversial, with the mineralogy and elemental chemistry suggesting they may be of asteroidal (Genge et al., 1997; Kurat et al., 1994) or cometary (Engrand & Maurette, 1998; Nakamura et al., 2005) origin. Similar controversy arises when addressing the origin of IDPs, most of which are meteoritic in terms of mineralogy and elemental composition and thus asteroidal in origin. However, the chondritic porous IDPs (rich in anhydrous silicates and presolar silicates whilst lacking hydrous silicates) are thought to derive from cometary material (Bradley, 1994b; Rietmeijer, 1998).

Although the broad mineralogy, elemental and isotopic composition of AMMs matches the carbonaceous chondrites (Genge & Grady, 1998; Kurat et al., 1994), AMMs do have a higher carbon content (Table 6 and Section 2.1.3), a pyroxene/olivine rations ~ x 10 of the carbonaceous chondrites and the presence of chondrules is scarce (Maurette 1998). In this study, AMMs also contain different percentage proportions of benzenes, thiophenes and their alkyl counterparts compared to Murchison. Differences in organic composition may derive from alteration during AMM atmospheric entry heating as discussed previously or be reflective of parent body composition. In the case of the carbonaceous chondrites and the ordinary chondrites, higher carbon abundance and absence of chondrules implies that the parent body of a meteorite originates at a greater heliocentric distance (Rubin & Wasson, 1995). Applying this principle to AMMs, suggests that their parent body/bodies may have formed at a larger heliocentric distance than the chondrites (Clemett et al., 1998; Maurette, 1998; Rubin & Wasson, 1995), favouring an outer asteroid-belt or cometary parent body.

Extraterrestrial dust particles thought to be of asteroidal origin inevitably sample chondritic components (chondrules, refractory inclusions and matrix material), which are heterogeneous on the sub-mm scale, reflected in the variety of MM compositions and their similarities to chondritic material (Section 1.3 and 1.4). However, chondrules and refractory inclusions are not exclusive to asteroidal material, they may account for the dense compact particles observed in the Leonids cometary meteor shower (Swindle &

Campins, 2004). In contrast, ultracarbonaceous MMs (Nakamura et al., 2005) and anhydrous IDPs (Bradley, 1994b) thought to originate from cometary material due to the high occurrence of pre solar silicates and their high carbon contents, could alternatively be derived from highly primitive bodies in the asteroid belt (for example D-type or P-type asteroids).

The reflectance spectra of hydrous silicate rich IDPs is similar to that of the C-type asteroids (Bradley et al., 1996) (within the main belt and beyond 2.7 AU), which are thought to be the parent bodies of the CM and CI meteorites (McSween, 1999). Chondritic porous IDPs have reflectance spectra similar to the P-type and D-type asteroids (Bradley et al., 1996), typically located in excess of 3.5 AU. Recent mineralogical analysis of hydrous MMs (Sakamoto et al., 2008) highlights similarities to Tagish Lake which is thought to originate from a D-type asteroid. The D-type asteroids comprise carbon, organic rich silicates and water ice (Lebofsky, 1991) which may have sourced the Tagish Lake meteorite (Ai, 2002; Noguchi et al., 2002). Although we do not have a substantial meteoritic record of the D-type asteroids, a consequence of their location in and beyond the outer asteroid belt, it is plausible that dust derived from these asteroids may travel to Earth via Poynting–Robertson drag (a process by which solar radiation causes solar system dust grains to slowly spiral inward) (Noguchi et al., 2002). However, analysis of Tagish Lake macromolecular fraction finds that it contains high abundances of O-bearing species compared to CI and CM2 meteorites (Yabuta et al., 2007), and is lacking in thiophenes and benzenes (Gilmour et al., 2001; Yabuta et al., 2007). In contrast, AMMs in this study contain a variety of C_0-C_5 benzenes and C_0-C_3 thiophenes which cannot be attributed to a consequence of atmospheric entry heating (Section 3.5.1); subsequently it is unlikely that they share a parent body with Tagish Lake.

Whilst it was not possible to identify AMM species larger than naphthalene in this study, Clemett et al (1993) found that IDPs are dominated by larger PAHs, suggesting that more volatile components (lower PAHs) are lost during atmospheric entry heating. In contrast, AMMs with CM-like mineralogy were found to contain PAHs with very few alkyl

derivatives, whilst AMMs with CI-like mineralogy demonstrated the highest degree of PAH alkylation (Clemett et al., 1998). There is a greater degree of PAH aromatisation and alkylation in AMMs than in carbonaceous chondrites (Clemett et al., 1998). Typically, cometary derived extraterrestrial dust particles have higher entry velocities > 18 km/s (Joswiak et al., 2000), subjecting particles to higher entry heating temperatures (up to 1175 °C based on stepped-He release measurements of IDPs) releasing the more volatile organic components. Although high molecular weight species (PAHs) have not been characterised in this study, the structural diversity of benzenes and the presence of naphthalene suggest that AMMs are unlikely to have experienced high temperatures on atmospheric entry and a subsequent high entry velocity.

The CI chondrites, based on a reconstruction of the Orgueil orbit (Gounelle et al., 2006) and amino acid compositions (Botta et al., 2000) are thought to be the remnants of cometary nuclei. The CI chondrites have undergone substantial aqueous alteration (Bullock et al., 2005) and comparisons of AMMs organic composition with CI material illustrates they are significantly different. Analysis of Orgueil demonstrates that it lacks C_0-C_1 benzenes (Pearson, 2003), containing large abundances of higher alkylated benzenes (C_2-C_4). This is inconsistent with AMMs, which display a complete series of C_0-C_4 alkyl benzenes and C_5 *n*-alkane substituted benzene. Although benzene and C_1-benzenes can be formed by secondary reactions during atmospheric entry heating (Section 3.5.1) it is unlikely that this process could produce all C_0-C_1 benzenes present in AMMs. It is therefore unlikely that AMMs are related to the CI parent body.

Directly sampled cometary material from the Stardust mission shows it does not contain a large abundance of presolar silicates as is predicted for material originating from the Kuiper belt (Ishii et al., 2008). Instead, they contain abundances of presolar grains equivalent to carbonaceous chondrites (Ishii et al., 2008), in addition to D/H and O isotopic compositions consistent with inner solar system objects (McKeegan et al., 2006). Refractory inclusions have also been identified in the cometary samples returned in the *Stardust* mission (Schmitz et al., 2008; Simon et al., 2008). It suggests Kuiper belt objects

may have accreted nearer to the Sun and later migrated or that they accreted in-situ from materials transported from the inner solar nebula (Ciesla, 2007). Certainly, observations of protoplanetary disks surrounding young stars detect the presence of warm C_2H_2, HCN (Gibb et al., 2007; Lahuis et al., 2005), complex aromatics such as PAHs (Geers et al., 2006; Habart et al., 2006) and high abundances of water vapour and OH within 3 AU of the host star.

L^2MS has revealed that Stardust samples of Comet Wild/2 contain 2 to 4-ringed PAHs with up to C_4 alkyl derivatives (Sandford et al., 2006), resembling Murchison matrix material and that of IDPs (Clemett et al., 1993). Raman spectra of Stardust particles (Sandford et al., 2006) suggest they contain relatively unmetamorphosed organic material similar to IDPs and primitive meteorites. FTIR along Stardust track walls also exhibit –OH (3222 cm^{-1}), aromatic –CH (3065 cm^{-1}), $-CH_3$ (2968 cm^{-1}), $-CH_2$ (2923 cm^{-1}), $-CH_3$ and CH2 (2855 cm^{-1}) and C=O (1706 cm^{-1}) features corresponding to aromatic, aliphatic, carboxylic species (Sandford et al., 2006). Additionally one Stardust particle contained a weak nitrile stretch feature at 2232 cm^{-1}. Complimentary C-, N- and O- XANES confirmed the presence of aromatic and carboxyl moieties in addition to nitriles, amides and keto-aldehydic species (Sandford et al., 2006). AMMs in this study contain a range of aromatic species, branched and straight chain aliphatic species, the carboxylic acid acetic acid, benzonitrile and acetonitrile, phenol and aliphatic alcohols that would be responsible for similar FTIR features. In addition, comets contain high abundances of unsaturated hydrocarbons (Kissel & Krueger, 1987), the dominant aliphatic species in AMMs.

More recently, the detection of activated asteroids (also known as main-belt comets) (Hammergren, 1996; Hsieh & Jewitt, 2006) suggests that there are no marked asteroidal and cometary formation regions. The similarities between comet Wild/2 and chondritic material suggests there is not even compositional differentiation between cometary and asteroidal materials within the solar system, but instead there exists a continuum. Some activated asteroids do not exhibit cometary-like orbits and reside in regions of the asteroid belt associated with the Themis family of C-class asteroids

(Hammergren, 1996), that are thought to resemble the carbonaceous chondrites (McSween, 1999).

Cometary organic molecules and ices are thought to have interstellar origins (Greenberg et al., 1995; Mumma et al., 1996), whilst others are thought to derive from nebula condensates (Mumma et al., 2001). Active comets progressively loose volatiles, with any organic material on their surface becoming polymerized and condensed kerogen-like aromatic units as is observed in Hale-Bopp (Milam et al. 2004) and Halley (Fomenkova, 1999; Huebner, 1987). Consequently, the composition of a comet is related to the length of time it has been active e.g. an "old" comet will be carbonized and contain condensed aromatic material analogous to thermally altered carbonaceous chondrites (Kitajima et al., 2002; Komiya., 1993; Shimoyama, 1997).

A number of S- and N- heterocyclic compounds are identified in AMMs, suggesting the presence of S- and N- heterocyclic bound species integrated with the macromolecule, in addition to large abundances of phenol, indicative of ether linkages prevalent in the macromolecular structure. Combined, this suggests that AMM macromolecular material is not substantially condensed and has therefore neither experienced intensive pre-terrestrial thermal alteration nor extreme heating on atmospheric entry. The AMM open macromolecular structure is not consistent with condensed structure of the organic material from "old" or long-term active comets. Until a detailed analysis of volatile organic species in cometary particles is conducted, it is not possible to fully assess their similarities to MMs.

4.5. Conclusions

Despite exposure to extreme heating conditions during atmospheric entry, both simulations of the process demonstrated in Chapter 3 and previous studies (Glavin & Bada, 1999; Matrajt et al., 2006) and the analysis of MMs in this study and others (Clemett et al., 1998; Matrajt et al., 2001; Matrajt et al., 2004; Suzuki et al., 2005) illustrate that the survival of organic material within the particles is possible. This study has

identified a variety of species in AMM fragments for the first time, including those of biological significance. However, some species are identified in the complementary Antarctic terrestrial particles, making it impossible to rule out the terrestrial origin of some AMM organics. Further analysis of more pristine AMMs from the Concordia collection, with well constrained terrestrial ages, may improve these results.

There are strong similarities in the organic composition of AMMs and the Murchison meteorite, with atmospheric entry heating and/ or a contribution by terrestrial sources accounting for any differences. AMMs comprise all functional organic groups that have been previously identified in Stardust cometary samples. It is entirely possible that MMs are sourced from both cometary and asteroidal dust, which may be resolved with detailed cometary analysis. Alternatively, cometary-like and asteroidal-like EDPs may originate from a parent body that is poorly or not yet represented by meteoritic samples. The primitive volatile and organic rich D-type or P-type asteroids existing at a greater heliocentric distance than the main belt asteroids, could be a potential source.

5. The Fate of EDP Material in the Atmosphere

The primary objectives of this thesis were to investigate the processes affecting the organic chemical composition of EDPs during atmospheric entry heating and to establish the nature of liberated volatiles and carbon (Chapter 3) and that of remaining organic carbon (Chapter 4) within particles. In this chapter, the results of experimental simulations (Chapter 3) are used, in combination with extraterrestrial flux estimates, to constrain the contribution of volatile and organic species to the early Earth atmosphere. The fate of EDPs and their organic species injected into the atmosphere is influenced by both physical and chemical processes, which may have been of significance not only for chemical evolution but also the development of early Earth environment.

5.1. AMM Macromolecular Material

A range of aromatic species are detectable in AMMs using pyrolysis GCxGC (Chapter 4), with cores up to 2-carbon rings in size accompanied by O-, N- and S-N bearing components. Previous studies using μL^2MS, have identified up to 5-carbon ringed aromatic units (Clemett et al., 1998). The presence of both small aromatic units (1 and 2 carbon rings) and their structurally diverse alkyl counterparts suggests that the AMM insoluble organic material has an open structure and has not been exposed to substantial thermal alteration during atmospheric entry heating. If it had, graphitisation of macromolecular material with subsequent loss of side chains would have occurred (Kitajima et al. 2002; Komiya et al., 1993), yielding pyrolysates lacking in these smaller aromatic and alkyl-substituted components.

The presence of S- and N-bearing species within the aromatic network are inferred from the identification of thiophenes and N- and S-N heterocycles within AMM pyrolysates (Chapter 4). However, AMMs appear to lack the structural diversity of N-heterocycles relative to Murchison (Chapter 4). Whilst it is thought that S-bearing species can be

generated during pyrolysis or thermal events (Juntgen, 1987a; Juntgen, 1987b; Komiya & Shimoyama, 1996; Simmonds et al., 1969 a), K edge sulphur XANES analysis of carbonaceous chondrites has identified the presence of thiophene units within the aromatic network (Derenne et al., 2002). As yet, this technique has not been extended to EDPs in the case of sulphur, and is required to clarify the indigeneity of S-bearing species within particles.

Aliphatic linkages within AMM aromatic network are inferred from the structural diversity of alkyl-substituted aromatic units (derived from predominantly the β- cleavage of the macromolecular-bound aromatic precursors (Hartgers et al., 1994)) and a variety of aliphatic species characterised in the pyrolysate. The presence of phenols, in addition to previous identification of C=O features in AMMs by STXM (Matrajt et al., 2001), suggests the presence of ester linkages within the AMM macromolecule akin to that in carbonaceous chondrites (Hayatsu et al., 1980; Sephton et al., 2000). This study (Chapter 4) suggests that EDP's contain an aromatic macromolecular network similar to that of carbonaceous chondrites that have experienced minimal thermal metamorphism (Remusat et al., 2007 and references therein). Subtle differences between the distribution of aromatic species in AMMs and the Murchison carbonaceous chondrite coincide with the liberation of species during atmospheric entry heating or Antarctic weathering processes (Chapter 4).

5.2. Estimating the Flux of Volatile and Organic Carbon to the Early Earth

5.2.1. The Early Earth EDP Flux

The flux of extraterrestrial material to the early Earth has been estimated using the lunar cratering record (Hartmann, 1980; Hartmann et al., 2000) and suggests that at the time of the Earth's formation the bombardment flux was ~ 2 x 10^9 that of the present day, with an estimated 10^7 times that of present day once the Earth had accreted. Soon after

the Earth's formation there was a rapid decline in the delivery of these materials, with an estimated 10^3 times the present day flux at 4.2 Ga and 10^2 times at 3.8 Ga (Hartmann et al., 2000). Assuming an average bombardment flux of 10^5 times that of the present day between 3.8-4.5 Ga, and an average present day 10 μm - 500 μm sized EDP flux of 4 x 10^7 kg/yr (Love & Brownlee, 1993), the average EDP flux to the early Earth would have been 4 x 10^{12} kg/yr. This flux estimate is similar to 3 x 10^{12} kg/yr calculated by Pasek and Lauretta (2008) which assumed a maximum extraterrestrial flux 3.8-4.1 Ga ~10^5 times (Zahnle & Sleep, 2006) that of the present IDP flux of 3 x 10^7 kg/yr (Pasek & Lauretta, 2008). Similarly, taking the extreme values for bombardment flux during the 3.8-4.5Ga time period, the minimum and maximum EDP flux would have been 4 x 10^9 kg/yr and 4 x 10^{14} kg/yr respectively.

5.2.2. The Flux of Carbon or Volatile-Bearing EDPs

Walter et al., (1995 a) found that 13.5 % of 303 extraterrestrial particles in the 100-400 μm fractions from Cap-Prudhomme were melted cosmic spherules. 86.5 % comprise partially melted and unmelted AMMs, 1% of which have trace elemental abundances similar to the ordinary chondrites (Walter et al., 1995 a). The remaining particles (85.5%) consist of unmelted MMs compositionally similar to CM and CI chondrites (Genge et al., 1997; Greshake et al., 1998; Kurat et al., 1992; Kurat et al., 1994), with partially melted MMs found to have trace element abundances (Walter et al., 1995 b) and oxygen isotopic compositions (Yada et al., 2006) also similar to the CM chondrites.

Similarly, 82.0 % of 200 of 4-40 μm sized IDPs comprise chondritic porous IDPs (containing carbonaceous materials) or chondritic smooth IDPs (containing hydrous components) (Schramm et al., 1989). Both classes of IDP are compositionally similar to CI or CM chondrites (Schramm et al., 1989). In the calculations that follow, it is assumed that an average of 83.8 % of present EDPs (4-400 μm) are of CM or CI composition prior to atmospheric entry heating, which subsequently dehydrates them liberating volatile and

organic material (Chapter 3) altering the mineralogy and morphology of particles (Greshake et al., 1998; Toppani et al., 2001). The early Earth EDP flux is also thought to have been dominated by carbonaceous and hydrous bearing components as is suggested by the presence of "fossil" microclasts (MMs) of CI and CM-like compositions incorporated into HED meteorites (Maurette et al., 2000; Zolensky et al., 1996) and lunar soil (Zolensky et al., 1996). It is assumed that the same percentage of early Earth EDPs is of volatile or carbon-bearing composition as that of those present day. Therefore the early Earth flux of carbon or volatile-bearing EDPs is calculated as 3.4×10^{12} kg/yr (with a minimum EDP flux of 3.4×10^{9} kg/yr and maximum EDP flux of 3.4×10^{14} kg/yr) across 3.8-4.5Ga.

5.2.3. The Abundance Carbon in EDPs

Using the upper limits of carbon contents from Table 6, an average of ~3 wt. % carbon is present in MMs (Engrand & Maurette, 1998; Matrajt et al., 2003; Maurette et al., 2001). This is similar to the carbon content in Murchison 1.6-2.7 wt % (Naraoka et al. 2004 and references therein; Pearson et al. 2006) and that of the Murchison reference material (2.7 wt % ± 0.06, this study) used in the experimental simulations. As carbonate minerals are lacking in the Cap-Prudhomme MM collection (Duprat et al., 2007) a consequence of collection procedures and/or their prolonged residence time on Earth, the carbon is primarily derived from organic material. It must be noted that MMs collected recently from Antarctic snow of shorter terrestrial ages at the Concordia and the Dome Fuji sites show the presence of dolomite (Duprat et al., 2007) and Fe-Mg carbonates (Sakamoto et al., 2008). As such, carbonate minerals will contribute to the carbon abundance in MMs from these sites.

Whilst the carbon content of MMs is well constrained, there is a large range of carbon abundances identified in IDPs between 0 – 48 wt % (Keller et al., 1994; Thomas et al., 1993). As experimental simulations were conducted on material with similar carbon contents to MMs, the calculations that follow assume the EDP flux consists of MM particles and therefore represent a lower limit of carbon flux to the early Earth. Assuming

the EDP flux consisted of only IDPs, the delivery of carbon to the early Earth would be higher reflecting their increased carbon content.

5.2.4. The Delivery of EDP Volatiles and Carbon to the Early Earth

Powdered SFE Murchison (Murchison reference material) was used as an analogue of EDP material during experimental simulations outlined in Chapter 3. Murchison reference material was of similar grain size, hydrous mineralogy, carbon content and organic composition as EDPs as summarised in sections 1.4 and 2.1.3. During and post simulation, the abundance of H_2O (derived from the dehydration of phyllosilicates) and CO_2 (derived from the decomposition and volatisation of organic material and carbonate minerals) were recorded (Table 26). In calculating the flux of volatiles and carbon to the early Earth, it is assumed that EDP mineralogical and organic compositions are identical to Murchison reference material, and that the ratios of these components released or retained by EDPs are the same as those recorded in simulations. A flux of 3.4×10^{12} kg/yr of carbon or volatile-bearing EDPs to the early Earth is assumed as calculated in Section 5.2.2). The annual early Earth flux of H_2O and organic and inorganic carbon delivered both to the surface in EDPs (Table 37) and deposited into the atmosphere (Table 38) are summarised dependant on the heating regime.

	Annual early Earth EDP flux retained in particles to the surface (kg)				
	H_2O	CO_2 derived from organic material	Equivalent $C_{organic}$	CO_2 derived from inorganic material	Equivalent $C_{inorganic}$
No Heating	2.9×10^{11}	7.4×10^{10}	2.0×10^{10}	1.3×10^{11}	3.7×10^{10}
Mild Heating (2 s, 400 °C)	2.3×10^{11}	5.7×10^{10}	1.6×10^{10}	1.3×10^{11}	3.7×10^{10}
Mild Heating (2 s, 600 °C)	2.0×10^{11}	5.0×10^{10}	1.4×10^{10}	1.3×10^{11}	3.7×10^{10}
Moderate Heating (2 s, 800 °C)	6.7×10^{9}	3.4×10^{9}	9.1×10^{8}	1.2×10^{11}	3.4×10^{10}
Extreme Heating (2 s, 1000 °C)	0	0	0	3.4×10^{10}	9.1×10^{09}

Table 37: Calculated abundances of water and CO_2 in addition to equivalent organic and inorganic carbon retained by early Earth EDPs to the surface. Calculated from average early Earth EDP flux and ratios of evolved gases from heated samples the unheated reference Murchison (Table 26, Chapter 3). These represent the midpoint values using a bombardment flux of 10^5 time that of present day. Accounting for the extremes of bombardment flux to the early Earth (10^2 and 10^7 times that of present flux), the minimum EDP flux values would be 1000 less than quoted in the table, whilst the maximum would be 100 times more. Full calculations are given in Appendix V

Table 37 demonstrates that the extent of heating has a significant effect on the quantity of H_2O and $C_{organic}$ that may be retained by EDPs and delivered to the early Earth surface. Under an extreme heating regime (up to 1000 °C) no organic carbon or water is estimated to survive to the early Earth surface. In contrast, under milder heating regimes (to 400 °C and 600 °C), similar quantities of H_2O and $C_{organic}$ are retained in EDPs.

Table 38 illustrates that up to one order of magnitude more H_2O and organic carbon could be released into the early Earth atmosphere annually by EDPs under extreme heating (to 1000 °C) than mild heating (to 400 °C). In the case of heating to 1000 °C (where almost complete volatile and organic loss from a particle occurs as summarised in Section 3.4.2) an estimated 1.7×10^{11} kg CO_2 was liberated into the early Earth atmosphere annually. 7.4×10^{10} kg of this would be derived from organic material, corresponding to 2.0×10^{10} kg organic carbon ($C_{organic}$). Conversely, EDPs exposed to low heating temperatures (< 600 °C) would liberate substantially less CO_2 into the atmosphere < 2.3×10^{10} kg CO_2 annually, corresponding to < 6.4×10^9 $C_{organic}$ with no contribution from the thermal decomposition of carbonate minerals.

For extreme values of bombardement flux to the early Earth during the 3.8-4.5Ga period, the maximum EDP volatile flux would be 100 times the values in Table 37 and Table 38, whilst the minimum would be 1000 times less.

	Annual early Earth EDP flux of volatiles released into the atmosphere (kg)				
	H_2O	CO_2 derived from organic material	Equivalent $C_{organic}$	CO_2 derived from inorganic material	Equivalent $C_{inorganic}$
No Heating[3]	0	0	0	0	0
Mild Heating (2 s, 400 °C)	6.0×10^{10}	1.7×10^{10}	4.6×10^9	0	0
Mild Heating (2 s, 600 °C)	9.1×10^{10}	2.3×10^{10}	6.4×10^9	0	0
Moderate Heating (2 s, 800 °C)	2.8×10^{11}	7.0×10^{10}	1.9×10^{10}	1.0×10^{10}	2.7×10^9
Extreme Heating (2 s, 1000 °C)	2.9×10^{11}	7.4×10^{10}	2.0×10^{10}	1.0×10^{11}	2.7×10^{10}

Table 38: Calculated abundances of water and CO_2 in addition to equivalent organic and inorganic carbon released by early Earth EDPs into the atmosphere. Calculated from average early Earth EDP flux and ratios of evolved gases from heated samples the unheated reference Murchison (Table 26, Chapter 3). These represent the midpoint values using a bombardment flux of 10^5 time that of present day. Accounting for the extremes of bombardment flux to the early Earth (10^2 and 10^7 times that of present flux), the minimum EDP flux values would be 1000 less than quoted in the table, whilst the maximum would be 100 times more. Full calculations are given in Appendix V.

5.2.5. Limitations of EDP Volatile Flux Calculations

Underpinning the above calculations is the estimation of early Earth bombardment flux (Section 5.2.1), which is derived from the lunar cratering record. During the time period 3.8-4.5 Ga, the estimated bombardment flux ranged from 10^7 and 10^2 times that of the present day (Hartmann, 1980; Hartmann et al., 2000) and is therefore the least constrained variable. As such, EDP volatile flux has been calculated for a mid-point bombardment flux of 10^5 times that of present day. However, using the minimum bombardment flux estimates decreases the EDP volatile flux calculations by 10^3 times that in Table 37 and Table 38, whilst the maximum increases the calculated volatile fluxes by 10^2 times.

The second least constrained variable is the composition of EDPs delivered to the early Earth. The majority of present EDPs are thought to originate from asteroidal dust bands (Kortenkamp & Dermott, 1998), accounting for their affinities to the carbonaceous chondrites (Section 1.4). The early Earth was initially bombarded by the left over debris following the formation of the Solar System. However, 3.8-4.1Ga the migration of the giant outer planets (Gomes et al., 2005) resulted in a sudden delivery of outer Solar System material into the inner Solar System known as the late heavy bombardment (LHB). EDPs delivered during the LHB would have been sourced from the more volatile-rich outer region of the Solar System.

The calculations of EDP volatile flux have been based on the carbon contents of MMs and the experimental heating simulation results of carbonaceous chondrites (MM-analagous material). IDPs are known to have compositional similarities to cometary material (Section 1.4) and contain higher carbon contents than MMs (Keller et al., 1994; Thomas et al., 1993). As such, the calculations represent the lower limits of EDP volatile flux to the early Earth. Assuming the early Solar System EDP flux consisted of only IDP-like particles, the delivery of carbon and volatiles to the early Earth would be significantly higher reflecting their increased carbon and volatile content.

5.2.6. A Comparison with Alternative EDP Flux Estimates

Maurette et al., (2000) have estimated a total of 1.3 x 10^{20} kg (equivalent to an annual flux of 1.3 x 10^{12} kg) of C released as CO_2 from MMs as a result of atmospheric entry heating during the first 100 Ma of heavy bombardment. Maurette et al., (2000) assumed a present day MM flux of 4 x 10^7 kg/yr with an early Earth bombardment factor was 10^6 times that of the present flux. They also assumed that 90 % of MMs were carbon or volatile bearing. This study (Table 38) demonstrates that 4.7 x 10^{10} kg of total C was released annually from EDPs exposed to extreme atmospheric entry heating (1000°C) during the same time period. Although this is two orders of magnitude lower than that estimated by Maurette et al (2000), this accommodates an early Earth bombardment flux of 10^5 times that of present day with constraints on the quantity of volatiles released derived from experimental simulations (Chapter 3).

Table 37 suggests that an annual flux of 1.6 x 10^{10} kg organic carbon could survive in EDPs to the early Earth surface if only exposed to mild (400 °C) atmospheric entry heating regimes. In contrast, Pasek and Lauretta, (2008) despite using a similar early Earth EDP flux to that of calculations in this study, estimated an annual flux of just 5 x 10^9 kg of organic C delivered to the early Earth by these particles. The order of magnitude difference in calculations between the two studies arise as Pasek and Lauretta (2008) considered that organic carbon could only be delivered by the hydrous fraction of EDPs (27.5 % the total EDP flux). The calculations in this study, in contrast, assume that 83.8% of EDPs (Section 5.2.2) are of CM or CI like composition prior to atmospheric entry heating and are therefore volatile or carbon-bearing. The dehydration, volatisation and thermal alteration of EDP components can give rise to the porous or vesicular textures identified in partially melted particles and account for differences in elemental abundances and mineralogical differences relative to unmelted particles (Greshake et al., 1998; Kurat et al., 1992; Kurat et al., 1994; Toppani et al., 2001), suggesting unmelted and melted EDPs may have the same composition prior to entry heating.

5.2.7. EDP Volatile Delivery vs. Volcanic Degassing

The present day annual flux of H_2O injected into the atmosphere by volcanism is between $5 \times 10^9 - 5.5 \times 10^{10}$ mols, equivalent to 9×10^{10} kg – 9.9×10^{11} kg (Martin et al., 2007). Martin et al., (2007) have suggested that increased volcanic activity on the early Earth would have led to an estimated ten times the present H_2O flux being injected into the atmosphere, equivalent to 9×10^{11} kg – 9.9×10^{12} kg. Whereas, $6 \times 10^{10} - 10 \times 10^{10}$ kg CO_2 is released annually into the atmosphere by volcanic activity (Walker, 1977; Williams et al., 1992), with therefore an estimated $6 \times 10^{11} - 10 \times 10^{11}$ kg CO_2 injected into the early Earth atmosphere. Table 2 suggests that EDPs could have annually contributed between 6.0×10^{10} kg - 2.9×10^{11}kg H_2O and 1.0×10^{10} - 1.0×10^{11} kg CO_2 (derived from inorganic components) to the early Earth atmosphere, depending on heating regime.

It is apparent that the contribution of CO_2 and H_2O from EDPs could have been comparable to that of early Earth volcanic eruptions, which are thought to have been primary source of early atmospheric gases (Kasting, 1993; Kasting et al., 1993; Walker, 1977; Walker, 1985). It suggests that EDP derived volatiles may have been a significant contributor to early atmospheric development.

5.3. Characterisation of EDP Organic Material Deposited into the Atmosphere

Experimental simulations (Chapter 3) have shown that meteoritic macromolecular material fragments on heating to temperatures as low as 400 °C, with a minimum of 600 °C is required to release some N-heterocycles. The cleaving of side chains from the macromolecule (Hartgers et al., 1994; Hambly, 1998; Sinninghe Damsté et al., 1989) result in the release monoaromatic and alkyl aromatic species including benzenes, thiophenes and N- heterocycles. Parental and alkyl PAHs are also liberated, in addition to phenol released on cleavage of ether linkages.

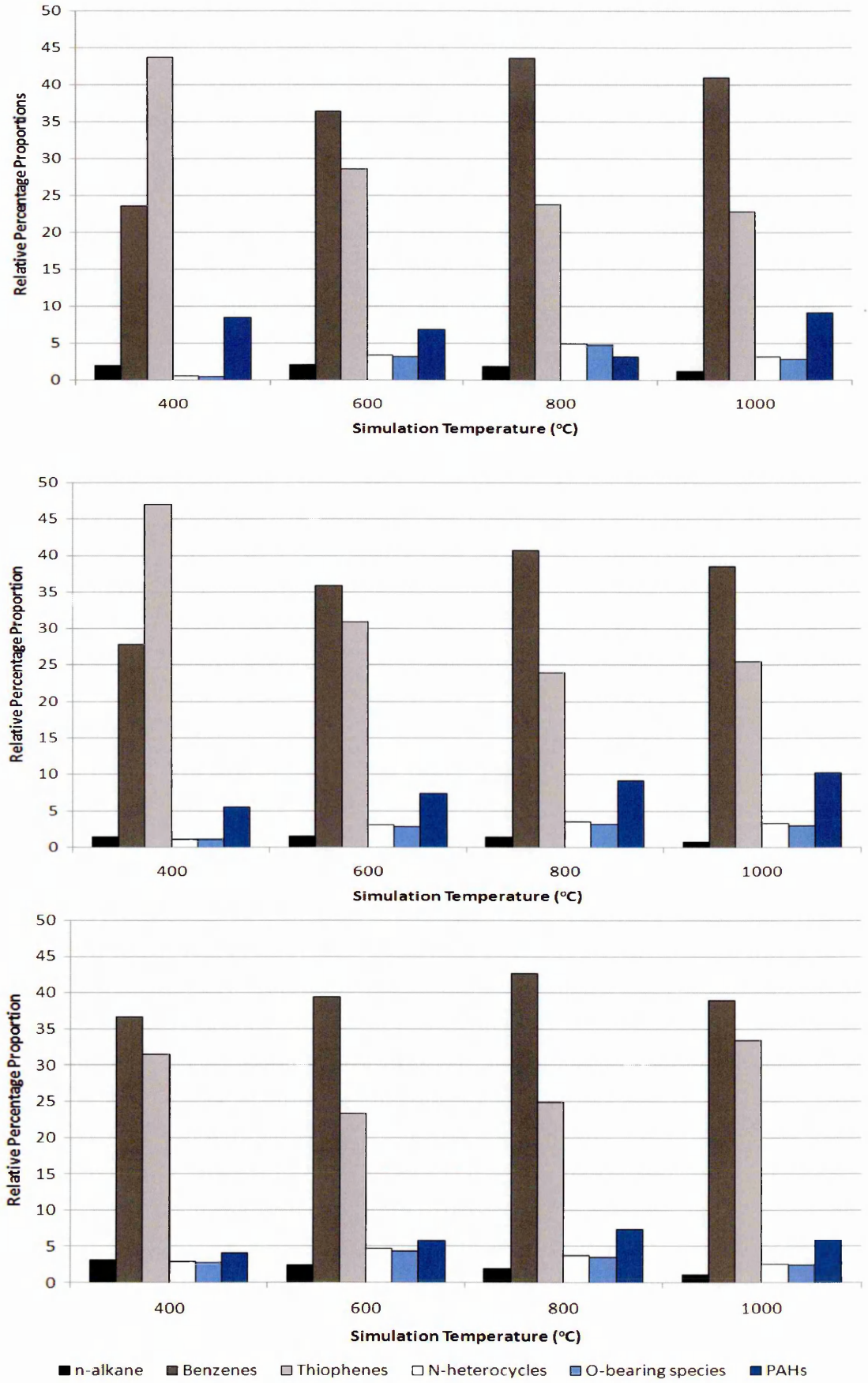

Figure 62: Proportions of various aromatic and aliphatic components as a percentage of total chromatogram peak areas of species identified in pyrolysates in Tables 27-29 for simulations for 2s (top), 5s (middle) and 20s (bottom)

The quantity of organic C (Section 5.2.4), and the variety of organic species deposited into the atmosphere by EDPs, is strongly dependant on atmospheric entry heating temperature. Figure 62 demonstrates that thiophenes (as a percentage proportion of species documented in Tables 27-29) dominate liberated species in simulations at low temperatures (400 °C) for short durations (2 s and 5 s), with very little contribution by N-heterocycles and O-bearing species. In contrast, at high temperatures (1000 °C) benzenes are the major liberated species, with a reduced contribution by thiophenes and increased contribution by PAHs, N-heterocycles and O-bearing species.

Combining the findings of experimental simulations conducted for 2 s (Chapter 3), and the predicted peak atmospheric entry heating temperatures of Love and Brownlee, (1994) for a variety of EDP sizes and entry velocities, three heating regimes are highlighted in Figure 63.

- Blue: signifying entry heating parameters that result in the retention of the majority of water, organic carbon and inorganic carbon in the particle. This is based on thermogravimetric measurements presented in Section 3.4.2.
- Purple: representing the conditions giving rise to significant thermal degradation of the macromolecular network. The limiting factor of this heating regime was the complete absence of pyridine and pyrimidine liberated in samples heated to 425 °C, suggesting a higher temperature is required for the release of these N-heterocycles from the aromatic network (Section 3.5.1.D). These conditions additionally evolve substantial volatile components (CO_2 and H_2O) (Section 3.4.2).
- Red: highlights heating conditions that would result in the volatisation and subsequent liberation of the majority of H_2O, organic carbon and inorganic carbon based on thermogravimetric measurements (Section 3.4.2)

Figure 63 demonstrates that that EDPs with an entry angle of 45° would have to be small (up to 15 μm-sized) with a low velocity (~10 km/s), or extremely small (a few microns) travelling up to 22km/s to enable the survival of the majority of their organic inventory. However, 100-400 μm sized particles like those analysed in Chapter 4, could

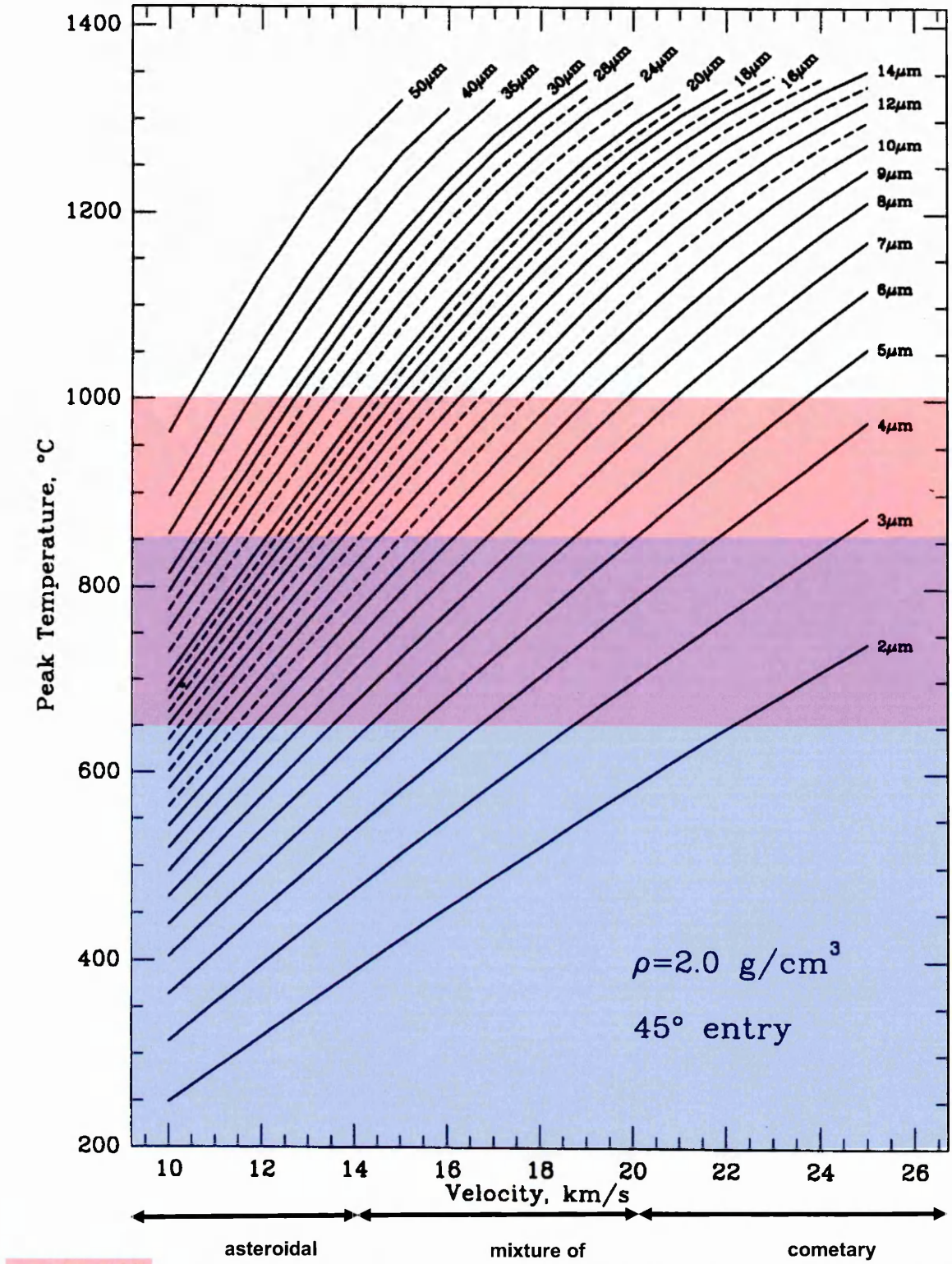

Extreme entry heating conditions – substantial volatile and organic loss from particle, possible aromatisation and condensation of residual macromolecular organic material

Entry heating conditions that liberate the majority of the organic and volatile components, retaining very little organic material within the particle. Aromatisation and condensation reactions start to occur.

Entry heating conditions that liberate a fraction of volatile and organic components and retain a fraction of these components.

Figure 63: The fate of EDP organic and volatile material as recorded in experimental simulations (Chapter 3) and applied to entry heating conditions modelled by Love and Brownlee (1993) for particles with an entry angle of 45° with varying particle size and entry velocity

experience peak entry heating temperatures <<1000 °C, making it possible to retain their a fraction of their components, if they had either an extremely low entry velocity (<< 10 km/s) or if they had a high entry angle (> 80°) (Love & Brownlee, 1991). EDP macromolecular material retained in particles could have been a viable source of organic species on deposition to the surface.

From the calculations in Section 5.2.4, it is apparent that large quantities (up to 2.0 x 10^{10} kg) of organic carbon, were deposited annually at 85-100 km altitude during the period of heavy bombardment up to 4.5 - 3.8 Ga, creating an organic-rich layer dominated by aromatic species. An organic rich atmospheric layer may have served as a location for further chemical evolution (Oberbeck et al., 1991). If concentrated enough, an organic haze would have shielded the surface from harmful UV radiation or contributed to a greenhouse effect therefore stabilising surface temperatures (Sagan & Chyba 1997; Trainer et al. 2006).

5.3.1. Secondary Reactions During Heating

Under flash heating (pyrolysis or atmospheric entry heating), mineral interactions or secondary reactions between released radicals may occur resulting in the production of new organic species which were not necessarily present within the original macromolecular material. For example, carbonaceous chondritic macromolecular material contains organic sulphur as both thiophenic units and aliphatic sulphide linkages (Anders et al. 1973; Derenne et al., 2002). Thiophenes present in carbonaceous chondritic pyrolysates arise via cleaving of thiophenic units from the macromolecule. In addition, the degradation of sulphide linkages similar to the process in coal pyrolysis (Remusat et al., 2005 b; Riboulleau et al., 2000), and their subsequent interaction with resident organic material, can also contribute to the generation of thiophenes in the simulation pyrolysates. The structure of AMM macromolecular material requires further

investigation to determine if sulphide linkages occur within the network, which may be thus contributing to the abundance of thiophenes in pyrolysates (Chapter 4).

Meteoritic clay minerals are spatially associated with inherent organic material (Pearson et al., 2002), suggesting that their catalytic properties may have influenced the origin of organic species in the early Solar System. During pyrolysis these clay minerals can also induce aromatisation via degradative, aromatisation or polymerisation reactions (e.g. Faure et al., 2006; Horsfield & Douglas, 1980). This may account for the decreasing percentage proportion of n-alkanes and increasing relative proportion of aromatic species such as benzene documented in Chapter 3.

5.3.2. A Comparison with Meteor Observations

Infra-red (Russell et al., 2002) and visible/near-UV (Jenniskens et al., 2004) observations of the Leonids and Geminids meteor streams (80-100 km altitude), have identified N_2, H_2O, CO, CO_2, minor CN and a C-H stretch vibration indicative of organic material in the wake of meteors. It must be noted that the Leonids and Geminids have a cometary and asteroidal source respectively. Atmospheric entry heating simulations (Chapter 3) correlate with meteor observations, and identify the release of CO_2 from the thermal decomposition of organic material and carbonate minerals, in addition to H_2O from the dehydration of phyllosilicates. Characterisation of evolved organic carbon under atmospheric entry heating conditions has been discussed extensively in Chapter 3. A range of aliphatic species, aromatic components, PAHs, N- S- and O-bearing species are liberated in all simulations, which will account for the infrared C-H stretching feature and CN previously observed in meteors.

In particular, these simulations demonstrate the ability for the liberation of complex organic material including up to 4-carbon ringed PAHs, confirming the plausibility that EDPs deposit these complex species into the atmosphere during entry heating. Jenniskens et al., (2004) targeted the identification of CN during the Leonids meteor entry heating and hypothesised that small molecular or atomic species (H, O, H_2, O_2, OH, H_2O,

CO, CO_2, C_2, CH, CH_4, C_2H, CN, HCN, and NH_3,) would be released during macromolecular carbonisation/graphitisation and via subsequent collisions in the wake e.g. sputtering by fast ions or energetic photons. The authors identified a low abundance of CN suggesting that larger components are released from meteoroids, which do not degrade into simple molecules in the meteor wake (Jenniskens et al., 2000; Jenniskens et al., 2004; Rairden et al., 1998), or that polymerisation and recombination reactions occurring in the meteor wake create more complex molecules.

5.4. Astrobiological Significance of Liberated EDP Organic Species

EDP entry heating simulations yield a variety of organic species, many of which are of direct biological significance or are precursors of biomolecules. With a mid range value for early Earth flux of EDPs up to x 10^5 (Hartmann et al., 2000) that of the present day (40,000 T/yr; Love and Brownlee, 1993), the deposition of organic material into the Earth's atmosphere, or delivery intact within EDPs to the Earth's surface, would have made them a substantial source of prebiotic molecules.

A diverse range of 5-6 ringed N-heterocycles are released from simulations (pyridine, pyrimidine, pyrazine, pyridazine, triazine, pyrrole and their alkyl derivatives), many of which form the basis of essential biomolecules. For example, the DNA and/or RNA nucleobases uracil, thymine and cytosine are all pyrimidine derivatives. Pyrazine is a constituent of folic acid and folate (its anion form), required for the production and maintenance of new cells and is essential for DNA synthesis, function and replication (Kamen, 1997). Pyrrole is a key component for the formation heme (found in haemoglobin) (Dailey, 1990) responsible for oxygen transfer during respiration. Similarly, chlorophyll, also comprised of pyrrole (Dailey, 1990), is necessary for the conversion of light to energy via the process of photosynthesis. The delivery of these species from EDPs, would have provided a source of nitrogen heterocycles essential for the formation of key biological components at the heart of the genetic code of living organisms and the compounds required for their replication. Importantly, pyrrole is critical for the

development of heme and chlorophyll, responsible for mechanisms of energy conversion and transfer in living organisms.

Acetonitrile and benzonitrile were released during simulations, and serve as biomolecule precursors or intermediates. For example nitriles are precursors of amino acids derived by Strecker synthesis (Strecker, 1850; Strecker, 1854) or Michael-addition reactions (Botta et al., 2002; Ehrenfreund et al., 2001; Michael, 1887; Michael, 1894). The hydrolysis of nitriles on their deposition into the Earth's atmosphere or delivery to the Earth's surface can derive carboxylic acids (Tewari & Goldberg, 2005), which can further be converted to amines via the Schmidt reaction (Schmidt, 1924). The reduction of nitriles can also produce amines directly (Caddick et al., 2000).

Aromatic species are not usually considered to be of prebiotic significance; however their fragmented products from heating, oxidation or hydrolysis may be. It has recently been proposed that aromatic species and PAHs could polymerise and form aggregates in water, eventually forming vesicles (Ehrenfreund et al., 2006) which could encapsulate solutions in a precursor to the cell.

5.5. Further Atmospheric Reactions and Processes

The hypothesised early atmospheric composition is believed to have been predominantly CO_2 in addition to CO, N_2 and H_2O (Kasting, 1993; Kasting & Ackerman, 1986; Walker, 1985). More recently, it has been suggested that CH_4 may have also been a major early atmospheric component (Kasting, 2005). The simulations presented in Chapter 3 have been conducted in the presence of He, representing an inert atmosphere. Further simulations conducted in the presence of gases representative of the early atmosphere (i.e. CO_2) are required to clarify the extent to which atmospheric composition affects the variety of species liberated from EDPs.

Following atmospheric entry heating in the mesosphere (50-100 km altitude), EDP liberated volatile and organic species may undergo further processes and reactions with

EDP products or atmospheric species prior to their deposition to the surface. The influence of these processes on EDP material is discussed below.

5.5.1. Atmospheric Reactions and Photolysis

Observations of T-Tauri stars analogous to the early Sun suggest that the young Sun may have emitted x 10^4 more UV radiation than the present day (Canuto et al., 1982). High levels of H_2O and CO_2 and organic carbon injected into the atmosphere by the devolatisation of EDPs (Section 5.2.4) would have been efficient "absorbers" of UV radiation at < 200 nm wavelengths (Jacobson, 2005) via the process of photolysis. Consequently. the UV flux to the Earth's surface would have been reduced, favourable for the emergence of life. EDPs resident in the atmosphere would have also scattered UV radiation, in the similar manner as present aerosol scattering of UV radiation (Bergstrom et al. 2007; Kalashnikova et al. 2005).

UV photo-disassociation of an early Earth CO_2 atmosphere would yield CO and atomic oxygen radicals ($O^{\bullet}$) (Lee & Grabowski, 1992; Mitsuke et al., 1990; Slanger & Black, 1978; Stolow & Lee, 1993). $O^{\bullet}$ is highly reactive and can combine with itself producing O_2, further reacting with atomic oxygen to yield O_3 (Kaplan et al., 1960) or react with liberated EDP organic species. The reaction of EDP liberated nitriles, benzenes, thiophenes and N-heterocycles with $O^{\bullet}$ would have generated both the radical ion and anion respective species in addition to H_2O, $^{\bullet}OH$, OH^- and $H^{\bullet}$. These organic radicals could have formed neutral products in the atmosphere, or could react with each other to produce polymers or higher carbon species.

Examples of the potential reaction pathways of liberated organic species (as identified in simulations, Chapter 3) with atmospheric radicals are given in Table 39. Ultimately, EDP derived organic species could react with radicals in the atmosphere eventually recombining, leading to oxygen or nitrogen enriched polymerised products (Jenniskens et al., 2004). The interaction of released species with atmospheric radicals can also be a degradative process, leading to products with less carbon atoms than the

parent compound (Atkinson, 1995; 2000). Similar radical interactions in the present atmosphere degrade organic species to simple molecules e.g. CO_2 and H_2O (Atkinson, 1995).

EDP liberated species	Examples of reaction pathways
alkanes	reaction with OH or NO_3 → alkyl radicals → alkylperoxy radicals → alkylnitrates, alcohols, carbonyls
alkenes	reaction with OH → hydroxyalkyl radicals reaction with NO_3 → nitrooxyalkyl radicals reaction with O_3 → carbonyl + biradicals
benzenes	reaction with OH → OH aromatic adduct → phenol, carbonyls, dicarbonyls and epoxy carbonyls benzyl radical reaction with NO → benzyl nitrate
PAHs	reaction with OH → OH-PAH adducts

Table 39: Examples of reactions of EDP derived organic species with OH, NO_3 and O_3 in the troposphere adapted from present day reactions from Atkinson (2000)

Photolysis and photo-ionisation can also act as mechanisms for the destruction of atmospheric species into simpler components. The photolysis lifetime of volatile organic species in the present day stratosphere is compound specific, ranging from days to years (Derwent, 1995). However, these lifetimes are likely to be in the order of hours to days in the early atmosphere, regardless of functional group, if UV fluxes were x 10^4 that of present (Canuto et al., 1982). Whether degradative, or processes that would produce higher molecular weight hydrocarbons, radical reactions and photolysis would have contributed to the range of organic species present in the EDP rich atmospheric layer.

5.5.2. Wet Deposition of EDP particles and Organic Species

Analyses of Li abundances and isotopes in 4.3-3.3Ga zircons (Ushikubo et al., 2008) suggest that liquid water existed on the early Earth at the time of their formation. Wet deposition is the method by which organic species can be removed from the atmosphere via the water cycle. It is the process that can ultimately provide an effective method of hydrolysing EDP organic material and delivering it to the early Earth's surface. On contact with water, the hydrolysis of EDP liberated organic species may be another process that can generate new organic compounds. For example nitriles liberated from EDPs, or those derived from the thermal decomposition of N-heterocycles, can be

converted by hydrolysis to carboxylic acids (Tewari & Goldberg, 2005) or from amino nitriles to amino acids (Strecker 1850; Strecker 1854).

Some EDP liberated organic species may be soluble in rainwater, whilst the particles themselves can be suspended in water, both can be deposited to the surface via wet precipitation like their present-day counterparts (Kawamura et al., 2001; Matsunaga et al., 2007). Major organic species in present-day wet precipitation are derived from anthropogenic sources and include C_1– C_{10} monocarboxylic acids and C_2-C_{10} dicarboxylic acids (Kawamura et al., 1996; Kawamura et al., 2001; Matsunaga et al., 2007), C_1-C_2 aldehydes (Kawamura et al., 1996; Kawamura et al., 2001; Matsunaga et al., 2007), a range of nitrogen-bearing species including amines, amino acids, urea, N-PAHs and N-heterocycles (Anastasio & McGregor, 2000; Cornell et al. 2003 and references therein) and particulates of 2- 4 carbon ringed PAHs (Ozaki et al., 2006; Park et al., 2001).

The equivalent EDP species which are known to be liberated during atmospheric entry heating simulations include acetic acid, aldehydes, ketones, alcohols, aromatic nitriles and N-heterocycles (Section 3.3.3), and would be soluble in rainwater. These would therefore be deposited to the surface via precipitation and incorporated into the water cycle on the Earth's surface. Certain aromatic species such as benzenes, larger PAHs and alkyl PAHs are not easily soluble in water, but may reside in rainwater as particulates and also deposited to the surface by rain water.

Once incorporated into the water cycle, opportunities for the concentration of organic species may have arisen e.g. in small pools or tidal areas with the further polymerisation of organic material occurring on clay mineral surfaces (Bernal, 1967; Lahav et al., 1978; Ferris, 1999;2005). Additionally some aromatic species and PAHs can polymerise and form aggregates in water, eventually forming vesicles (Ehrenfreund et al., 2006) which could encapsulate concentrated organic solutions in a precursor to the cell.

5.5.3. Dry Deposition

Following atmospheric entry heating and the liberation of volatile species, the remaining particles (which may still retain organic compounds), could be deposited on the planet's surface via gravitational settling. The residence time of EDPs in the atmosphere is of interest, as these particles may have had an impact on the environment in a similar way as aerosols do in the present day.

The aerodynamic breaking of EDPs in the upper atmosphere would result in them slowly settling to the Earth's surface. The settling of EDPs out of the atmosphere is comparable to that of ash particles injected into the present day atmosphere following volcanic eruptions. It is not unusual for explosive rhyolite and dacite Plinian eruptions to inject ash particles and gas into the lower stratosphere, up to 55 km altitude (Cas & Wright 1998). These volcanic particles are up to 20mm in diameter (Rose et al. 2001), coarser particles > 1 mm typically settle to the surface within an hour (Riley et al., 2003). Settling velocity is a function of particle size, larger particles have higher velocities and settle to the surface in a shorter time period than smaller particles (Bonadonna et al., 1998). Although settling rates are well constrained for the troposphere based on observations of ash fall, the same is not true for the stratosphere or mesosphere.

Settling rates for present day EDPs range from days to weeks for particles tens of microns in size, and months for particles <10 μm (Rietmeijer, 1998). In an early Earth atmosphere, dominated by CO_2, with a near-surface atmospheric pressure 15 times that of present day and a surface temperature of ~100 °C (Kasting & Ackerman, 1986) the early atmospheric density would have been ~ 3 times that of present (see appendix VI for calculations). Similar to those of present day, early Earth EDPs < 10 μm would have settling rates of the order of months (Appendix VI), whilst those in the range of tens of microns would have residence times of days. Larger particles, hundreds of microns in size, have estimated residence times of hours to days.

EDPs in terms of their composite nature (comprising organic, refractory and elemental carbon) and their particle sizes are also analogous to carbonaceous aerosols.

Carbonaceous aerosols are primarily formed from incomplete combustion of fossil fuels or biomass and include graphitised carbon, organic material and elemental carbon (Andreae & Gelencsér, 2006; Gelencsér, 2005) and are typically < 10 μm in size. Other atmospheric aerosols can be up to 150 μm in size (Exton et al., 1986). Carbonaceous aerosols in particular, are thought to have atmospheric residence times in the order of days to weeks and are known to absorb sunlight, consequently heating the surrounding air contributing to present day global warming (Andreae & Gelencsér, 2006; Gelencsér, 2005; Hansen et al., 2000; Menon et al., 2002; Penner et al., 1998). An estimated 1.2 x 10^{10} kg/yr of carbonaceous aerosols are thought to be released into the present atmosphere (Liousse et al., 1996a; Liousse et al., 1996b); this is two orders of magnitude lower than the estimated early Earth EDP flux of 3.4 x 10^{12} kg/yr (Section 5.2.2). With estimated atmospheric residence times in the order of days to months, EDPs may have affected the early Earth climate, potentially increasing global temperatures.

Furthermore, EDPs resident in the atmosphere could have provided a surface for atmospheric species to condense onto, similar to present day aerosols (Hoose et al., 2008; Novakov & Penner, 1993; Schaefer, 1975; Zhang et al., 2001). Present day carbonaceous aerosols are known to act as cloud condensation nuclei (CCN) (Hitzenberger et al., 1999), which facilitate the phase transition of water from gaseous to liquid form. With smaller EDPs resident in the atmosphere for prolonged periods of time (in excess of several days) they could have acted as CCN, seeding cloud formation and leading to eventual precipitation.

5.6. Summary

Liberated EDP volatiles are estimated to be of similar magnitudes as estimated volcanic degassing into the early Earth atmosphere (Section 5.1). Their evolved organic compounds would have undergone a various reactions and processes (summarised in Figure 64) including photolytic degradation or reaction with resident atmospheric radicals.

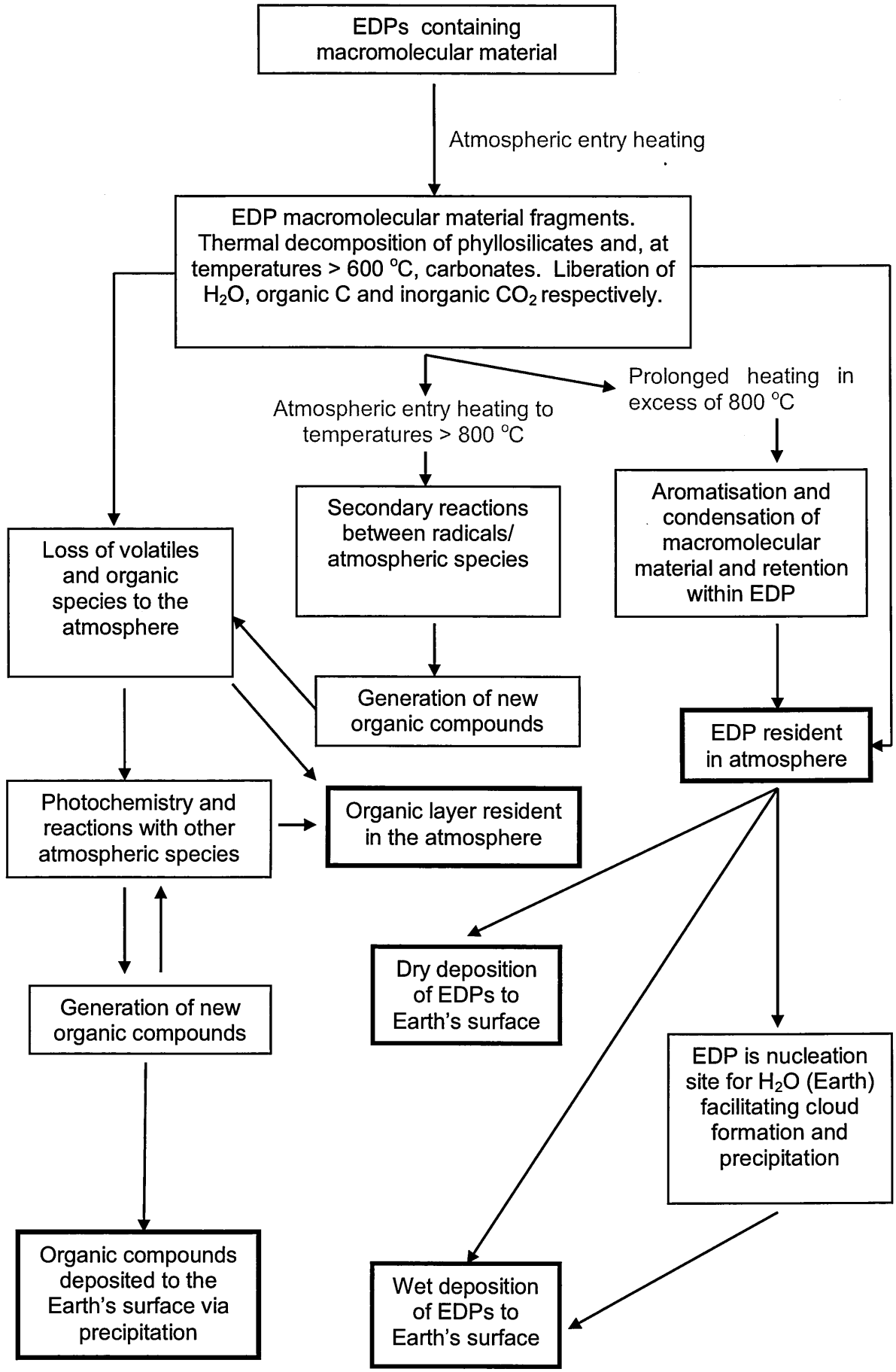

Figure 64: Processes affecting EDP on atmospheric entry and their fate (bold boxes)

These processes may have provided the opportunity to generate more complex molecules, with the EDP derived organic atmospheric layer/haze or meteor wakes serving as sites for prebiotic chemical evolution. Alternatively these species, depending on solubility, may have been deposited to the surface via precipitation, with incorporation into the water cycle offering opportunities and further sites for chemical evolution.

EDPs and their liberated volatile and organic material would also have had environmental effects. EDPs would have scattered incoming UV radiation, reducing its flux to the surface. Both EDPs and atmospheric organic species potentially resident as haze encompassing the planet (Sagan & Chyba, 1997) would have absorbed UV radiation, limiting the flux to the surface and contributing to increased surface and atmospheric temperatures. Furthermore, EDPs deposited into the stratosphere have estimated resident times in the order of days to months depending on grain size (Section 5.5.3). Such particles would have also acted as CCN, enabling cloud formation and precipitation without the need for water supersaturating the atmosphere.

The abundance and composition of volatile and organic species liberated and retained in EDPs during entry heating and their subsequent atmospheric reactions have served as a source of prebiotic molecules, or provided sites for chemical evolution. Ultimately, they played a role in atmospheric or climate development and may have aided regulation of the extreme surface conditions on the and Earth.

6. Conclusions and Future Work

The aim of this study was to investigate the influence of atmospheric entry heating on the release of volatile and organic species from EDPs, in order to assess the contribution of biologically significant material to the early Earth by these micron-sized particles.

6.1. Entry Heating Simulation Methods

A review of previous flash heating methods and the subsequent development of a pyrolysis-based atmospheric entry heating simulation method is documented in Chapter 2. During experimental development, it became apparent that simulation conditions using the Pt coil (pyroprobe) heating method were not reproducible (Section 2.2.2). In particular, the Pt coil pyroprobe method failed to heat samples to the preset temperatures, questioning its validity as a method for organic analysis and heating simulation studies.

In contrast, the Pt-ribbon (Pyrola) flash heating method was the most appropriate simulation tool, due to its reproducibility of simulation conditions. It was possible to control simulation temperatures using a photodiode and the resistance of the Pt ribbon. The main limitation of the Pt ribbon heating method was that although it was ideal for the pyrolysis of small samples during online simulations (coupled to GCxGC-TOFMS, Section 2.4) and AMM fragments (Chapter 4), it was incapable of flash heating enough sample in one instance to produce the residue required for post-heating analysis (~10 mg). For some simulation conditions, it was necessary to conduct up to 80 replicates of simulations on EDP analogous materials and collect the residues for later analyses.

6.2. The Effect of Atmospheric Entry Heating on EDP Analogues

Thermogravimetric and evolved gas analyses have identified organic carbon, inorganic carbon and water as the major components liberated from samples during offline atmospheric entry heating simulations (Section 3.4.1). The release of volatile and

organic material from is dependent on simulation conditions, as is indicated by the progressive dehydration of phyllosilicates, loss of organic material and the decarbonation of carbonates with increasing simulation temperature and duration (Section 3.4.2).

The volatile losses recorded in simulations (Chapter 3) have been used to constrain the EDP contribution to the early Earth volatile and organic inventory (Section 5.2.1). Calculations for varying atmospheric entry heating regimes (Table 38) demonstrate an order of magnitude increase in organic carbon liberated into the early atmosphere during an extreme heating regime (heating to 1000 °C), compared to a mild heating regime (400 °C). Considering an extreme heating regime, EDPs could have deposited up to 2.9×10^{11} kg/yr of water, 2.0×10^{10} kg/yr organic carbon and 2.7×10^{10} kg/yr inorganic carbon (in the form of carbonate-derived CO_2) annually into the early atmosphere. The contribution of CO_2 and H_2O from EDPs during atmospheric entry heating are comparable to that predicted by early Earth volcanic eruptions (Section 5.2.6), which are thought to have been primary source of early atmospheric gases (Kasting, 1993; Kasting et al., 1993; Walker, 1977; Walker, 1985). It suggests that EDP derived volatiles may have been a significant contributor to early atmospheric development.

Further investigations, with online simulations conducted coupled to a GCxGC-TOFMS (Section 3.5), characterised the organic species liberated. A range of organic species volatised from samples during heating experiments including benzenes, thiophenes, N- and S-N heterocycles, nitriles, PAHs and aliphatic species. The identification of complex organic species liberated during simulations is consistent with spectral observations of meteor streams (Jenniskens et al., 1998; Rairden et al., 1998; Jenniskens et al., 2004). Meteor observations (*ibid.*) identify very low abundances of molecular and atomic species, leading authors to suggest that larger more complex species are present in the meteor wake.

Relative abundances of these organic species released during simulations is dependant not only on peak temperature and heating durations in order to release them from macromolecular material, but also on their reaction with other fragments, leading to

their production as secondary products (Section 5.3.1). Furthermore, there is evidence that some components (N-heterocycles and N-S heterocycles in particular) have an optimal release temperature in the region of ~800 °C during short simulation durations (Section 3.5.1D). In particular, biomolecule precursors pyridine and pyrimidine are not released during gentle heating simulations (425 °C for 2 s).

6.2.1. The Astrobiologicval Significance of EDP Materials to the early Earth

EDP entry heating simulations yield a variety of organic species (Chapter 3), some of which are known pollutants detrimental to the environment or human health (GHS, 2009). If concentrated, these may have had a similar impact on emerging life. However, many EDP derived species are of direct biological significance or are precursors of biomolecules (Sections 4.4.8 and 5.4) and would have been made available for prebiotic chemical evolution. Additionally liberated species would have undergone various reactions and processes (summarised in Figure 64) including photolytic degradation or reaction with resident atmospheric radicals, providing the opportunity to generate more complex molecules within the atmosphere. The atmosphere itself or the wake of meteors themselves could have provided sites for chemical evoloution. Furthermore, depending on solubility, EDP derived species may have been deposited to the surface via precipitation, with incorporation into the water cycle offering opportunities and further sites for chemical evolution.

EDPs and their liberated volatile and organic material would also have had environmental effects, with the potential to absorb or scatter UV radiation from the planetary surface. Furthermore, EDPs deposited into the stratosphere would have also acted as CCN, enabling cloud formation and precipitation.

EDPs offer a mechanism by which organic material can be deposited across the early Earth into a variety of environments, many of which can act as sites of chemical evoloution. Additionally, EDP derived organic material can subsequently be incorporated

into a number of atmospheric or environmental processes (e.g. photochemical reations, the water cycle) that can facilitate the generation of more complex organic species and/or provide a means of concentrating organic material. Combined, these processes are favourable for the emergence of life on our planet.

6.3. AMM Organic Characterisation

In a complimentary investigation, the first comprehensive volatile organic analysis of AMMs (exploiting the high sensitivity and separation power of GCxGC-TOFMS) has been undertaken (Chapter 4), drawing comparisons to chondritic organic composition. A range of aromatic species are identified including aromatic cores of up to 2-carbon rings, with structurally diverse alkyl counterparts in addition to N-, S-N and O-bearing components. The presence of both small aromatic units, and their structurally diverse alkyl substituted species, suggests that the AMM insoluble organic material has an open structure and has not been exposed to substantial thermal alteration/metamorphism during atmospheric entry heating. Both aliphatic and ester linkages occur in AMM macromolecular material, as is deduced from the structural diversity of alkyl-substituted aromatic units and the presence of phenols, respectively.

6.3.1. The Origin of AMMs

The AMMs in this study appear to comprise an aromatic macromolecular network akin to that of carbonaceous chondrites that have experienced minimal thermal metamorphism. A reduced number and diversity of organic species are identified in AMMs relative to Murchison (Section 4.4.3), which is a consequence of analysing a reduced sample mass. However, variations in the distribution of aromatic species in AMMs and the Murchison carbonaceous chondrite are consistent with the liberation of species during atmospheric entry heating (Section 4.4.4), alteration via the Antarctic weathering processes (Section 4.4.6) and a contribution from terrestrial particles (Section 4.4.5). Alternatively these may reflect different parent body compositions.

A comparison of AMM organic compositions to that of well characterised CIs and Tagish Lake was also carried out (Section 4.4.9). Compared to AMMs in this study, these meteorites comprise differences in benzene and thiophene ranges and structural diversity. The AMM open macromolecular structure is not consistent with condensed structure of the organic material from "old" or long-term active comets. This suggests that AMMs do not share a common parent body with either CI meteorites or Tagish Lake, sourced by cometary nuclei remnants (Botta et al., 2000; Gounelle et al., 2006) and D-type asteroids respectively.

The analysis of directly sampled cometary material (Stardust) suggests it contains relatively unmetamorphosed organic material similar to IDPs and primitive meteorites (Sandford et al., 2006). AMMs in this study comprise an organic composition characteristic of exposure to minimal thermal alteration/metamorphism, with a range of aliphatic, aromatic, N- S- and O- bearing species responsible for similar FTIR features observed in Stardust samples. In addition, comets are known to contain high abundances of unsaturated hydrocarbons (Kissel & Krueger, 1987), the dominant aliphatic species in AMMs in this study.

There are strong similarities in the organic composition of AMMs and the CM2 Murchison meteorite, with atmospheric entry heating and/ or a contribution by terrestrial sources and processes accounting for some of the differences. However there remain substantial differences between AMMs and CIs and Tagish Lake meteorites. From this study, a carbonaceous chondrite parent body is not consistent with all features of AMM organic composition, despite atmospheric entry heating and post-terrestrial processing. AMMs comprise all functional organic groups that have been previously identified in Stardust cometary samples including the high abundance of unsaturated hydrocarbons. It is entirely plausible that MMs could be sourced from cometary dust. However, until a detailed analysis of volatile organic species in cometary particles (Stardust or otherwise) is conducted, it is not possible to fully assess their similarities to MMs.

6.4. Future Work

EDP-derived organic species are of substantial astrobiological significance, potentially serving as the primary source of prebiotic organic material to the early atmosphere and the planet's surface (Section 5.4). This study has been a preliminary investigation characterising changes in EDP organic and volatile composition during atmospheric entry heating, which has also identified a number of areas requiring further focus and research. Ultimately, the quantification of individual species or functional groups liberated during different heating regimes is required to assess their direct contribution to the early atmosphere. Although it was beyond the remit of this study, this can be achieved utilising the same analytical techniques described in this study, inclusive of calibration curves from customised standards.

Both offline and online simulations were conducted in an inert gas flow (He) and consequently in the absence of oxygen. There is scope to continue such simulations under gas mixtures pertaining to the early Earth (e.g. CO_2, N_2 and CO) or early Mars (CO_2) atmospheres in order to determine atmospheric compositional effects on EDP released species. It is thought that a CO_2-rich early Martian atmosphere was at least 0.5 – 5 bars (Craddock & Howard, 2002; Pollack & Yung, 1980) and, like the early Earth, would have been capable of decelerating and subsequently heating incoming EDPs. However, as Mars has a lower planetary mass and surface gravity compared to Earth, EDP velocities in Martian atmosphere are lower. Consequently, Martian EDP peak heating temperatures would have been lower, with 80 % of 10 μm sized particles and 20 % of 100 μm particles experiencing peak temperatures < 530 °C (Flynn & McKay, 1990). Flynn and McKay (1990) have calculated EDPs as large as 1200 μm could survive unmelted during Martian atmospheric entry heating. Entry heating simulations (Chapter 3) to < 600 °C suggest that the majority of H_2O and organic carbon are retained in these particles. Consequently, EDP organic material is likely to have been retained in particles and delivered directly to the Martian surface than liberated into the atmosphere. With early Mars once located in the habitable zone, it is plausible that the delivery of EDP

organic material to the Martian surface may have led to Martian prebiotic chemistry. The repetition of atmospheric entry heating simulations under early Martian atmospheric conditions is of significant interest.

Minimising the simulated sample mass in future simulations could reduce the effects of grain insulation or the possibility of released species recondensing back onto the sample. The ideal scenario would be to conduct simulations on individual particles, to establish the relationship between particle size and simulation conditions. Initial tests (Wilson et al., 2007b) suggest comprehensive organic analysis (using pyrolysis-GCxGC-TOFMS), may feasible on individual grains of Murchison as small as 223 μm. However, further effort in GCxGC optimisation is required. Determining the volatile abundance of individual flash heated particles presents a challenge, however textural and compositional features in simulated products could be investigated via techniques such as FIB SEM or NanoSIMS. The organic material remaining in individually simulated grains could be constrained using Raman spectroscopy, FTIR spectroscopy and L^2MS which have all been employed to determine the organic nature of Stardust material (Sandford et al. 2006).

Using py-GCxGC-TOFMS, this study has successfully identified a range of organic species in AMMs for the first time (Chapter 4; Wilson et al., 2008), demonstrating it is a feasible method of analysing small extraterrestrial samples. There is a possibility that some species identified in AMMs (i.e. phenol, aliphatic ketones, aliphatic aldehydes, pyrrole, alkanes and alkenes) may be terrestrially sourced as they were also identified in Antarctic terrestrial particles. Analysis of AMMs derived from the CONCORDIA collection (Duprat et al. 2007), that are better preserved than those extracted elsewhere, may enhance these findings. The CONCORDIA particles have well constrained terrestrial ages and have been exposed to lower levels of alteration from terrestrial weathering compared to previous collections, their analysis could provide vital information regarding the organic composition and origin of MMs.

The fate of EDP particles and organic species has been addressed related to present-day processes occurring in the early Earth atmosphere (Chapter 5). It is apparent that EDPs may have had a direct impact on the early Earth atmosphere, not just adding to its volatile inventory, but potentially facilitating cloud formation and precipitation. The water cycle is critical to life on our planet. Another area of future focus would be to investigate the photolysis/radical reactions of EDP liberated species under early stratospheric conditions. This would help constrain the fate EDP derived organic species deposited in the early atmosphere, and ultimately characterise a variety of prebiotic chemical pathways.

This study has highlighted the significance of EDPs as a large source of volatile and organic species, including a number of biological precursors that survive entry heating conditions. EDP entry heating, and subsequent interaction in the early atmosphere, would have had substantial impact on the pre-biotic chemical evolution of life on Earth (and other planetary surfaces) that justifies a continued investigation.

References

Abreu, N.M., 2007. Fine-scale mineralogical study of the matrices of CR carbonaceous chondrites: Insights on early solar system processes. Ph.D. New Mexico: University of Mexico.

Ai, K., 2002. Photometric and near-IR spectroscopic observations of a D-type asteroid, (773) Irmintraud, by SUBARU/IRCS. *Astronomical Herald*, 95(11), 507-514.

Alexander, C.M.O. et al., 1998. The origin of chondritic macromolecular organic matter: a carbon and nitrogen isotope study. *Meteoritics & Planetary Science*, 33(4), 603-22.

Alpern, B. & Benkheiri, Y., 1973. Distribution de la matière organique dans la météorite d'orgueil par microscopie en fluorescence. *Earth and Planetary Science Letters*, 19(4), 422-428.

Amari, S. et al., 1990. Interstellar graphite in meteorites. *Nature*, 345, 238-240.

Amini, B. & Lowenkron, S., 2003. Aniline and its derivatives. In *Kirk-Othmer Encyclopedia of Chemical Technology*. John Wiley & Sons.

Anastasio, C. and McGregor, K.G. 2000. Photodestruction of dissolved organic nitrogen species in fog waters. *Aerosol Science and Technology*, 32, 2, 106-119.

Anders, E. & Grevesse, N., 1989. Abundances of the elements - meteoritic and solar. *Geochimica et Cosmochimica Acta*, 53, 197-214.

Anders, E. & Owen, T., 1977. Mars and Earth - origin and abundance of volatiles. *Science*, 198(4316), 453-465.

Anders, E. & Zinner, E., 1993. Interstellar grains in primitive meteorites - Diamond, silicon carbide, and graphite. *Meteoritics*, 28, 490-514.

Anders, E., 1968. Chemical processes in the early solar system, as inferred from meteorites. *Accounts of Chemical Research*, 1(10), 289-298.

Anders, E., 1989. Pre-biotic organic-matter from comets and asteroids. *Nature*, 342(6247), 255-257.

Anders, E. et al., 1973. Organic compounds in meteorites. *Science*, 182, 781-790.

Andreae, M. O. and Gelencsér, A. 2006. Black carbon or brown carbon? The nature of light-absorbing carbonaceous aerosols. *Atmospheric Chemistry and Physics*, 6, 3131-3148.

Anon., 2005. Fisher Material Safety Data Sheet: Calcium Carbonate. Available at http://www.catalogue.fisher.co.uk/scripts/search.dll?ViewMSDS&SheetNumber=03880.

Anon., 2007. *Handbook of Chemistry and Physics* 88th ed., CRC Press. Available at http://www.hbcpnetbase.com/ [Accessed October 19 2007]

Anon., 2008. *Properties of Organic Compounds*. CHEMnetBASE. Available at: http://www.chemnetbase.com/scripts/pocweb.exe [Accessed September 13, 2008].

Arndt, P. et al., 1996. The elemental abundances in interplanetary dust particles. *Meteoritics* and Planetary *Science*, 31, 817-833.

Artemieva, N.A. & Shuvalov, V.V., 2008. Numerical simulation of high-velocity impact ejecta following falls of comets and asteroids onto the Moon. *Solar System Research*, 42(4), 329-334.

Atkinson, R. 1995. Gas phase tropospheric chemistry of organic compounds. In *Issues in Environmental Science and Technology 4 - Volatile Organic Compounds in the Atmosphere.* Royal Society of Chemistry, Cambridge.pp. 65-89.

Atkinson, R. 2000. Atmospheric chemistry of VOCs and NOx. *Atmospheric Environment*, 34, 12-14, 2063-2101.

Bada, J.L., 1991. Amino acid cosmogeochemistry. *Philosophical Transactions: Biological Sciences*, 333(1268), 349-358.

Baker, E.G., 1967. *Fundamental Aspects of Petroleum Geochemistry*. New York: Elsevier, p. 299.

Baker, L. et al., 1998. Measurement of oxygen isotopes in water from CI and CM chondrites. In *29th Lunar and Planetary Science Conference* p. 1740.

Barber, D.J., 1981. Matrix phyllosilicates and associated minerals in CM2 carbonaceous chondrites. *Geochimica et Cosmochimica Acta*, 45(6), 945-970.

Barber, D.J., 1985. Phyllosilicates and other layer-structured materials in stony meteorites. *Clay Minerals*, 20(4), 415-454.

Barker, J.L. & Anders, E., 1968. Accretion rate of cosmic matter from iridium and osmium contents of deep-sea sediments. *Geochimica et Cosmochimica Acta*, 32, 627-645.

Barlow, A. et al., 1961. Direct examination of polymer degradation by gas chromatography: I. Applications to polymer analysis and characterization. *Polymer*, 2, 27-40.

Baross, J.A. & Hoffman, S.E., 1985. Submarine hydrothermal vents and associated gradient environments as sites for the origin and evolution of life. *Origins of Life*, 15(4), 327-345.

Basu, P., 2006. *Combustion and Gasification in Fluidized Beds*, CRC Press.

Becker, L. et al., 1997. Polycyclic aromatic hydrocarbons (PAHs) in Antarctic martian meteorites, carbonaceous chondrites, and polar ice. *Geochimica et Cosmochimica Acta*, 61(2), 475-481.

Becker, R.H. & Epstein, S., 1982. Carbon, hydrogen and nitrogen isotopes in solvent-extractable organic matter from carbonaceous chondrites. *Geochimica et Cosmochimica Acta*, 46, 97-103.

Belsky, T. & Kaplan, I.R., 1970. Light hydrocarbon gases, C 13 , and origin of organic matter in carbonaceous chondrites. *Geochimica et Cosmochimica Acta*, 34, 257-278.

Benedix, G.K. et al., 2003. Carbonates in CM2 chondrites: constraints on alteration conditions from oxygen isotopic compositions and petrographic observations. *Geochimica et Cosmochimica Acta*, 67(8), 1577-1588.

Bergstrom, R.W. et al., 2007. Spectral absorption properties of atmospheric aerosols. *Atmospheric Chemistry and Physics Discussions*, 7, 10669-10686.

Bernal, J.D., 1961. Significance of Carbonaceous Meteorites in Theories on the origin of Life. *Nature*, 190(4771), 129-131.

Bernal, J. D. 1967. Origin of Life. Weidenfeld & Nicholson, London.

Binet, L. et al., 2002. Heterogeneous distribution of paramagnetic radicals in insoluble organic matter from the Orgueil and Murchison meteorites. *Geochimica et Cosmochimica Acta*, 66(23), 4177-4186.

Bischoff, A. et al., 1993. Acfer 182 and paired samples, an iron-rich carbonaceous chondrite: Similarities with ALH85085 and relationship to CR chondrites. *Geochimica et Cosmochimica Acta*, 57(11), 2631-2648.

Bischoff, A., 1998. Aqueous alteration of carbonaceous chondrites: Evidence for preaccretionary alteration. A review. *Meteoritics and Planetary Science*, 33, 1113-1122.

Bischoff, A., 2001. Meteorite classification and the definition of new chondrite classes as a result of successful meteorite search in hot and cold deserts. Planetary and Space *Science*, 49, 769-776.

Bitz, M.C. & Nagy, B., 1966. Ozonolysis of "polymer-type" amterial in coal, kerrogen and the orgueil meteorite: a preliminary report. *Proceedings of the National Academy of Sciences of the United States of America*, 56(5), 1383-1390.

Blake, P.G. & Jackson, G.E., 1969. High- and low-temperature mechanisms in the thermal decomposition of acetic acid. *Journal of the Chemical Society B: Physical Organic*, 94-96.

Bland, P. et al., 1996. The flux of meteorites to Earth over the last 50,000 years. *Monthly Notices of the Royal Astronomical Society*, 283, 551-565.

Blazek, A., 1973. *Thermal Analysis*, London: Van Nostrand Reinhold.

Bloomberg, J. et al., 1997. Compehensive two-dimensional gas chromatography (GC×GC) and its applicability to the characterization of complex (petrochemical) mixtures. *Journal of High Resolution Chromatography*, 20(10), 539-544.

Blumberg, L.M., 2003. Comprehensive two-dimensional gas chromatography: metrics, potentials, limits. *Journal of Chromatography A*, 985(1-2), 29-38.

Bonadonna et al., C. Thickness variations and volume estimates of tephra fall deposits: the importance of particle Reynolds number. *Journal of Volcanology and Geothermal Research*, 81(3-4), 173-187.

Bonal, L. et al., 2007. Organic matter and metamorphic history of CO chondrites. *Geochimica et Cosmochimica Acta*, 71, 1605-1623.

Botta, O. & Bada, J.L., 2002. Extraterrestrial Organic Compounds in Meteorites. *Surveys in Geophysics*, 23(5), 411-467.

Botta, O. et al., 2000. A cometary origin of the amino acids in the Orgueil meteorite? In *31st Lunar and Planetary Science Conference* p. 1398.

Botta, O. et al., 2002. Relative amino acid concentrations as a signature for parent body processes of carbonaceous chondrites. *Origins of Life and Evolution of the Biosphere*, 32, 143-163.

Boynton, W.V. et al., 2001. Thermal and Evolved Gas Analyzer: Part of the Mars Volatile and Climate Surveyor integrated payload. *Journal of Geophysical Research*, 106(E8), 17683–17698.

Bradley, J. et al., 1988. Interplanetary dust particles. In *Meteorites and the Early Solar System*. pp. 861-895.

Bradley, J.P. & Brownlee, D.E., 1991. An interplanetary dust particle linked directly to type CM meteorites and an asteroidal origin. *Science*, 251, 549-552.

Bradley, J.P. et al., 1996. Reflectance spectroscopy of interplanetary dust particles. *Meteoritics and Planetary Science*, 31, 394-402.

Bradley, J.P., 1994a. Chemically anomalous, preaccretionally irradiated grains in interplanetary dust from comets. *Science*, 265, 925-929.

Bradley, J.P., 1994b. Nanometer-scale mineralogy and petrography of fine-grained aggregates in anhydrous interplanetary dust particles. *Geochimica et Cosmochimica Acta*, 58(9), 2123-2134.

Bradley, J.P. et al., 1984. Carbon compounds in interplanetary dust: Evidence for formation by heterogeneous catalysis. *Science*, 223, 56-58.

Bradley, J.P. et al., 1989. Automated thin-film analyses of anhydrous interplanetary dust particles in the analytical electron microscope. *Earth and Planetary Science Letters*, 93, 1-13.

Brearley, A.J. & Jones, R.H., 1998. Chondritic meteorites. In *Planetary Materials. Reviews in Mineralogy*. pp. 3.1-3.398

Brearley, A.J. et al., 1999. Carbonates in the Murchison CM chondrite: CL characteristics and oxygen isotopic compositions. In *30th Lunar and Planetary Science Conference* p. 1301.

Brearley, A.J., 2002. Heterogeneous distribution of carbonaceous material in Murchison matrix: In situ observations using energy filtered transmission electron microscopy. In *33rd Lunar and Planetary Science Conference* p. 1388.

Bregman, J.D. et al., 1987. Airborne and groundbased spectrophotometry of comet P/Halley from 5-13 micrometers. *Astronomy and Astrophysics*, 187, 616-620.

Brezinsky, K. et al., 1998. Pyrolysis and oxidation of phenol. *Journal of Physical Chemistry A*, 102(44), 8614-8619.

Briggs, M., 1961. Organic constituents of meteorites. *Nature*, 191, 1137-1140.

Brinton, K.L. et al., 1998. A search for extraterrestrial amino acids in carbonaceous Antarctic micrometeorites. *Origins of Life and Evolution of Biospheres*, 28(4-6), 413-424.

Broido, A., 1969. A simple, sensitive graphical method of treating thermogravimetric analysis data. *Journal of Polymer Science Part A-2: Polymer Physics*, 7(10), 1761-1773.

Brown, P.G. et al., 2000. The fall, recovery, orbit, and composition of the Tagish Lake meteorite: A new type of carbonaceous chondrite. *Science*, 290, 320-325.

Browning, L.B., McSween, H.Y. & Zolensky, M.E., 1996. Correlated alteration effects in CM carbonaceous chondrites. *Geochimica et Cosmochimica Acta*, 60(14), 2621-2633.

Brownlee, D.E. et al., 2001. Carbonaceous meteor ash - A significant carrier of carbon, organic material and noble gas to the surfaces of terrestrial planets? In *32nd Annual Lunar and Planetary Science Conference*. Houston, Texas, p. 2170.

Brownlee, D.E. et al., 2002. Survival of carbon in moderately to strongly heated IDPs and micrometeorites . In *33rd Lunar and Planetary Science Conference* p. A1786.

Brownlee, D.E., 1978. Interplanetary Dust: Possible implications for comets and presolar interstellar grains. In *Protostars & Planets*. pp. 134-150.

Brownlee, D.E., 1985. Cosmic dust - Collection and research. Annual Review of Earth and Planetary *Science*s, 13, 147-173.

Bruckner, H. et al., 1989. Chromatographic detection of bioactive AIB-peptides in molds of the genus Stilbella. *Fresenius Zeitschrift Fur Analytische Chemie*, 333(7), 777-778.

Bullock, E.S. et al., 2005. Mineralogy and texture of Fe-Ni sulfides in CI1 chondrites: Clues to the extent of aqueous alteration on the CI1 parent body. *Geochimica et Cosmochimica Acta*, 69, 2687-2700.

Bunch, T.E. & Chang, S., 1980. Carbonaceous chondrites. II - Carbonaceous chondrite phyllosilicates and light element geochemistry as indicators of parent body processes and surface conditions. *Geochimica et Cosmochimica Acta*, 44, 1543-1577.

Burgess, R. et al., 1991. Determination of sulphur-bearing components in C1 and C2 carbonaceous chondrites by stepped combustion. *Meteoritics*, 26, 55-64.

Buseck, P.R. & Hua, X., 1993. Matrices of carbonaceous chondrite meteorites. *Annual Review of Earth and Planetary Sciences*, 21, 255-305.

Caddick, S. et al., 2000. Convenient synthesis of protected primary amines from nitriles. *Tetrahedron Letters*, 41(18), 3513-3516.

Canuto, V.M. et al., 1982. UV radiation from the young Sun and oxygen and ozone levels in the prebiological palaeoatmosphere. *Nature*, 296, 5860, 816-820

Cas, R.A.F. and Wright, J.V. 1998. *Volcanic Successions - Modern and Ancient.* Chapman and Hall, London. p. 528.

Chang, S. & Bunch, T.E., 1986. *Clay Minerals and the Origin of Life*. Cambridge University Press.

Christoffersen, R. & Buseck, P.R., 1986. Refractory minerals in interplanetary dust. *Science*, 234, 590-592.

Chyba, C.F. & McDonald, G.D., 1995. The Origin of Life in the Solar System: Current Issues. *Annual Review of Earth and Planetary Sciences*, 23, 215-249.

Chyba, C.F. & Sagan, C., 1992. Endogenous production, exogenous delivery, and impact-shock synthesis of organic molecules: an inventory for the origins of life. *Nature*, 355, 125-132.

Chyba, C.F. et al., 1990. Cometary delivery of organic-molecules to the early Earth. *Science*, 249(4967), 366-373.

Chyba, C.F., 1993. The violent environment of the origin of life - Progress and uncertainties. *Geochimica et Cosmochimica Acta*, 57(14), 3351-3358.

Ciesla, F.J. & Lauretta, D.S., 2005. Radial migration and dehydration of phyllosilicates in the solar nebula. *Earth and Planetary Science Letters*, 231(1-2), 1-8.

Ciesla, F.J. et al., 2003. A Nebular Origin for Chondritic Fine-Grained Phyllosilicates. *Science*, 299(5606), 549-552.

Ciesla, F.J., 2007. Outward transport of high-temperature materials around the midplane of the Solar nebula. *Science*, 318, 613.

Classen, N., 2008. List of Martian Meteorites. Available at: http://www.meteoris.de/mars/list.html [Accessed June 4, 2008].

Clemett, S.J. et al., 1993. Identification of complex aromatic molecules in individual interplanetary dust particles. *Science*, 262, 721-725.

Clemett, S.J. et al., 1998. Observation of indigenous polycyclic aromatic hydrocarbons in 'giant' carbonaceous Antarctic micrometeorites. *Origin of Life and Evolution of Biospheres*, 28(4-6), 425-448.

Cody, G.D. & Alexander, C.M.O., 2005. NMR studies of chemical structural variation of insoluble organic matter from different carbonaceous chondrite groups. *Geochimica et Cosmochimica Acta*, 69(4), 1085-1097.

Cody, G.D. et al., 2008. Organic thermometry for chondritic parent bodies. *Earth and Planetary Science Letters*, 272, 446-455.

Cody, G.D. et al., 1999. New Insights into the chemistry of Murchison organic macromolecule using high field 13C solid state NMR. In *30th Lunar and Planetary Science Conference* p. 1582.

Cody, G.D. et al., 2002. Solid-state (1H and 13C) nuclear magnetic resonance spectroscopy of insoluble organic residue in the Murchison meteorite: a self-consistent quantitative analysis. *Geochimica et Cosmochimica Acta*, 66, 1851-1865.

Commins, B.T. & Harington, J.S., 1966. Polycyclic aromatic hydrocarbons in carbonaceous meteorites. *Nature*, 212(5059), 273-274.

Cooper, G. et al., 2001. Carbonaceous meteorites as a source of sugar-related organic compounds for the early Earth. *Nature*, 414(6866), 879-883.

Cooper, G.W. & Cronin, J.R., 1995. Linear and cyclic aliphatic carboxamides of the Murchison meteorite: Hydrolyzable derivatives of amino acids and other carboxylic acids. *Geochimica et Cosmochimica Acta*, 59, 1003-1015.

Cooper, G.W. et al., 1997. Sulfur and hydrogen isotope anomalies in meteorite sulfonic acids. *Science*, 277(5329), 1072-1074.

Cooper, G.W., 1993. Organic Analyses of the Murchison Meteorite. Ph.D. Tempe: Arizona State University.

Cooper, G.W. et al., 1992. Alkyl phosphonic acids and sulfonic acids in the Murchison meteorite. *Geochimica et Cosmochimica Acta*, 56(11), 4109-4115.

Corliss, J.B. et al., 1981. An hypothesis concerning the relationship between submarine hot springs and the origin of life on Earth. *Oceanologica Acta*, 4(supplement), 59-69.

Cornell, S. E. et al., 2003. Organic nitrogen deposition on land and coastal environments: a review of methods and data. *Atmospheric Environment*, 37, 16, 2173-2191.

Craddock, R. A. and Howard, A. D. 2002. The case for rainfall on a warm, wet early Mars. *Journal of Geophysical Research*, 107(E11), 5111.

Cronin, J.R. & Chang, S., 1993. Organic matter in meteorites: molecular and isotopic analyses of the Murchison meteorite. In *The Chemistry of Life's Origins* pp. 209-258.

Cronin, J.R. & Moore, C.B., 1971. Amino acid analyses of Murchison, Murray, and Allende carbonaceous chondrites. *Science*, 172(3990), 1327-1329

Cronin, J.R. & Pizzarello, S., 1983. Amino acids in meteorites. *Advances in Space Research*, 3(9), 5-18.

Cronin, J.R. & Pizzarello, S., 1990. Aliphatic hydrocarbons of the Murchison meteorite. *Geochimica et Cosmochimica Acta*, 54, 2859-2868.

Cronin, J.R. et al., 1995. Characteristics and formation of amino acids and hydroxy acids of the Murchison meteorite. *Advances in Space Research*, 15(3), 91-97.

Cronin, J.R. et al., 1988. Organic matter in carbonaceous chondrites, planetary satellites, asteroids and comets. In *Meteorites and the Early Solar System*. pp. 819-857.

Cronin, J.R. et al., 1987. 13C NMR spectroscopy of the insoluble carbon of carbonaceous chondrites. *Geochimica et Cosmochimica Acta*, 51, 299-303.

Cullis, C.F. & Harris, A.C.T., 1972. Pyrolysis of organic compounds under conditions of carbon formation. *Carbon*, 10, 525-537.

Dailey, H.A., 1990. *Biosynthesis of Heme and Chlorophylls*, McGraw-Hill.pp. 594.

Dalrymple, G., 1991. *The Age of the Earth*, Stanford, California: Stanford University Press.

David, C., 1975. Thermal Degredation of Polymers. In *Chemical Kinetics: Degredation of Polymers*. Amsterdam: Elsevier *Science* Publication Company, pp. 1-173.

Delsemme, A.H., 1984. The cometary connection with prebiotic chemistry. *Origins of Life and Evolution of Biosphere*, 14(1-4), 51-60.

Derenne, S. & Robert, F., 2008. The chemical structure of the insoluble organic matter from carbonaceous meteorites. *European Planetary Science Congress Abstracts*, 3, A-00179.

Derenne, S. et al., 2002. Use of combined spectroscopic and microscopic tools for Ddeciphering the chemical structure and origin of the insoluble organic matter in the Orgueil and Murchison meteorites. In *33rd Lunar and Planetary Science Conference*, p. 1182.

Derwent, R. G. 1995. Sources, Distributions and Fates of VOCs in the Atmosphere. In *Issues in Environmental Science and Technology 4 - Volatile Organic Compounds in the Atmosphere*. Royal Society of Chemistry, Cambridge. pp. 1-15.

Docobo, J. et al., 2008. March 1, 2005 Daylight Fireball Over Galicia (NW of Spain) and Minho (N. Portugal). *Earth, Moon and planets*, 102, 537-542.

Doyle, C., 1961. Estimating thermal stability of experimental polymers by empirical thermogravimetric analysis. *Analytical Chemistry*, 33(1), 77.

Duchesne, J. et al., 1964. Concerning the nature of free radicals in the Cold Bokkeveld meteorite. *Geochemistry International*, 1, 1022-1024.

Duprat, J. et al., 2007. Micrometeorites from Central Antarctic snow: The CONCORDIA collection. *Advances in Space Research*, 39, 605-611.

Ehrenfreund, P. et al., 2001. Extraterrestrial amino acids in Orgueil and Ivuna: Tracing the parent body of CI type carbonaceous chondrites. *Proceedings of the National Academy of Sciences of the United States of America*, 98(5), 2138-2141.

Ehrenfreund, P. et al., 2006. Experimentally tracing the key steps in the origin of life: The aromatic world. *Astrobiology*, 6(3), 490-520.

Elsila, J.E. et al., 2005. Alkylation of polycyclic aromatic hydrocarbons in carbonaceous chondrites. *Geochimica et Cosmochimica Acta*, 69, 1349-1357.

Engler, P. et al., 1988. Non-isothermal in situ analysis of dolomite decomposition. *The Rigaku Journal*, 5(2), 3-8.

Engrand, C. & Maurette, M., 1998. Carbonaceous micrometeorites from Antarctica. *Meteoritics* and Planetary *Science*, 33(4), 565-580.

Engrand, C. et al., 1999. Extraterrestrial water in micrometeorites and cosmic spherules from Antarctica: An ion microprobe study. *Meteoritics* and Planetary *Science*, 34(5), 773-786.

Epstein, S. et al., 1987. Unusual stable isotope ratios in amino acid and carboxylic acid extracts from the Murchison meteorite. *Nature*, 326, 477-479.

Etemad-Rad, S. T. & Metcalfe, E., 1993. The pyrolysis of benzonitrile. *Fire and Materials*, 17(1), 33-37.

Exton, H.J. et al., 1986. The production and dispersal of maritime aerosol. In *Oceanic Whitecaps and Their Role in Air–Sea Exchange Processes*. Springer. pp. 175-193.

Faure, P. et al., 2006. Aromatization of organic matter induced by the presence of clays during flash pyrolysis-gas chromatography–mass spectrometry (PyGC–MS): A major analytical artefact. *The Journal of Analytical and Applied Pyrolysis,* 75(1), 1-10.

Ferris, J. P. 1999. Prebiotic synthesis on minerals: bridging the prebiotic and RNA worlds. *The Biological Bulletin*, 196(3), 311-314.

Ferris, J. P. 2005. Mineral Catalysis and Prebiotic Synthesis: Montmorillonite-Catalyzed Formation of RNA. *Elements*, 1(3), 145-149.

Flynn, G.J., 1989a. Atmospheric entry heating of micrometeorites. In *19th Lunar and Planetary Science Conference*, pp. 673-682.

Flynn, G.J., 1989b. Atmospheric entry heating: A criterion to distinguish between asteroidal and cometary sources of interplanetary dust. *Icarus*, 77(2), 287-310.

Flynn, G.J., 1991. Volatile trace elements in large micrometeorites from Greenland. *Meteoritics*, 26, 334-335.

Flynn, G.J., 1995. Atmospheric entry heating of large interplanetary dust particles. *Meteoritics*, 30, 504. *Journal of Geophysical Research*, 95, 14497-14509.

Flynn, G. J. and McKay, D.S. 1990. An assessment of the meteoritic contribution to the Martian soil.

Flynn, G.J. et al., 1993. The volatile content of anhydrous interplanetary dust. *Meteoritics*, 28, 349.

Flynn, G.J. et al., 1998. FTIR detection of organic carbon in interplanetary dust particles. In *29th Lunar and Planetary Institute Conference*. p. 1157.

Flynn, G.J. et al., 2002. Infrared analysis of organic carbon in anhydrous and hydrated interplanetary dust particles: FTIR identification of carbonyl (C=O) in IDPs. In *33rd Lunar and Planetary Science Conference*, p. 1320.

Flynn, G.J. et al., 2003. The origin of organic matter in the solar system: evidence from the interplanetary dust particles. *Geochimica et Cosmochimica Acta*, 67, 4791-4806.

Flynn, G.J. et al., 2004. An assessment of the amount and types of organic matter contributed to the Earth by interplanetary dust. *Advances in Space Research*, 33, 57-66.

Folsome, C.E. et al., 1971. Heterocyclic Compounds indigenous to the Murchison Meteorite. *Nature*, 232, 108-109.

Folsome, C.E. et al., 1973. Heterocyclic compounds recovered from carbonaceous chondrites. *Geochimica et Cosmochimica Acta*, 37, 455-465.

Fomenkova, M., 1999. On the Organic Refractory Component of Cometary Dust. *Space Science Reviews*, 90(1), 109-114.

Fox, M.A. & Whitesell, J.K., 2004. *Organic Chemistry*. 3rd ed., Jones and Bartlett Publishers.

Fraundorf, P. et al., 1982. Deceleration heating of interplanetary dust in the Earth's atmosphere, and its simulation using analogue materials. In *13th Lunar and Planetary Science Conference*, p. 227-228.

Fraundorf, P., 1980. The distribution of temperature maxima for micrometeorites decelerated in the Earth's atmosphere without melting. *Geophysical Research Letters*, 7(10), 765-768.

Frysinger, G. & Gaines, R., 2001. Separation and identification of petroleum biomarkers by comprehensive two-dimensional gas chromatography. *Journal of Separation Science*, 24(2), 87-96.

Frysinger, G. et al., 2003. Resolving the unresolved complex mixture in petroleum-contaminated sediments. *Environmental Science & Technology*, 37(8), 1653-1662.

Fuchs, L.H. et al., 1973. Mineralogy, mineral-chemistry, and composition of the Murchison (C2) meteorite. *Smithsonian Contributions to Earth Sciences*, 10.

Gaines, R. et al., 1999. Oil spill source identification by comprehensive two-dimensional gas chromatography. *Environmental Science & Technology*, 33(12), 2106-2112.

Gao, X. & Thiemens, M.H., 1993. Isotopic composition and concentration of sulfur in carbonaceous chondrites. *Geochimica et Cosmochimica Acta*, 57(13), 3159-3169.

Geers, V.C. et al., 2006. C2D Spitzer-IRS spectra of disks around T Tauri stars. II. PAH emission features. *Astronomy and Astrophysics*, 459(2), 545-556.

Geiger, T and Bischoff, A. 1991. The CK chondrites-Conditions of parent body metamorphism. *Meteoritics*, 26, 337.

Gelencsér, A. 2005. *Carbonaceous aerosol*. Springer. p. 350.

Genge, M.J., 2005. The Parent Bodies of Micrometeorites. *LPI Contributions,* 1280, 52.

Genge, M.J., 2006. Igneous rims on micrometeorites. *Geochimica et Cosmochimica Acta*, 70, 2603-2621.

Genge, M.J., 2008. Koronis asteroid dust within Antarctic ice. *Geology*, 36(9), 687-690.

Genge, M.J., 2008. Micrometeorites and their implications for meteors. *Earth, Moon, and Planets*, 102(1), 525-535.

Genge, M.J. et al., 1997. The textures and compositions of fine-grained Antarctic micrometeorites - Implications for comparisons with meteorites. *Geochimica et Cosmochimica Acta*, 61, 5149.

Genge, M.J. & Grady, M.M., 1998a. A petrological-chemical classification scheme for coarse-grained micrometeorites. *Meteoritics and Planetary Science*, 33 (4) Supplement, A56-A57.

Genge, M.J. & Grady, M.M., 1998b. Melted micrometeorites from Antarctic ice with evidence for the separation of immiscible Fe-Ni-S liquids during entry heating. *Meteoritics and Planetary Science*, 33, 425-434.

Genge, M.J. & Grady, M.M., 2000. The thermal evolution of micrometeoroids during atmospheric entry. In *31st Lunar and Planetary Science Conference* p. 1361.

Genge, M.J. et al., 2008. The classification of micrometeorites. *Meteoritics and Planetary Science,* 43(3), 497-515.

George, S.C., 1992. Effect of igneous intrusion on the organic geochemistry of a siltstone and an oil shale horizon in the Midland Valley of Scotland. *Organic Geochemistry*, 18(5), 705-723.

GHS, 2009. *Globally Harmonized System of Classification and Labelling of Chemicals*, 3rd edition, United Nations Economic Commission for Europe.

Gibb, E.L. et al., 2007. Warm HCN, C2H2, and CO in the disk of GV Tau. *Astrophysical Journal*, 660, 1572.

Gibson, E.K. & Hubbard, N.J., 1972. Thermal volatilization studies on lunar samples. In *3rd Lunar and Planetary Science Conference*. p. 2003-2014.

Gibson, E.K. & Johnson, S., 1972. Thermogravimetric-quadrupole mass-spectrometric analysis of geochemical samples. *Thermochimica Acta*, 4, 49-56.

Gilmour, I., 2003. Structural and isotopic analysis of organic matter in carbonaceous chondrites. In *Treatise on Geochemistry: Meteorites Comets and Planets*. 1, Meteorites Comets and Planets: Elsevier-Pergamon.

Gilmour, I. & Pillinger, C.T., 1994. Isotopic Compositions of Individual Polycyclic Aromatic Hydrocarbons from the Murchison Meteorite. *Monthly Notices of the Royal Astronomical Society*, 269, 235.

Gilmour, I. et al., 2001. Analysis of Tagish Lake macromolecular organic material. In *32nd Lunar and Planetary Science Conference*. p. 1993.

Glavin, D.P. & Bada, J.L., 1999. The sublimation and survival of amino acids and nucleobases in the Murchison meteorite during a simulated atmospheric heating event. In *30th Lunar and Planetary Science Conference*. p. A1085.

Glavin, D.P. & Bada, J.L., 2001. Survival of amino acids in micrometeorites during atmospheric entry. *Astrobiology*, 1(3), 259-269.

Glavin, D.P. et al., 2006. Amino acid analyses of Antarctic CM2 meteorites using liquid chromatography-time of flight-mass spectrometry. *Meteoritics and Planetary Science*, 41, 889-902.

Glavin, D.P. et al., 2004. Re-examination of amino acids in Antarctic micrometeorites. *Advances in Space Research*, 33, 106-113.

Gohlke, R.S. & McLafferty, F.W., 1993. Early gas chromatography/mass spectrometry. *Journal of the American Society for Mass Spectrometry*, 4(5), 367-371.

Gooding, J.L., 1986. Weathering of stony meteorites in Antarctica. In *Lunar and Planetary Institute International Workshop on Antarctic Meteorites*. pp. 48-54.

Gomes, R. et al., 2005. Origin of the cataclysmic Late Heavy Bombardment period of the terrestrial planets. *Nature,* 435, 466-469.

Gounelle, M. et al., 1999. Comparison of the 1998 "Cap-Prudhomme" and "Astrolabe" Antarctic micrometeorite collections with the 1996 "South Pole" collection: Preliminary implications. In *30th Lunar and Planetary Science Conference*. p. 1564.

Gounelle, M. et al., 2001. Refractory phases of micrometeorites and the ``primitivity" of cometary nuclei. In *32nd Lunar and Planetary Science Conference*. p. 1626.

Gounelle, M. et al., 2005. Hydrogen isotopic composition of water from fossil micrometeorites in howardites. *Geochimica et Cosmochimica Acta*, 69(13), 3431-3443.

Gounelle, M. et al., 2006. The orbit and atmospheric trajectory of the Orgueil meteorite from historical records. *Meteoritics and Planetary Science*, 41, 135-150.

Greenberg, J.M. et al., 1995. Origin of organic matter in the protosolar nebula and in comets. *Advances in Space Research*, 16(2), 9-16.

Greenberg, J.M., 1984. Chemical Evolution in Space. *Origins of Life*, 14, 25-36.

Greenwood, R.C. & Hutchison, R., 1993. Atmospheric entry heating of macro- and micrometeorites: A comparative study. *Meteoritics*, 28, 356.

Greenwood, R.C. et al., 2007. The Moss (CO3) meteorite: An integrated isotopic, organic and mineralogical study. In *38th Lunar and Planetary Science Conference*. p. 2267.

Gregor, B., 1992. Some ideas on the rock cycle: 1788-1988. *Geochimica et Cosmochimica Acta*, 56, 2993-3000.

Greshake, A. et al., 1995a. Trace element abundances in refractory inclusions from Antarctic micrometeorites. *Meteoritics*, 30(5), 513.

Greshake, A. et al., 1995b. Volatile element abundances in micrometeorites:evidence for the losss of copper, germanium and zinc during atmospheric entry heating. In *26th Lunar and Planetary Science Conference*, 26, 509.

Greshake, A. et al., 1995c. Flash-heating of pyrrhotite from Orgueil (CI): Evidence for the loss of sulphur and selenium during atmospheric entry heating of polar micrometeorites. In *26th Lunar and Planetary Science Conference*. P. 511.

Greshake, A. et al., 1996. Mineralogy, chemistry, and oxygen isoptopes of refractory inclusions from stratospheric interplanetary dust particles and micrometeorites. *Meteoritics and Planetary Science*, 31, 739-748.

Greshake, A. et al., 1998. Heating experiments simulating atmospheric entry heating of micrometeorites: clues to their parent body sources. *Meteoritics and Planetary Science*, 33, 267-290.

Grimm, R.E. & McSween, H.Y., 1989. Water and the thermal evolution of carbonaceous chondrite parent bodies. *Icarus*, 82(2), 244-280.

Habart, E. et al., 2006. Spatially resolved PAH emission in the inner disks of Herbig Ae/Be stars. *Astronomy and Astrophysics*, 449, 1067-1075.

Halliday, I. et al., 1996. Detailed data for 259 fireballs from the Canadian camera network and inferences concerning the influx of large meteoroids. *Meteoritics and Planetary Science*, 31, 185-217.

Hambly, E.M., 1998. The chemical structure of coal tar and char during devolatilisation. M.Sc. Provo: Brigham Young University.

Hammer, C. & Maurette, M., 1996. Micrometeorite flux on the melt zone of the West Greenland ice sheet. *Meteoritics and Planetary Science*, 31, A56.

Hammergren, M., 1996. The Main Asteroid Belt - Comet graveyard or nursery? *Bulletin of the American Astronomical Society*, 28, 1299.

Han, J. et al., 1969. Organic analysis on the Pueblito de Allende meteorite. *Nature*, 222, 364-365.

Hansen, J. et al., 2000. Global warming in the twenty-first century: An alternative scenario. *Proceedings of the National Academy of Sciences of the United States of America*, 97(18), 9875-9880.

Haraldson, L., 1962. An investigation of the products of pyrolysis in the determination of oxygen in sulphur-containing organic substances. *Microchimica Acta*, 50(4), 650-670.

Harding, S., 2003. The Toarcian oceanic anoxic event : organic and inorganic geochemical anomalies in organic-carbon-rich mudrocks from the North Yorkshire coast, UK and Dotternhausen Quarry, SW Germany. Ph.D. Milton Keynes: Open University.

Hartgers, W.A. et al., 1994. Geochemical significance of alkylbenzene distributions in flash pyrolysates of kerogens, coals, and asphaltenes. *Geochimica et Cosmochimica Acta*, 58(7), 1759-1775.

Hartmann, W.K. 1980. Dropping stones into magma oceans: Effects of early lunar cratering. *Proceedings of the Lunar Highlands Crust Conference*. Pergamon, New York. pp. 155-171.

Hartmann, W.K. et al., 2000. The time-dependent intense bombardment of the primordial Earth/Moon system. In *Origin of the Earth and Moon*. Tucson: University of Arizona Press, pp. 493-512.

Hayatsu, R., 1964. Orgueil Meteorite: Organic Nitrogen Contents. *Science*, 146(1964), 1291-1293.

Hayatsu, R. & Anders, E., 1981. Organic compounds in meteorites and their origins. *Topics in Current Chemistry*, 99, 1-37.

Hayatsu, R. et al., 1975. Purines and triazines in the Murchison meteorite. *Geochimica et Cosmochimica Acta*, 39, 471-488.

Hayatsu, R. et al., 1977. Origin of organic matter in the early solar system--VII. The organic polymer in carbonaceous chondrites. *Geochimica et Cosmochimica Acta*, 41(9), 1325-1339.

Hayatsu, R. et al., 1980. Phenolic Ethers in the Organic Polymer of the Murchison Meteorite. *Science*, 207(4436), 1202-1204.

Hayes, J.M., 1967. Organic constituents of meteorites -A review. *Geochimica et Cosmochimica Acta*, 31, 1395-1440.

Hayes, J.M. & Biemann, K., 1968. High resolution mass spectrometric investigations of the organic constituents of the Murray and Holbrook chondrites. *Geochimica et Cosmochimica Acta*, 32, 239-267.

Henning, T. & Salama, F., 1998. Carbon in the universe. *Science*, 282(5397), 2204-2210.

Herbst, E. & Klemperer, W., 1973. The formation and depletion of molecules in dense interstellar clouds. *Astrophysical Journal*, 185, 505-534.

Herbst, E., 2001. The chemistry of interstellar space. *Chemical Society Reviews*, 30(3), 168-176.

Hewins, R. & Radomsky, P., 1990. Temperature conditions for chondrule formation. *Meteoritics*, 25, 309-318.

Hewins, R.H. & Connolly, H.C., 1994. Experimental constraints on models for origins of chondrules: Peak temperatures. *LPI Contributions*, 844, 11-12.

Hezel, D.C. et al., 2003. Evidence for fractional condensation and reprocessing at high temperatures in CH chondrites. *Meteoritics and Planetary Science*, 38, 1199-1215.

Hitzenberger, R. et al., 1999. Contribution of carbonaceous material to cloud condensation nuclei concentrations in European background (Mt. Sonnblick) and urban (Vienna) aerosols. *Atmospheric Environment*, 33(17), 2647-2659.

Holleman, A.F. & Wiberg, E., 2001. *Inorganic Chemistry*, San Diago: Academic Press.

Hoose, C. 2008. The global influence of dust mineralogical composition on hetergeneous ice nucleation in mixed-phase clouds. *Environmental Research Letters*, 2(3), 025003.

Hoppe, P. et al., 1996. Small SiC grains and a nitride grain of circumstellar origin from the Murchison meteorite: implications for stellar evolution and nucleosynthesis. *Geochimica et Cosmochimica Acta*, 60(5), 883-907.

Horowitz, H. & Metzger, G., 1963. A New Analysis of Thermogravimetric Traces. *Analytical Chemistry*, 35, 1464-1468.

Horsfield, B. & Douglas, A. G., 1980. The influence of minerals on the pyrolysis of kerogens. *Geochimica et Cosmochimica Acta,* 44, 8, 1119-1131.

Hsieh, H.H. & Jewitt, D., 2006. A population of comets in the main asteroid belt. *Science* (New York, N.Y.), 312(5773), 561-3.

Huang, Y. et al., 2005. Molecular and compound-specific isotopic characterization of monocarboxylic acids in carbonaceous meteorites. *Geochimica et Cosmochimica Acta*, 69, 1073-1084.

Huebner, W.F., 1987. First polymer in space identified in comet Halley. *Science*, 237(4815), 628-630.

Huss, G.R. & Lewis, R.S., 1995. Presolar diamond, SiC, and graphite in primitive chondrites: Abundances as a function of meteorite class and petrologic type. *Geochimica et Cosmochimica Acta*, 59, 115-160.

Hyötylainen, T. et al., 2002. Modulator design for comprehensive two-dimensional gas chromatography: Quantitative analysis of polyaromatic hydrocarbons and polychlorinated biphenyls. *Analytical Chemistry*, 74(17), 4441-4446.

Ishii, H.A. et al., 2008. Comparison of Comet 81P/Wild 2 Dust with interplanetary dust from comets. *Science*, 319, 447.

Iwata, N. & Imae, N., 2001. The collection of antarctic micrometeorites by JARE-41 in 2000. *Meteoritics & Planetary Science*, vol. 36, Supplement, p.A89, 36, 89.

Jacobson, M.Z. 2005. Fundamentals of atmospheric modelling. Cambridge University Press, Cambridge.

Jarosewich, E., 1990. Chemical analyses of meteorites - A compilation of stony and iron meteorite analyses. *Meteoritics*, 25, 323-337.

Jenniskens, P. et al., 2000. Meteors: A Delivery Mechanism of Organic Matter to the Early Earth. *Earth, Moon, and Planets*, 82-83, 57-70.

Jenniskens, P. et al., 2004. Meteors do not break exogenous organic molecules into high yields of diatomics. *Astrobiology*, 4(1), 67-79.

Jessberger, E.K. et al., 2001. Properties of interplanetary dust: Information from collected samples. In *Interplanetary Dust*. Springer. pp. 253-294

Joswiak, D.J. et al., 2000. Characteristics of Asteroidal and Cometary IDPs Obtained from Stratospheric Collectors: Summary of Measured He Release Temperatures, Velocities and Descriptive Mineralogy. In *31st Lunar and Planetary Institute Conference*. p. 1500.

Joswiak, D.J. et al., 2007. Densities and Mineralogy of Cometary and Asteroidal Interplanetary Dust Particles Collected in the Stratosphere. *Dust in Planetary Systems*, 643, 141-144.

Jungclaus, G.A. et al., 1976a. Aliphatic amines in the Murchison meteorite. *Nature*, 261, 126-128.

Jungclaus, G.A. et al., 1976b. Evidence for the presence of low molecular weight alcohols and carbonyl compounds in the Murchison meteorite. *Meteoritics*, 11, 231-237.

Juntgen, H., 1987a. Coal characterisation in relation to coal combustion, part 1: structural aspects and combustion. *Erdol und Kohle-Erdgras-Petrochemie*, 40,153-165.

Juntgen, H., 1987b. Coal characterisation in relation to coal combustion, part 2: evironmental problems of combustion. *Erdol und Kohle-Erdgras-Petrochemie*, 40, 204-208.

Kalashnikova, O.V. et al., 2005. The effects of smoke and dust aerosols on UV-B radiation in Australia from ground-based and satellite measurements. *Proceedings of SPIE - The International Society for Optical Engineering*, p. 5886

Kallemeyn, G.W. & Rubin, A.E., 1995. Coolidge and Loongana 001: A new carbonaceous chondrite grouplet. *Meteoritics*, 30(1), 20-27.

Kallemeyn, G.W. & Wasson, J.T., 1981. The compositional classification of chondrites. I - The carbonaceous chondrite groups. *Geochimica et Cosmochimica Acta*, 45, 1217-1230.

Kallemeyn, G.W. & Wasson, J.T., 1982. The compositional classification of chondrites. III - Ungrouped carbonaceous chondrites. *Geochimica et Cosmochimica Acta*, 46, 2217-2228.

Kallemeyn, G.W. et al., 1991. The compositional classification of chondrites. V - The Karoonda (CK) group of carbonaceous chondrites. *Geochimica et Cosmochimica Acta*, 55(3), 881-892.

Kamen, B., 1997. Folate and antifolate pharmacology. *Seminars in Oncology*, 24(5 Suppl 18), 30-39.

Kaplan, J. et al., 1960. Atomic reactions in the upper atmosphere. *Canadian Journal Chemistry*, 38, 10, 1688-1692.

Kasting, J.F. 1993. Earths Early Atmosphere. *Science*, 259, 5097, 920-926.

Kasting, J.F. 2005. Methane and climate during the Precambrian era. *Precambrian Research*, 137, 3-4, 119-129.

Kasting, J.F. and Ackerman, T.P. 1986. Climatic consequences of very high carbon dioxide levels in the earth's early atmosphere. *Science*, 234, 4782, 1383-1385.

Kasting, J.F. et al., 1993. Mantle Redox Evolution and the Oxidation-State of the Archean Atmosphere. *The Journal of Geology*, 101, 2, 245-257.

Kawamura, K. et al., 1996. Concentrations of monocarboxylic and dicarboxylic acids and aldehydes in southern California wet precipitations: Comparison of urban and nonurban samples and compositional changes during scavenging. *Atmospheric Environment*, 30, 7, 1035-1052.

Kawamura, K. et al., 2001. Wet deposition of low molecular weight mono- and di-carboxylic acids, aldehydes and inorganic species in Los Angeles. *Atmospheric Environment*, 35, 23, 3917-3926.

Kearsley, A. et al., 2007. The chemical composition of micrometeoroids impacting upon the solar arrays of the Hubble Space Telescope. *Advances in Space Research*, 39(4), 590-604.

Keil, K. et al., 1997. Constraints on the role of impact heating and melting in asteroids. *Meteoritics and Planetary Science*, 32, 349-363.

Keil, K., 2000. Thermal alteration of asteroids: evidence from meteorites. *Planetary and Space Science*, 48(10), 887-903.

Keller, L. et al., 1992. An interplanetary dust particle with links to CI chondrites. *Geochimica et Cosmochimica Acta*, 56, 1409-1412.

Keller, L.P. et al., 1994. Carbon in primitive interplanetary dust particles. In Analysis *of interplanetary dust particles*. New York.

Keller, L.P. et al., 2006. Infrared Spectroscopy of Comet 81P/Wild 2 Samples Returned by Stardust. *Science*, 314(5806), 1728-1731.

Kerridge, J.F., 1983. Isotopic composition of carbonaceous-chondrite kerogen Evidence for an interstellar origin of organic matter in meteorites. *Earth and Planetary Science Letters*, 64, 186-200.

Kerridge, J.F. et al., 1979. Magnetite in CI carbonaceous meteorites - Origin by aqueous activity on a planetesimal surface. *Science*, 205, 395-397.

Kissel, J. & Krueger, F.R., 1987. The organic component in dust from comet Halley as measured by the PUMA mass spectrometer on board Vega 1. *Nature*, 326(6115), 755-760.

Kitajima, F. et al., 2002. Evaluating the thermal metamorphism of CM chondrites by using the pyrolytic behavior of carbonaceous macromolecular matter. *Geochimica et Cosmochimica Acta*, 66(1), 163-172.

Klöck, W. et al., 1994. Heating experiments simulating atmospheric entry of micrometeorites. In *25th Lunar and Planetary Science Conference*. p. 713.

Koeberl, C. & Cassidy, W.A., 1991. Differences between Antarctic and non-Antarctic meteorites: An assessment. *Geochimica et Cosmochimica Acta*, 55(1), 3-18.

Koeberl, C. et al., 1992. Bulk major and trace element analyses of unmelted micrometeorites from CAP Prudhomme, Antartica. In *23rd Lunar and Planetary Science Conference*. p. 709.

Kolodny, Y. et al., 1980. Deuterium in carbonaceous chondrites. *Earth and Planetary Science Letters*, 46, 149-158.

Komiya, M. & Shimoyama, A., 1996. Organic compounds from insoluble organic matter isolated from the Murchison carbonaceous chondrite by heating experiments. *Bulletin of the Chemical Society of Japan*, 69, 53-58.

Komiya, M. et al., 1993. Examination of organic compounds from insoluble organic matter isolated from some Antarctic carbonaceous chondrites by heating experiments. *Geochimica et Cosmochimica Acta*, 57(4), 907-914.

Korotev, R., 2008. List of Lunar Meteorites. Available at: http://meteorites.wustl.edu/lunar/moon_meteorites_list_alumina.htm [Accessed June 4, 2008].

Kortenkamp, S.J. and Dermott, S.F. 1998. Accretion of Interplanetary Dust Particles by the Earth. *Icarus,* 135, 2, 469-495.

Kress, M. & Brownlee, D.E., 2002. Chemical alteration of extraterrestrial organics during atmospheric entry of micrometeorites. In *34th COSPAR Scientific Assembly*.

Kress, M. et al., 2002. Pyrolysis of carbonaceous micrometeorites during atmospheric entry: Implications for early Earth. *Meteoritics & Planetary Science*, 37(Supplement), A82.

Krishnamurthy, R.V. et al., 1992. Isotopic and molecular analyses of hydrocarbons and monocarboxylic acids of the Murchison meteorite. *Geochimica et Cosmochimica Acta*, 56, 4045-4058.

Kristensen, E., 1990. Characterization of biogenic organic matter by stepwise thermogravimetry (STG). *Biogeochemistry*, 9(2), 135-159.

Kortenkamp, S. J. and Dermott, S. F. Accretion of interplanetary dust particles by the Earth. *Icarus,* 135, 2, 469-495.

Kurat, G. et al., 1992. Bulk compositions of Antarctic micrometeorites: Nebular and terrestrial signatures. *Meteoritics*, 27(3), A246.

Kurat, G. et al., 1994. Petrology and geochemistry of Antactic micrometeorites. *Geochimica et Cosmochimica Acta*, 58(18), 3879-3904.

Kvenvolden, K. et al., 1970. Evidence for extraterrestrial amino-acids and hydrocarbons in the Murchison meteorite. *Nature*, 228, 923-926.

Kvenvolden, K.A. et al., 1971. Non-protein amino acids in the Murchison meteorite. Proceedings of the National Academy of *Science*, 68, 486-490.

Lahav, N. et al., 1978. Peptide formation in the prebiotic era: thermal condensation of glycine in fluctuating clay environments. *Science*, 201(4350), 67-69.

Lahuis, F. et al., 2005. Hot organic molecules toward a young low-mass star: A look at inner disk chemistry. *Astrophysical Journal*, 636, L-145-L148.

Larimer, J.W. & Anders, E., 1967. Chemical fractionations in meteorites-II. Abundance patterns and their interpretation. *Geochimica et Cosmochimica Acta*, 31, 1239-1270.

Larson, J.W. & Ji, H., 2000. Kerogen chemistry. 8. Hydrous pyrolysis of rundle kerogen : Source of the oxygen in CO2 and mineral catalysis. *Energy and Fuels*, 20(1), 278-280.

Laue, T. & Plagens, A., 2005. *Named Organic Reactions*. 2nd ed., John Wiley & Sons.

Lauer, H.V. et al., 2000. Thermal and evolved gas analyses at reduced pressures: A mineral database for the Thermal Evolved Gas Analyzer (TEGA). In *31st Lunar and Planetary Science Conference*. p. 1990.

Lauer, H.V. et al., 2006. Thermal and evolved gas analysis of geologic samples containing organic materials: Implications for the 2007 Mars Phoenix Scout Mission. In *37th Lunar and Planetary Science Conference*. p. 1780.

Lawless, J.G., 1973. Amino acids in the Murchison meteorite. *Geochimica et Cosmochimica Acta*, 37, 2207-2212.

Lawless, J.G. & Yuen, G.U., 1979. Quantification of monocarboxylic acids in the Murchison carbonaceous meteorite. *Nature*, 282(5737), 396-398.

Lawless, J.G. et al., 1974. Dicarboxylic acids in the Murchison meteorite. *Nature*, 251(5470), 40-42.

Lazcano, A. & Miller, S.L., 1996. The origin and early evolution of life: Prebiotic chemistry, the pre-RNA world, and time. *Cell,* 85, 793-798.

Lebofsky, L.A., 1991. An infrared reflectance study of low albedo surface constituents. *NASA Technical Report N92-10830*, University of Arizona.

Lee, T. et al., 1976. Demonstration of Mg-26 excess in Allende and evidence for Al-26. *Geophysical Research Letters*, 3, 41-44.

Lee, J. And Grabowski, J. 1992. Reactions of the atomic oxygen radical anion and the synthesis of organic reactive intermediates. *Chemical Reviews*, 92, 1611-1647.

Levy, R.L. et al., 1973. The organic analysis of the Murchison meteorite. *Geochimica et Cosmochimica Acta*, 37(3), 467-483.

Lifshitz, A. & Tamburu, C., 1998. Thermal decomposition of acetonitrile: Kinetic modeling. *International Journal of Chemical Kinetics*, 30(5), 341-347.

Liousse, C. et al., 1996 a. A global three-dimensional model study of carbonaceous aerosols. *Journal of Geophysical Research*, 101(D14), 19411-19432.

Liousse, C. et al., 1996 b. Modeling biomass burning aerosols. In *Biomass Burning and Global Change*, 1. The MIT Press. pp. 492-508.

Lisse, C.M. et al., 2005. Spitzer and Chandra observations of the Deep Impact encounter with Comet 9P/Tempel 1. *Bulletin of the American Astronomical Society*, 207, 1484

Lisse, C.M. et al., 2007. Comparison of the composition of the Tempel 1 ejecta to the dust in Comet C/Hale Bopp 1995 O1 and YSO HD 100546. *Icarus*, 191, 223-240.

Liu, Z.Y. & Phillips, J., 1991. *Journal of Chromatographic Science*, 29, 227.

Lofgren, G.E., 1994. Experimental constraints on models for the origin of chondrules: Cooling rates. *LPI Contributions*, 844, 19-20.

Love, S.G. & Brownlee, D.E., 1991. Heating and thermal transformation of micrometeoroids entering the earth's atmosphere. *Icarus*, 89, 26-43.

Love, S.G. & Brownlee, D.E., 1993. A direct measurement of the terrestrial mass accretion rate of cosmic dust. *Science*, 262(5133), 550-553.

Love, S.G. & Brownlee, D.E., 1994. Peak atmospheric entry temperature of micrometeorites. *Meteoritics*, 29, 69-70.

MacKinnon, I.D.R. & Rietmeijer, F.J.M., 1987. Mineralogy of chondritic interplanetary dust particles. *Reviews of Geophysics*, 25, 1527-1553.

MacKinnon, I.D.R. et al., 1982. Classification of the Johnson Space Center stratospheric dust collection. In *13th Lunar and Planetary Science Conference*. p. 413.

Maher, K.A. & Stevenson, D.J., 1988. Impact Frustration of the Origin of Life. *Nature*, 331(6157), 612-614.

Marriott, P. & Shellie, R., 2002. Principles and applications of comprehensive two-dimensional gas chromatography. *TrAC Trends in Analytical Chemistry*, 21(9), 573-583.

Martin, R.S. et al., 2007. Volcanic emissions and the early Earth atmosphere. *Geochimica et Cosmochimica Acta*, 71, 15, 3673-3685.

Martins, Z. et al., 2006. Free dicarboxylic and aromatic acids in the carbonaceous chondrites Murchison and Orgueil. *Meteoritics and Planetary Science*, 41, 1073-1080.

Martins, Z. et al., 2008. Extraterrestrial nucleobases in the Murchison meteorite. *Earth and Planetary Science Letters*, 270, 130-136.

Marty, B. et al., 2005. Nitrogen and noble gases in micrometeorites. *Meteoritics and Planetary Science*, 40, 881.

Matrajt, G. et al., 2001. FTIR and STXM Detection of Organic Carbon in Scoriaceous-type Antarctic Micrometeorites. In *32nd Lunar and Planetary Science Conference*. p. A1336.

Matrajt, G. et al., 2003. A nuclear microprobe study of the distribution and concentration of carbon and nitrogen in Murchison and Tagish Lake meteorites, Antarctic micrometeorites, and IDPs: Implications for *Astrobiology*. *Meteoritics and Planetary Science*, 38(11), 1585-1600.

Matrajt, G. et al., 2004. Concentration and variability of the AIB amino acid in polar micrometeorites: Implications for the exogenous delivery of amino acids to the primitive Earth. *Meteoritics and Planetary Science*, 39(11), 1849-1858.

Matrajt, G. et al., 2005 a. FTIR analysis of the organics in IDPs: Comparison with the IR spectra of the diffuse interstellar medium. *Astronomy and Astrophysics*, 433, 979-995.

Matrajt, G. et al., 2005 b. Atmospheric entry heating effects on organic carbonaceous phases of IDPs and polar micrometeorites: An EELS study. In *36th Lunar and Planetary Science Conference*. p. 1553.

Matrajt, G. et al., 2006. Survival of organic phases in porous IDPs during atmospheric entry: A pulse-heating study. *Meteoritics and Planetary Science*, 41, 903-911.

Matsunaga, S. N. et al., 2007. Importance of wet precipitation as a removal and transport process for atmospheric water soluble carbonyls. *Atmospheric Environment*, 41, 4, 790-796.

Maurette, M., 1998. Carbonaceous Micrometeorites and the Origin of Life. *Origins of Life and Evolution of the Biosphere*, 28, 385-412.

Maurette, M., 2006. *Micrometeorites and the Mysteries of Our Origins*. Berlin: Springer.

Maurette, M., 2006. The ``Hunt" for Micrometeorites Parent Bodies. In *Micrometeorites and the Mysteries of Our Origins*. Berlin: Springer, pp. 199-210.

Maurette, M. et al., 1987. Characteristics and mass distribution of extraterrestrial dust from the Greenland ice cap. *Nature*, 328, 699-702.

Maurette, M. et al., 1990. Multidisciplinary investigations of new collections of Greenland and Antarctica micrometeorites. In *From Mantle to Meteorites*. Banglore: Indian Academy of Sciences. p. 87.

Maurette, M. et al., 1991. A collection of diverse micrometeorites recovered from 100 tonnes of Antarctic blue ice. *Nature*, 351, 44-47.

Maurette, M. et al., 1994a. Collection and curation of IDPs in the Stratosphere and below: Part 2: The Greenland and Antarctic Ice sheets. In *Analysis of Interplanetary Dust. AIP Conference. Proceedings of the American Institute of Physics*, pp. 277-289.

Maurette, M. et al., 1994b. The 1994 EUROMET collection of micrometeorites at Cap-Prudhomme, Antarctica. *Meteoritics*, 29, 499.

Maurette, M. et al., 1995a. Were micrometeorites a source of prebiotic molecules on the early Earth? *Advances in Space Research*, 15(3), 113-126.

Maurette, M. et al., 1995b. Carbonaceous phases in Antarctic micrometeorites and their mineralogical environment. Their contribution to the possible role of Micrometeorites as "chondritic chemical reactors" in atmospheres, waters and/or ices. In *26th Lunar and Planetary Science Conference*, 26, 913.

Maurette, M. et al., 2000. Accretion of neon, organics, CO2, nitrogen and water from large interplanetary dust particles on the early Earth. *Planetary and Space Science*, 48, 1117-1137.

Maurette, M. et al., 2001. EMMA and the Early Earth's Hydrosphere. In *32nd Lunar and Planetary Science Conference*. p. 1586.

McAuliffe, C., 1963. Solubility in Water of C1-C9 Hydrocarbons. *Nature*, 200(4911), 1092-1093.

McKay, C.P. & Borucki, W.J., 1997. Organic synthesis in experimental impact shocks. *Science*, 276(5311), 390-392.

McKeegan, K.D. et al., 2006. Isotopic compositions of cometary matter returned by Stardust. *Science*, 314, 1724.

McSween, H.Y., 1987. Aqueous alteration in carbonaceous chondrites: Mass balance constraints on matrix mineralogy. *Geochimica et Cosmochimica Acta* , 51(9), 2469-2477.

McSween, H.Y., 1989. Achondrites and igneous processes on asteroids. *Annual Review of Earth and Planetary Sciences*, 17, 119-140.

McSween, H.Y., 1994. What we have learned about Mars from SNC meteorites. *Meteoritics*, 29, 757-779.

McSween, H.Y., 1999. *Meteorites and Their Parent Planets*. 2nd ed., Cambridge: Cambridge University Press.

Meinschein, W.G., 1963a. Benzene extracts of the Orgueil meteorite. *Nature*, 197, 833-836.

Meinschein, W.G., 1963b. Hydrocarbons in terrestrial samples and the Orgeuil meteorite. *Space Science Reviews*, 2, 653-679.

Menon, S. et al., 2002. Climate Effects of Black Carbon Aerosols in China and India.. *Science*, 297(5590), 2250.

Michael, A., 1887. Ueber die addition von natriumacetessig- und natriummalonsäureäthern zu den aethern ungesättigter säuren. *Journal für Praktische Chemie*, 35(1), 349-356.

Michael, A., 1894. Ueber die addition von natriumacetessig- und natriummalonsäureäther zu den aethern ungesättigter säuren. *Journal für Praktische Chemie,* 49(1), 20-25.

Milam, S.N. et al., 2004. HCO+ observations toward Comet Hale-Bopp (C/1995 O1): Ion-molecule chemistry and evidence for a volatile secondary source. *The Astrophysical Journal*, 615(2), 1054-1062.

Miller, S. & Lazcano, A., 1995. The origin of life - did it occur at high temperatures. *Journal of Molecular Evolution*, 41, 689-692.

Miller, S. & Urey, H.C., 1959. Organic Compound Synthes on the Primitive Eart: Several questions about the origin of life have been answered, but much remains to be studied. *Science*, 130(3370), 245-251.

Miller, S., 1953. A production of amino acids under possible primitive Earth conditions. *Science*, 117(3046), 528-529.

Miller, S.L. & Bada, J.L., 1988. Submarine hot springs and the origin of life. *Nature*, 334(6183), 609-611.

Milodowski, A.E. & Morgan, D.J., 1980. Identification and estimation of carbonate minerals at low-levels by evolved CO_2 Analysis. *Nature*, 286(5770), 248-249.

Mita, H. & Shimoyama, A., 1996. Amino acid analysis of the Cretaceous/Tertiary boundary sediments at Kawaruppu, Hokkaido, Japan. *Origins of Life and Evolution of the Biosphere*, 26, 330.

Mitsuke, K. et al., 1990. Negative-ion mass spectrometric study of ion-pair formation in the vacuum ultraviolet. II. OCS→S-+CO+, O-+CS+, and CO2→O-+CO+. *Journal of Chemical Physics*, 93, 3, 1710.

Mochida, I. & Yoneda, Y., 1967. Linear free energy relationships in heterogeneous catalysis : I. Dealkylation of alkylbenzenes on cracking catalysts. *Journal of Catalysis*, 7(4), 386-392.

Morgan, W.A. et al., 1991. A new mechanism for the formation of meteoritic kerogen-like material. *Meteoritics*, 26, 374.

Morris, A.A. et al., 2005. Evolved gas analysis of hydrated phases in Murchison and Orgueil. In *36th Lunar and Planetary Science Con*ference. p. 1925.

Morris, A.A., 2008. *Understanding the origin and evolution of water in the early Solar System*. Ph.D. Milton Keynes: The Open University.

Mumma, M.J. et al., 1996. Detection of abundant ethane and methane, along with carbon monoxide and water, in Comet C/1996 B2 Hyakutake: Evidence for interstellar origin. *Science*, 272(5266), 1310-1314.

Mumma, M.J. et al., 2001. Organic composition of C/1999 S4 (LINEAR): A comet formed near Jupiter? *Science*, 292(5520), 1334-1339.

Murchison, D.G. & Raymond, A.C., 1989. Igneous activity and organic maturation in the Midland Valley of Scotland. *International Journal of Coal Geology*, 14(1-2), 47-82.

Nakamura, T. et al., 2001. Bulk mineralogy of individual micrometeorites determined by X-ray diffraction analysis and transmission electron microscopy. *Geochimica et Cosmochimica Acta*, 65, 4385-4397.

Nakamura, T. et al., 2005. Mineralogy of Ultracarbonaceous Large Micrometeorites. *Meteoritics & Planetary Science*, 40(Supplement), p.5046.

Naraoka, H. et al., 2004. A chemical sequence of macromolecular organic matter in the CM chondrites. *Meteoritics and Planetary Science*, 39(3), 401-406.

Noguchi, T. et al., 2002. Mineralogy of phyllosilicate-rich micrometeorites and comparison with Tagish Lake and Sayama meteorites. *Earth and Planetary Science Letters*, 202(2), 229-246.

Nooner, D.W. & Oro, J., 1967. Organic compounds in meteorites-I. Aliphatic hydrocarbons. *Geochimica et Cosmochimica Acta*, 31, 1359-1394.

Norman, D.I. & Palin, J.M., 1982. Volatiles in phyllosilicate minerals. *Nature*, 296(5857), 551-553.

Novakov, T. And Penner, J.E. 1993. Large contribution of organic aerosols to cloud-condensation-nuclei concentrations. *Nature*, 365(6449), 823-826.

Oberbeck, V.R. et al., 1991. Prebiotic chemistry in clouds. *Journal of Molecular Evolution*, 32, 296-303.

Olah, G.A. & Molnar, A., 2003. Hydrocarbon from Petroleum and Natural Gas. In *Hydrocarbon Chemistry*. Wiley, pp. 30-84.

Olson, E.S., 1992. Amino-Acids from Coal-Gasification. *Nature*, 357(6375), 202-202.

Ong, R. et al., 2003. Pressurised liquid extraction–comprehensive two-dimensional gas chromatography for fast-screening of polycyclic aromatic hydrocarbons in soil. *Journal of Chromatography A*, 1019(1-2), 221-232.

Oparin, A.I., 1938. *The Origin of Life*, New York: Macmillan.

Orgel, L.E., 1998. The origin of life—a review of facts and speculations. *Trends in Biochemical Sciences*, 23(12), 491-495.

Oro, J. & Nooner, D.W., 1967. Aliphatic Hydrocarbons in Meteorites. *Nature*, 213, 1085-1087.

Oro, J., 1961. Comets and formation of biochemical compounds on primitive Earth. *Nature*, 190(477), 389-390.

Osawa, T. et al., 2001. Mid-infrared transmission spectra of individual Antarctic micrometeorites and carbonaceous chondrites. *Antarctic Meteorite Research*, 14, 71-88.

Osawa, T. & Nagao, K., 2002. Noble gas compositions of Antarctic micrometeorites collected at the Dome Fuji Station in 1996 and 1997. *Meteoritics and Planetary Science*, 37(7), 911-936.

Ozaki, N. et al., 2006. Dispersion and dry and wet deposition of PAHs in an atmospheric environment. *Water Science and Technology*, 53, 2, 215-24

Palma, R. et al., 2001. Helium and neon in carbon-rich phases of interplanetary dust particles. In *32nd Lunar and Planetary Science Conference*. p. 2074.

Parsons, A.J. et al., 1997. Evolved gas analysis (EGA) of brick clays. *Journal of Thermal Analysis*, 48(1), 49-62.

Pasek, M. & Lauretta, D., 2008. Extraterrestrial flux of potentially prebiotic C, N, and P to the early Earth. *Origins of Life and Evolution of the Biosphere*, 38, 5-21.

Pearson, V. K., 2003. Organic-Inorganic Relationships in the Carbonaceous Chondrites. Ph.D. Milton Keynes: The Open University.

Pearson, V.K. et al., 2002. Clay mineral-organic matter relationships in the early solar system. *Meteoritics and Planetary Science*, 37, 1829-1833.

Pearson, V.K. et al., 2006. Molecular and isotopic indicators of alteration in CR chondrites. *Meteoritics and Planetary Science*, 41(9), 1291-1303.

Pearson, V.K. et al., 2007a. Organic constitution of the CO3 chondrites and implications for asteroidal processes. In *38th Lunar and Planetary Science Conference*. p. 1846.

Pearson, V.K. et al., 2007b. Identification of trace organic components in the CR chondrites by 4D TOFMS. In *38th Lunar and Planetary Science Conference*. p. 1833.

Peltzer, E.T. et al., 1984. The chemical conditions on the parent body of the murchison meteorite: Some conclusions based on amino, hydroxy and dicarboxylic acids. *Advances in Space Research*, 4, 69-74.

Penner, J.E. et al., 1998. Climate forcing by carbonaceous and sulfate aerosols. *Climate Dynamics*, 14(12), 839-851.

Pering, K.L. & Ponnamperuma, C., 1971. Aromatic Hydrocarbons in the Murchison Meteorite. *Science*, 173, 237-239.

Peucker-Ehrenbrink, B. & Schmitz, B., 2001. *Accretion of extraterrestrial matter throughout earth's history*, Springer. pp. 466.

Phillips, J.B. & Xu, J., 1995. Comprehensive multi-dimensional gas chromatography. *Journal of Chromatography A*, 703(1-2), 327-334.

Pierazzo, E. et al., 1998. Hydrocode simulation of the Chicxulub impact event and the production of climatically active gases. *Journal of Geophysical Research*, 103, 28607-28626.

Pierazzo, E. et al., 1997. A Reevaluation of Impact Melt Production. *Icarus*, 127(2), 408-423.

Pizzarello, S. et al., 1994. Isotopic analyses of nitrogenous compounds from the Murchison meteorite: ammonia, amines, amino acids, and polar hydrocarbons. *Geochimica et Cosmochimica Acta*, 58(24), 5579-5587.

Pizzarello, S. et al., 2001. The Organic Content of the Tagish Lake Meteorite. *Science*, 293(5538), 2236-2239.

Pizzarello, S., 2002. The chiral amines of the Murchison meteorite: A preliminary characterization. In *33rd Lunar and Planetary Science Conference*, p. 1233.

Pollack, J.B. and Yung, Y.L. 1980. Origin and evolution of planetary-atmospheres. *Annual Review of Earth and Planetary Sciences*, 8, 425-487.

Pratt, A.R. & Nesbitt, H.W., 1997. Pyrrhotite leaching in acid mixtures of HCl and H_2SO_4. American Journal of *Science*, 297(8), 807-828.

Presper, T. et al., 1993. Elemental depletions in Antarctic micrometeorites and Arctic cosmic spherules: Comparison and relationships. In *24th Lunar and Planetary Science Conference*, pp. 1177-1178.

Radke, M. et al., 1982. Aromatic components of coal: relation of distribution pattern to rank. *Geochimica et Cosmochimica Acta*, 46(10), 1831-1848.

Rairden, R.L. et al., 1998. Search for Organic Matter in Leonid Meteoroids. *Earth, Moon, and Planets*, 82-83, 71-80.

Raseev, S. & Suciu, G.D., 2003. *Thermal and Catalytic Processes in Petroleum Refining*, CRC Press.

Rasmussen, K.L. et al., 1995. No iridium anomaly after the 1908 Tunguska impact: Evidence from a Greenland ice core. *Meteoritics*, 30, 634.

Raymond, A.C. & Murchison, D.G., 1992. Effect of igneous activity on molecular-maturation indices in different types of organic matter. *Organic Geochemistry*, 18(5), 725-735.

Remusat, L. et al., 2005a. New insight on aliphatic linkages in the macromolecular organic fraction of Orgueil and Murchison meteorites through ruthenium tetroxide oxidation. *Geochimica et Cosmochimica Acta*, 69 (17), 4377-4386.

Remusat, L. et al., 2005b. New pyrolytic and spectroscopic data on Orgueil and Murchison insoluble organic matter: A different origin than soluble? *Geochimica et Cosmochimica Acta*, 69 (15), 3919-3932.

Remusat, L. et al., 2007. The insoluble organic matter in carbonaceous chondrites: Chemical structure, isotopic composition and origin. *Comptes Rendus Geosciences*, 339, 14-15, 895-906.

Riboulleau, A. et al., 2000. Pyrolytic and spectroscopic study of a sulphur-rich kerogen from the "Kashpir oil shales" (Upper Jurassic, Russian platform). *Organic Geochemistry,* 31, 12, 1641-1661.

Rietmeijer, F.J.M., 1990. Salts in two chondritic porous interplanetary dust particles. *Meteoritics*, 25, 209-213.

Rietmeijer, F.J.M., 1992. Interplanetary dust particle L20005T12 directly linked to type CM chondrite petrogenesis. In *23rd Lunar and Planetary Science Conference*. p. 1153.

Rietmeijer, F.J.M., 1998. Interplanetary Dust Particles. In *Planetary Materials*. Mineralogical Society of America, pp. 28-119.

Riley, C.M. et al., 2003. Quantitative shape measurements of distal volcanic ash. *Journal of Geophysical Research*, 108 (B10), 2504.

Robert, F. & Epstein, S., 1982. The concentration and isotopic composition of hydrogen, carbon and nitrogen in carbonaceous meteorites. *Geochimica et Cosmochimica Acta*, 46, 81-95.

Rodante, F., 1992. Thermodynamics and kinetics of decompostion processes for standard a-amino acids and some oftheir dipeptides in the solid state. *Thermochimica Acta*, 200, 47-60.

Rose, W.I. et al., 2001. Observations of volcanic clouds in their first few days of atmospheric residence: The 1992 erruptions of Crater Peak, Mount Spurr volcano, Alaska. *Journal of Geology*, 109, 677-694.

Rubin, A.E. & Wasson, J.T., 1995. Variations of chondrite properties with heliocentric distance. *Meteoritics*, 30, 569.

Russell, R.W. et al., 2002. Mid-infrared spectroscopy of persistent Leonid trains. *Earth Moon Planets*, 82-83, 429-438.

Sagan, C. and Chyba, C. 1997. The early faint sun oaradox: Organic shielding of ultraviolet-labile greenhouse gases. *Science*, 276, 5316, 1217-1221.

Sakamoto, K. et al., 2008. Possible mineralogical variation of D-type asteroids deduced from new type hydrous micrometeorites collected from Antarctic snow. *Meteoritics and Planetary Science*, 43 (Supplement), 5140.

Sandford, S.A., 1996. The inventory of interstellar materials available for the formation of the solar system. *Meteoritics and Planetary Science*, 31, 449-476.

Sandford, S.A. & Allamandola, L.J., 1993a. Condensation and vaporization studies of CH3OH and NH3 ices: Major implications for astrochemistry. *Astrophysical Journal*, 417, 815-825.

Sandford, S.A. & Allamandola, L.J., 1993b. The condensation and vaporization behavior of ices containing SO_2, H_2S, and CO_2 - Implications for Io. *Icarus*, 106, 478.

Sandford, S.A. & Walker, R.M., 1985. Laboratory infrared transmission spectra of individual interplanetary dust particles from 2.5 to 25 microns. *Astrophysical Journal*, 291, 838-851.

Sandford, S.A. et al., 1993. Spectroscopic detection of molecular hydrogen frozen in interstellar ices. *Science*, 262, 400-402.

Sandford, S.A. et al., 2006. Organics captured from Comet 81P/Wild 2 by the Stardust spacecraft. *Science*, 314(5806), 1720-1724.

Schaefer, V. 1975. The inadvertant modification of the atmosphere by air pollution. In *The Changing Global Environment*. D. Resdel Publishing Company. pp. 177-196.

Schlosberg, R.H. et al., 1981. Pyrolysis of benzyl ether under hydrogen starvation conditions. *Fuel*, 60(2), 155-157.

Schlosberg, R.H. et al., 1983. Pyrolysis studies of organic oxygenates: 3. High temperature rearrangement of aryl alkyl ethers. *Fuel*, 62(6), 690-694.

Schmidt, K.F., 1924. Ü ber den Imin-Rest. *Berichte der deutschen chemischen Gesellschaft (A and B Series)*, 57(4), 704-706.

Schmitz, S. et al., 2008. CAI-like fragments detected in Wild 2 Cometary impact track C 2012, 110. In *39th Lunar and Planetary Science Conference*. p. 1137.

Schramm, L.S. et al., 1989. Major element composition of stratospheric micrometeorites. *Meteoritics*, 24, 99-112.

Schulz, K. & Elofson, R., 1965. Electron spin resonance studies of organic matter in the Orgueil meteorite. *Geochimica et Cosmochimica Acta*, 29(3), 157-160.

Scrutton, C. 1994. The Lower Jurrasic rocks between Staithes and Port Mulgrave. In *Yorkshire rocks and landscape.* pp. 150-163.

Sears, D.W.G. & Dodd, R.T., 1988. Overview and classification of meteorites. In *Meteorites and the Early Solar System*. pp. 3-31.

Sephton, M.A., 2002. Organic compounds in carbonaceous meteorites. *Natural Product Reports*, 19(3), 292-311.

Sephton, M.A. & Gilmour, I., 1998. A "unique" distribution of polycyclic aromatic hydrocarbons in Allan Hills 84001, or a selective attack in meteorites from Mars? *Meteoritics & Planetary Science*, 33, 142.

Sephton, M.A. et al., 1999. Cyclic diaryl ethers in a Late Permian sediment. *Organic Geochemistry*, 30(4), 267-273.

Sephton, M.A. et al., 2003. Investigating the variations in carbon and nitrogen isotopes in carbonaceous chondrites. *Geochimica et Cosmochimica Acta*, 67(11), 2093-2108.

Sephton, M.A. et al., 2004a. The preservation state of organic matter in meteorites from Antarctica. *Meteoritics and Planetary Science*, 39, 747-754.

Sephton, M.A. et al., 2004b. Hydropyrolysis of insoluble carbonaceous matter in the Murchison meteorite: new insights into its macromolecular structure. *Geochimica et Cosmochimica Acta*, 68, 1385-1393.

Sephton, M.A. et al., 1998a. d13C of free and macromolecular aromatic structures in the murchison meteorite. *Geochimica et Cosmochimica Acta*, 62(10), 1821-1828.

Sephton, M.A. et al., 1998b. Small-scale hydrous pyrolysis of macromolecular material in meteorites. *Planetary and Space Science*, 47(1-2), 181-187.

Sephton, M.A. et al., 2000. Aromatic moieties in meteoritic macromolecular materials: analyses by hydrous pyrolysis and 13 C of individual compounds. *Geochimica et Cosmochimica Acta*, 64, 321-328.

Sephton, M.A. et al., 2001a. Normal alkanes in meteorites: molecular d13C values indicate an origin by terrestrial contamination. *Precambrian Research*, 106(1-2), 47-58.

Sephton, M.A. et al., 2001b. Supercritical fluid extraction of the non-polar organic compounds in meteorites. *Planetary and Space Science*, 49(1), 101-106.

Shimoyama, A. & Katsumata, H., 2001. Polynuclear aromatic thiophenes in the Murchison carbonaceous chondrite. *Chemistry Letters*, 30(3), 202.

Shimoyama, A., 1997. Complex organics in meteorites. *Advances in Space Research*, 19(7), 1045-1052.

Shiota, Y. et al., 2005. Mechanism for the direct oxidation of benzene to phenol by FeO^+. *Organometallics*, 24(14), 3532-3538.

Shiu, M. & Ma, K., 2000. Temperature dependence of physical-chemical properties of selected chemicals of environmental interest. I. Mononuclear and polynuclear aromatic hydrocarbons. *Journal of Physical and Chemical Reference Data*, 29(1), 41-130.

Shock, E.L. & Schulte, M.D., 1990. Amino-acid synthesis in carbonaceous meteorites by aqueous alteration of polycyclic aromatic hydrocarbons. *Nature*, 343, 728-731.

Simmonds, P.G. et al., 1969a. Unextractable organic fraction of Pueblito De Allende meteorite. Evidence for its indigenous *Nature. Proceedings of the National Academy of Sciences of the United States of America*, 64(3), 1027-1034.

Simmonds, P.G. et al., 1969b. Organic analysis by pyrolysis-gas chromatography-mass spectrometry. A candidate experiment for the biological exploration of Mars. *Journal of Chromatographic Science*, 7, 36-41.

Simon, S.B. et al., 2008. A refractory inclusion returned by Stardust from Comet P81/Wild2. *Meteoritics and Planetary Science. (In press).*

Sinninghe Damsté, J.S. et al., 1989. Organic sulphur in macromolecular sedimentary organic matter: I. Structure and origin of sulphur-containing moieties in kerogen, asphaltenes and coal as revealed by flash pyrolysis. *Geochimica et Cosmochimica Acta*, 53(4), 873-889.

Siskin, M. & Aczel, T., 1983. Pyrolysis studies on the structure of ethers and phenols in coal. *Fuel*, 62(11), 1321-1326.

Slanger, T.G. and Black, T. G. 1978. CO_2 photolysis revisited. *Journal of Chemical Physics*, 68, 1844-1849.

Smith, J.W. & Kaplan, I.R., 1970. Endogenous carbon in carbonaceous meteorites. *Science*, 167, 1367-1370.

Smith, R.E. & Hinshelwood, C.N., 1940. The thermal decomposition of gaseous benzaldehyde. *Royal Society of London Proceedings Series A*, 175, 131-142.

Solomon, P.M. & Werner, M.W., 1971. Low energy cosmic rays and the abundance of atomic hydrogen in dark clouds. *Astrophysical Journal*, 165, 41-49.

Solomon, P.R. & Colket, M.B., 1978. Evolution of fuel nitrogen in coal devolatilization. *Fuel*, 57(12), 749-755.

Stöffler, D. et al., 1991. Shock metamorphism of ordinary chondrites. *Geochimica et Cosmochimica Acta*, 55(12), 3845-3867.

Stoks, P.G. & Schwartz, A.W., 1979. Uracil in carbonaceous meteorites. *Nature*, 282(5740), 709-710.

Stoks, P.G. & Schwartz, A.W., 1981. Nitrogen-heterocyclic compounds in meteorites: significance and mechanisms of formation. *Geochimica et Cosmochimica Acta*, 45(4), 563-569.

Stoks, P.G. & Schwartz, A.W., 1982. Basic nitrogen-heterocyclic compounds in the Murchison meteorite. *Geochimica et Cosmochimica Acta*, 46, 309-315.

Stolow, A. And Lee, Y.T. 1993. Photodissociation dynamics of CO2 at 157.6 nm by photofragment-translational spectroscopy. *Journal of Chemical Physics*, 98, 3, 2066-2076.

Strecker, A., 1850. Ueber die künstliche Bildung der Milchsäure und einen neuen, dem Glycocoll homologen Körper. *Annalen der Chemie und Pharmacie*, 75(1), 27-45.

Strecker, A., 1854. Ueber einen neuen aus Aldehyd - Ammoniak und Blausäure entstehenden Körper. *Annalen der Chemie und Pharmacie*, 91(3), 349-351.

Stuart, J.P. & Binzel, R.P., 2004. Bias-corrected population, size distribution, and impact hazard for the near-Earth objects. *Icarus*, 170(2), 295-311.

Studier, M.H. et al., 1968. Origin of organic matter in early solar system---I. Hydrocarbons. *Geochimica et Cosmochimica Acta*, 32, 151-173.

Studier, M.H. et al., 1972. Origin of organic matter in early solar system--V. Further studies of meteoritic hydrocarbons and a discussion of their origin. *Geochimica et Cosmochimica Acta*, 36, 189-215.

Suzuki, A. et al., 2005. Infrared micro-spectroscopy of organic and hydrous components in some Antarctic micrometeorites. In *36th Lunar and Planetary Science Conference*. p. A1176.

Suzuki, A. et al., 2007. Infrared and Raman spectroscopy of Antarctic micrometeorites. In *Abstracts of the 31st Symposium on Antarctic Meteorites*.

Svetsov, V.V., 2002. Assessment of organic delivery by comets to the early Earth. In *33rd Annual Lunar and Planetary Science Conference*. p. 1451.

Swindle, T.D. & Campins, H., 2004. Do comets have chondrules and CAIs? Evidence from the Leonid meteors. *Meteoritics and Planetary Science*, 39(10), 1733-1740.

Szydlik, P. & Flynn, G.J., 1992. The internal temperature profiles of large micrometeorites during atmospheric entry. *Meteoritics*, 27(3), 294.

Taylor, M.J. et al., 2007. First 0.96-1.46 micron near-IR spectra of meteors. *Advances in Space Research*, 39(4), 544-549.

Taylor, S. et al., 1998. Accretion rate of cosmic spherules measured at the South Pole. *Nature*, 392, 899.

Taylor, S. et al., 2000. Numbers, types, and compositions of an unbiased collection of cosmic spherules. *Meteoritics and Planetary Science*, 35, 651-666.

Tewari, Y.B. & Goldberg, R.N., 2005. Thermodynamics of the hydrolysis reactions of nitriles. *The Journal of Chemical Thermodynamics*, 37(7), 720-728.

Thomas, K.L. et al., 1990. Mineralogical descriptions of eight hydrated interplanetary dust particles and their relationship to chondrite matrix. In *21st Lunar and Planetary Science Conference*. p. 1250.

Thomas, K.L. et al., 1992. Carbon in anhydrous interplanetary dust particles: Correlations with silicate mineralogy and sources of anhydrous IDPs. In *23rd Lunar and Planetary Science Conference*. p. 1425.

Thomas, K.L. et al., 1993. Carbon abundance and silicate mineralogy of anhydrous interplanetary dust particles. *Geochimica et Cosmochimica Acta*, 57(7), 1551-1566.

Thomas, R.N. & Whipple, F.L., 1951. The physical theory of meteors .2. Astroballistic heat transfer. *Astrophysical Journal*, 114(3), 448-465.

Tomeoka, K. & Buseck, P.R., 1985a. Hydrated interplanetary dust particle linked with carbonaceous chondrites? *Nature*, 314, 338-340.

Tomeoka, K. & Buseck, P.R., 1985b. Indicators of aqueous alteration in CM carbonaceous chondrites: Microtextures of a layered mineral containing Fe, S, O and Ni. *Geochimica et Cosmochimica Acta* , 49(10), 2149-2163.

Tomeoka, K. & Buseck, P.R., 1986. A carbonate-rich, hydrated, interplanetary dust particle Possible residue from protostellar clouds. *Science*, 231, 1544-1546.

Toppani, A. & Libourel, G., 2001. Conditions of atmospheric entry of micrometeorites. In *32nd Lunar and Planetary Science Conference*. p. A1520.

Toppani, A. et al., 2000. Experimental simulation and modeling of atmospheric entry of micrometeorites. *Meteoritics & Planetary Science*, 35(Supplement), A158.

Toppani, A. et al., 2001. Experimental simulation of atmospheric entry on micrometeorites. *Meteoritics and Planetary Science*, 36, 1377-1396.

Toppani, A. et al., 2003. Simulation of nitrogen and noble gases released during atmospheric entry of micrometeorites. In *34th Lunar and Planetary Science Conference*. p. 2028.

Trainer, M.G. et al., 2006. Organic haze on Titan and the early Earth. *Proceedings of the National Academy of Sciences of the United States of America*, 103, 48, 18035-18042.

Trigo-Rodriguez, J.M. et al., 2006. Non-nebular origin of dark mantles around chondrules and inclusions in CM chondrites. *Geochimica et Cosmochimica Acta*, 70(5), 1271-1290.

Tsuchiyama, A. et al., 2004. Density and porosity measurement of Antarctic micrometeorites using microtomography. *Meteoritics and Planetary Science,* 39 (Supplement). p. 5058.

Tyburczy, J.A. et al., 1986. Shock-induced volatile loss from a carbonaceous chondrite: implications for planetary accretion. *Earth and Planetary Science Letters*, 80, 201-207.

Ushikubo, T et al., 2008. Lithium in Jack Hills zircons: Evidence for extensive weathering of Earth's earliest crust. *Earth and Planetary Science Letters*, 272, 3-4, 666-676.

Van der Velden, W. & Schwartz, A.W., 1977. Search for purines and pyrimidines in the Murchison meteorite. *Geochimica et Cosmochimica Acta*, 41(7), 961-968.

Van Schmus, W. & Wood, J., 1967. A chemical-petrologic classification for the chondritic meteorites. *Geochimica et Cosmochimica Acta*, 31, 747-765.

Vandenabeele-Trambouze, O. et al., 2001. Identification of amino acids by capillary gas chromatography. Application to martian samples. *Chromatographia*, 53(0), S332-S339.

Velbel, M.A. et al., 1991. Terrestrial weathering of Antarctic stone meteorites - Formation of Mg-carbonates on ordinary chondrites. *Geochimica et Cosmochimica Acta*, 55, 67-76.

Watts, S. et al., 1999. The Organic Geochemistry of Jet: Pyrolysis-gas Chromatography/ Mass Spectrometry (Py-GCMS) Applied to Identifying Jet and Similar Black Lithic Materials—Preliminary Results. *Journal of Archaeological Science,* 26(8), 923-933.

Walker, J.C.G. 1977. Evoloution of the atmosphere. Macmillan, New York. p. 318.

Walker, J.C.G. 1985. Carbon dioxide on the early earth. *Origins of Life and Evolution of Biospheres*, 16, 2, 117-127.

Walter, et al., 1995 a. The Abundance of Ordinary Chondrite Debris Among Antarctic Micrometeorites. *Meteoritics*, 30, 592.

Walter et al., 1995 b. Cosmic Spherules, Micrometeorites, and Chondrules. *Lunar and Planetary Institute Conference Abstracts,* 26, 1457.

Watson, B.A. et al., 1997. Catalytic cracking of alkylbenzenes: Modeling the reaction pathways and mechanisms . *Applied Catalysis A: General*, 160(1), 13-39.

Watson, J.S. et al., 2005. Pyrolysis-GCxGC-TOFMS to characterize carbonaceous chondrites. In *36th Lunar and Planetary Science Conference*. p. 1842.

Watson, J.S. et al., 2005. Oxygen-containing aromatic compounds in a Late Permian sediment. *Organic Geochemistry*, 36, 371-384.

Weisberg, M.K. et al., 2001. A new metal-rich chondrite grouplet. *Meteoritics and Planetary Science*, 36, 401-418.

Whipple, F.L., 1950. The theory of micro-meteorites .1. In an isothermal atmosphere. Proceedings of the National Academy of *Sciences U. S. A.,* 36(12), 687-695.

Whipple, F.L., 1951. The theory of micro-meteorites .2. In heterothermal atmospheres. Proceedings of the National Academy of *Sciences U. S. A.*, 37(1), 19-30.

Wicks, F.J. & Ramik, R.A., 1990. Vacuum thermogravimetric analysis and evolved gas analysis by mass spectrometry. In *Thermal Analysis in Clay Science*. pp. 160-189.

Wiley, W.C. & McLaren, I.H., 1955. Time-of-flight mass spectrometer with improved resolution. *Review of Scientific Instruments*, 26(12), 1150-1157.

Williams, S.N. et al., 1992. Global carbon dioxide emission to the atmosphere by volcanoes. *Geochimica et Cosmochimica Acta*, 56, 4, 1765-1770.

Wilson, J.T., 1963. Hypothesis of Earth's behaviour. *Nature*, 198(4884), 925-929.

Wilson, R.C. et al., 2007a. Experimental simulation of volatile organic contributions to planetary atmospheres and surfaces. In *38th Lunar and Planetary Science Conference*. p. 1799.

Wilson, R.C. et al., 2007b. Simulating the organic and volatile contributions to planetary surfaces and atmospheres from extraterrestrial dust. *Meteoritics and Planetary Science*, 42(Supplement), 5115

Wilson, R.C. et al., 2008. Comprehensive organic analysis of Antarctic micrometeorites. In *Lunar and Planetary Institute Conference Abstracts*, 39, 1763.

Winkler, J.K. et al., 2002. Gas-phase pyrolysis of heterocyclic compounds, part 1 and 2: flow pyrolysis and annulation reactions of some sulfur heterocycles: thiophene, benzo[b]thiophene, and dibenzothiophene. A product-oriented study. *Journal of Analytical and Applied Pyrolysis*, 62(1), 123-141.

Wirick, S. et al., 2007. Carbonates found in Stardust aerogel tracks. In *38th Lunar and Planetary Science Conference* p. 1534.

Wopenka, B., 1987. Raman observations of individual interplanetary dust particles. In *18th Lunar and Planetary Science Conference*. p. 1102.

Wright, I.P. & Pillinger, C.T., 1998. Mars, Modulus and MAGIC. The measurement of stable isotopic compositions at a planetary surface. *Planetary and Space Science*, 46(6-7), 813-823.

Wright, I.P. et al., 1997. The content and stable isotopic composition of carbon in individual micrometeorites from Greenland and Antarctica. *Meteoritics and Planetary Science*, 32(79-89).

Wright, I.P. et al., 2000. Effects of atmospheric heating on infalling meteorites and micrometeorites; relevance to conditions on the early Earth. In *Impacts and the Early Earth (Lecture Notes in Earth Science)*, 91, 51-72

Wynberg, H. & Bantjer, A., 1959. Pyrolysis of thiophene. *Journal of Organic Chemistry*, 24, 1421-1423.

Yabuta, H. et al., 2007. Chondritic organic matter as an indicator of nebular and parent body processing: Extended pyrolysis studies for CM, CI, CR, CO, CV, ordinary, and Tagish Lake group meteorites. In *38th Lunar and Planetary Science Conference*. p. 2304.

Yada, T. et al., 2006. High abundances of presolar silicates in Antarctic micrometeorites; Implications for their cometary origins. In *37th Lunar and Planetary Science Conference*. p. 1470.

Yang, J. & Epstein, S., 1983. Interstellar organic matter in meteorites. *Geochimica et Cosmochimica Acta*, 47, 2199-2216.

Yuen, G.U. & Kvenvolden, K.A., 1973. Monocarboxylic acids in Murray and Murchison carbonaceous meteorites. *Nature*, 246, 301-303.

Yuen, G.U. et al., 1984. Carbon isotope composition of low molecular weight hydrocarbons and monocarboxylic acids from Murchison meteorite. *Nature*, 307, 252-254.

Zahnle, K.J. and Sleep, N.H. 2006. Impacts and the early evolution of life. *In Comets and the Origin and Evolution of Life.* Springer-Verlag, New York. pp. 175-208.

Zhang, D. et al., 2001. Soot particles and their impacts on the mass cycle in the Tibetan atmosphere. *Atmospheric Environment*, 35(34), 5883-5894.

Zhao, M.X. & Bada, J.L., 1989. Extraterrestrial amino-acids in Cretaceous Tertiary boundary sediments at Stevns-Klint, Denmark. *Nature*, 339(6224), 463-465.

Zolensky, M.E. & Barrett, R.A., 1994. Compositional variations of olivines and pyroxenes in chondritic interplanetary dust particles. *Meteoritics*, 29, 616-620.

Zolensky, M.E. & Lindstrom, D.J., 1992. Mineralogy of 12 large 'chondritic' interplanetary dust particles. In *22nd Lunar and Planetary Science Conference*. pp. 161-169.

Zolensky, M.E. & Thomas, K.L., 1995. Iron and iron-nickel sulfides in chondritic interplanetary dust particles. *Geochimica et Cosmochimica Acta*, 59, 4707-4712.

Zolensky, M.E. et al., 1996. Mineralogy of carbonaceous chondrite clasts in HED achondrites and the Moon. *Meteoritics and Planetary Science*, 31, 518-537.

Appendix I a: Raw Data Heating Method 1 (Pt Coil)

Sample	~mass (mg)	Heating Duration (s)	Date	Sample Number	Temperature Pyroprobe (°C)	Temperature Thermocouple (°C)
Murchison	9	5	250106	b1	600	368
Murchison	9	5	250106	b2	800	542
Murchison	9	5	250106	b3	800	510
Murchison	9	5	060306	a1	800	511
Murchison	9	5	060306	a2	800	497
Murchison	9	5	060306	a4	800	240
Murchison	9	5	060306	a5	800	385
Murchison	9	5	060306	a10	900	456
Murchison	9	5	060306	a6	1000	569
Murchison	9	5	060306	a7	1000	658
Murchison	9	5	060306	a8	1000	645
Murchison	9	5	060306	a9	1000	751
Murchison	9	5	250106	a2	1200	886
Murchison	9	5	250106	a3	1200	845
Murchison	9	5	250106	a4	1200	745
Murchison	9	5	250106	a5	1200	809
Murchison	9	10	130306	a10	600	485
Murchison	9	10	130306	b1	600	403
Murchison	9	10	130306	b2	600	500
Murchison	9	10	130306	a7	800	598
Murchison	9	10	130306	a8	800	576
Murchison	9	10	130306	a9	800	629
Murchison	9	10	130306	a4	1000	768
Murchison	9	10	130306	a5	1000	618
Murchison	9	10	130306	a6	1000	737
Murchison	9	10	130306	a1	1200	884
Murchison	9	10	130306	a2	1200	874
Murchison	9	10	130306	a3	1200	935
Murchison	9	20	160106	c3	600	537
Murchison	9	20	160106	c5	600	535
Murchison	9	20	160106	b5	800	473
Murchison	9	20	160106	c1	800	565
Murchison	9	20	160106	c2	800	704
Murchison	9	20	230206	a2	800	405
Murchison	9	20	230206	a3	800	674
Murchison	9	20	230206	a4	800	661
Murchison	9	20	230206	a5	800	684
Murchison	9	20	230206	a10	800	646
Murchison	9	20	230206	a8	900	727
Murchison	9	20	230206	a9	900	732
Murchison	9	20	160106	b3	1000	801
Murchison	9	20	160106	b4	1000	763
Murchison	9	20	230206	a1	1000	740
Murchison	9	20	230206	a6	1000	809
Murchison	9	20	230206	a7	1000	819
Murchison	9	20	110106	a2	1200	947
Murchison	9	20	160106	a5	1200	907
Murchison	9	20	160106	b1	1200	931

Sample	~mass (mg)	Heating Duration (s)	Date	Sample Number	Temperature Pyroprobe (°C)	Temperature Thermocouple (°C)
Toarcian	7	5	181105	c3	400	206
Toarcian	7	5	181105	c4	400	206
Toarcian	7	5	181105	c5	400	200
Toarcian	7	5	181105	b5	600	323
Toarcian	7	5	181105	c1	600	350
Toarcian	7	5	181105	c2	600	325
Toarcian	7	5	181105	b2	800	423
Toarcian	7	5	181105	b3	800	470
Toarcian	7	5	181105	b4	800	459
Toarcian	7	5	181105	a4	1000	590
Toarcian	7	5	181105	a5	1000	603
Toarcian	7	5	181105	b1	1000	582
Toarcian	7	5	181105	a2	1200	748
Toarcian	7	5	181105	a3	1200	719
Toarcian	7	10	151105	d3	400	279
Toarcian	7	10	151105	d4	400	269
Toarcian	7	10	151105	d5	400	225
Toarcian	7	10	151105	c4	600	431
Toarcian	7	10	151105	d1	600	412
Toarcian	7	10	151105	d2	600	426
Toarcian	7	10	151105	c1	800	417
Toarcian	7	10	151105	c2	800	528
Toarcian	7	10	151105	c3	800	530
Toarcian	7	10	151105	b3	1000	709
Toarcian	7	10	151105	b4	1000	694
Toarcian	7	10	151105	b5	1000	975
Toarcian	7	10	151105	a1	1200	684
Toarcian	7	10	151105	b1	1200	853
Toarcian	7	10	151105	b2	1200	752
Toarcian	7	20	141105	d3	400	325
Toarcian	7	20	141105	d4	400	304
Toarcian	7	20	141105	d5	400	323
Toarcian	7	20	141105	d1	600	543
Toarcian	7	20	141105	d2	600	496
Toarcian	7	20	151105	e1	600	452
Toarcian	7	20	141105	c2	800	654
Toarcian	7	20	141105	c3	800	679
Toarcian	7	20	141105	c4	800	689
Toarcian	7	20	141105	b4	1000	686
Toarcian	7	20	141105	b5	1000	694
Toarcian	7	20	141105	c1	1000	726
Toarcian	7	20	141105	b1	1200	908
Toarcian	7	20	141105	b2	1200	912
Toarcian	7	20	141105	b3	1200	879

Sample	~mass (mg)	Heating Duration (s)	Date	Sample Number	Temperature Pyroprobe (°C)	Temperature Thermocouple (°C)
Permian	9	20	280405	2c	400	264
Permian	9	20	280405	2a	400	278
Permian	9	20	280405	2b	400	316
Permian	9	20	140805	a5	400	113
Permian	9	20	140805	b5	400	207
Permian	9	20	140805	c5	400	263
Permian	9	20	230805	a5	400	228
Permian	9	20	230805	b5	400	273
Permian	9	20	280405	2c	600	505
Permian	9	20	280405	2a	600	454
Permian	9	20	280405	2b	600	476
Permian	9	20	140805	a4	600	331
Permian	9	20	140805	b4	600	212
Permian	9	20	140805	c4	600	377
Permian	9	20	230805	a4	600	408
Permian	9	20	230805	b4	600	335
Permian	9	20	280405	2c	800	640
Permian	9	20	280405	2a	800	645
Permian	9	20	280405	2b	800	684
Permian	9	20	140805	a3	800	495
Permian	9	20	140805	b3	800	467
Permian	9	20	140805	c3	800	442
Permian	9	20	230805	a3	800	470
Permian	9	20	230805	b3	800	466
Permian	9	20	280405	2c	1000	801
Permian	9	20	280405	2a	1000	845
Permian	9	20	280405	2b	1000	632
Permian	9	20	140805	a2	1000	650
Permian	9	20	140805	b2	1000	517
Permian	9	20	140805	c2	1000	654
Permian	9	20	230805	a2	1000	485
Permian	9	20	230805	b2	1000	583
Permian	9	20	280405	2c	1200	867
Permian	9	20	280405	2a	1200	969
Permian	9	20	280405	2b	1200	982
Permian	9	20	140805	a1	1200	826
Permian	9	20	140805	c1	1200	513
Permian	9	20	230805	a1	1200	915
Permian	9	20	230805	b1	1200	664
Permian	14	2	310305	A5	400	156
Permian	14	2	50404	a5	400	178
Permian	14	2	50404	b5	400	106
Permian	14	2	50404	c5	400	90
Permian	14	2	310305	A4	600	183
Permian	14	2	50404	a4	600	263
Permian	14	2	50404	b4	600	85
Permian	14	2	50404	c4	600	158
Permian	14	2	310305	A3	800	248
Permian	14	2	310305	A6	800	210
Permian	14	2	310305	A7	800	205
Permian	14	2	50404	a3	800	369
Permian	14	2	50404	b3	800	157

Sample	~mass (mg)	Heating Duration (s)	Date	Sample Number	Temperature Pyroprobe (oC)	Temperature Thermocouple (oC)
Permian	14	2	50404	c3	800	239
Permian	14	2	310305	A2	1000	431
Permian	14	2	50404	a2	1000	379
Permian	14	2	50404	b2	1000	273
Permian	14	2	50404	c2	1000	331
Permian	14	2	50404	d1	1000	318
Permian	14	2	50404	f1	1000	239
Permian	14	2	50404	f2	1000	236
Permian	14	2	310305	A1	1200	388
Permian	14	2	50404	a1	1200	448
Permian	14	2	50404	b1	1200	357
Permian	14	2	50404	c1	1200	210
Permian	14	2	50404	d2	1200	471
Permian	14	40	60705	a5	400	316
Permian	14	40	60705	b5	400	336
Permian	14	40	60705	c5	400	354
Permian	14	40	60705	a4	600	486
Permian	14	40	60705	b4	600	473
Permian	14	40	60705	c4	600	534
Permian	14	40	60705	a3	800	553
Permian	14	40	60705	b3	800	659
Permian	14	40	60705	c3	800	677
Permian	14	40	60705	a2	1000	732
Permian	14	40	60705	b2	1000	682
Permian	14	40	60705	c2	1000	802
Permian	14	40	60705	a1	1200	942
Permian	14	40	60705	b1	1200	861
Permian	14	40	60705	c1	1200	919

Raw data from simulation experiments using Pt coil (flash heating method 1)

Appendix I b: Raw Data Heating Method 1 (Pt Coil)

Sample	set pyroprobe temperature (°C)	average temperature thermocouple (°C)	Error (2σ)
~9mg Permian, 20s duration	400	242.75	123.56
	600	370.43	177.94
	800	538.63	198.68
	1000	645.88	251.21
	1200	819.43	344.77
~14mg Permian, 2s duration	400	132.50	82.71
	600	172.25	146.82
	800	238.00	143.38
	1000	315.29	145.14
	1200	374.80	205.58
~14mg, Permian, 40s duration	400	335.33	38.02
	600	497.67	86.27
	800	629.67	134.00
	1000	738.67	120.55
	1200	907.33	83.48
~7mg Toarcian, 5s duration	400	204.00	6.93
	600	332.67	30.09
	800	450.67	49.17
	1000	591.67	21.20
	1200	733.50	41.01
~7mg Toarcian, 10s duration	400	257.67	57.46
	600	423.00	19.70
	800	491.67	129.34
	1000	792.67	316.17
	1200	763.00	170.07
~7mg Toarcian, 20s duration	400	317.33	23.18
	600	497.00	91.02
	800	674.00	36.06
	1000	702.00	42.33
	1200	899.67	36.02
~9mg Murchison, 5s duration	600	368.00	0.00
	800	447.50	230.27
	900	456.00	0.00
	1000	655.75	149.30
	1200	754.00	119.56
~9mg Murchison, 10s duration	600	462.67	104.43
	800	601.00	53.25
	1000	707.67	158.37
	1200	897.67	65.43
~9mg Murchison, 20s duration	600	536.00	2.83
	800	601.50	219.80
	900	729.50	7.07
	1000	786.40	66.99
	1200	928.33	40.27

Average thermocouple temperatures for each simulation. Errors given are 2 standard deviation.

Appendix II: Chromatogram Peak Areas

This appendix contains the chromatogram peak areas used to derive the relative abundances of species and presented in graphs in Chapters 3 and 4 for all simulation conditions using SFE Murchison residue, AMMs and Antarctic terrestrial particles (T2 sample). Peak areas were mass specific; ions are indicated in brackets or in figure text.

n-ALKANES (amu 57)

Duration (s)	Simulation Temperature (°C)	C_5	C_6	C_7	C_8	C_9	C_{10}	C_{11}	C_{12}	C_{13}
2	425	40574	429513	70782	65314	98914	113288	267900	371256	400355
2	632	1979982	2240158	203460	167165	359378	216030	430885	497783	162638
2	834	2030457	2095589	210386	171054	338773	308219	451475	475178	116032
2	1026	802396	1016263	215400	74913	107344	122462	360450	487068	194766
5	404	576939	660153	78099	88839	123764	169704	97012	69629	102489
5	599	1232172	1294057	141962	122507	237989	228986	142093	120376	50729
5	802	1954909	2003201	125248	183051	165941	322469	312824	159035	57596
5	1009	496559	578911	148354	75593	71893	120409	185122	146763	63987
20	438	1694612	1931299	438309	378999	437476	449562	629902	1079918	359845
20	614	1991270	2082940	137406	217243	289752	261626	774825	640390	1048198
20	801	1356406	1344548	164137	123859	255322	249108	686960	56787	443329
20	992	247747	390683	55207	39342	21184	41188	330255	396547	445774

***n*-alkane RIC (mass 57) peak areas**

BENZENES

C_0-C_2 Benzenes

Duration (s)	Temperature (°C)	Benzene (52)	toluene (65)	ethylbenzene (91)	m & p-xylene (106)	o-xylene (91)	Total C_2-Benzene
2	425	**1052761**	**2313100**	4196526	1436964	1566817	**7200307**
2	632	**19432064**	**14370337**	17150639	8306194	11456806	**36913639**
2	834	**51996823**	**17980713**	18826893	9393178	13538843	**41758914**
2	1026	**41838530**	**17805666**	12590731	8073125	11637616	**32301472**
5	404	**2737025**	**4131048**	6108309	2295406	2886282	**11289997**
5	599	**15524274**	**10468779**	11684052	6338479	8377474	**26400005**
5	802	**31122103**	**18444661**	17954111	9790625	13374722	**41119458**
5	1009	**32114613**	**14348522**	9284807	6575296	9085325	**24945428**
20	438	**9758185**	**8810114**	13558109	6842105	9031619	**29431833**
20	614	**24534818**	**14689783**	16405507	9012551	12229654	**37647712**
20	801	**26165591**	**13414437**	12736850	7060286	10061697	**29858833**
20	992	**25561890**	**10587549**	5613907	12593765	6050220	**24257892**
AMMs		**655384**	**80951**	232970	131888	109645	**474503**
Terrestrial Particles T2		**21085823**	**1419766**	1240281	556379	868355	**2665015**

C_0-C_2 Benzene peak areas from RIC (mass 52+65+91+106)

C_3 Benzenes

Duration (s)	Simulation Temperature (°C)	1-methylethylbenzene (105)	propylbenzene (91)	1-ethyl-3-methylbenzene (105)	1-ethyl-4-methylbenzene (105)	1-ethyl-2-methylbenzene (105)	1,2,4-trimethylbenzene (105)	1,2,3-trimethylbenzene (105)	Total C_3-benzenes
2	425	405982	3887255	1565876	205141	556016	1383520	491095	**8494885**
2	632	1408830	10112323	7129725	1392142	2666722	5780850	1979556	**30470148**
2	834	1137760	9195610	6876899	1423394	3007355	5605057	2040331	**29286406**
2	1026	546375	4226807	4921440	1055035	1754635	4497298	1576019	**18577609**
5	404	539493	5079221	2314861	435100	907875	1808928	609896	**11695374**
5	599	859690	7360594	5235776	1021237	2086754	4248987	1531546	**22344584**
5	802	1317810	9130087	7826721	1736418	3117520	6303114	2318252	**31749922**
5	1009	460921	3331725	4287214	845875	1286961	3946476	1490233	**15649405**
20	438	1054169	9886663	6466414	1207049	2384282	5495470	1932949	**28426996**
20	614	1306963	10454238	7760592	1493405	3156721	6479185	2283321	**32934425**
20	801	832196	6346356	5500342	1048294	2172950	4469394	1623242	**21992774**
20	992	206628	1730532	2322179	553934	763517	2389955	818385	**8785130**
AMMs		0	49745	21894	0	9600.2	86776	43034	**211049.2**
Terrestria particles T2		137362	0	0	0	78411	129568	59671	**405012**

C_3 benzene peak areas from RIC (mass 52+ 61+91+105+106)

C_4 benzenes

Duration (s)	Simulation temperature (°C)	tertiary butylbenzene (119)	isobutylbenzene (92)	sec-butylbenzene (105)	1-methyl-3-isopropylbenzene (119)	1-methyl-4-isopropylbenzene (119)	1-methyl-2-isopropylbenzene (134)	1-methyl-3-propylbenzene (105)	1-methyl-4-propylbenzene (105)	1,4-diethylbenzene (91)
2	425	14812	29902	309628	146199	756004	13731	413428	160263	137711
2	632	73748	156075	963506	527299	603731	56825	1660703	569209	1547943
2	834	61836	134734	816637	492543	594208	47291	1410949	125842	226304
2	1026	26117	51922	288431	299689	318556	56339	796801	144166	562463
5	404	22001	62380	415449	245489	348725	20743	551254	114524	5055088
5	599	78201	153187	713207	398297	420605	38602	1045961	308392	234424
5	802	63201	218003	786084	386853	441575	59750	16722292	628978	572285
5	1009	16745	69840	293281	325851	307037	49587	729842	257136	283329
20	438	94473	218710	888575	557894	1434948	49731	1395045	468169	352026
20	614	83079	184902	902261	574925	689421	59232	1907810	678914	968993
20	801	37761	123299	483973	378082	354135	34453	1162076	437788	613230
20	992	7121.5	27439	141728	165343	165402	7829.9	336414	71789	281241
AMMs		14727	0	0	75922	43741	0	7722	7945.3	1986.3
Terrestrial particles T2		215673	37477	36052	6737.2	269755	1491.6	8950	7515.4	0

C_4 benzene peak areas from RIC (mass 91+92+105+119)

C_4 benzenes (continued)

Duration (s)	Simulation temperature (°C)	n-butyl benzene (134)	1,2 Diethyl benzene (119)	1-methyl-2-propyl benzene (105)	1,4-Dimethyl-2-ethyl benzene &1,3-dimethyl-2-ethyl benzene (119)	1,2-dimethyl-4-ethyl benzene (119)	1,3-dimethyl-2-ethyl benzene (119)	1,2-dimethyl-3-ethyl benzene (119)	1,2,4,5-tetramethyl benzene (119)	1,2,3,5-tetramethyl benzene (119)	1,2,3,4-tetramethyl benzene (119)	**TOTAL C4 thiophenes**
2	425	67397	15390	158256	349187	201339	0	89759	67375	201116	176628	**3308125**
2	632	9165.7	63574	914003	1578982	868247	178632	589051	356558	801207	697344	**12215802.7**
2	834	123872	92523	841696	1468103	829246	154736	514302	337797	719621	367698	**9359938**
2	1026	51885	29253	375094	958274	553662	87336	312947	233225	510988	240009	**5897157**
5	404	51579	24694	309232	552272	306849	59010	199232	129083	180215	129854	**8777673**
5	599	59171	50196	679954	1168840	666139	265482	254378	258047	455589	474226	**7722898**
5	802	193669	55139	1006553	1693679	845459	168306	520005	243914	705407	383473	**25694625**
5	1009	83551	38646	362018	796728	455637	0	250743	196934	414881	220385	**5152171**
20	438	287189	18624	940448	1569622	967648	347656	602242	230705	715497	550736	**11689938**
20	614	126522	70015	1151038	446970	1045983	195632	647109	391174	789644	809772	**11723396**
20	801	82814	67253	6555641	1129250	696601	119017	397424	241635	316751	462678	**13693861**
20	992	23029	6975.9	169905	446729	275850	39923	150742	122191	162005	136703	**2738360.3**
AMMs		2573.2	0	0	0	6549.5	0	0	0	7967.3	0	**169133.6**
Terrestrial particles T2		11770	0	16360	9641.9	0	0	6021.5	3806.5	5887.3	6157	**643295.4**

Further C_4 benzene peak areas from RIC (mass 105+119+134)

THIOPHENES

C_0-C_1 Thiophenes

Duration (s)	Peak Temperature (°C)	Thiophene (57)	2-methylthiophene (98)	3-methylthiophene (98)	Total C_1-Thiophene
2	425	**10569245**	7141279	13301983	**20443262**
2	632	**18021008**	16382948	25302242	**41685190**
2	834	**17996077**	15624937	23825205	**39450142**
2	1026	**13598537**	19799908	16582302	**36382210**
5	404	**22714534**	11189181	18770219	**29959400**
5	599	**12705546**	20998668	17520312	**38518980**
5	802	**18250970**	16094407	25380116	**41474523**
5	1009	**25525795**	14118414	12172081	**26290495**
20	438	**14222817**	13946180	22425804	**36371984**
20	614	**17486110**	15198452	24089219	**39287671**
20	801	**12486933**	17801248	15723753	**33525001**
20	992	**31246897**	8561787	15485924	**24047711**
AMMs		**3811920**	514737	1171843	**1686580**
Terrestrial Particles T2		**420805**	29196	60562	**89758**

C_0-C_1 thiophene peak areas from RIC (mass 57+97+98+111)

C_2 Thiophenes

Duration (s)	Temp (°C)	2-ethylthiophene (97)	2,5-DMthiophene (111)	2,4-DMthiophene (97)	2,3-DMthiophene (97)	3,4-DMthiophene (111)	Total C_2-Thiophene
2	425	1824906	1745793	1837602	842858	986389	**7237548**
2	632	5156711	4804052	5905410	3817592	2702343	**22386108**
2	834	4662757	3650241	5383838	3151242	2456439	**19304517**
2	1026	2561717	2347726	2982868	1919611	1644024	**11455946**
5	404	2389027	2269980	899415	1729769	1226317	**8514508**
5	599	3512085	3276467	3940879	2598671	1763363	**15091465**
5	802	5047254	4782469	4831147	3524802	2779903	**20965575**
5	1009	593320	2050939	1754936	991480	1314074	**6704749**
20	438	4407735	3041417	4842470	3490012	2439367	**18221001**
20	614	4597265	3857722				**8454987**
20	801	2640127	2285979	3184483	1801083	1536212	**11447884**
20	992	1008439	1100124	1199408	820808	777028	**4905807**
AMMs		104853	68051	125882	68207	67848	**434841**
Terrestrial Particles T2		0	3790.8	0	0	0	**3790.8**

C_2 thiophene peak areas from RIC (mass 57+ 97+98+111)

C_3 Thiophenes

Duration (s)	Temperature (°C)	2-isopropylthiophene (111)	3-isopropylthiophene (111)	2-propylthiophene (97)	2-Ethyl-4-methylthiophene (111)	2-Ethyl-5-methylthiophene (111)	C_3-Thiophene (111)	C_3-Thiophene (111)	Total C_3-Thiophene
2	425	182858	290217	607041	411721	958635	367446	295958	**3113876**
2	632	463744	764579	1276167	624379	2217649	777278	802972	**6926768**
2	834	349742	670752	1192548	861408	636106	823447	704062	**5238065**
2	1026	173818	302699	484322	548876	1097659	370525	452184	**3430083**
5	404	190879	390410	661324	872635	1191113	478974	354897	**4140232**
5	599	330995	525952	940417	535800	1550695	635690	86355	**4605904**
5	802	412304	768654	391258	1002109	2174586	873908	760509	**6383328**
5	1009	120020	229093	158399	401685	889190	354302	376217	**2528906**
20	438	414097	649134	1354671	742157	2059680	713083	736901	**6669723**
20	614	416706	708926	1305589	638605	2103048	872534	796208	**6841616**
20	801	219268	373728	680399	564233	1133802	455094	347414	**3773938**
20	992	35882	101567	196984	219920	428582	163044	201530	**1347509**
AMMs		36265	176616	193580	16157	118166	76909	30231	**647924**
Terrestrial Particles T2		35181	0	0	0	0	0	0	**35181**

C_3 thiophene peak areas from RIC (mass 57+97+98+111)

NITRILES

Duration (s)	Simulation Temperature (°C)	Benzonitrile (76)	Acetonitrile (38)
2	425	781143	15648072
2	632	8569759	52150717
2	834	11931281	54004690
2	1026	10454593	44850355
5	404	1037430	18577209
5	599	6710581	35539862
5	802	13155018	50729281
5	1009	9557534	34263006
20	438	3681079	38404974
20	614	13376216	50809881
20	801	9726237	30726065
20	992	6433948	22463411

Nitrile peak areas from RIC (mass 52+76+38)

NITROGEN AND SULPHUR-NITROGEN HETEROCYCLES

duration (s)	simulation temperature (°C)	Pyrrole (67)	Pyridine (67)	Pyrazine (80)	Pyrimidine (80)	Thiozole (80)
2	425	333864	0	103382	0	138792
2	632	2595804	6301803	657536	329017	1540415
2	834	6181503	8831086	956676	420684	1833200
2	1026	1813623	5385732	476634	322342	637699
5	404	745771	587210	109173	32620	404792
5	599	2111811	3912483	375904	236342	637699
5	802	3226006	7096591	891325	462843	1917747
5	1009	1537739	5245380	41901	338193	511886
20	438	2898904	3218140	389645	212012	1629427
20	614	2516231	9738204	863373	392484	1903355
20	801	1526544	6359428	315495	255886	893514
20	992	942297	3013236	249660	166709	221068

N- and S-N heterocycle peak areas from RIC (mass 67+80+94+107+108)

OXYGEN BEARING SPECIES

Duration (s)	Simulation temperature (°C)	Phenol (94)	Methyl phenol 1 (108)	Methyl phenol 2 (108)	Total C_1 - Phenol (108)	Benzaldehyde (106)
2	425	**239417**	17787	11988	**29775**	3831508
2	632	**2715614**	143959	262795	**406754**	5900231
2	834	**4134873**	178154	363480	**541634**	6527615
2	1026	**3493368**	140495	282025	**422520**	5274650
5	404	**299956**	27635	17906	**45541**	3679609
5	599	**1866227**	103632	154322	**257954**	4231309
5	802	**4163728**	234325	456901	**691226**	7352356
5	1009	**3222143**	160396	296110	**456506**	4231309
20	438	**1807707**	92741	142122	**234863**	6661659
20	614	**3112525**	144439	285098	**429537**	6472485
20	801	**2646456**	121577	225635	**347212**	4252441
20	992	**1869523**	91369	135982	**227351**	2485813
AMMs		**596396**	5183.9	9448.7	**14632.6**	-
Terrestrial particles T2		**497733**	0	0	**7691.2**	-

O-bearing species peak areas from RIC (57+94+106+108)

PAHs

Core PAHs

Time (s)	Simulation Temperature (°C)	Naphthalene (128)	Acenaphthylene (152)	Acenaphthene (153)	Phenanthrene (178)	Anthracene (178)	Pyrene (202)	Fluoranthene (202)
2	395	7189736	220465	52919	5642.3	28433	42253	33742
2	598	17867370	433498	79390	582480	105204	462229	390255
2	829	9187595	335288	62645	303515	65955	112727	72303
2	1005	21852704	561562	75261	887330	183427	278332	220958
5	396	6544594	208024	41752	270874	44576	45178	55827
5	505	14093845	457946	68881	138332	683557	209176	164882
5	805	28185672	942470	150585	888655	186498	218356	179420
5	999	21121971	647299	87883	546042	120328	142670	114970
20	420	8139751	333778	57020	437612	88721	94750	72734
20	634	15349402	422673	66607	581585	120027	162709	131380
20	810	15145936	537840	64620	688112	145488	186453	151340
20	962	8860999	350271	44813	484740	108975	148759	118791

Core PAH peak areas from RIC (mass128+152+153+178+202)

C_1 Naphthalenes

Duration	Simulation Temperature (°C)	**1-methylnaphthalene (142)**	2-methylnaphthalene (142)	**Total C_1 Naphthelenes**
2	395	**197469**	357845	**555314**
2	598	**557975**	971952	**1529927**
2	829	**313369**	497710	**811079**
2	1005	**769548**	1234292	**2003840**
5	396	**188279**	344384	**532663**
5	505	**486210**	853881	**1340091**
5	805	**1023636**	1712435	**2736071**
5	999	**844114**	1256384	**2100498**
20	420	**279697**	521982	**801679**
20	634	**458969**	824595	**1283564**
20	810	**510358**	876567	**1386925**
20	962	**354300**	580574	**934874**

C_1 naphthalene peak areas derived from RIC (mass 142)

C_2 Naphthalenes

Duration (s)	Simulation temperature (°C)	1,2-dimethylnaphthalene	1,3 dimethylnapthalene	1,4 &2,3 dimethylnaphthalene	1,5-dimethylnaphthalene	1,6-dimethylnaphthalene	1,7-dimethylnaphthalene	1,8-dimethylnaphthalene	2,6-dimethylnaphthalene	2,7-dimethylnaphthalene	**Total C_2 Naphthalene**
2	395	18541	2572.6	11402	12724	24690	29417	1212.7	26467	5755.4	**132781.7**
2	598	39125	13235	52377	9767.3	40542	85574	3402.9	23066	59174	**326263.2**
2	829	27788	7209.4	22862	6084	23604	62867	2139.1	13188	33741	**199482.5**
2	1005	62508	39232	70271	24981	47195	116062	4867	50026	56038	**471180**
5	396	13707	3426.4	23609	3565.6	15707	39351	1235.1	30497	4660.7	**135758.8**
5	505	44500	2882.1	56043	8996.1	39190	107526	3109	21800	53337	**337383.2**
5	805	67995	7314.4	117325	42625	77816	222899	7350.6	43119	94759	**681203**
5	999	51319	3716.3	68589	33970	54772	162585	3658.1	29554	61225	**469388.4**
20	420	22014	5501.3	39184	6599.7	37846	48083	2199.2	13245	39812	**214484.2**
20	634	32808	2621.6	53678	8030	37266	84792	3318	20060	49173	**291746.6**
20	810	35949	10557	35705	9836.1	40555	104507	3527.4	30107	58669	**329412.5**
20	962	25060	5865.5	46586	7210.6	28657	76071	2674.6	12649	43293	**248066.7**

C_2 naphthalene peak areas of mass 141 from TIC

C_3 Naphthalenes

Duration (s)	Simulation temperature (°C)	1,3,7-trimethylnaphthalene (170)	1,3,6 trimethylnaphthalene (170)	1,3,5- & 1,4,6- & 2,3,6-trimethylnaphthalene (170)	1,6,7- & 1,2,6- & 1,2,7-trimethylnaphthalene (170)	1,2,4-trimethylnaphthalene (170)	1,2,5-trimethylnaphthalene (170)	**Total C_3 naphthalenes**
2	395	2460.6	2923.1	6145.8	3946.7	1417.8	0	**16894**
2	598	7109.8	7961.7	16351	12901	3351.3	2393.8	**50068.6**
2	829	5899.9	4519	10493	6500.4	1836.4	1032	**30280.7**
2	1005	11147	11781	21313	17586	4537.4	3807	**70171.4**
5	396	3769.8	3394.5	5962.2	4906.1	900.06	0	**18932.66**
5	505	9725.3	7741.8	15317	11985	2597.3	1946.9	**49313.3**
5	805	22047	17164	27642	21260	4465	3133.5	**95711.5**
5	999	13278	8979.6	19518	13930	3496.8	2401	**61603.4**
20	420	4879.9	5165.9	7044.9	7501.1	1522.2	1515.1	**27629.1**
20	634	8801.8	8111.6	15223	11579	2324.7	1676.4	**47716.5**
20	810	8890.9	7862	16916	13062	2415.5	2113.3	**51259.7**
20	962	9273.5	5935.5	13785	11725	1884.5	1438.8	**44042.3**

C_3 naphtalene TIC peak areas

Appendix III: Micrometeorite SEM Analysis

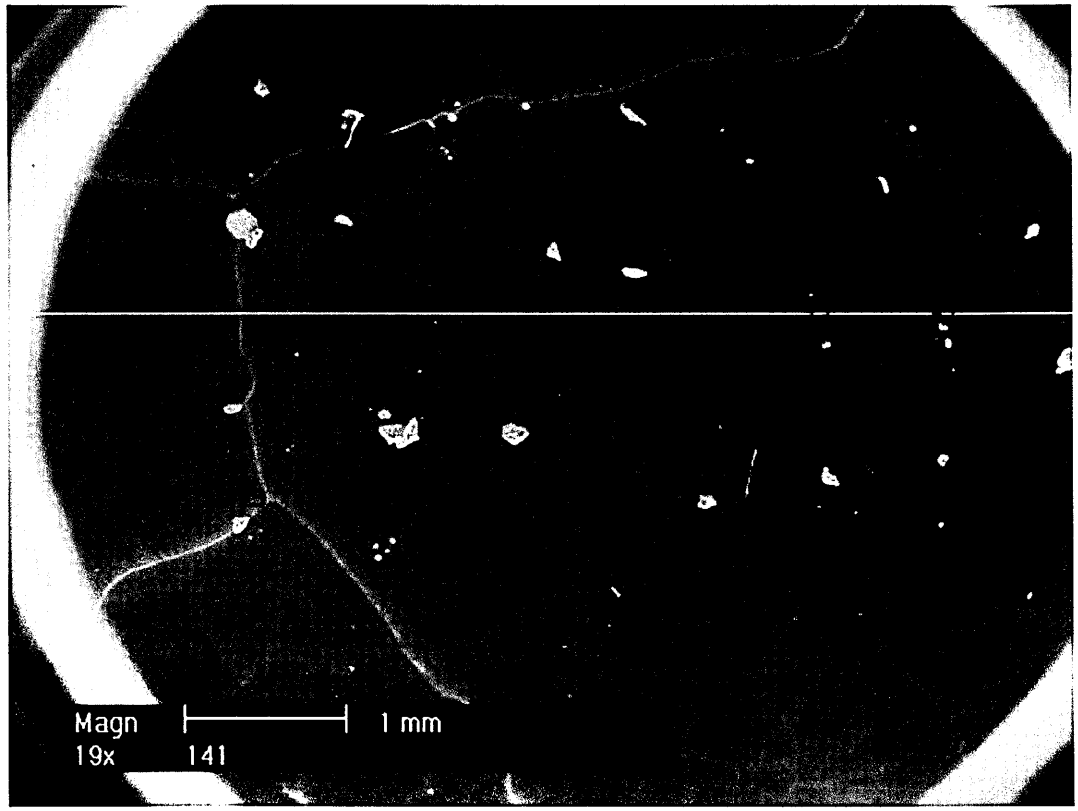

22

A back scattered electron image of the stub comprising 24 particles

The scanning electron microscope analyses in this appendix were conducted by Elena Dobrica, CSNSM CNRS-Univ. Paris Sud, 91405 Orsay Campus. Above is a back scattered electron image of the whole stub, comprising 24 particles. Below, a backscattered electron image (left), secondary electron image (right) and energy dispersive x-ray spectrum (bottom) for each particle is given. From these, it was established which of 24 Antarctic dark particles separated from sample #141 were terrestrial and which were extraterrestrial.

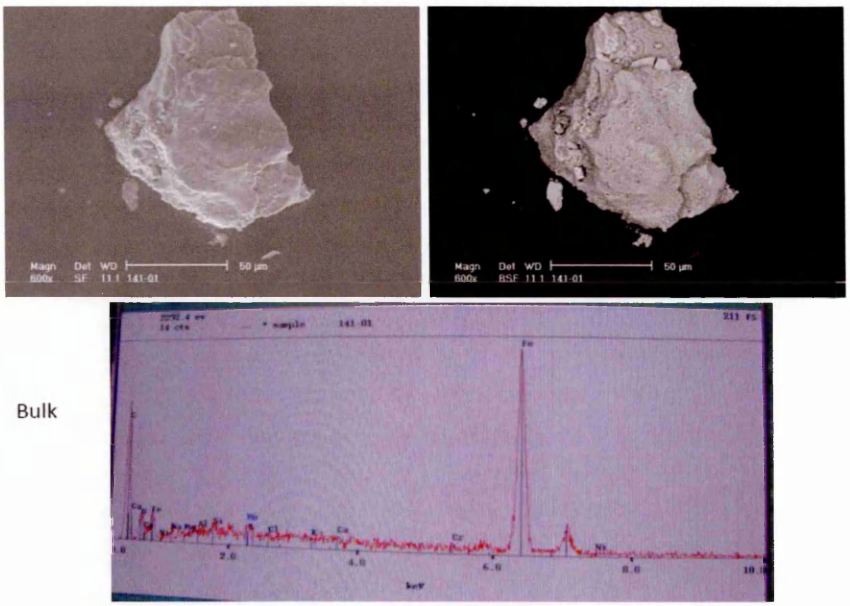

Particle 1 = Terrestrial

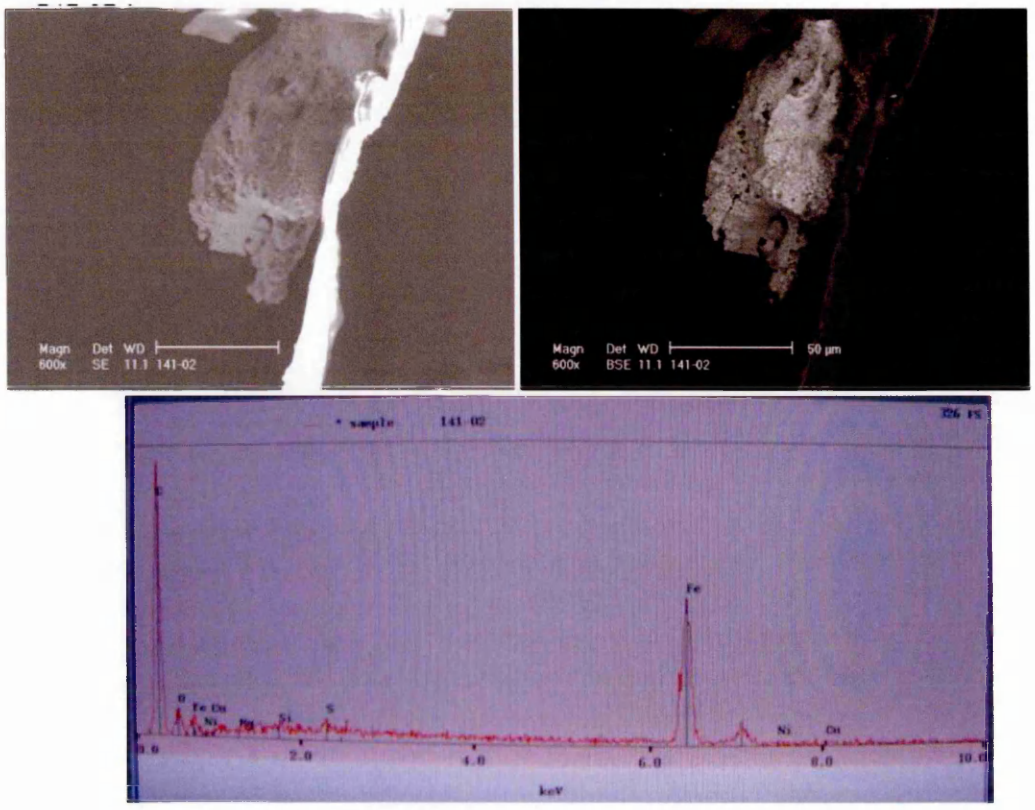

Particle 2 = Terrestrial

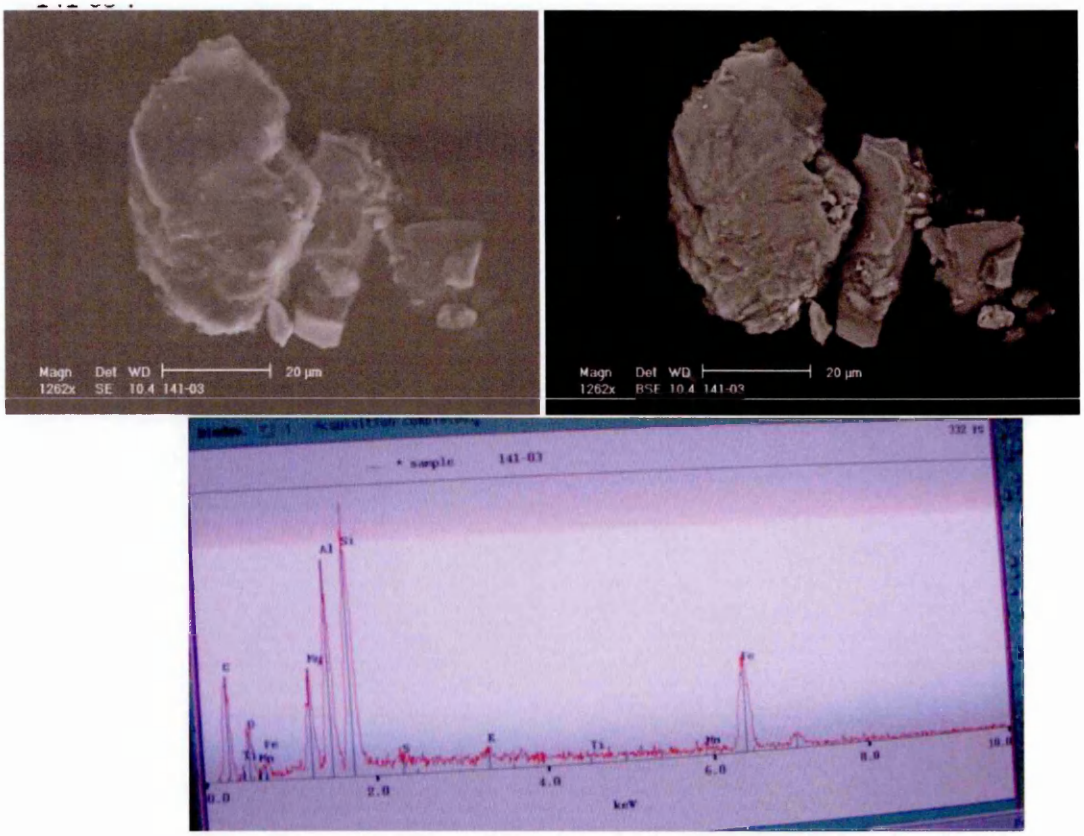

Particle 3 = Terrestrial

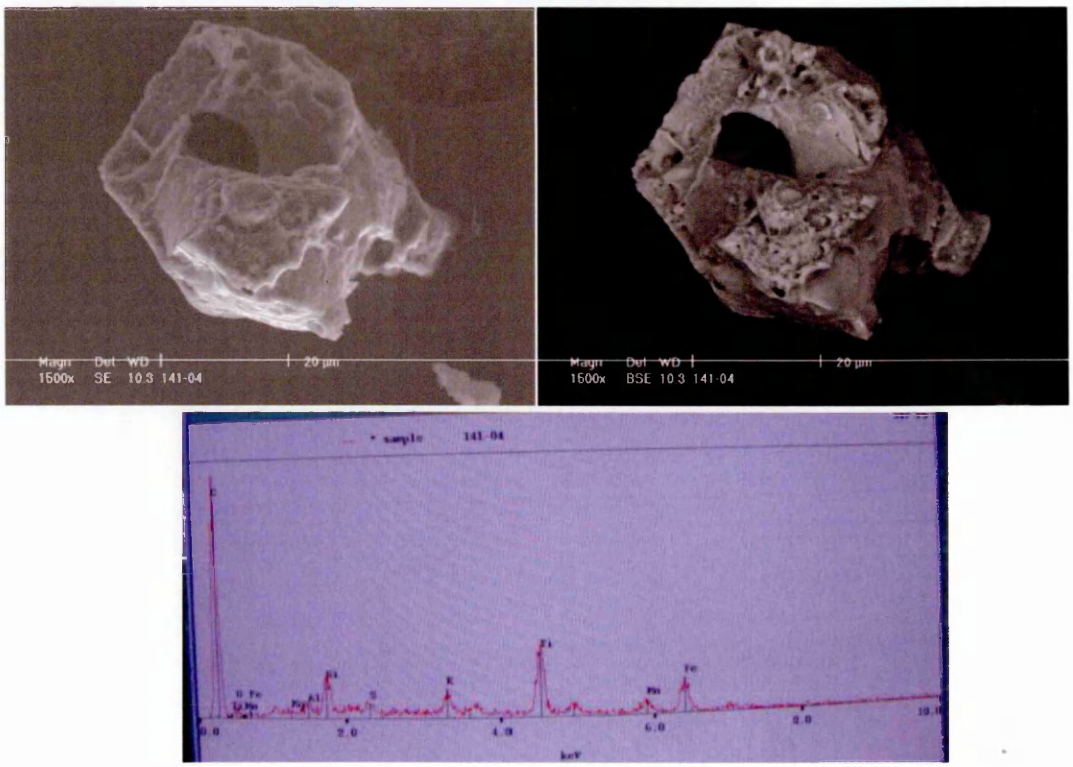

Particle 4 = Terrestrial

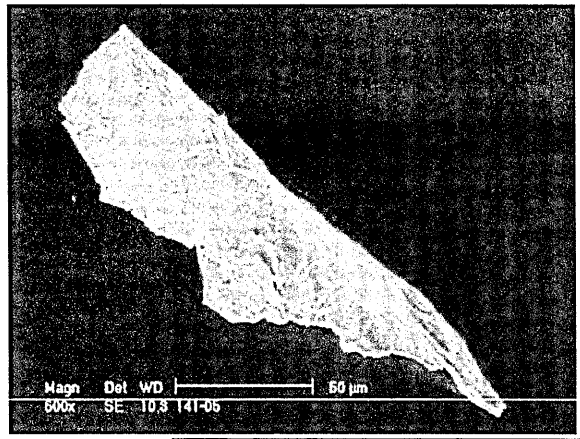

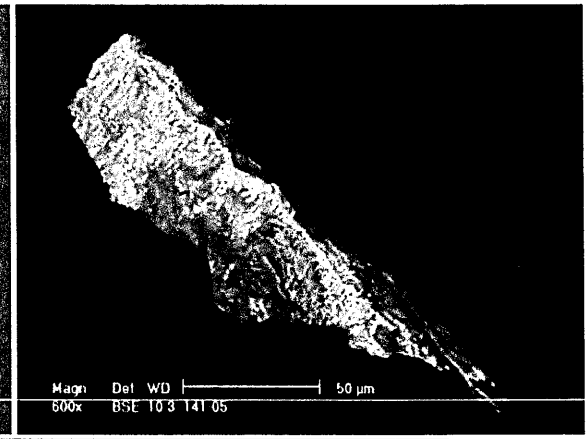

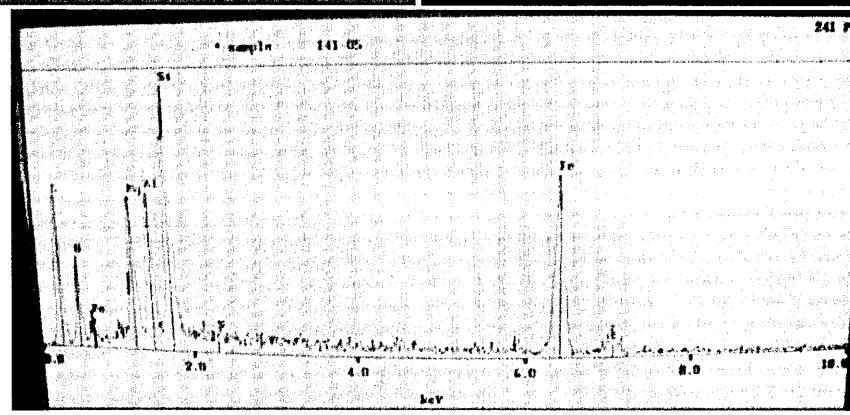

Particle 5 = Terrestrial

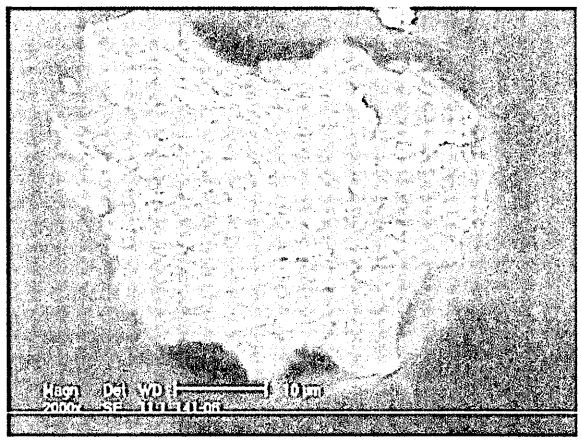

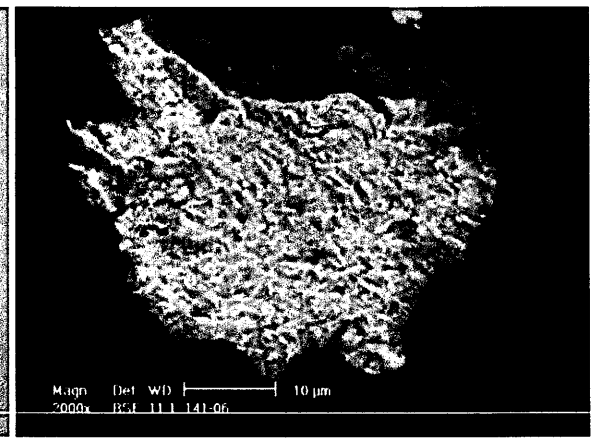

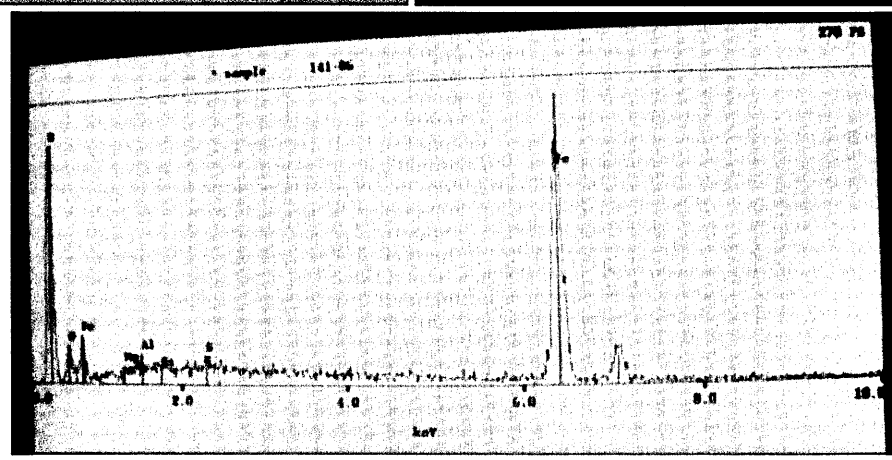

Particle 6 = Terrestrial

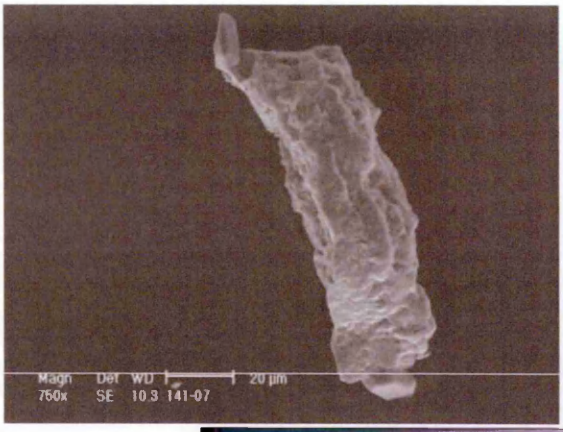

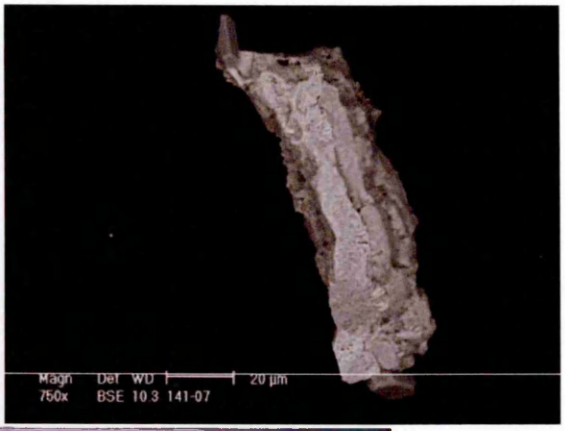

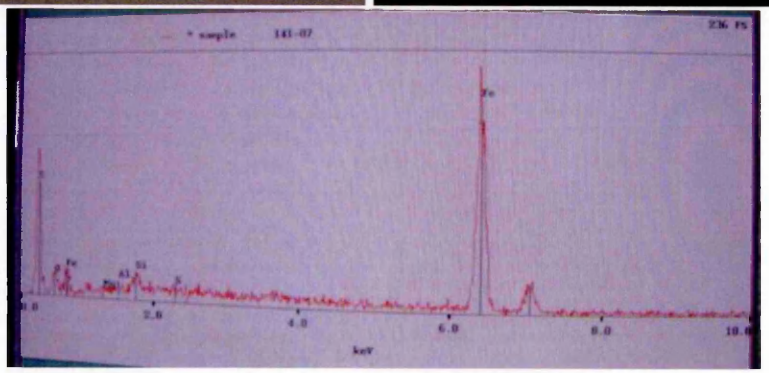

Particle 7 = Terrestrial

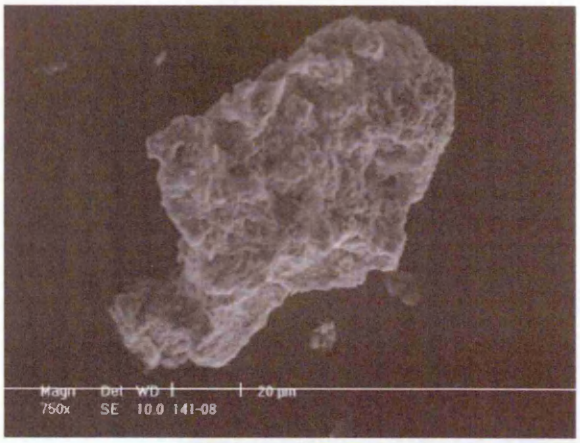

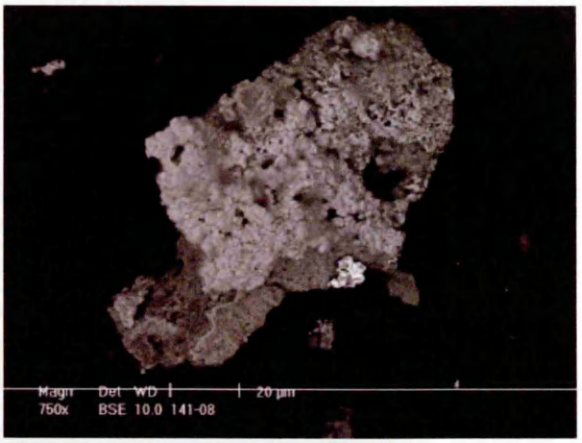

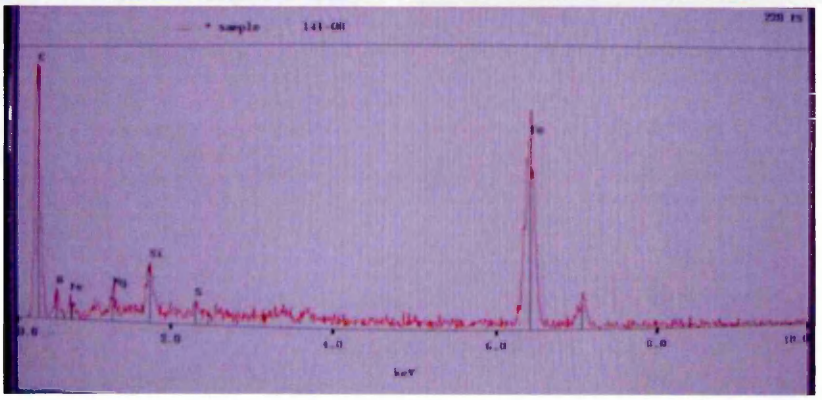

Particle 8 = Extraterrestrial

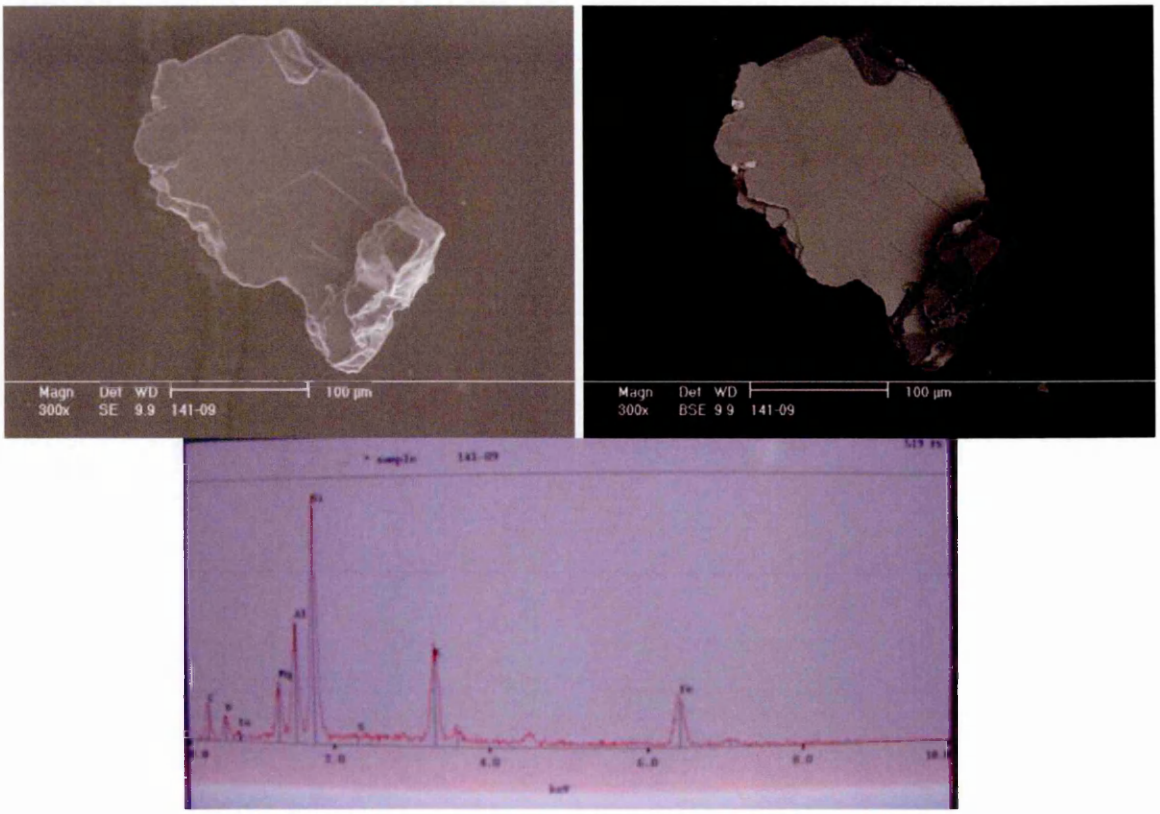

Particle 9 = Terrestrial

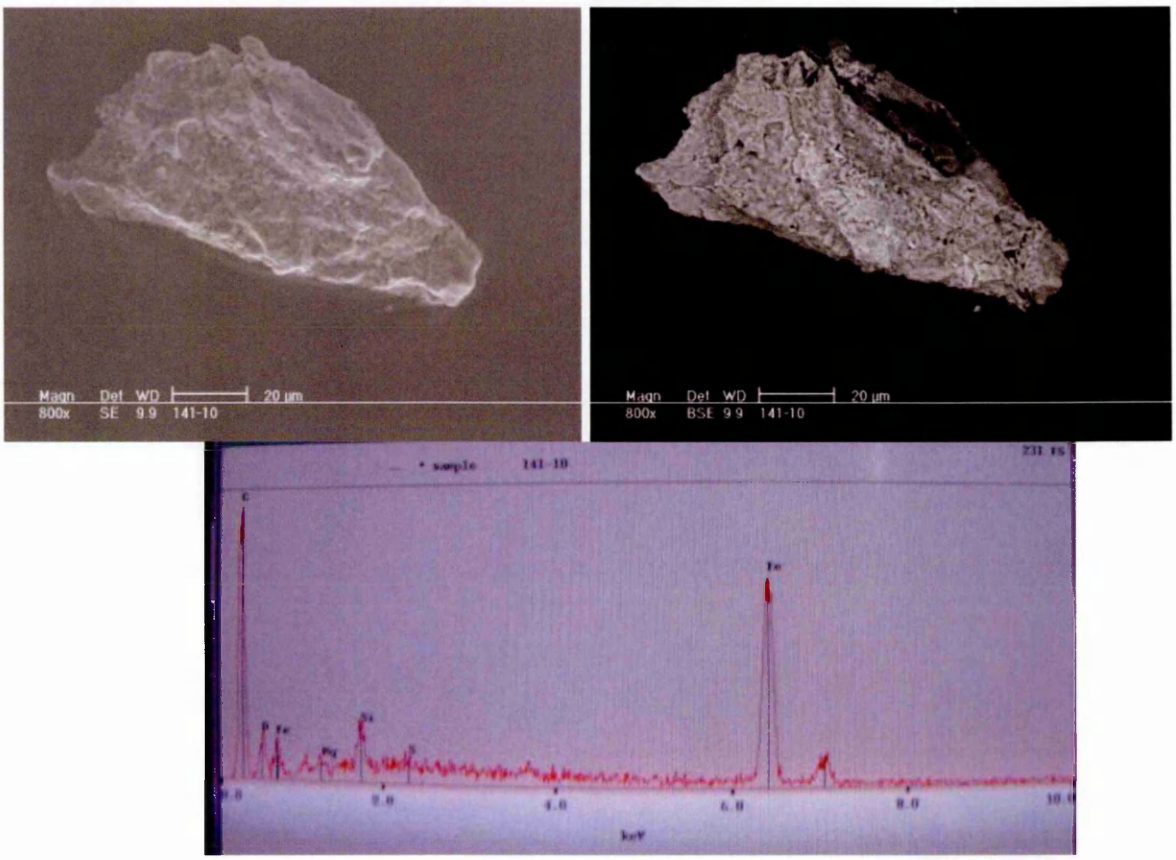

Particle 10 = Terrestrial

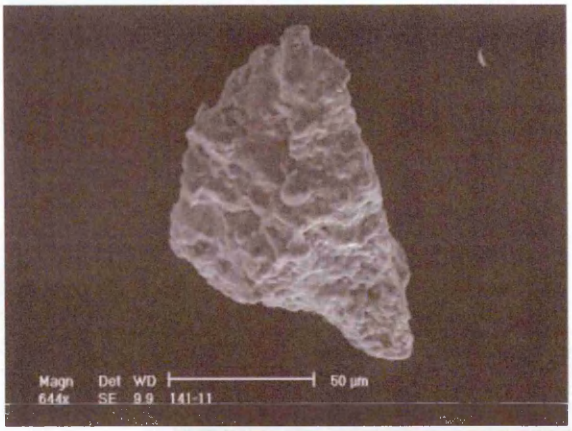

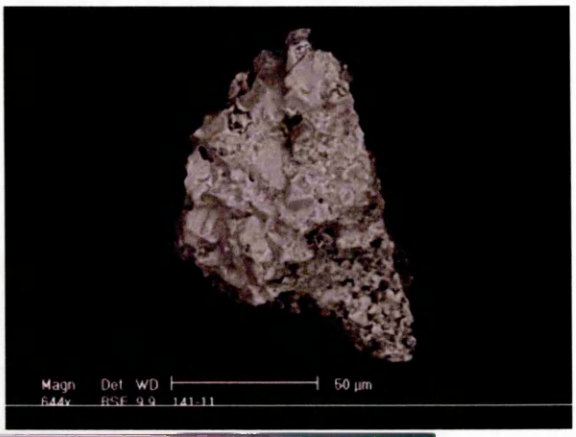

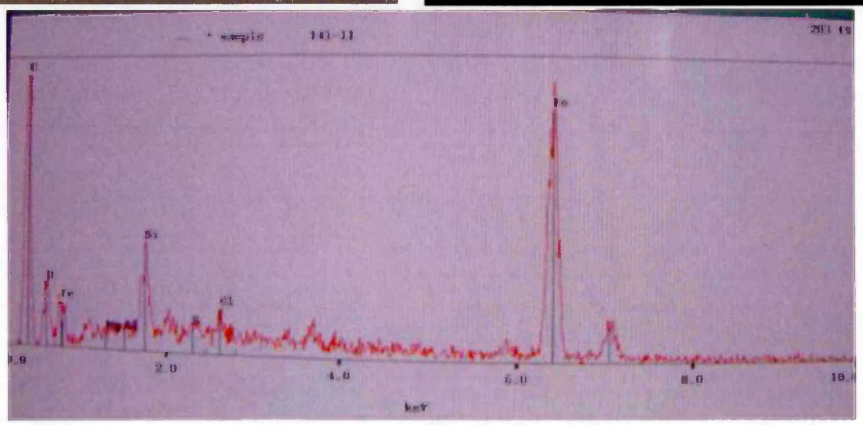

Particle 11 = Terrestrial

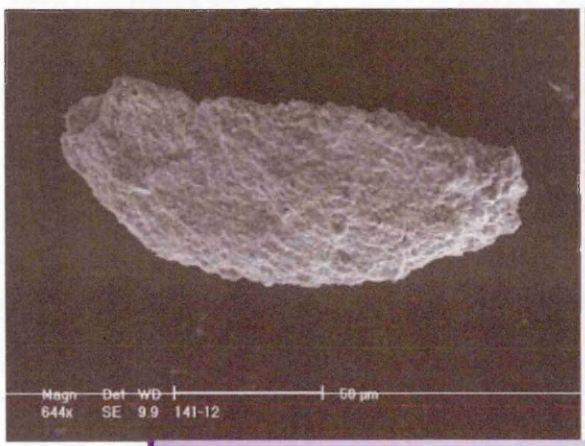

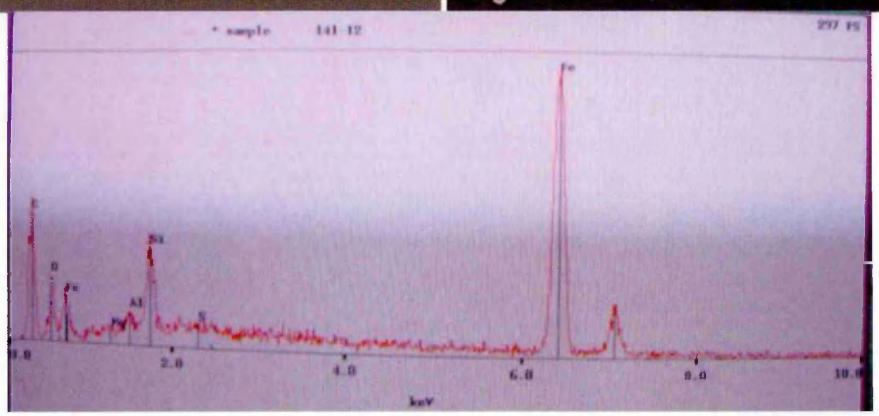

Particle 12 = Terrestrial

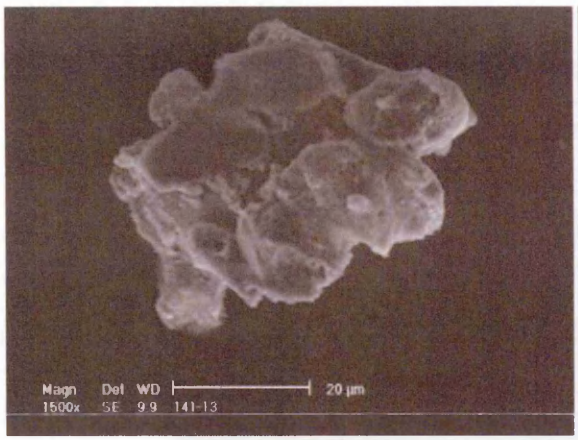

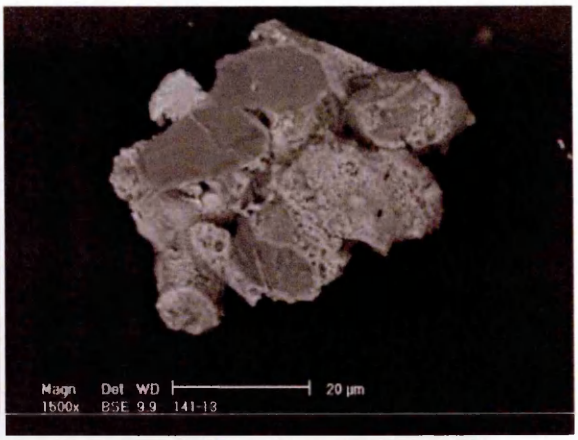

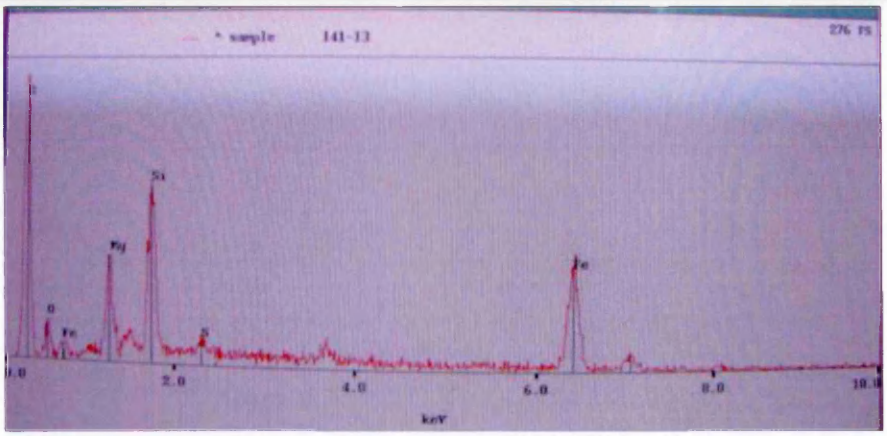

Particle 13 = Extraterrestrial

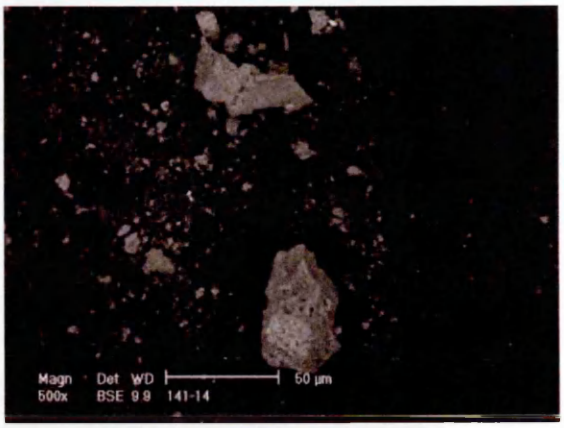

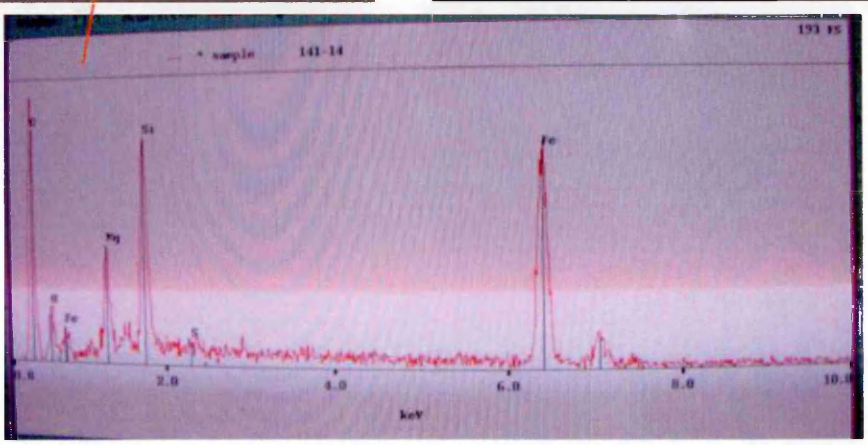

Fragments of particle 14 = Extraterrestrial

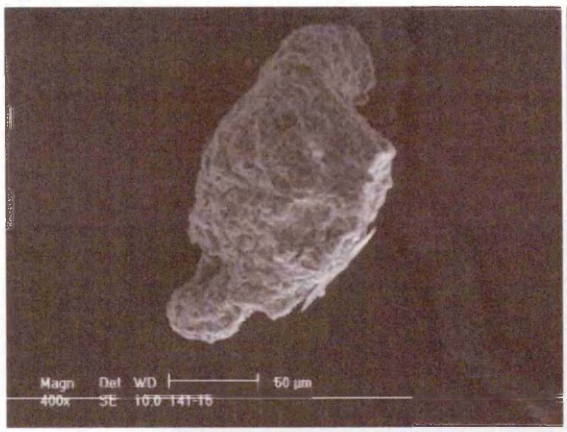

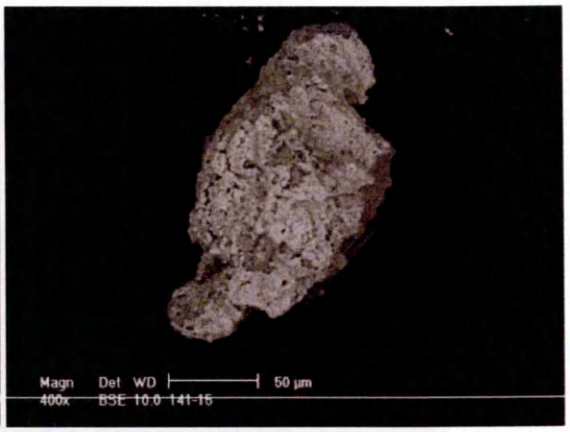

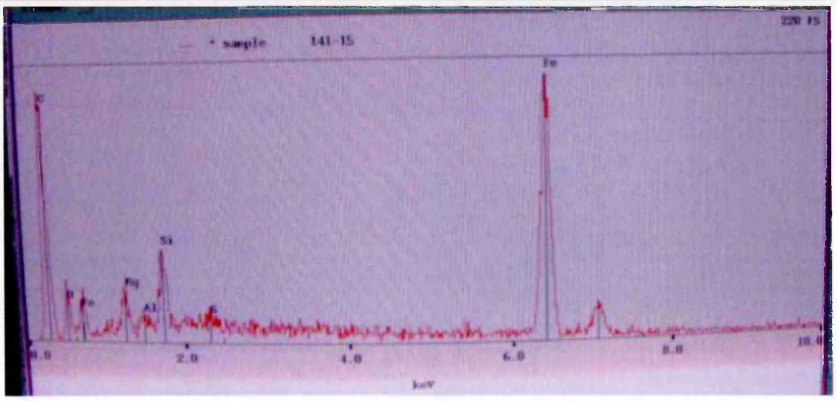

Particle 15 = Extraterrestrial

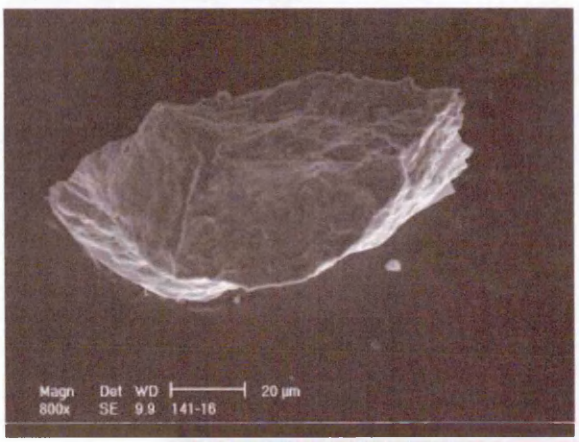

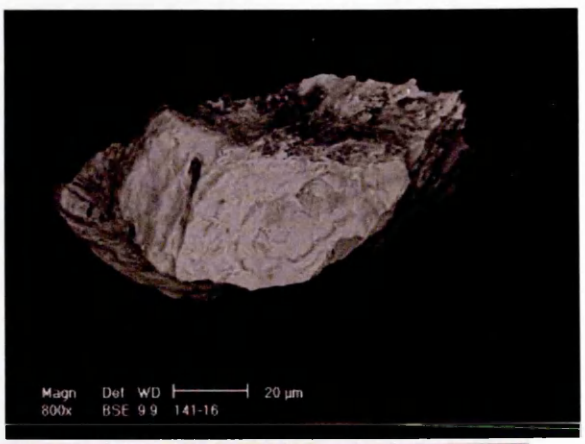

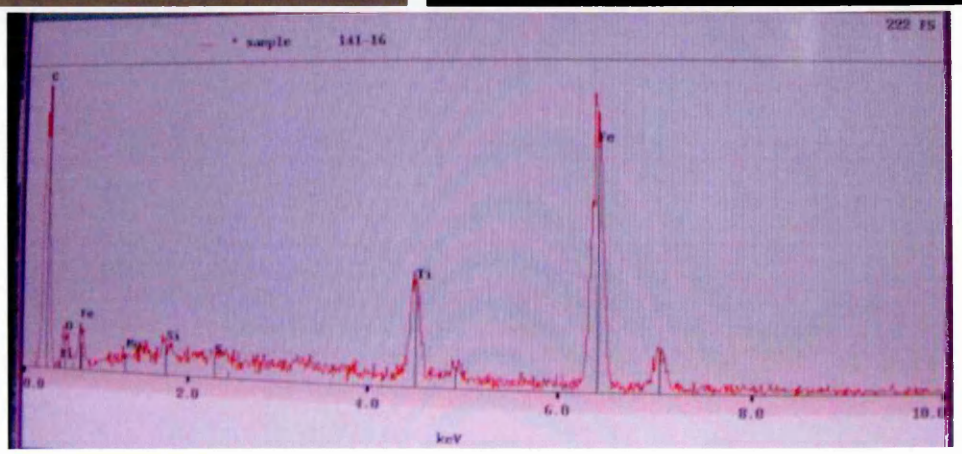

Particle 16 = Terrestrial

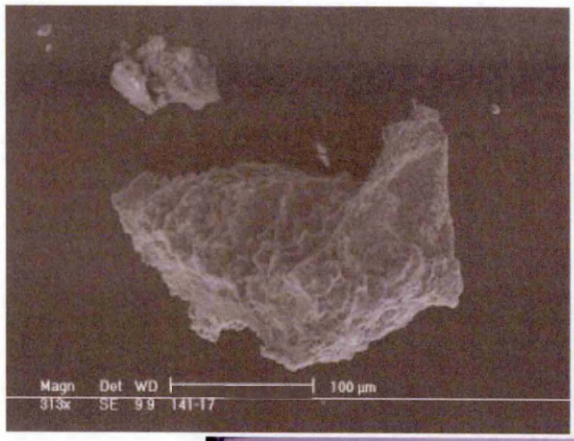

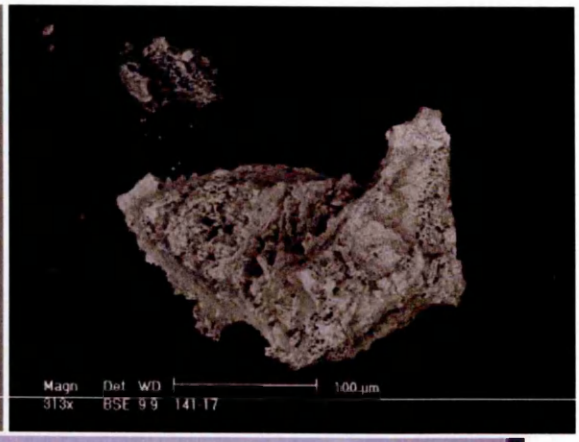

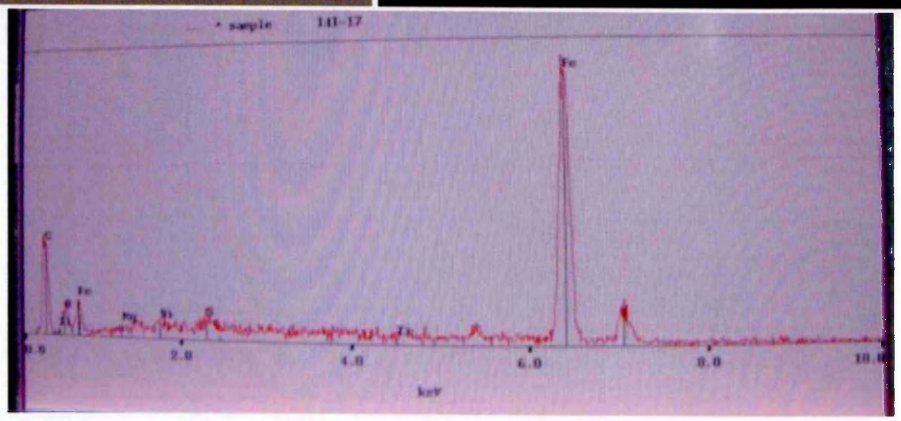

Particle 17 = Terrestrial

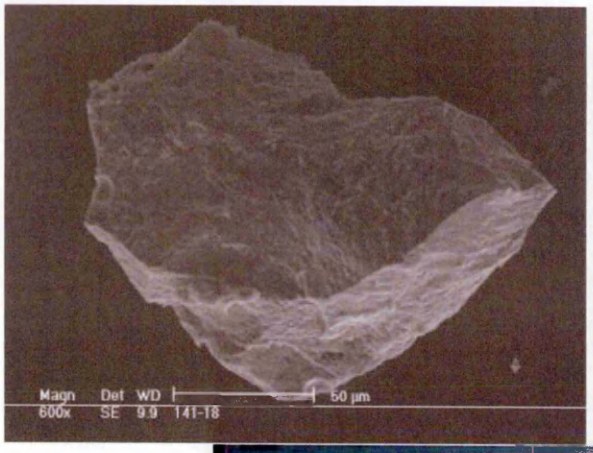

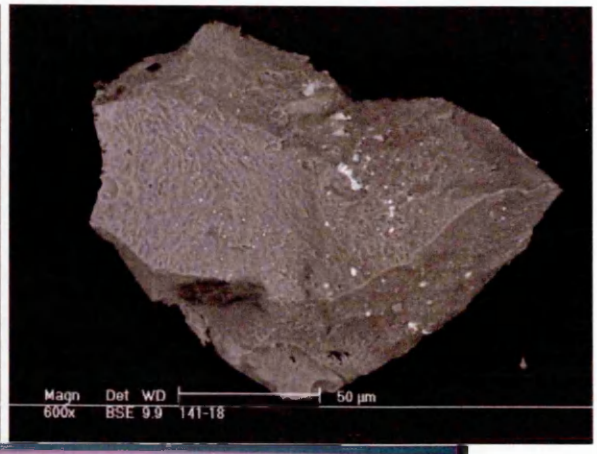

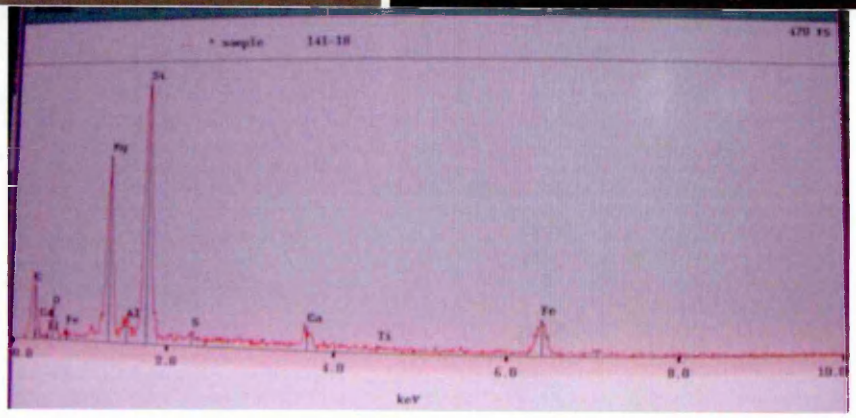

Particle 18 = Extraterrestrial

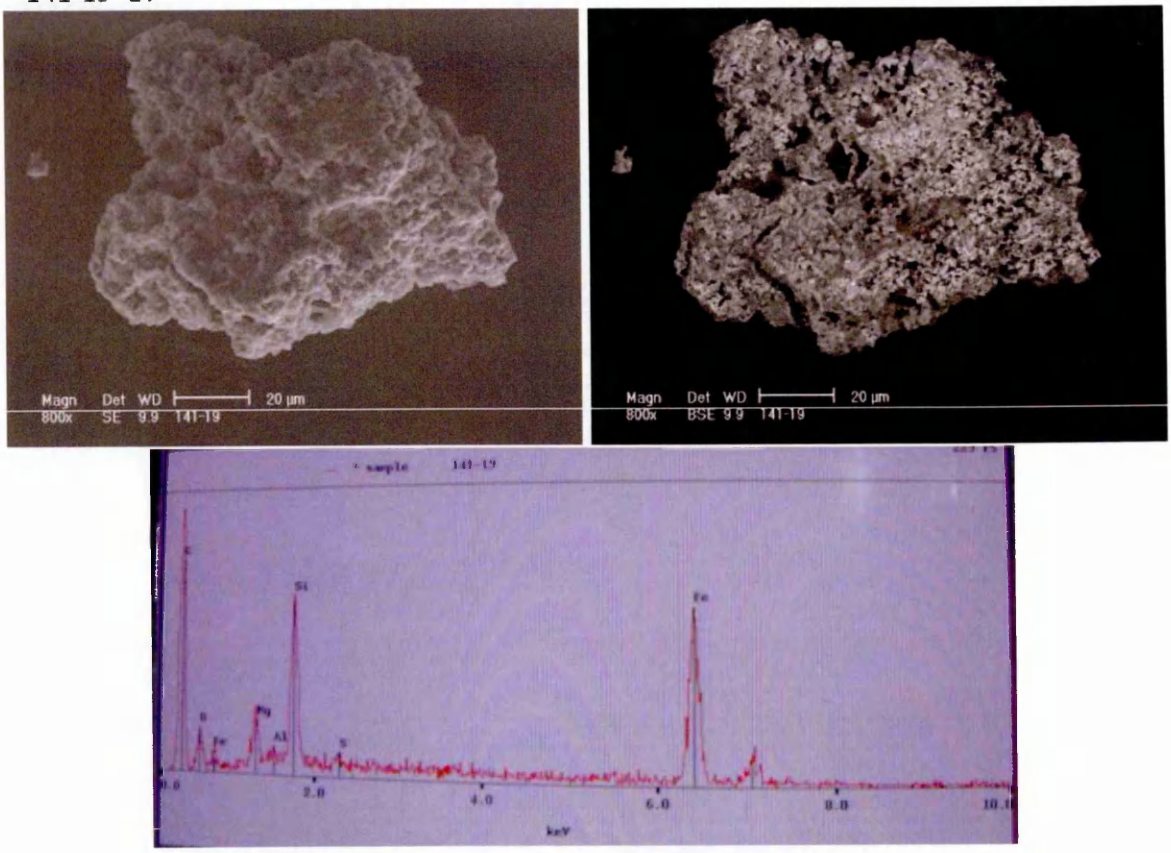

Particle 19 = Extraterrestrial

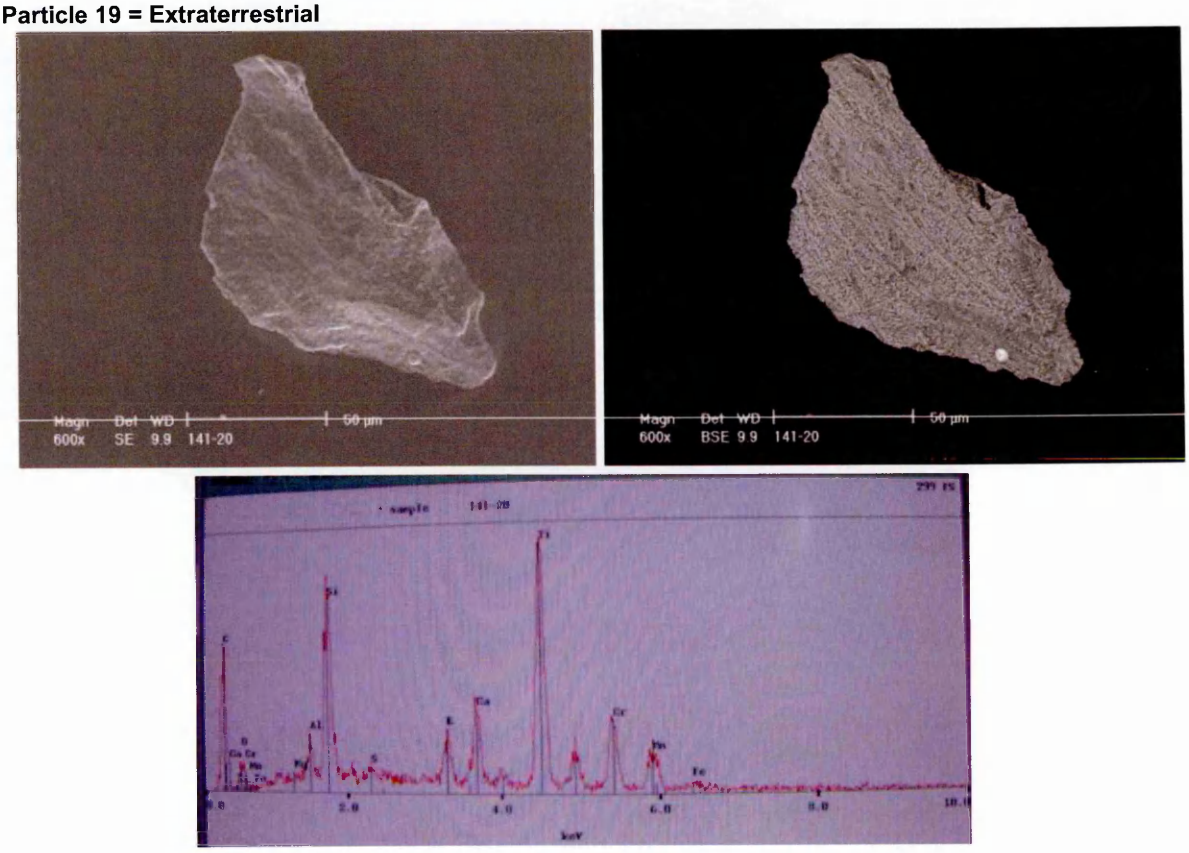

Particle 20 = Terrestrial

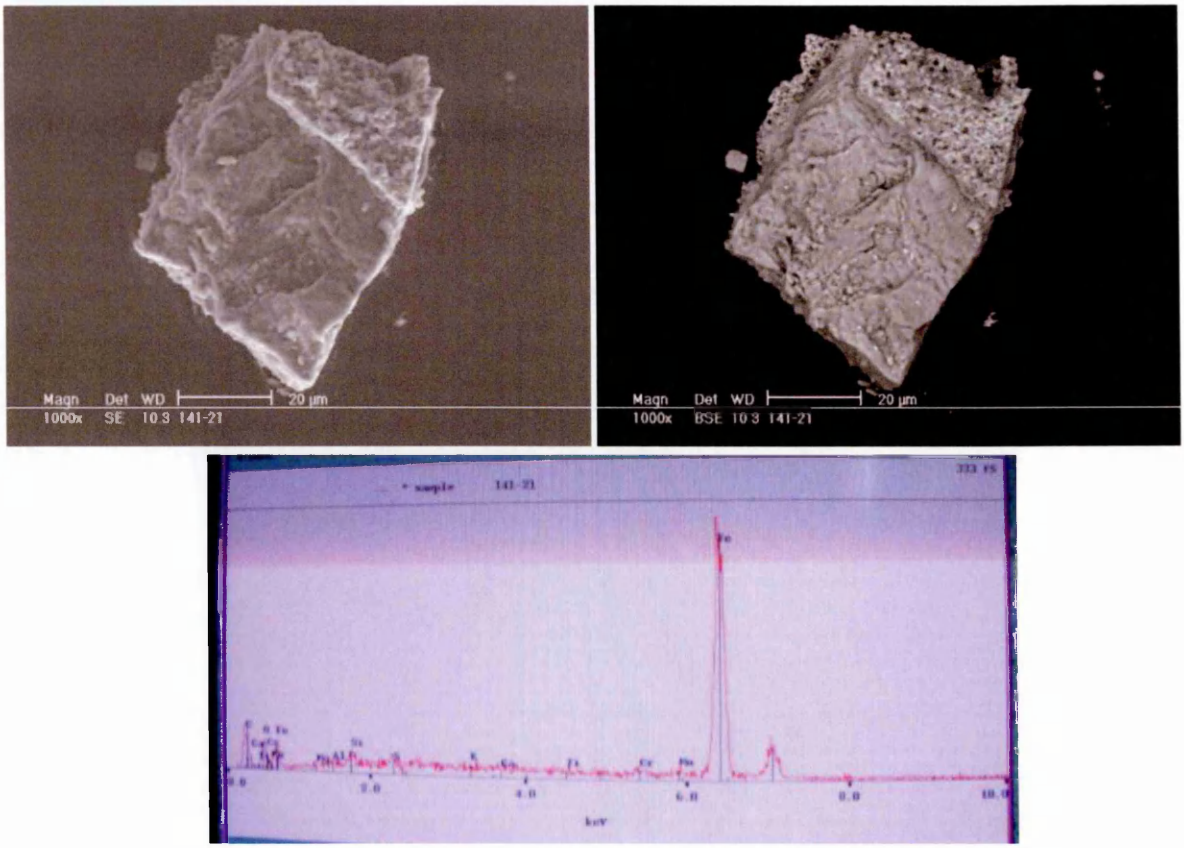

Particle 21 = Terrestrial

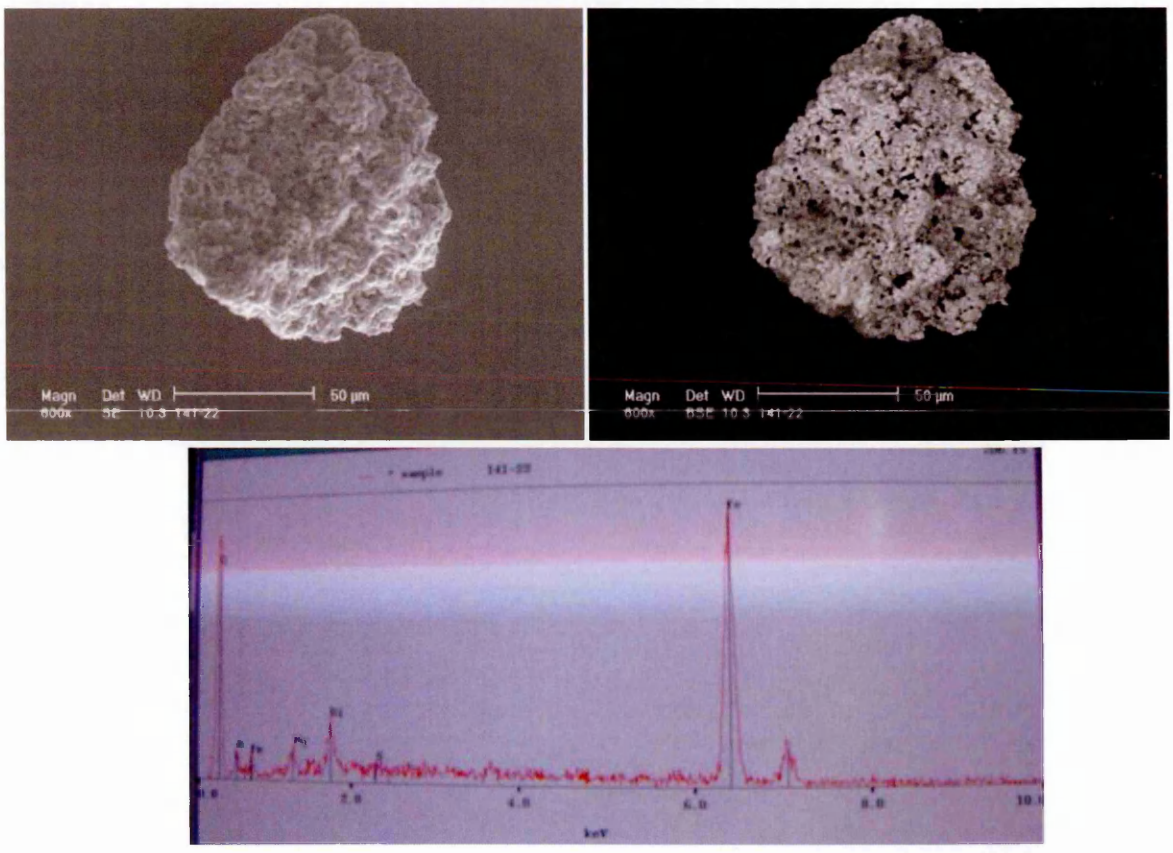

Particle 22 = Extraterrestrial

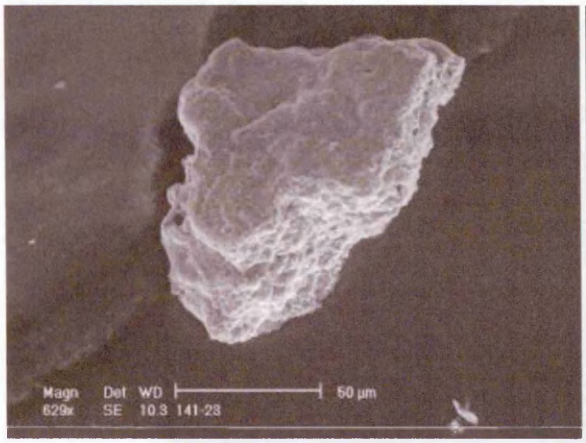

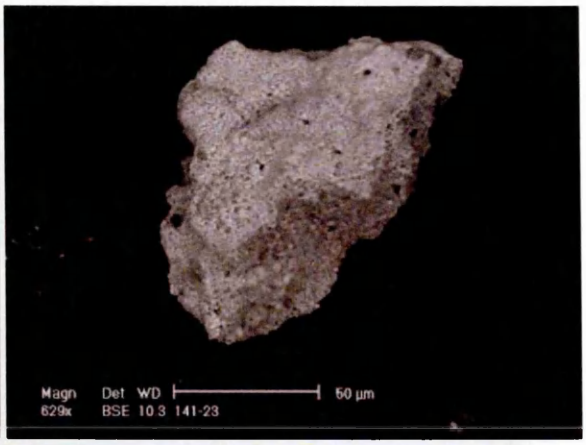

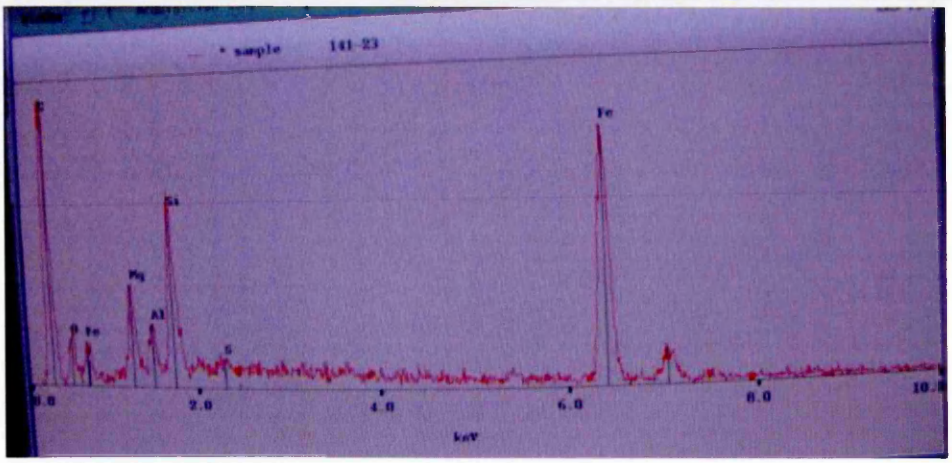

Particle 23 = Extraterrestrial

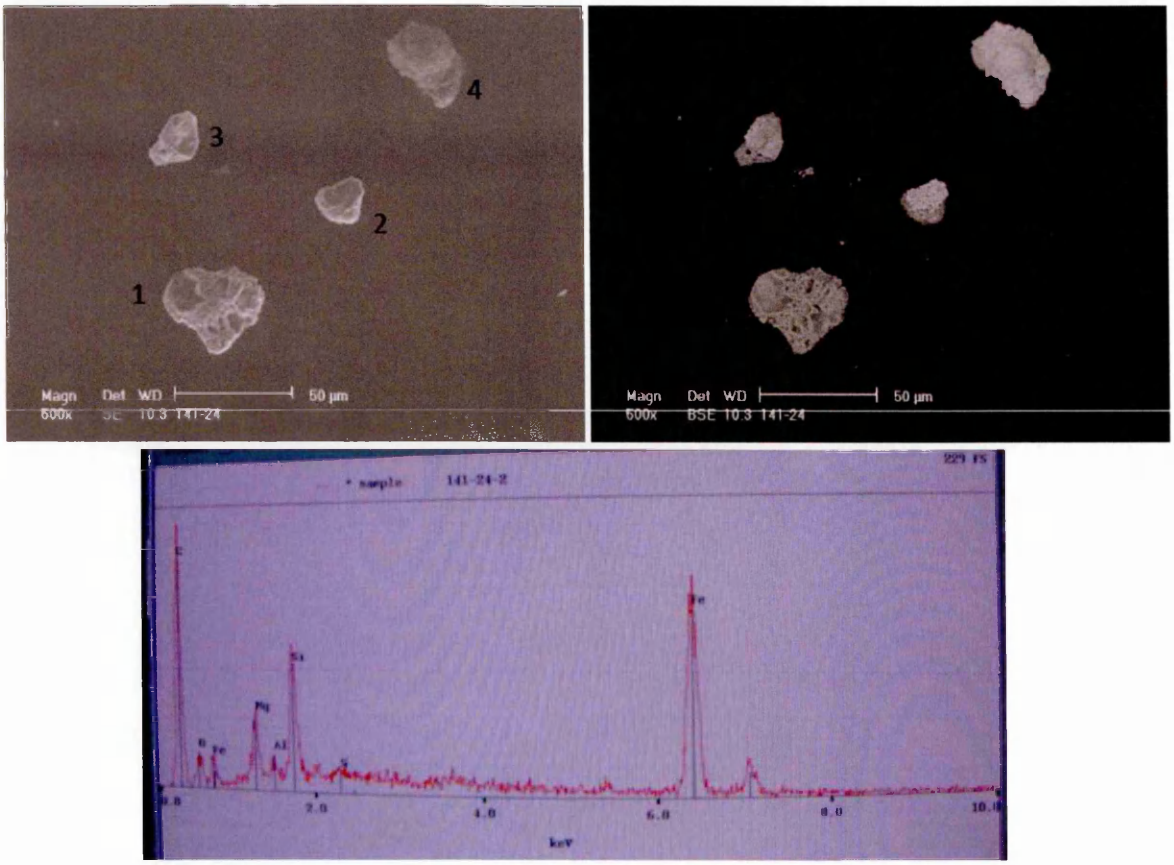

Four fragments of particle 24 = Extraterrestrial

Appendix IV: Antarctic Particle Masses

Fragments of AMMs and terrestrial particles prepared for organic analysis, were imaged under a light microscope in order to determine particle diameter. Assuming Antarctic particles are spherical the volume of particle fragments was calculated. With an average density as outlined in the tables below, the mass was subsequently determined.

Calculation of AMM fragment masses

Sample fragment	radius (μm)	radius (m)	volume (m^3) ^	density (kg/m^3)*	Mass (kg)
A1 1a	88	8.80E-05	2.85E-12	2100	5.99E-09
A1 1b	124	1.24E-04	7.99E-12	2100	1.68E-08
A1 2	95	9.50E-05	3.59E-12	2100	7.54E-09
A2	175	1.75E-04	2.24E-11	2100	4.71E-08
A3 1	113	1.13E-04	6.04E-12	2100	1.27E-08
A3 2	120	1.20E-04	7.24E-12	2100	1.52E-08
A6 1	110	1.10E-04	5.58E-12	2100	1.17E-08
A6 2	157	1.57E-04	1.62E-11	2100	3.40E-08
A7 2a	51	5.10E-05	5.56E-13	2100	1.17E-09
A7 2b	62	6.20E-05	9.98E-13	2100	2.10E-09
a7 1a	102	1.02E-04	4.45E-12	2100	9.33E-09
a7 1b	51	5.10E-05	5.56E-13	2100	1.17E-09
a7 1c	47	4.70E-05	4.35E-13	2100	9.13E-10
a7 1d	51	5.10E-05	5.56E-13	2100	1.17E-09
a7 1e	51	5.10E-05	5.56E-13	2100	1.17E-09
A10 1	131	1.31E-04	9.42E-12	2100	1.98E-08
A10 2	168	1.68E-04	1.99E-11	2100	4.17E-08
A11	113	1.13E-04	6.04E-12	2100	1.27E-08
A12 1	110	1.10E-04	5.58E-12	2100	1.17E-08
A12 2	120	1.20E-04	7.24E-12	2100	1.52E-08
				total estimated MM mass (kg)	2.69E-07
				total estimated MM mass (mg)	**2.69E-01**

Assumptions

^ particles assumed to be spherical

*** assumed density of 2100 kg/m^3 based on (Tsuchiyama et al., 2004)**

Theoretical maximum mass of 8 particles of 400um diameters

Sample fragment	radius (μm)	radius (m)	volume (m^3) ^	density (kg/m^3)*	Mass	
Maximum mass	200	2.00E-04	3.35E-11	2100	7.04E-08	kg
				Max mass one particle	7.04E-02	mg
				Mass of 8 particles	**0.56**	**mg**

Calculation of Antarctic terrestrial fragment masses

Sample	radius (μm)	radius (m)	volume (m^3)	Density (kg/m^3) **	Mass (kg)
B1 1	248	2.48E-04	6.39E-11	2700	1.73E-07
B1 2a	128	1.28E-04	8.78E-12	2700	2.37E-08
B1 2b	113	1.13E-04	6.04E-12	2700	1.63E-08
B2 a	197	1.97E-04	3.20E-11	2700	8.65E-08
B2 b	84	8.40E-05	2.48E-12	2700	6.70E-09
B3	245	2.45E-04	6.16E-11	2700	1.66E-07
B5	226	2.26E-04	4.84E-11	2700	1.31E-07
B6 1a	218	2.18E-04	4.34E-11	2700	1.17E-07
B6 1b	145	1.45E-04	1.28E-11	2700	3.45E-08
B6 2	107	1.07E-04	5.13E-12	2700	1.39E-08
B6 3	111	1.11E-04	5.73E-12	2700	1.55E-08
B9	200	2.00E-04	3.35E-11	2700	9.05E-08
B10 1	104	1.04E-04	4.71E-12	2700	1.27E-08
B10 2	111	1.11E-04	5.73E-12	2700	1.55E-08
B11	293	2.93E-04	1.05E-10	2700	2.84E-07
				total estimated T2 mass (kg)	1.19E-06
				total estimated T2 mass (mg)	**1.19E+00**

Theoretical maximum mass of 8 particles of 400um diameters

Sample	radius (μm)	radius (m)	volume (m^3)	Density (kg/m^3) **	Mass	
Maximum mass	200	2.00E-04	3.35E-11	2700	9.05E-08	kg
				Max mass one particle	0.091	mg
				Maximum mass of 8 terrestrial particles (mg)	**0.72**	**mg**

** assumed density of Earths crust

The discrepancy between theoretical maximum mass for 8 particles and the total T2 mass may be due to T2 particles not being spherical as is assumed in the calculation.

Sample	Mass of 18 play sand particles (mg)
1	1.38
2	1.42
3	1.56
4	1.59
Average	**1.49**
2σ	**0.21**

The average mass of 18 play sand particles taken from four measurements

Appendix V – EDP Volatile Flux Calculations

. Experimental simulations (Section 3.4) identified the following percentage mass losses in H_2O, CO_2 derived from organic material and CO_2 derived from the decomposition of carbonate minerals Table 26 is duplicated below).

Duration (s)	Peak Temperature (°C)	Retained in Samples[1]			Released during simulations[2]		
		H_2O (wt. %)	CO_2: organic material (wt. %)	CO_2: inorganic (wt. %)	H_2O (wt. %)	CO_2: organic material (wt. %)	CO_2: inorganic (wt. %)
0[3]	0	8.6	2.2	4.0	n/a	n/a	n/a
2	406 ± 8	6.8	1.7	4.0	1.8	0.5	0.0
2	603 ± 9	5.9	1.5	4.0	2.7	0.7	0.0
2	814 ± 13	0.2	0.1	3.7	8.4	2.1	0.3
2	1006 ± 59	0.0	0.0	1.0	8.6	2.2	3.0
5	409 ± 12	7.2	1.8	4.4	1.4	0.4	-0.5
5	599 ± 16	3.5	0.9	4.3	5.1	1.3	-0.3
5	790 ± 18	0.1	0.0	3.2	8.6	2.1	0.8
5	1003 ± 30	0.0	0.0	0.7	8.6	2.2	3.3

Table 26, Chapter3: Calculated percentages of water, organic carbon and inorganic carbon based on thermogravimetric measurements of evolved gases from heated samples (1) and the average of duplicate Murchison reference sample (3). The percentage of water, organic carbon and inorganic carbon released during simulations (2) is determined by comparison between flash heated samples and the average composition of duplicate Murchison reference samples (3)

The table below applies the measured mass losses of Table 26 (Chapter 3) to the early Earth flux of carbon/volatile-bearing EDPs (calculated in Section 5.2.2 as 3.4×10^{12} kg/yr). Subsequently, the table below estimates the quantity (kg/yr) of H_2O and CO_2 (derived from organic material and carbonates) delivered to the early Earth.

Duration (s)	Peak Temperature (°C)	Retained in Samples (kg/yr)			Released during simulations (kg/yr)		
		H_2O	CO_2: organic material	CO_2: inorganic	H_2O	CO_2: organic material	CO_2: inorganic
0	0	2.9E+11	7.4E+10	1.3E+11	0.0E+00	0.0E+00	0.0E+00
2	406 ± 8	2.3E+11	5.7E+10	1.3E+11	6.0E+10	1.7E+10	0.0E+00
2	603 ± 9	2.0E+11	5.0E+10	1.3E+11	9.1E+10	2.3E+10	0.0E+00
2	814 ± 13	6.7E+09	3.4E+09	1.2E+11	2.8E+11	7.0E+10	1.0E+10
2	1006 ± 59	0.0E+00	0.0E+00	3.4E+10	2.9E+11	7.4E+10	1.0E+11

Calculated total abundances of water, organic carbon and inorganic carbon deposited into the atmosphere by EDPS, based on thermogravimetric measurements of evolved gases from heated samples

Furthermore, the abundance of both organic and inorganic carbon can be calculated as the carbon molar proportion of CO_2 (equating to 12/44). The abundances of

organic and inorganic carbon as a carbon molar proportion of the total EDP CO_2 abundances in the table above, is given in the table below.

		Retained in Samples (kg/yr)		Released during simulations (kg/yr)	
Duration (s)	Peak Temperature (°C)	C organic	C inorganic	C organic	C inorganic
0	0	2.0E+10	3.7E+10	0.0E+00	0.0E+00
2	406 ± 8	1.6E+10	3.7E+10	4.6E+09	0.0E+00
2	603 ± 9	1.4E+10	3.7E+10	6.4E+09	0.0E+00
2	814 ± 13	9.1E+08	3.4E+10	1.9E+10	2.7E+09
2	1006 ± 59	0.0E+00	9.1E+09	2.0E+10	2.7E+10

Carbon abundances delivered by EDPs to the early Earth

Appendix VI – Calculation of EDP Settling Rates

In order to calculate the settling rate of EDPs through the early Earth atmosphere, estimations of the physical properties (dynamic viscosity and density) of an early Earth atmosphere had to be made. The following calculations assume an early Earth atmosphere composed of CO_2 and that EDPs are settling to the surface from a height of ~85 km. Dynamic viscosity is directly related to temperature[1]. According to the U.S. standard atmosphere[2] the average present atmospheric temperature between 0 - 84.5 km altitude is -35.6 °C. The early Earth is thought to have been dominated by CO_2, enabling surface temperatures of ~100 °C[3], 85 °C higher than present. Assuming the temperature profile of the early Earth atmosphere varies in the same way as today, yet scaled by +85 °C, the average early Earth atmospheric temperature (T) would be 49.4 °C.

The dynamic viscosity (μ) for a CO_2 atmosphere can be calculated using:

$$\mu = \mu_0 \left(\frac{T_0 + 273.15 + C}{T + 273.15 + C}\right)\left(\frac{T + 273.15}{T_0 + 273.15}\right)^{\frac{3}{2}}$$

Equation 1

where μ_0 is the reference viscosity at the reference temperature (T_0) and C is Sutherland's constant. In a CO_2 atmosphere, C = 240 [1], and for T_0 = 20 °C [4] , μ_0 = 0.01480 x10^{-3} kg/ms [4]. Therefore with T estimated at 49.4 °C, the average early Earth atmospheric dynamic viscosity would be 1.62 x 10^{-5} kg/ms.

The present day atmospheric pressure at the Earth's surface is 1 bar. Estimates for the early Earth are fifteen times this, with an average near-surface atmospheric pressure of 15 bars based on a CO_2 atmosphere [3]. The average atmospheric pressure for 0 – 84.5 km altitude is 0.16 bars based on the U.S. Standard Atmosphere [2], hence it is estimated that of the average early atmospheric pressure, P, would have been x15 this at 2.35 bars.

---

[1] Crane Company, 1988. Flow of fluids through valves, fittings and pipes. *Technical Paper No. 410.*
[2] U.S Standard Atmosphere, 1976. U.S. Government Printing Office, Washington D.C.
[3] Kasting, J.F. and Ackerman, T.P. 1986. Climatic consequences of very high carbon dioxide levels in the earth's early atmosphere. *Science*, 234(4782), 1383-1385.
[4] Anon, 2008. Handbook of Chemistry and Physics, 89th ed., CRC Press. Available at http://www.hbcpnetbase.com/ [Accessed September 13, 2008].

The early Earth atmospheric density can be calculated using the ideal gas equation [4]:

$$\rho = \frac{PM}{RT}$$

Equation 2

where the molecular weight (M) of CO_2 is 0.044 Kg/mol, the ideal gas constant (R) is 8.31 x 10^{-5} m^3bar/molK and the estimated average atmospheric temperature (T) is 322.55K (equivalent to 49.4 °C). The average density of the early Earth atmosphere is therefore 3.86 kg/m^3.

The settling of ash particles to the surface following injection into the atmosphere during a volcanic eruption is analogous to the atmospheric settling of EDPs. Settling rate of particles through the atmosphere is a function of terminal velocity (v_t), which in turn is dependent on the Reynolds numbers (Re) used to characterise flow regimes. Bonadonna et al., (1998) modelled the settling of volcanic ash between 1 μm and 10 cm in size[5], and determined that particles settled in a laminar (smooth) flow when Re <0.4, an intermediate flow when 0.4 < Re < 500 and a turbulent flow when Re >500. Using the standard Reynolds number equation and rearranging it to solve the transitional terminal velocity (X):

$$X = \frac{0.4\mu}{\rho d}$$

Equation 3

Inputting Re for laminar, intermediate and turbulent flows the transitional velocities between these flow regimes can be determined. For example, for a laminar flow regime, the following must be satisfied:

$$X < \frac{0.4\mu}{\rho d}$$

Equation 4

[5] Bonadonna et al., 1998. Thickness variations and volume estimates of tephra fall deposits: the importance of particle Reynolds number. *Journal of Volcanology and Geothermal Research*, 81(3-4), 173-187.

Similarly for an intermediate flow regime X must satisfy the following:

$$\frac{0.4\mu}{\rho d} < X < \frac{500\mu}{\rho d}$$

Equation 5

Whilst for a turbulent flow regime X must satisfy:

$$X > \frac{500\mu}{\rho d}$$

Equation 6

Depending on the flow type (laminar, intermediate or turbulent), the terminal velocity (V_t) is governed by:

$$V_t \approx \frac{g\sigma d^2}{18\mu}$$ [for laminar flow]

Equation 7

$$V_t \approx d\left(\frac{4\sigma^2 g^2}{225\mu\rho}\right)^{\frac{1}{3}}$$ [for intermediate

Equation 8

$$V_t \approx \left(\frac{3.1g\sigma d}{\rho}\right)^{\frac{1}{2}}$$ [for turbulent flow]

Equation 9

where σ is particle density and g is gravitational acceleration [5]. Assuming an EDP particle settles through the atmosphere at its terminal velocity, Equations 7, 8 and 9 can be used to calculate the terminal velocity of an EDP (with a density of 2500 kg/m^3), dependant on the flow regime. The settling time to the surface can then be calculated for particles from ~85 km altitude (see table below).

Particle Size (μm)	V_t (laminar) (m/s)	Satisfy Equation 4?	V_t (intermediate) (m/s)	Satisfy Equation 5?	Settling time to surface (days)
10	**0.01**	✓	-	-	116.28
20	**0.03**	✓	-	-	29.07
30	0.08	×	**0.20**	✓	4.98
40	0.13	×	**0.26**	✓	3.73
50	0.21	×	**0.33**	✓	2.99
100	0.84	×	**0.65**	✓	1.49
200	3.36	×	**1.31**	✓	0.75
300	7.57	×	**1.96**	✓	0.50
400	13.46	×	**2.62**	✓	0.37
500	21.03	×	**3.27**	✓	0.30

The settling time of EDP particles, of varying diameter, from 84.5km altitude in a CO_2 atmosphere on the early Earth. Terminal velocities have been calculated to satisfy Reynolds numbers governing laminar and intermediate flow regime